

**AN INVESTIGATION OF OPTICAL METHODS FOR THE  
MAPPING OF MICROGRADIENTS OF HYDROGEN-ION  
CONCENTRATION WITHIN DENTAL BIOFILMS**

Thesis submitted by

**Dallas Peter Roulston**

for the degree of

DOCTOR OF PHILOSOPHY

in the

Faculty of Medical Sciences

University College London

Division of Microbial Diseases

UCL Eastman Dental Institute for Oral Health Care Sciences

256 Gray's Inn Road

LONDON

WC1X 8LD

United Kingdom

**-2017-**



# Declaration

I, Dallas Peter Roulston, hereby confirm that the work embodied in this thesis is as a result of my own investigations, except where otherwise stated. Where information has been derived from other sources, I confirm that this has been indicated in the thesis.

The dual-fluorophore, ratiometric, pH-sensitive nanosensors used in this thesis were designed and developed at the Department of Analytical Biosciences, School of Pharmacy at the University of Nottingham. They were produced in conjunction with Dr. Veeren Chauhan and Prof. Jon Aylott at the above department.

The work pertaining to this thesis was partly funded by GlaxoSmithKline.

Signed: .....

Name: .....

Date: .....



## ABSTRACT

The oral cavity is the most complex and accessible microbial ecosystem in the human body. It is the entrance to the respiratory and gastrointestinal tracts and, as such is exposed to unique environmental constraints. The human mouth is home to a myriad of microorganisms, many of which are exclusively found in this unique habitat. These microbial inhabitants can establish themselves and thrive in this environment by attaching to the various surfaces of the oral cavity. Following attachment, they form three-dimensional, complex and highly-integrated microbial communities. Despite their complexity and natural fluctuations in environmental parameters, in health, these communities remain relatively stable over time. This stability is termed microbial homeostasis. Disruption of the microbial homeostasis occurs as a result of regular or prolonged challenges in the form of an altered environment. These disruptions favour a shift in the microbial populations, suppressing the metabolism of the beneficial inhabitants and allowing unfavourable microorganisms to thrive in the lack of competition. This change in the oral microbiota facilitates the progression from oral health to disease. Despite continuing research and development in preventative measures dental caries, characterised by localised dissolution of the dental hard tissues, remain one of the most prevalent disorders affecting man today. This decay occurs as a result of strong organic acids produced by the microbiota within dental plaque following exposure to fermentable carbohydrates. Furthermore, prolonged and regular exposure to acids suppresses the growth of 'beneficial' bacteria allowing acidogenic, aciduric microorganisms, such as *Streptococcus mutans* and lactobacilli to thrive in the lack of competition. The presence of these acidogenic microorganisms causes

an increase in acid production and an increase in the duration of exposure to those acids. Although rarely life-threatening, they create an enormous economic burden to healthcare providers worldwide and cause significant physical and social impact on those affected, including diet, communication and self-esteem. Greater understanding is required to appreciate the dynamic relationship that exists between the environment, the microbiota and the host. To gain a greater understanding of how the microbial ecology is affected, it is necessary to be able to determine how pH changes during and following fermentation and the effect these perturbations have upon the microbial community. At present, the most commonly employed methods include the use of microelectrodes, whether through insertion into laboratory grown biofilm or incorporated within in vivo prosthetics devices. These methods are not without their drawbacks. In the act of measurement, microelectrodes are inserted into the biofilm resulting in, at least partial, disruption of the biofilm and this may have a detrimental effect on the results. In vivo prosthetics provides measurement at the biofilm interfaces and in physiological conditions, however almost certainly require partially dentate individuals and are difficult to use. Novel methods are required to investigate pH within biofilms which provide a multidimensional determination, including temporal, and do not cause a detrimental effect upon the biofilm. Here, I examine two optical methods which utilised different properties of fluorescence to investigate pH microgradients within biofilms designed to mimic cariogenic dental plaque. The two methods are dual-fluorophore, ratiometric, pH-sensitive nanosensors imaged through confocal laser scanning microscopy and SNARF<sup>®</sup>-4F 5-(and-6)-carboxylic acid imaged through time-correlated single-photon counting and fluorescence-lifetime imaging microscopy. The nanosensors were designed, produced and characterised prior to calibration.

The nanosensors were applied to biofilms with limited success, likely due to poor penetration. The optical properties of SNARF<sup>®</sup>-4F 5-(and-6)-carboxylic acid were characterised, including the two-photon molecular excitation wavelength for use here. The fluorophore was calibrated and applied to bacterial sediment and biofilms and the localised environmental pH assessed following exposure to a fermentable carbohydrate to decrease the pH. Many of the drawbacks experienced with currently employed methods have been addressed by these methods, however further research and development is required.



## STATEMENT OF IMPACT

Dental caries affects between 60% and 90% of school-aged children and approaching 100% of adults. Treatment of dental caries remains a huge economic burden upon healthcare providers. Dental caries also has a major effect on the health and well-being of the patient. Left untreated, dental caries can lead to considerable discomfort and effect nutritional intake from a varied diet. Cavitated teeth may also result in the sufferer experiencing effects upon their emotional well-being, due to self-confidence, speech and communication through expression. The driving force behind the development and progression of dental caries is the generation of organic acids produced by the microbial inhabitants of the oral cavity as a result of fermentation of carbohydrates. To greater understand, and to combat, the development and progression of dental caries the determination of pH within the microbial communities is highly desirable. The currently employed methods for the determination of pH in biofilms have a number of drawbacks. Therefore, methods which address these drawbacks are advantageous. The methods described address many of the disadvantages of previously employed methods.

The employment of the described methods will appeal to industry. The ability to determine multidimensional microgradients in pH in real-time will be of particular interest. The ability to observe the effect of active ingredients upon pH over time is attractive. Active ingredients of interest would include those which suppress the production of acids following fermentation or promote the return to the resting pH, shifting the homeostatic balance towards remineralisation. With respect to the clinic, the methods described may be employed to understand the interactions between various microbial inhabitants, whether detrimental or beneficial. This may give rise to probiotics to address dental caries.

The imaging methods employed here may also allow the determination of other environmental parameters, with the selection and characterisation of appropriate sensors.



*"Life is a struggle, not against sin, not against the Money Power, not against malicious animal magnetism, but against hydrogen ions."*

*H.L. MENCKEN*

---



# ACKNOWLEDGEMENTS

I would like to express my deepest gratitude to my supervisors during this project, **Prof. David Spratt** and **Dr Jonathan Pratten**. Your constant guidance, support, encouragement and friendship were invaluable. Thank you for introducing me to this exciting field of research and providing me the opportunity to become the research scientist that I am today. I never once left a meeting feeling more uncertain than prior to it. Thank you.

I would like to express my appreciation to The **Biotechnology and Biological Sciences Research Council (BBSRC)** and **GlaxoSmithKline (GSK)** for providing funding to permit this research and the ability to present my work to an international audience. Furthermore, a special thank you to those at GSK who provided assistance and advice along the way, particularly but not excluded to; **Dr David Bradshaw**, **Dr Gary Burnett** and **Dr Richard Lynch**.

I am grateful to a many number of people who throughout my project provided support and guidance. They include; **Dr Veeren Chauhan** and **Assoc. Prof. Jon Aylott** at University of Nottingham. Your assistance with the development, production and characterisation of the pH-sensitive nanoparticle allowed this work. **Dr Ee Zhuan 'Chris' Chong**, **Dr Dylan Herzog** and **Dr Fred Festy** at King's College London Dental Institute. Thank you for allowing me to use the fluorescence lifetime imaging microscope and various analysers during the conceptual analysis of seminaphthorhodafluor dyes. I would like to thank **Dr Chris Thrasivoulou** and the staff at UCL Centre for Cell & Molecular Dynamics, Imaging Unit for their continual assistance with the fluorescence lifetime imaging. I would like to thank **Dr Nicola Mordan** at the UCL Eastman Dental Institute for your assistance with the confocal laser scanning microscope. Likewise to **Dr George Georgiou**, also at the UCL Eastman Dental Institute, for your assistance with the production of hydroxyapatite discs.

Finally, I would like to thank my family. To my caring, loving, and supportive wife, **Kerry**: my deepest gratitude. Your encouragement when the times got rough was much appreciated. To my daughter, **Jessica**, you had the ability to cheer me up when things got tough. To my extended family, for the sacrifices you have made, my heartfelt thanks.



# CONTENTS

## AN INVESTIGATION OF OPTICAL METHODS FOR THE MAPPING OF MICROGRADIENTS OF HYDROGEN-ION CONCENTRATION WITHIN DENTAL BIOFILMS

<b>ABSTRACT.....</b>	<b>i</b>
<b>STATEMENT OF IMPACT .....</b>	<b>v</b>
<b>ACKNOWLEDGEMENTS.....</b>	<b>ix</b>
<b>CONTENTS.....</b>	<b>ix</b>
<b>TABLE OF FIGURES.....</b>	<b>xviii</b>
<b>TABLE OF UNITS .....</b>	<b>xxv</b>
<b>Chapter 1 Introduction .....</b>	<b>1</b>
1.1 The Human Oral Cavity .....	1
1.1.1 <i>The Calcified Dental Tissue</i> .....	2
1.1.2 <i>The Mucosal Surfaces of the Human Oral Cavity</i> .....	4
1.2 Saliva.....	5
1.2.1 <i>Buffering Capacity of Saliva</i> .....	6
1.3 Gingival Crevicular Fluid .....	12
1.4 Dental Plaque .....	13
1.4.1 <i>Formation of Dental Plaque</i> .....	14
1.5 Parameters Which Influence the Oral Environment and Microbial Ecology .....	19

1.5.1	<i>Hydrogen-Ion Concentration (pH)</i> .....	19
1.5.2	<i>Oxygen Concentration and Oxidation-Reduction (Redox) Potential (Eh)</i> .....	26
1.5.3	<i>Temperature</i> .....	27
1.5.4	<i>Nutrient Sources</i> .....	28
1.6	The Formation of Spatial Microgradients .....	30
1.7	Dental Caries .....	31
1.8	The Role of Fermentable Carbohydrates in Dental Caries .....	33
1.9	The Concept of Microbial Homeostasis .....	33
1.10	Plaque Hypotheses .....	35
1.10.1	<i>Specific Plaque Hypothesis</i> .....	36
1.10.2	<i>Non-Specific Plaque Hypothesis</i> .....	36
1.10.3	<i>Ecological Plaque Hypothesis</i> .....	37
1.10.4	<i>Extended Ecological Plaque Hypothesis</i> .....	39
1.11	The Microbiota of the Oral Cavity .....	40
1.11.1	<i>The Microbiota Pertaining to Human Dental Caries</i> .....	42
1.11.2	<i>The Oral Streptococci</i> .....	42
1.11.3	<i>The Oral Lactobacilli</i> .....	43
1.11.4	<i>The Oral Neisseria spp.</i> .....	43
1.12	Dental Plaque as a Microbial Community .....	44
1.12.1	<i>Genetic Exchange</i> .....	45
1.12.2	<i>Bacterial Communication and Regulation of Gene Expression</i> .....	45
1.13	Acid Tolerance of Oral Bacteria .....	46
1.14	Preventative Measures and Treatments of Dental Caries .....	47
1.14.1	<i>Mechanical Removal of Dental Plaque</i> .....	48
1.14.2	<i>Chemical Control</i> .....	48
1.14.3	<i>Nutritional Intervention</i> .....	49
1.14.4	<i>Beneficial Foodstuffs</i> .....	50

1.15	Methods for the Measurement of Hydrogen-Ion Concentration within Dental Biofilms .....	52
	1.15.1 <i>The Harvest Method</i> .....	53
	1.15.2 <i>Microelectrodes</i> .....	53
	1.15.3 <i>In vivo Prosthetic Devices Incorporating Electrodes</i> .....	56
	1.15.4 <i>Optical methods</i> .....	57
1.16	Fluorescence .....	58
	1.16.1 <i>The Fluorescence Spectra</i> .....	60
	1.16.2 <i>Fluorescence Lifetime</i> .....	61
	1.16.3 <i>Fluorescent Molecular Probes</i> .....	63
1.17	Fluorescence-Based Microscopy Techniques .....	63
	1.17.1 <i>Epifluorescence Microscopy</i> .....	63
	1.17.2 <i>Confocal Laser Scanning Microscopy</i> .....	64
	1.17.3 <i>Two-Photon Excitation Microscopy</i> .....	69
	1.17.4 <i>Two-Photon Molecular Excitation Scanning Microscopy</i> .....	71
	1.17.5 <i>Fluorescence-Lifetime Imaging Microscopy</i> .....	71
	1.17.6 <i>Time-Correlated Single Photon Counting</i> .....	73
1.18	Nanosensors .....	77
1.19	Benzo[c]xanthene Fluorescent Dyes .....	79
1.20	Biofilm Models .....	83
	1.20.1 <i>Static Biofilms</i> .....	84
	1.20.2 <i>The Constant Depth Film Fermenter</i> .....	85
1.21	Rationale for the Study .....	87
1.22	Aims & Objectives .....	90

## Chapter 2 General Materials and Methods ..... 91

2.1	Reagents .....	91
2.2	Media.....	91
2.3	Storage of Bacterial Isolates .....	91
2.4	Production of Citric Acid-Sodium Phosphate Buffer Solutions .....	92
2.5	Selection of Organisms to Mimic a Dental Caries Biofilm.....	93
2.6	Preparation of Static Biofilms.....	94
2.7	Preparation of Microtitre Plate Biofilms .....	95
2.8	Set-up of the Constant Depth Film Fermenter.....	95
2.8.1	<i>Selection of an Appropriate Environmental Temperature .....</i>	<i>95</i>
2.8.2	<i>Selection of an Appropriate Gaseous Environment.....</i>	<i>96</i>
2.8.3	<i>Selection of an Appropriate Nutrient Source.....</i>	<i>96</i>
2.8.4	<i>Selection of an Appropriate Biofilm Substratum for the Constant Depth Film Fermenter .....</i>	<i>97</i>
2.8.5	<i>Production of Hydroxyapatite Discs for Use in the Constant Depth Film Fermenter .....</i>	<i>97</i>
2.8.6	<i>Preparation of the Peripheral Devices.....</i>	<i>97</i>
2.8.7	<i>Preparation of an Artificial Saliva Medium Containing Mucin .....</i>	<i>99</i>
2.8.8	<i>Calibration of the Peristaltic Pump.....</i>	<i>100</i>
2.8.9	<i>Preparation of the Constant Depth Film Fermenter .....</i>	<i>101</i>
2.8.10	<i>Set-up of the Constant Depth Film Fermenter.....</i>	<i>103</i>
2.8.11	<i>Preparation of the Inoculum for the Constant Depth Film Fermenter.....</i>	<i>104</i>
2.8.12	<i>Inoculation of the Constant Depth Film Fermenter .....</i>	<i>104</i>

## **Chapter 3 Investigation of Processes Which Effect the Microbial Ecology of Biofilms Formed in the Oral Cavity.... 106**

3.1	Introduction.....	106
3.1.1	<i>Aims and Objectives</i> .....	107
3.2	Materials and Methods.....	107
3.2.1	<i>Preparation of Bacterial Suspensions for Fermentation Assays</i> .....	107
3.2.2	<i>Fermentation Assay 1</i> .....	107
3.2.3	<i>Fermentation Assay 2</i> .....	107
3.3	Results .....	108
3.3.1	<i>Fermentation Assay 1</i> .....	108
3.3.2	<i>Fermentation Assay 2</i> .....	109
3.4	Discussion.....	110

## **Chapter 4 Design, Production and Characterisation of Dual-Sensitive Fluorophore, Ratiometric, pH-Sensitive Nanosensors ..... 112**

4.1	Introduction.....	112
4.1.1	<i>Aims and Objectives</i> .....	123
4.2	Materials and Methods.....	123
4.2.1	<i>Design of Nanosensors</i> .....	123
4.2.2	<i>Production of pH-Sensitive, Dual-Fluorophore Ratiometric Nanosensors</i> .....	125
4.2.3	<i>Characterisation of the Nanosensor</i> .....	128
4.3	Results .....	130
4.3.1	<i>Design of the Nanosensors</i> .....	130
4.3.2	<i>Analysis of the Fluorescent Spectra of Nanosensors</i> .....	132
4.3.3	<i>Analysis of Nanosensor Size and Shape Using Environmental Scanning Electron Microscopy</i> .....	135

4.3.4	<i>Analysis of Nanosensor Size Using Dynamic Light Scattering</i> .....	136
4.3.5	<i>Analysis of Nanosensor Fluorescence Spectra</i> .....	137
4.4	Discussion .....	138
4.4.1	<i>Summary</i> .....	140

## **Chapter 5 Investigation of Suitability and Calibration of Dual-Fluorophore, Ratiometric, pH-Sensitive Nanosensors for the Determination of pH ..... 141**

5.1	Introduction.....	141
5.1.1	Aims and Objectives .....	142
5.2	Materials and Methods .....	143
5.2.1	<i>Analysis of Bacterial Cell Viability Following Exposure to Polyacrylamide Nanoparticles</i> .....	143
5.2.2	<i>Calibration</i> .....	147
5.2.3	<i>Imaging of the Buffered Nanosensor Suspensions</i> .....	149
5.2.4	<i>Determination of pH Changes in Planktonic Bacteria Using Dual-Fluorophore, pH-Sensitive, Ratiometric Nanosensors</i> .....	150
5.3	Results .....	151
5.3.1	<i>Analysis of Bacterial Cell Viability Following Exposure to Polyacrylamide Nanoparticles</i> .....	151
5.3.2	<i>Serial Dilution</i> .....	155
5.3.3	<i>Calibration</i> .....	157
5.4	Discussion .....	160
5.4.1	<i>Summary</i> .....	162

## Chapter 6 Analysis of Seminaphthorhodafluor (SNARF)

### Dyes to Determine Hydrogen-Ion Concentration..... 163

6.1	Introduction.....	163
6.1.1	<i>Aims and Objectives</i> .....	165
6.2	Materials and Methods.....	166
6.2.1	<i>Instrumentation</i> .....	166
6.2.2	<i>Determination of Optimal Two-Photon Excitation Wavelength</i> .....	167
6.2.3	<i>Preparation of SNARF®-4F 5-(and-6)-Carboxylic Acid Dye</i> .....	169
6.2.4	<i>Investigation of Detrimental Effect of SNARF®-4F 5-(and-6)-Carboxylic Acid upon Bacteria</i> .....	169
6.2.5	<i>Preparation of Citric Acid – Sodium Phosphate Buffer Solutions</i> .....	170
6.2.6	<i>Production of Reduced Transport Fluid</i> .....	170
6.2.7	<i>Instrument Set-Up and Optimisation</i> .....	171
6.2.8	<i>Imaging a Specimen</i> .....	171
6.2.9	<i>Obtaining the Fluorescence Emission Spectra of SNARF®-4F 5-(and-6)-Carboxylic Acid</i> .....	171
6.2.10	<i>Calibration of SNARF®-4F 5-(and-6)-Carboxylic Acid With Respect to pH</i> .....	172
6.2.11	<i>Investigation of Fluorescence Emission of Various Biofilm Substrata</i> .....	172
6.2.12	<i>Investigation of Factors Which May Influence Fluorophore Accuracy</i> .....	173
6.3	Results .....	174
6.3.1	<i>Determination of the Optimal Two-Photon Excitation Wavelength for SNARF Dyes</i> .....	174
6.3.2	<i>Investigation of Detrimental Effect of SNARF®-4F 5-(and-6)-Carboxylic Acid upon Bacteria</i> .....	177
6.3.3	<i>Calibration of SNARF®-4F 5-(and-6)-Carboxylic Acid for Two-Photon Excitation Fluorescence Lifetime Imaging Microscopy</i> .....	178
6.3.4	<i>Investigation of Factors Which May Influence Fluorophore Accuracy</i> .....	183
6.4	Discussion.....	187
6.4.1	<i>Summary</i> .....	190

<b>Chapter 7</b>	<b>Application of Dual-Fluorophore, Ratiometric, pH-sensitive Nanosensors and SNARF®-4F 5-(and-6)-Carboxylic Acid Dye to Bacteria to Visualise pH Microgradients.....</b>	<b>191</b>
7.1	Introduction.....	191
7.1.1	<i>Aims and Objectives</i> .....	194
7.2	Materials and Methods .....	194
7.2.1	<i>Preparation of the Nanosensor Suspension</i> .....	194
7.2.2	<i>Application of Nanosensors to Biofilms</i> .....	195
7.2.3	<i>Growth of Biofilms Incorporating Nanosensors</i> .....	195
7.2.4	<i>Preparation of SNARF®-4F 5-(and-6)-Carboxylic Acid Suspension</i> .....	196
7.2.5	<i>Preparation of a Suspension of Streptococcus mutans</i> .....	196
7.2.6	<i>Determination of pH in Bacterial Sediment Exposed to Sucrose</i> .....	196
7.2.7	<i>Determination of pH in Bacterial Biofilm Exposed to Sucrose</i> .....	197
7.3	Results .....	198
7.3.1	<i>Dual-Fluorophore, Ratiometric, pH-sensitive Nanosensors</i> .....	198
7.3.2	<i>Imaging of Planktonic Bacterial Sediment of S. mutans using SNARF®-4F 5-(and-6)-Carboxylic Acid and Two-Photon Molecular Excitation Fluorescence Lifetime Imaging</i> .....	199
7.3.3	<i>Comparison of pH Values Determined Through the Use of a pH Microelectrode to SNARF®-4F 5-(and-6)-Carboxylic Acid Imaged Through the Use of Two-Photon Molecular Excitation Fluorescence Lifetime Imaging Following Exposure to a Fermentable Carbohydrate</i> .....	201
7.3.4	<i>Imaging of S. mutans Biofilm using SNARF®-4F 5-(and-6)-Carboxylic Acid and Two-Photon Molecular Excitation and Fluorescence Lifetime Imaging</i> .....	204
7.4	Discussion .....	208

**Chapter 8    General Discussion ..... 212**

8.1 Project Background ..... 212

8.2 Summary of Main Findings..... 213

8.3 Challenges and Difficulties ..... 218

8.4 Future Work ..... 220

8.5 Conclusion ..... 221

**REFERENCES ..... 225**

**APPENDICES ..... 262**

*Appendix 1.    Abbreviations Used..... 263*

*Appendix 2.    Glossary of Terms Used ..... 264*

# TABLE OF FIGURES

Figure 1.1	Locations of stagnation offering dental plaque and food protection from mechanical removal and the effects of saliva. (Image credit: adapted from healthtap.com). .....	2
Figure 1.2	Cross section of the adult human molar. (Encyclopaedia Britannica CC BY 2.0).	4
Figure 1.3	Dissociation equation of carbonic acid by bicarbonate under the action of salivary carbonic anhydrase IV. ....	7
Figure 1.4	The role of carbonic anhydrase IV in the neutralisation of acidic products of bacterial metabolism. (Adapted from Leinonen et al. 1999) .....	8
Figure 1.5	The effect of bicarbonate concentration on saliva pH .....	10
Figure 1.6	Dissociation equilibrium of the phosphate buffer system. ....	11
Figure 1.7	Alkali generating pathways in the oral cavity. ....	12
Figure 1.8	Spatiotemporal model of colonisation of oral bacteria, showing recognition of salivary receptors within the salivary pellicle by early colonisers and co-aggregation between early colonisers, fusobacteria and late colonisers, (Kolenbrander et al. 2002). ....	17
Figure 1.9	A diagram showing various synergistic feeding interactions which may occur in dental plaque (Image adapted from Marsh & Martin 2009). ....	19
Figure 1.10	The Stephan curve, an archetypal profile of pH with respect to time following exposure of dental plaque to fermentable carbohydrates (Stephan 1940). ....	22
Figure 1.11	Stephan curves demonstrating the differences in pH decreases in patients with different caries activity (Stephan & Miller 1943). ....	22
Figure 1.12	Diagram of a basic food chain showing the effect of the presence and absence of <i>Veillonella</i> spp. (Marsh and Martin 2009). ....	24
Figure 1.13	Plots of dental plaque pH following (A) numerous and frequent carbohydrate exposures through diet and (B) limiting carbohydrate intake (Marsh & Martin 2009). ....	26

Figure 1.14	Chemical structure of sucrose, showing a glucose molecule and a fructose molecule joined by a glycosidic linkage.....	30
Figure 1.15	Representation of the dental plaque composition and the transition from health to disease under ecological pressure. (Marsh 2009). .....	38
Figure 1.16	The ecological plaque hypothesis, factors leading to the progression of dental caries and how control of these factors can reinstate oral health (Marsh 2003). .....	39
Figure 1.17	The concept of the extended ecological plaque hypothesis, showing the various stages of disease progression (Takahashi & Nyvad 2008). .....	40
Figure 1.18	A diagrammatic representation of the pH range for growth for some oral bacterial species (Marsh & Martin 2009). .....	47
Figure 1.19	An example of a pH microelectrode (Ewers & Greener 1985).....	54
Figure 1.20	An example of A) an in vivo prosthetic device incorporating a pH electrode and B) the device in situ, (Image credit: Mühlemann & de Boever 1970). .....	57
Figure 1.21	Fluorescent emission shift with respect to changes in concentration.....	57
Figure 1.22	Fluorescent wavelength shift with respect to changes in concentration. ....	58
Figure 1.23	A Jablonski diagram showing the various energy states that may be achieved following excitation by electromagnetic radiation and the consequential internal conversion (heat loss) and fluorescence emission (release of a photon). .....	60
Figure 1.24	An example of a fluorescence spectra showing excitation (blue) and emission (red) peaks. The right pane shows the effect of different excitation wavelength on emission intensity (Thermo Fisher Scientific CC BY 2.0). .....	61
Figure 1.25	Schematic of a typical fluorescence microscope.....	64
Figure 1.26	Cut away diagram of a filter cube used in fluorescence microscope (Leica Microsystems). .....	64

Figure 1.27	A schematic of a typical CLSM. Laser light (red line) travels through an objective aperture, which removes light of unwanted wavelength. The light continues through a dichroic mirror allowing light of the excitation wavelength (CC BY 2.0).....	65
Figure 1.28	Conventional (single-photon) molecular excitation demonstrating out-of-focus fluorescence emission. (Image credit: Steve Ruzin) .....	66
Figure 1.29	Images demonstration a comparison of image resolution. A) shows a lack of resolution caused by out-of-focus fluorescence emission. B) shows an improvement to image resolution by blocking out-of-focus light through the use of a pinhole aperture (Image credit: University of Texas CC BY 2.0) .....	67
Figure 1.30	The numerical aperture of an objective lens. A is the aperture of the objective lens and $\vartheta$ is the one half the angular aperture. ....	68
Figure 1.31	Fluorescent emission as a result of single-photon excitation (left) and two-photon excitation (right) (Cornell University CC BY 2.0). ....	70
Figure 1.32	Detector signal for fluorescence detection at 80 Hz laser pulse repetition rate. a) shows the excitation pulse sequence at 80 Hz. b) shows the expected fluorescence signal and fluorescence decay. c) shows the actual detector signal achieved.....	74
Figure 1.33	Fluorescence exponential decay curve and determination of fluorescence lifetime.....	75
Figure 1.34	Diagram demonstrating oscillation of random longitudinal modes within a laser cavity and the resulting output signal. ....	76
Figure 1.35	Diagram demonstrating 'locked' longitudinal modes within a laser cavity and the resulting output signal, a train of intense and regular pulses.....	77
Figure 1.36	Schematic of PEBBLE construct (Koo Lee et al. 2009). ....	78
Figure 1.37	Diagram demonstrating the similarity in chemical structure between A) SNARF B) SNAFL and C) BCECF dyes. ....	79
Figure 1.38	Chemical structure of SNARF dyes. A) As pH decreases, protonation of the phenol group occurs. B) As pH increases, this is reversed. The site of protonation is indicated. C) indicates R groups and $pK_a$ values. ....	80

Figure 1.39	Chemical structures of a. SNARF-1 and b. SNAFL-1, showing the substitution at the 10 position of nitrogen for oxygen, respectively. ....	81
Figure 1.40	Chemical structure of SNARF dyes, demonstrating a. the protonated (low pH) form, exhibiting a monoanionic naphthol group at the site of protonation (blue) and b. the deprotonated (high pH) form exhibiting the naphtholate group. ....	82
Figure 1.41	Side aspect view and components of the CDFP (Pratten & Wilson 1999). ....	86
Figure 1.42	Top aspect of the turn table of the constant depth film fermenter (Adapted image, used with permission from J Pratten). ....	87
Figure 2.1	Schematic drawing of a secretory mucin glycoprotein depicting a MUC protein backbone and its O-glycans. ....	96
Figure 2.2	Schematic diagram of the CDFP when set-up. ....	100
Figure 2.3	CDFP tools including A) tamping tool, B) PTFE pan removal tool, and C) PTFE plug recession tool. (Wiecek 2015). ....	102
Figure 2.4	Recession of PTFE plugs and substratum at desired depth using the PTFE plug recession tool (Wiecek 2015). ....	102
Figure 2.5	Use of the tamping tool to situate the PTFE pans flush with the turn table (Wiecek 2015). ....	103
Figure 2.6	Application of high vacuum silicone grease to each side of the PTFE seals (Wiecek 2015). ....	103
Figure 3.1	Graph showing the average change in pH following after 2 hours of exposure to sucrose or non-exposed (saline). Lighter bars indicate those exposed to sucrose. The error bars shows 1 standard deviation, n = 12. ....	109
Figure 3.2	Graph of pH with respect to time following exposure to sucrose. n = 1 for each isolate. ....	110
Figure 4.1	An example of a fluorescence spectra, Oregon Green <sup>®</sup> -488, showing relative excitation and emission intensity and various wavelengths and the Stoke's shift (ThermoFisher Spectraviewer) ....	114

Figure 4.2	Chemical structure of A) N,N'-methylbis(acrylamide), B) acrylamide and C) polyacrylamide.....	117
Figure 4.3	The principle of obtaining nanoparticle size through the use of dynamic light scattering (Image credit Mike Jones CC BY 2.0).....	121
Figure 4.4	Chemical structure of N-(3-aminopropyl)methacrylamide hydro- chloride (APMA).....	126
Figure 4.5	Chemical reaction of conjugation of fluorophores to N-(3-amino- propyl)methacrylamide hydrochloride (APMA), in sodium tetra- borate decahydrate ( $\text{Na}_2\text{B}_4\text{O}_7 \cdot 10\text{H}_2\text{O}$ , 50 nM at pH 9.5) buffer solution. ....	127
Figure 4.6	Chemical structure of Oregon Green <sup>®</sup> -488, succinidyl ester. ....	131
Figure 4.7	Chemical structure of 5-(and-6)-carboxyfluorescein, succinidyl ester.....	131
Figure 4.8	Chemical structure of 5-(and-6)-carboxytetramethylrhodamine,.....	131
Figure 4.9	Fluorescence excitation (dotted) and emission (solid) spectra for carboxyfluorescein (green line) and Oregon Green <sup>®</sup> -488 (blue line). The vertical blue line indicates the excitation laser line (488 nm) utilised throughout. The green bar indicates the emission filter (520/30 nm) applied .....	133
Figure 4.10	Fluorescence excitation (dotted) and emission (solid) spectra for tetramethylrhodafluor (yellow line). The vertical blue line indicates the excitation laser line (543 nm) utilised throughout. The yellow bar indicates the emission filter (590/70 nm) applied .....	134
Figure 4.11	Graphic representation of the dynamic range of nanosensors incorporating various ratios of FAM to Oregon Green. The extension of the dynamic range is visible when utilised in a 1:1 ratio. ....	135
Figure 4.12	Environmental scanning electron micrograph of the produced dual- fluorophore, ratiometric, pH-sensitive nanosensors.....	136
Figure 4.13	Particle size distribution obtained through dynamic light scattering. (Image used with permission of V. Chauhan). ....	137
Figure 4.14	The fluorescence emission spectra of dual-fluorophore, ratiometric, pH- sensitive nanosensors.....	138

Figure 5.1	Diagram of 96 well plate layout, showing concentration of nanoparticles, in mg/L, for each column. NC refers to the control well in which nanoparticles were replaced with sterile dH <sub>2</sub> O. ....	144
Figure 5.2	Diagram demonstrating the location of the ‘multi-point’ tool utilised for counting in the ImageJ image analysis software package.....	146
Figure 5.3	Live/dead images of a suspension of <i>N. subflava</i> . A) Not exposed to nanoparticles B) Exposed to nanoparticles. ....	152
Figure 5.4	A comparison of cell viability, determined by colony-counting, following exposure to polyacrylamide nanoparticles. Error bars show standard deviation from the mean. n = 3.....	153
Figure 5.5	Relative proportions of live (green) and dead (red) bacteria following exposure to nanosensors for 24 h for a.) <i>S. mutans</i> , b.) <i>S. sanguinis</i> , c.) <i>N. subflava</i> , and d.) <i>L. casei</i> . n = 1. ....	154
Figure 5.6	Plot of CFU/mL following exposure to varying concentration of polyacrylamide nanoparticles for a.) <i>S. mutans</i> , b.) <i>S. sanguinis</i> , c.) <i>N. subflava</i> , and d.) <i>L. casei</i> . The green dotted line represents the mean bacterial concentration and the red dotted lines represent 2 standard deviations from the mean across the varying nanoparticle concentrations. The yellow solid line shows the trend in bacterial concentration values across the varying nanoparticle concentrations. ....	156
Figure 5.7	Matrix of images of nanosensors in buffers of varying values, showing separate images and merged images.....	158
Figure 5.8	Graphic representation of obtained intensities with respect to pH. A) Intensities obtained prior to normalisation. B) Intensities following normalisation. The red line represents fluorescence intensity values in the red channel, while the green line represents fluorescence intensity values in the green channel. The yellow line represents the line-of-best-fit and represents the calibration curve. ....	159
Figure 5.9	Calibration curve of pH-sensitive nanosensors in pH buffer solutions ranging from pH 3.0 to 7.4, and the residual values .....	160
Figure 6.1	The Spectra-Physics Tsunami Ultra-fast tuneable Ti:sapphire oscillator .....	168
Figure 6.2	Layout of the Spectra-Physics Tsunami Ti:sapphire oscillator .....	169

Figure 6.3	Mean number of photons per pixels generated by two-photon excitation between 760 and 940 nm .....	175
Figure 6.4	Fluorescence emission spectrum when excited at $\lambda$ 840 nm showing an emission peak maximum at approximately $\lambda$ 646 nm .....	176
Figure 6.5	Cell concentrations following exposure to various concentrations of SNARF <sup>®</sup> -4F 5-(and-6)-carboxylic acid for a) <i>S. mutans</i> , b) <i>S. sanguinis</i> , c) <i>L. casei</i> , and d) <i>N. subflava</i> . Error bars represent standard deviation from the mean, n = 3.....	178
Figure 6.6	Matrix of colour-coded fluorescence lifetime images at various pH values. ..	180
Figure 6.7	Calibration curve of fluorescence lifetime values for the calibration of SNARF <sup>®</sup> -4F 5-(and-6)-carboxylic acid in citric acid-sodium phosphate buffer and the residual values. The plot of residuals represents the variation between the observed values and the line-of-best-fit.....	181
Figure 6.8	Calibration curve for of SNARF <sup>®</sup> -4F 5-(and-6)-carboxylic acid in citric acid-sodium phosphate buffers and the residual values. The plot of residuals represents the variation between the observed values and the line-of-best-fit. . .....	182
Figure 6.9	Plot of the number of photons obtained under differing redox potential environments. Error bars represent standard deviation from the mean.....	183
Figure 6.10	Plot of the number of photons obtained under differing temperatures. Error bars represent standard deviation from the mean .....	184
Figure 6.11	Mean fluorescence lifetimes at various temperatures. Error bars represent standard deviation from the mean.....	185
Figure 6.12	Number of photons detected at various protein concentrations. Error bars represent standard deviation from the mean .....	185
Figure 6.13	Mean fluorescence lifetimes at various protein concentrations. Error bars represent standard deviation from the mean .....	186
Figure 6.14	Number of photons detected at various glycoprotein concentrations .....	187
Figure 6.15	Mean fluorescence lifetimes at various glycoprotein concentrations. Due to a lack of photons detected, fluorescence lifetime values were not able to be determined at 10 and 20 mg/mL .....	187

Figure 7.1	Diagram demonstrating the structural heterogeneity of biofilms. The diagram displays projections and interstitial water channels facilitating the exchange of nutrients and waste products (Image credit: Peg Dirckx, Image used with permission) .....	192
Figure 7.2	Colour-coded fluorescence lifetime images of a bacterial sediment of <i>S. mutans</i> using SNARF®-4F 5-(and-6)-carboxylic acid. Images demonstrate fluorescence lifetime prior to sucrose (left), and 15 min post-exposure (right). .....	200
Figure 7.3	Matrix of colour-coded fluorescence lifetime images over time following exposure to fermentable carbohydrates, in the form of sucrose. The images are taken at introduction of fermentable carbohydrate and subsequently at intervals of approximately 3 min over a period of 1 h. ....	201
Figure 7.4	Plot of pH values determined using a glass microelectrode, pH meter and plotting software package, with respect to time. Points correspond to the average pH values recorded every second over the period of a minute. ....	203
Figure 7.5	Plot of average pH values determined through the use of SNARF®-4F 5-(and-6)-carboxylic acid excited through the utilisation of two-photon molecular excitation fluorescence lifetime imaging microscopy, with respect to time. Images were collected every 3 min and are observed in Figure 7.3. ....	203
Figure 7.6	Plot of pH values with respect to time extrapolated from the average fluorescence lifetime values and the calibration data for SNARF®-4F 5-(and-6)-carboxylic acid. ....	204
Figure 7.7	Colour-coded fluorescence lifetime images of <i>S. mutans</i> biofilm in 15 minute increments following exposure to sucrose .....	206
Figure 7.8	Colour-coded fluorescence lifetime image following 1 hour incubation in the presence of sucrose. Fluorescence lifetime values of each pixel obtained from the Becker-Hickl SPCImage software are converted to pH through use of the calibration equation and converted colour using Microsoft Excel. ....	207

# TABLE OF EQUATIONS

Equation 1-1 .....	8
Equation 1-2 .....	9
Equation 1-3 .....	9
Equation 1-4 .....	12
Equation 1-5 .....	49
Equation 1-6 .....	59
Equation 1-7 .....	62
Equation 1-8 .....	62
Equation 1-9 .....	68
Equation 1-10 .....	69
Equation 1-11 .....	69
Equation 1-12 .....	69
Equation 1-13 .....	72
Equation 1-14 .....	72
Equation 1-15 .....	74
Equation 4-1 .....	114
Equation 4-2 .....	120
Equation 5-1 .....	150
Equation 5-2 .....	150

## TABLE OF UNITS

<b>Concentration</b>	M:	molar
	$\mu$ M:	micromolar
<b>Electromotive Force</b>	kV:	kilovolts
<b>Energy</b>	eV:	electronvolt
<b>Frequency</b>	MHz:	megahertz
	Hz:	hertz
<b>Frequency of rotation</b>	rpm:	revolutions per minute
<b>Length</b>	m:	metre
	mm:	millimetre
	$\mu$ m:	micrometre
	nm:	nanometre
<b>Number of Viable Cells</b>	CFU:	colony-forming unit
<b>Power</b>	mW:	milliwatt
<b>Pressure</b>	mbar:	millibar
<b>Relative Centrifugal Force</b>	g:	acceleration of gravity
<b>Temperature</b>	$^{\circ}$ C:	degree centigrade
<b>Time</b>	h:	hour
	min:	minute
	s:	second
<b>Volume</b>	L:	litre
	mL:	millilitre
	$\mu$ L:	microlitre
<b>Weight</b>	t:	tonne
	g:	gram
	mg:	milligram
	$\mu$ g:	microgram

**pH:** potential of hydrogen. It is the negative of the logarithm to base 10 of the activity of hydrogen ion (Bates 1973).

**pK<sub>a</sub>:** the negative log of the acid dissociation constant ( $K_a$ ). It is a quantitative measure of the strength of acid in solution (Miessler & Tarr 2004).





# Chapter 1 Introduction

## 1.1 The Human Oral Cavity

The oral cavity is the most complex and accessible microbial ecosystem in the human body (Lamont & Jenkinson 2010). It is the entry to both the respiratory and gastrointestinal tracts and as such is exposed to unique environmental parameters. It is moist, warm and has a steady stream of nutrients in the form of diet, saliva and gingival crevicular fluid (GCF). It is the only site within the human body where calcified, non-shedding surfaces are exposed to the environment and are therefore vulnerable to bacterial colonisation and unhindered by desquamation. It is ecologically distinct from all other surfaces of the body providing a myriad of environmental niches within which a multitude of bacteria thrive, many of which are exclusive to the oral cavity (Paster et al. 2001). However, it is important to consider that it is not the enamel of the tooth which is colonised, but the acquired salivary pellicle-coating upon the surface. Diversity in many environmental parameters makes it ideal for the growth of numerous and varied microorganisms. These ecological niches include; the various surfaces of the hard, non-shedding teeth in addition to many soft, desquamating surfaces of the oral mucosa (buccal and lingual mucosa, gingiva, hard and soft palate, tonsils and tongue). Each of these sites offers diverse environmental conditions and as such will reveal a differing distinct microbiota. Dental plaque sampled from different locations within the oral cavity vary in microbial composition due to the variety of surfaces available for colonisation (Aas et al. 2005). Upon these various surfaces, a wide variety of complex and integrated bacterial communities are able to form. The tooth has a number of distinct surfaces which offer sites of protection and stagnation. These stagnation sites include the gum line (gingival margin), the pits and fissures of the occlusal surface and the interdental space (Figure 1.1). These sites afford the bacterial communities protection from mechanical removal, such as chewing and scraping, and saliva flow. This affords the bacterial community with an opportunity to thrive and promote the growth of dental plaque at these sites. This protection

and stagnation explains the increased prevalence of dental caries at these locations (Moynihan & Petersen 2007; Caufield et al. 2015).



**Figure 1.1** Locations of stagnation offering dental plaque and food protection from mechanical removal and the effects of saliva. (Image credit: adapted from healthtap.com).

### **1.1.1 The Calcified Dental Tissue**

The surfaces of the dental hard tissue constitutes approximately 20% of the surface area of the oral cavity (Wilson 2005). The primary function of the teeth is to mechanically break down food through mastication to allow passage to the gastrointestinal tract for subsequent digestion. The teeth consist of enamel, dentin, cementum and dental pulp (Figure 1.2).

#### **1.1.1.1 Enamel**

Dental enamel, the outermost surface of the tooth structure, is the hardest tissue in the human body (Eastoe 1960). The enamel layer of teeth allows one to tolerate extremes in heat and cold, as well as the withstanding hard foodstuffs, e.g. nuts, confectionaries, etc. Native enamel consists of approximately 96% mineral, primarily calcium phosphate in the form of large hexagonal hydroxyapatite ( $\text{Ca}_{10}(\text{PO}_4)_6(\text{OH})_2$ ) crystals, both carbonated and defective (Cuy et al. 2002). The

remaining composition consists of approximately 3% water and organic matter (Berkovitz 2016). In spite of its hardness, enamel can lose its structural integrity through prolonged exposure to acids, through diet (dental erosion) or produced by the microbial inhabitants of the oral cavity as a result of metabolism of fermentable carbohydrates (dental caries). The enamel of the tooth also possesses a 'sacrificial' layer, more readily disposed to demineralisation than the underlying enamel (Hornby et al. 2009). Saliva also plays a role in this sacrificial layer, acting as an abundant and readily available source of calcium and phosphate dissolving preferentially before the enamel beneath (Abou Neel et al. 2016). The balance between demineralisation and remineralisation is a dynamic one. When exposed to acid, the solution (saliva) will be unsaturated with respect to calcium and phosphate and, as a result of Le Châtelier's Principle, calcium and phosphate ions will be removed from the hydroxyapatite structure. Fluoride acts as a promoter for the deposition of calcium and phosphate onto the tooth surface (Selwitz et al. 2007). The deposited mineral is in the form of fluorapatite and fluorinated hydroxyapatite (Selwitz et al. 2007). In contrast to hydroxyapatite, with a critical pH in the vicinity of 5.5, fluorapatite has a critical pH of 4.5 meaning that it is more resistant to demineralisation as a result of exposure to acids (Dawes 2003; Lussi et al. 2012).

#### **1.1.1.2 Dentine**

Underlying the enamel is dentine (also called dentin), a mineralised connective tissue. Dentine is less mineralised than enamel but more mineralised than bone and cementum (Goldberg et al. 2011). Dentine consists of 70% inorganic compounds predominantly hydroxyapatite, 20% organic and 10% water (Nanci 2014). Because it is less mineralised, it decays at a more rapid rate than enamel.

#### **1.1.1.3 Cementum**

Cementum is a mineralised tissue which covers the root of the tooth. The calcium and magnesium content of cementum is roughly 26% (of dry weight), while phosphorus constitutes roughly 12%, regardless of the age of the patient (Selvig and

Selvig, 1962). The fibres of the periodontal membrane are imbedded in cementum and hold the tooth within its socket.

#### **1.1.1.4 Dental Pulp**

Dental pulp is the only non-mineralised tissue of the tooth. It is the layer under the dentine and consists of blood vessels, connective and nervous tissue. Due to the nervous tissue, it is where pain originates when the caries lesion approaches or penetrates the level.

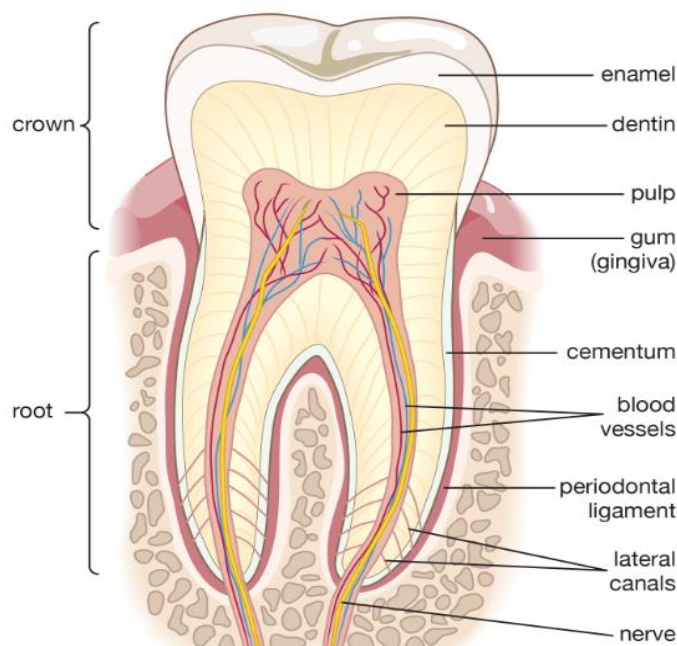


**Figure 1.2 Cross section of the adult human molar. (Encyclopaedia Britannica CC BY 2.0)**

#### **1.1.2 The Mucosal Surfaces of the Human Oral Cavity**

The mucosal surfaces of the oral cavity consist of stratified epithelium cells and the underlying fibrous connective tissue, the lamina propria (Nanci 2013). It includes the gingiva (gums), the buccal and lingual mucosa, the hard and soft palate, the tongue and tonsils. Interspersed throughout the oral cavity are the major (parotid, submandibular and sublingual) and numerous minor salivary glands (Edgar 1992; Whelton 2004). The gingiva consists of mucosal tissue which covers the maxillary

and mandibular bone and provides a seal to prevent bacterial colonisation of the gingival sulcus, underlying lamina propria and the alveolar bone. The complex surface of the tongue differs from other surfaces of the oral cavity. Numerous papillae, (filiform, fungiform, vallate and foliate papillae) offer protective sites for bacterial colonisation (Kolenbrander, Jakobovics and Bachrach, 2009). Mucosal surfaces, such as the buccal mucosa, the soft palate and the gingiva, are colonised by bacteria to a lower extent due to the shedding of the epithelium (Mager et al. 2003). The redox potential of the tongue varies greatly at different sites. Locations of low redox potential and the highly papillated surfaces of the tongue provide a niche for obligately anaerobic species (Greenman et al. 2005). The mucosal surfaces of the cheeks, lips and soft palate offer various sites for biofilm attachment and formation. Biofilm formation is limited by desquamation. Some bacterial species are able to persist as a result of buccal epithelial invasion.

## **1.2 Saliva**

Saliva is a clear, watery substance produced by the salivary glands in the oral cavity. It is a viscoelastic fluid with distinct surface activity (Preetha & Banerjee 2005). It consists of approximately 98% water with the remainder comprising electrolytes, mucus, antibacterial compounds and various enzymes. In health, approximately half a litre of saliva is secreted daily (Whelton 2004). It coats all surfaces of the oral cavity and provides a number of important functions; aiding in swallowing and digestion, lubrication and cleansing. The flow of saliva contributes to the removal of acidic by-products from dental plaque and helps to maintain a near-neutral, resting pH. Saliva also works in a number of ways to assist in the return to neutral pH values following pH challenge. The importance of saliva flow in maintaining oral health, particularly pertaining to dental caries, is evident. Those with diminished saliva flow, such as Sjögren's syndrome sufferers or those taking certain medications, are predisposed to an increased incidence of dental caries (Papas et al. 1993; Rudney 1995). Xerostomia is the subjective sensation of dry mouth, while hyposalivation is the objective finding of a reduced salivary flow rate (Dawes 2004). Due to the fact that saliva is so beneficial in terms of buffering, much interest has

been applied to agents that stimulate saliva flow (Edgar et al. 2004). Saliva forms the salivary acquired pellicle which facilitates the attachment of the oral microbiota to the tooth allowing dental plaque formation. The acquired pellicle assists in maintaining the tooth mineralisation equilibrium. The main determinant of pH in the oral cavity is saliva, except in the gingival crevice where gingival crevicular fluid (GCF) is of greater significance (Mandel 1987). This pH is maintained around neutral, predominantly by the action of saliva. The pH of saliva remains in the region of 6.75 to 7.25 (Marsh & Martin 2009), and varies significantly depending upon the flow rate. Resting, unstimulated saliva is pH 6.5 - 6.9, while stimulated saliva is slightly less acidic, at pH 7.0 - 7.5. Saliva also has a number of mechanisms to buffer or neutralise the acid by-products within plaque. The beneficial effect of saliva is apparent with discrepancies between the maxillary and mandibular surfaces. pH responses to sucrose are more apparent (Aamdal-Scheie et al. 1996) and the prevalence of dental caries are higher on maxillary teeth. This is likely due to gravity removing saliva from the maxillary surfaces and pooling upon the mandibular surfaces.

### **1.2.1 Buffering Capacity of Saliva**

Salivary buffering systems neutralise the acidic end-products of carbohydrate metabolism. The buffering capacity of saliva is a factor of primary importance in maintaining oral homeostasis (Kivelä et al. 1999). The flowing action of saliva is of importance in returning dental plaque to a resting pH. Saliva expels and dilutes metabolites. The bicarbonate and phosphate systems and those based on proteins are the most significant systems known to contribute to the total buffer capacity of saliva (Margolis et al. 1998; Newbrun 1992; Edgar & Higham 1995; Bardow et al. 2000; Bardow et al. 2008). The effectiveness of these systems is highly dependent on the flow of saliva (Tenovuo 1997). These systems have different pH ranges of maximal buffer capacity, the bicarbonate and phosphate systems having  $pK_a$ , i.e. the negative logarithm of the dissociation constant, of 6.1 to 6.3 and 6.8 to 7.0, respectively. Proteins contribute to the salivary buffer capacity at very low pH values only (Kivelä et al. 1999).

### 1.2.1.1 Bicarbonate/Salivary Carbonic Anhydrase IV System

The predominant system for maintaining a healthy resting pH is bicarbonate (Edgar 1992; Kimoto et al. 2006). When bicarbonate is removed from saliva, buffering capacity is considerably impaired (Lenander-Lumikari & Loimaranta 2000). When bacterial fermentation results in acid production within dental plaque the increase in hydrogen ion concentration drives the dissociation equation to the left (**Error! Reference source not found.**). Acids, designated as H<sup>+</sup> in the equation react with bicarbonate (HCO<sub>3</sub><sup>-</sup>) producing carbonic acid (H<sub>2</sub>CO<sub>3</sub>) which, under the action of salivary carbonic anhydrase IV, produces CO<sub>2</sub> and H<sub>2</sub>O. This effectively terminates available protons and, since the mouth is an open system, the carbon dioxide is lost to the atmosphere and the acid is removed from the system. Therefore, the acid is neutralised, not buffered. This reversible reaction is catalysed by salivary carbonic anhydrase IV (SCA IV).

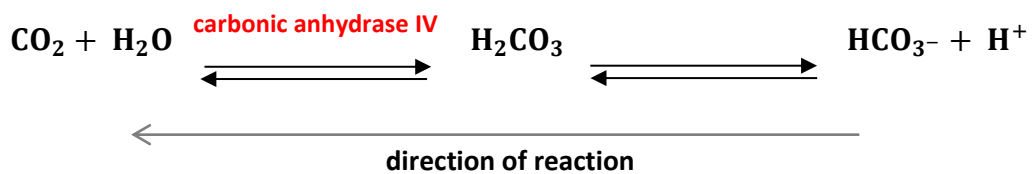


**Figure 1.3** Dissociation equation of carbonic acid by bicarbonate under the action of salivary carbonic anhydrase IV.

SCA IV is an isoenzyme secreted by serous acinar cells of the parotid and submandibular salivary glands (Kivelä et al. 1999). It is found in higher levels in caries-free children compared with caries-active children (Szabó 1974). It has been shown that SCA IV forms part of the tooth pellicle making it available to convert protons produced by overlying dental plaque to carbon dioxide and water, provided bicarbonate is accessible (Leinonen et al. 1999). Therefore, SCA IV is situated beneath dental plaque where it is likely to provide the greatest protection from demineralisation (Figure 1.4).

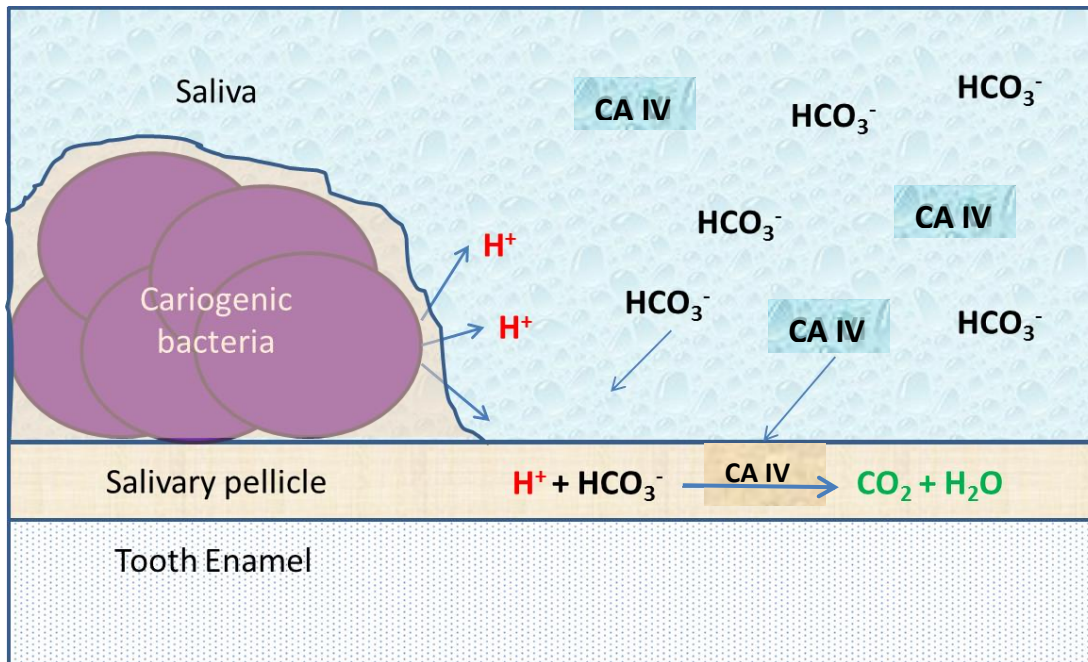


**Figure 1.4** The role of carbonic anhydrase IV in the neutralisation of acidic products of bacterial metabolism. (Adapted from Leinonen et al. 1999)

This will only happen if sufficient bicarbonate ions are present to interact with the hydrogen ions. The concentration of bicarbonate in saliva is proportional to the flow rate. As the rate of saliva production increases, more bicarbonate ions are produced as a by-product of cell metabolism. Consequently, stimulated saliva contains more bicarbonate than resting saliva. This is beneficial as during eating saliva flow is raised and plaque acid is produced in the greatest quantity. This ensures there is enough bicarbonate present to terminate surplus hydrogen ions. However, bicarbonate concentration is responsible for determining the actual pH of saliva in the first place. The pH of the oral cavity and the buffering capacity are able to be calculated using the Henderson-Hasselbalch Equation (Equation 1-1).

$$\text{pH} = \text{pK}_a + \log \frac{[\text{A}^-]}{[\text{HA}]} \quad \text{Equation 1-1}$$

In the mouth, the concentration of carbonic acid stays remarkably constant at approximately 1.3 mM per L (Bardow et al. 2008). It has been demonstrated that the  $pK_a$  of carbonic acid is 6.1 (Siggaard-Andersen 1974). Both are very important to how saliva protects teeth. Two things do change however; the pH of the oral cavity and the bicarbonate concentration in saliva. By applying the values to the Henderson-Hasselbalch equation, the effects of bicarbonate concentration can be visualised. Equation 1-2 shows the Henderson-Hasselbalch Equation with the base and acid substituted with bicarbonate and carbonic acid, respectively.

$$pH = pK_a + \log \frac{[HCO_3^-]}{[H_2CO_3]} \quad \text{Equation 1-2}$$

Following substitution of known values into the equation, pH can be calculated. Therefore, pH can be plotted with respect to the concentration of bicarbonate (Figure 1.5). This is shown below with bicarbonate and carbonic acid concentrations substituted for the anion and acid concentrations respectively (Equation 1-3).

$$y = 6.1 + \log \frac{[x]}{[1.3]} \quad \text{Equation 1-3}$$

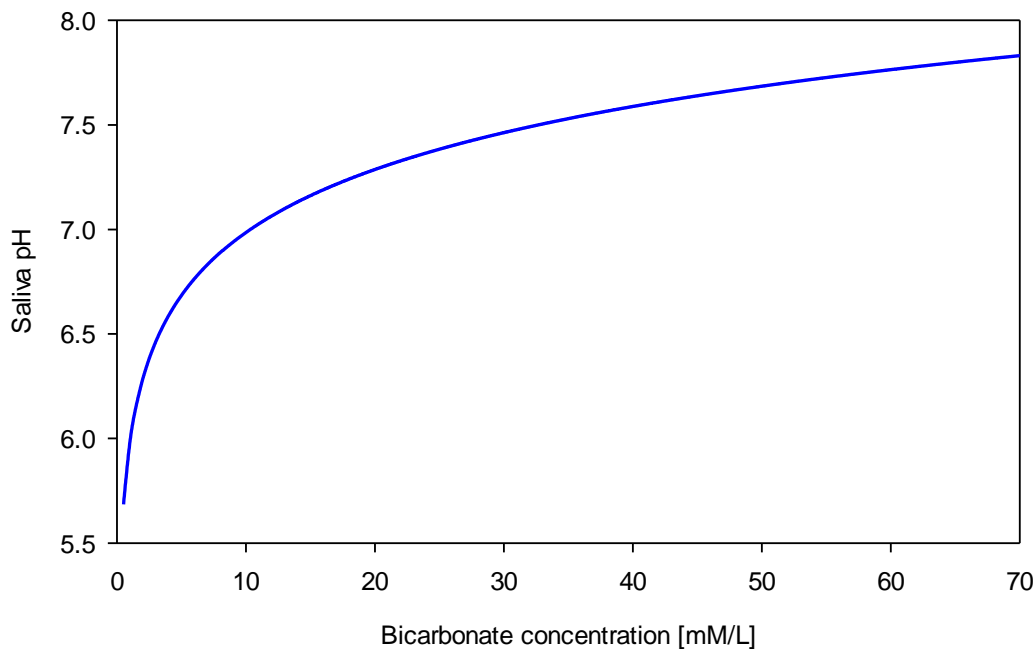


**Figure 1.5** The effect of bicarbonate concentration on saliva pH

### 1.2.1.2 Phosphate

The mode of action for the phosphate buffer system revolves around the ability of a secondary phosphate ion ( $\text{HPO}_4^{2-}$ ) to bind a hydrogen ion and form a primary phosphate ion ( $\text{H}_2\text{PO}_4^-$ ) removing hydrogen ions from the system (Figure 1.6). Phosphate concentration, like bicarbonate, is affected by flow rate. However, the concentration of phosphate decreases as flow rate increases (Bardow et al. 2000). This acid-base pair has a  $\text{pK}_a$  value in the range of 6.8 and 7.2, which has a maximum buffering capacity that is relatively close to the salivary pH range, i.e. pH 6 to 8. Therefore, the phosphate buffer has the potential to be an effective buffer in the mouth. However, its effectiveness is limited due to insufficient concentrations of phosphate in the oral cavity. Nonetheless, in the resting state where there is no food in the mouth, the concentration of inorganic phosphate is rather high while the concentration of carbonic acid/bicarbonate is low in comparison. Hence, the phosphate buffer is moderately efficient in unstimulated saliva (Bardow et al. 2008). It appears that the phosphate buffer system plays a significant role in the maintenance of microbial homeostasis.

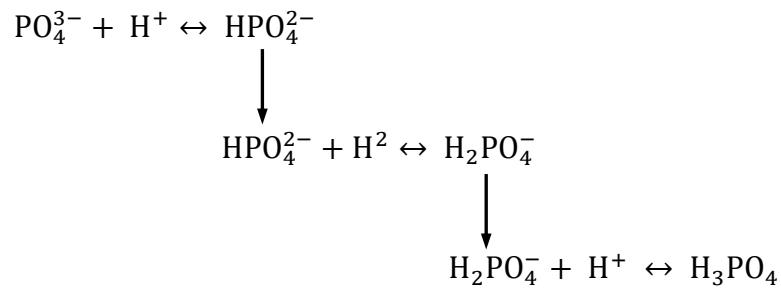


**Figure 1.6** Dissociation equilibrium of the phosphate buffer system.

### 1.2.1.3 Protein

Protein is not a very effective buffer as it does not have a preponderance of ionised groups; nearly all of the charged groups of amino acids are involved in the peptide bonds (Berg et al. 2002). Therefore, it does not possess sufficient acidic and basic groups to remove  $\text{OH}^-$  and  $\text{H}^+$ , respectively. Saliva also contains immunoglobulins, predominantly IgA, which limits bacterial attachment by blocking adhesins, reducing hydrophobicity and aggregating bacteria. They also neutralise enzymes and toxins and produce synergistic interactions with other antibacterial factors. Total protein is elevated in caries active children compared with caries free children (Preethi et al. 2010).

### 1.2.1.4 The Arginine Deiminase System

The arginine deiminase system (ADS) protects bacterial cells against the damaging effects of acidic environments encountered as a result of fermentation (Casiano-Colon & Marquis 1988). The ADS occurs in a number of lactic acid bacteria found in the oral cavity, including *Streptococcus sanguinis*, *Streptococcus gordonii*, *Streptococcus parasanguis* and *Streptococcus mitis* (Liu et al. 2012; Cunin et al. 1986) and appears to be involved in the return to neutral pH following acidic attack (Kanapka & Kleinberg 1983). The system also appears to have an important role in microbial ecology, protecting acid susceptible bacteria during episodes of decreased pH. L-citrulline produced as a product of the action of arginine deiminase is acted upon by ornithine transcarbamylase, producing carbamyl-P. Carbamyl-P is further

reduced to CO<sub>2</sub> and NH<sub>3</sub>, under the action of carbamate kinase, and removed from the system (Figure 1.7).

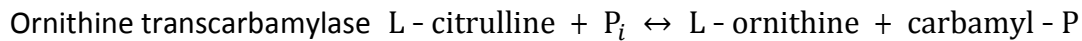
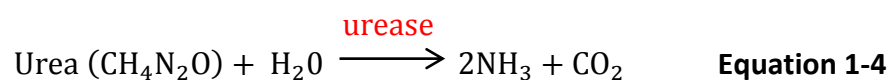


**Figure 1.7 Alkali generating pathways in the oral cavity.**

### 1.2.1.5 Urea

Urea is found in salivary secretions and gingival crevicular fluid excreted into the oral cavity and is readily converted into alkali products (ammonia and carbon dioxide) by the action of bacterial ureases (Liu et al. 2012).



## 1.3 Gingival Crevicular Fluid

Gingival crevicular fluid (GCF) is a serum transudate or inflammatory exudate which is secreted into the gingival sulcus (Lamster & Ahlo 2007). GCF is a mixture of plasma proteins (albumin), inflammatory products and constituents released from phagocytic cells. During the host inflammatory response the pH of the gingival crevice may increase (Marcotte & Lavoie 1998). This is likely to be due to bacterial metabolism and/or deamination of amino acids in GCF. The microbial population shifts to contain fewer aciduric, acidogenic species (Marsh 2003), and the proteolytic nature of the plaque will result in peptides, such as foul smelling diamines (putrescine and cadaverine), being released. In health, the gingival crevice has a pH of ~6.9 which can increase to above 8.0 during disease (McDermid et al. 1988). This can alter gene expression in subgingival bacteria (Marsh 2003), thereby

increasing the competitiveness of putative pathogens, such as *Porphyromonas gingivalis*, which has an optimal growth pH of approximately 7.5 (Takahashi & Schachtele 1990).

## 1.4 Dental Plaque

The microorganisms that inhabit the oral cavity are able to do so by adhering to the salivary pellicle coating the surfaces of the oral cavity, including the mucosal surfaces (Spratt & Pratten 2003). However, the formation of visible biofilm on the mucosal surfaces is limited by desquamation of the oral epithelium. Following attachment, the microorganisms form complex, highly organised communities (Kuramitsu et al. 2007). These intricate communities are a biofilm, characterised by microorganisms encapsulated in an extracellular polymeric substance (EPS, also referred to as the biofilm matrix), and attached to an underlying surface. The biofilms which form in the oral cavity are termed dental plaque, with oral microorganisms attaching to the salivary pellicle coating the oral cavity surfaces. According to McHugh, '*Dental plaque consists predominantly of micro-organisms plus extra-cellular polysaccharides, and usually an underlying pellicle of salivary origin*' (McHugh 1970). It was later recognised that '*the oral and gingival surfaces of dental plaque are often covered with leucocytes and desquamated epithelial cells and, at times, food debris*'. (McHugh 1999). As a result, the term extracellular polysaccharides became obsolete. Through the use of confocal laser scanning microscopy, it has been shown that dental plaque has an open architecture, similar to other biofilms, with projections, channels and voids (Marsh 2004). Dental plaque preferentially develops at stagnant sites, such as along the gingival margin, and on rough surfaces of the tooth, such as interdental spaces and in pits and fissure (Figure 1.1). These sites afford dental plaque and food protection from mechanical removal forces and the action of saliva. The bacterial species which thrive at these sites are mainly dominated by gram-positive, facultative anaerobes such as streptococci and actinomycetes. The formation of dental plaque is a natural process which assists in the protection of colonisation by exogenous species (Marsh 1994). When growing as biofilm, the properties of the bacteria differ greatly from

planktonic bacteria. Following attachment, growth rate slows and gene expression altered (Socransky & Haffajee 1992). Bacterial attachment is mediated by receptors within the acquired salivary pellicle, a thin film which coats the surfaces of the oral cavity. Moreover, the tolerance of biofilm bacteria to antimicrobials may be increased up to 1000 fold (Rasmussen & Givskov 2006). This may occur through neutralisation of inhibitors, novel gene expression and protection of sensitive organisms as a result of  $\beta$ -lactamase production by neighbouring cells (Marsh 2004; Marsh & Martin 2009). Within the proximity of dental plaque, a number of genetic and molecular processes can occur (Roberts & Mullany 2010). Dental plaque is the major etiological agent of two dominant dental pathologies, dental caries and periodontal disease. Development and maturation of dental plaque are driven by microbial competition (particularly pertinent to pH microgradients) and interspecies communication (complex feeding and antagonistic interactions) (Kolenbrander et al. 2010; Kolenbrander 2011).

#### **1.4.1 Formation of Dental Plaque**

The formation of dental plaque occurs in a step-wise manner, complicated by a multitude of synergistic and antagonistic events. The process begins with the formation of a salivary pellicle, which provides bacteria with ligands, such as mucins and proteins, to promote attachment. Due to specific recognition only some bacteria are able to attach to the salivary pellicle and colonise the tooth surface. Following attachment, these so-called 'pioneer species' provide sites of attachment to subsequent bacterial species. These attachment events are often observed between species that benefit from feeding interactions, such as *Fusobacterium* spp. providing ammonium ions to, for example, *Actinomyces* spp. (Marsh & Martin 2009). *Veillonella* spp. also co-aggregate with streptococci and *Actinomyces* spp. to obtain a source of lactate (Marsh 1995).

#### **1.4.1.1 The Acquired Salivary Pellicle**

Following mechanical plaque removal, an acellular film termed the 'acquired salivary pellicle' coats all surfaces of the oral cavity. The acquisition of the salivary pellicle occurs within a matter of seconds (Hannig 1999). The pellicle is composed of different host-derived molecules, including mucins, proteins and agglutinins, which act as a source of receptors that are recognised by various oral bacteria. Also, there are other host proteins, for example, lysozyme and histatins, which are present in the pellicle and are believed to protect from bacterial colonisation (Hannig et al. 2005; Siqueira et al. 2010). The acquired pellicle consists primarily of salivary glycoproteins, phosphoproteins and lipids and is critical to a number of processes within the oral environment, both beneficial and detrimental. An example of the protection it offers the tooth is that against demineralisation from acidic foodstuffs (von der Fehr & Steinnes 1966; Jenkins 1966; Meckel 1968; Holly & Gray 1968). Conversely, the glycoproteins available in the acquired pellicle act as ligands providing sites of adhesion to early colonisers and host molecules to the tooth surface (Al-Hashimi & Levine 1989).

#### **1.4.1.2 Bacterial Attachment and Co-aggregation**

Oral bacteria are passively transported to the tooth surface where reversible, physicochemical interactions between the bacterial cell surfaces and the pellicle-coated teeth occur. These weak, long-range interactions include electrostatic and Van der Waal's forces (Busscher & Van Der Mei 1997). Once in proximity, strong, irreversible intermolecular attachment occurs between specific cell adhesins and receptor proteins within the salivary pellicle including proline-rich proteins, statherin, sialyated mucin and  $\alpha$ -amylase (Jenkinson & Lamont 1997, Lamont & Jenkinson 2000). These intermolecular interactions are represented in Figure 1.8. Fundamentally, each bacterial species which inhabit the oral cavity possess multiple adhesins on their surface facilitating coaggregation (Kolenbrander & London 1992). These early colonisers are predominantly streptococci, (*Streptococcus oralis*, *S. mitis*, *S. gordonii*) consisting of between 47 and 85% of recovered cultivatable cells during the first four hours post professional cleaning (Nyvad & Kilian 1987). Other

early colonisers able to recognise various receptors and bind to the pellicle-covered surface include; *Actinomyces* spp., *Capnocytophaga* spp., *Eikenella* spp., *Haemophilus* spp., *Prevotella* spp., *Propionibacterium* spp. and *Veillonella* spp. (Kolenbrander et al. 2010). This provides a new surface for colonisation. Following the adhesion of the early colonisers, other bacteria utilise specific adhesion-receptor interactions, often involving lectins, to adhere to the already established microorganisms. This co-adhesion may facilitate functional organisation. Co-aggregation between pairs of early colonisers is common but relatively rare between late colonisers (Faust et al. 2012). *Fusobacterium nucleatum* however can co-aggregate to many members of both the early and late colonisers, and as such, acts as a microbial bridge between the two populations (Zilm & Rogers 2007; Kolenbrander & London 1993). *F. nucleatum* may also adhere to many host-derived molecules found in the pellicle as observed in Figure 1.8 (Kolenbrander et al. 2002). Within twelve hours, the population diversifies and the biofilm is colonised by the late colonisers, which include more gram-negative organisms such as *Haemophilus* spp., *Capnocytophaga* spp., *Actinobacillus* spp., *Prevotella* spp., *Eubacterium* spp., *Porphyromonas* spp. and *Treponema* spp. (Takeshita et al. 2015). The bacterial populations that constitute the dental plaque are highly organised and engage in a range of synergistic and antagonistic biochemical interactions (Marsh & Bradshaw 1999). There is fierce competition for nutrients within dental plaque. Environmental gradients are formed in pH, oxygen concentration, redox potential and ion concentrations. Obligately anaerobic microorganisms may enhance their chances of survival due to their proximity to aerobic species (Bradshaw et al. 1998).

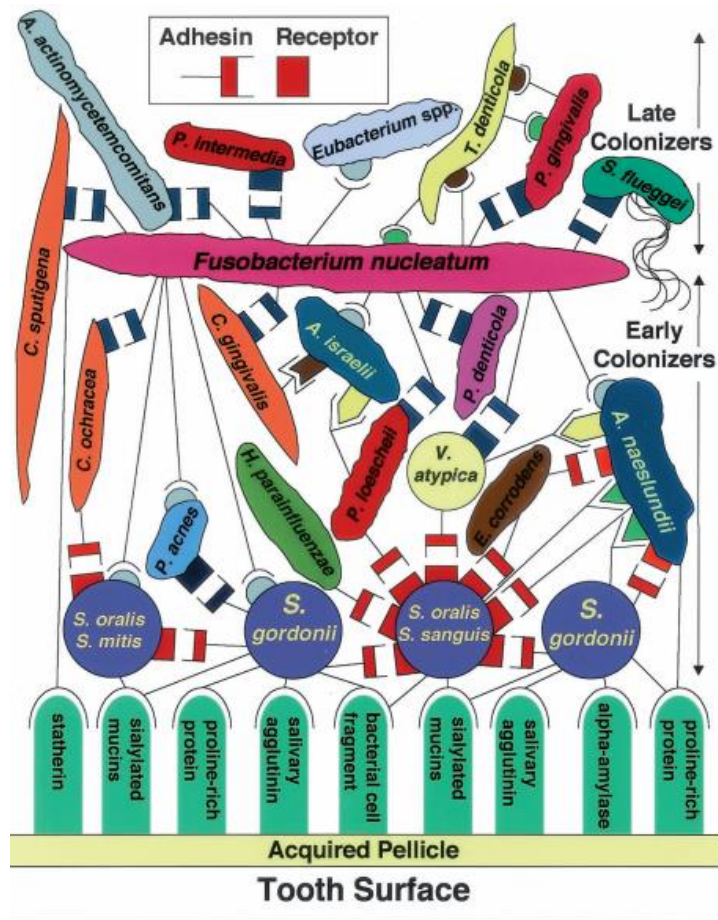


**Figure 1.8** Spatiotemporal model of colonisation of oral bacteria, showing recognition of salivary receptors within the salivary pellicle by early colonisers and co-aggregation between early colonisers, fusobacteria and late colonisers, (Kolenbrander et al. 2002).

Pioneer species bind with high affinity to components of the salivary pellicle. Additionally, bacteria expressing glucan binding proteins may bind to glucan polysaccharides which become incorporated into the salivary pellicle (Gibbons et al. 1983; Marsh et al. 2011). Secondary colonisers, unable to compete with the primary colonisers, are able to bind directly to pioneer species through lectin-like (protein-carbohydrate) interactions. This leads to the development of spatially-defined groups of microorganisms. Secondary colonisers are also able to bind to glucan polysaccharides and salivary components incorporated in the extracellular polymeric substance (EPS) matrix.

### **1.4.1.3 Multiplication and Maturation**

The organisms which initially colonise the tooth surface are predominantly aerobic and aerotolerant species (Foster & Kolenbrander 2004). As the dental plaque matures, anaerobic species predominate (Kolenbrander et al. 2006). Mature dental plaque is also characterised by considerable species diversity. Cell division occurs resulting in confluent growth, increase in biomass and later three-dimensional growth of projections, voids and water channels consistent with biofilm formation (De Beer et al. 1996). These water channels facilitate the removal of waste and allow the transport of nutrients throughout the biofilm. The complex structure, constant metabolic activity and solute transport and diffusion give rise to physicochemical spatial microgradients; characterised by varied and distinct environments within short distances. An essential element of the biofilm lifestyle is the formation of an extracellular matrix that encapsulates the colony (Branda et al. 2005). This matrix affords the biofilm protection from desiccation and phagocytosis. The matrix consists of bacterial polysaccharides, proteins, lipids, nucleic acids and lipooligosaccharides (Koo et al. 2013). These processes lead to the maturation of a diverse dental plaque community. Development and maturation of dental plaque is driven by microbial competition and interspecies communication. Species within dental plaque co-exist and cooperate in a number of metabolic and physical interactions. Within mature dental plaque feeding synergies exist in which by-products of metabolism by one species are used by a second as a nutrient source (Figure 1.9). Additionally, some species provide glycosidases for the metabolism of available carbohydrates allowing complete utilisation of nutrients. This results in a degree of stability within the community, known as microbial homeostasis.

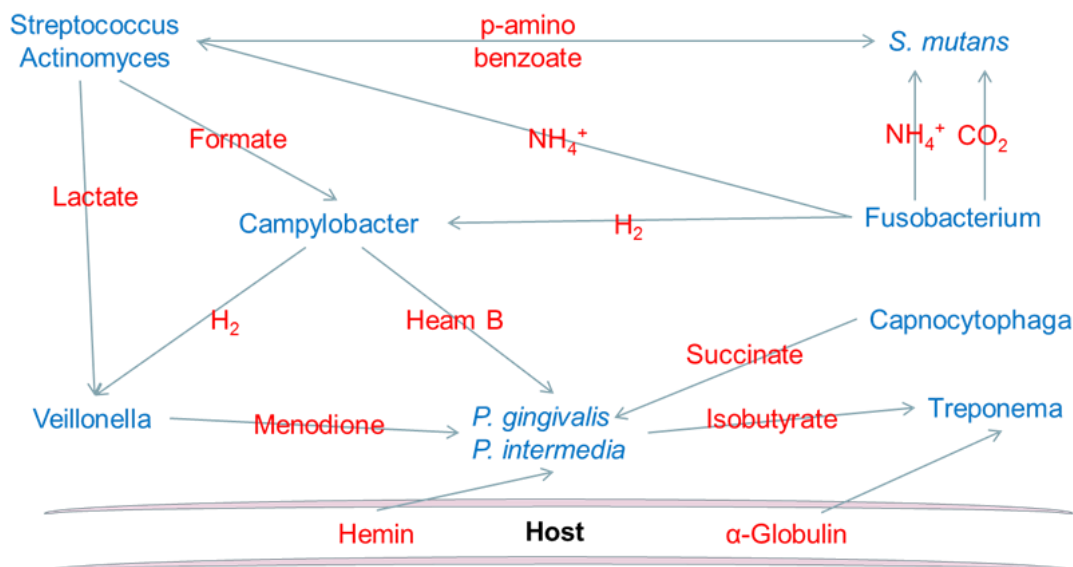


**Figure 1.9** A diagram showing various synergistic feeding interactions which may occur in dental plaque (Image adapted from Marsh & Martin 2009).

## 1.5 Parameters Which Influence the Oral Environment and Microbial Ecology

As the gateway to the respiratory and gastrointestinal tracts, the oral cavity is exposed to constant fluctuation in numerous environmental parameters. These fluctuations result from respiration, diet, endogenous sources such as saliva and gingival crevicular fluid and as a result of dental plaque formation and metabolism. Environmental factors pertinent to the oral cavity include pH, oxygen availability and oxidation-reduction potential (redox potential), temperature and nutrient sources.

### 1.5.1 Hydrogen-Ion Concentration (pH)

The main challenge to the dental enamel is acidification of the oral cavity, from the metabolism of fermentable carbohydrates by the bacterial microbiota (Kivelä et al. 1999). The metabolism of the microbiota attached to the dental surfaces produces considerable amounts of acid, mainly in the form of lactic, acetic, formic and

propionic acids (Clarke 1924; Muntz 1943; Stephan 1944; Geddes 1975; Geddes 1981) which decreases the pH. Acidification initiates dissolution of the mineral component of the dental hard tissue as well as applying positive selective pressure to cariogenic bacterial species.

In health, microbial homeostasis maintains the pH of the oral cavity and it remains relatively stable, between pH 6.75-7.25 (Marsh & Martin 2009). Many of the microorganisms that inhabit the oral cavity require an approximately neutral pH to grow and are sensitive to extremes in pH (Figure 1.18). The neutrality of the oral cavity is dramatically disrupted following the consumption of easily fermented carbohydrate, particularly sucrose. These changes are unable to be prevented (Kidd & Fejerskov 2004; Fejerskov 2004; Kidd 2011). Metabolism by microorganisms can have a considerable effect on pH in the oral cavity. This *“environmental acidification is the main determinant of the phenotypic and genotypic changes that occur in the microflora during caries”* (Takahashi & Nyvad 2011). It has long been understood that the main cause of fluctuations in pH is the ingestion of foods high in fermentable carbohydrates which causes the pH to become more acidic (Grossman & Brickman 1937). The variations of pH following the ingestion of sugar is best visualised in the Stephan curve (Figure 1.10) (Stephan 1944). The Stephan curve is principally a plot of dental plaque pH with respect to time following a challenge, possibly a fermentable carbohydrate. Immediately following the ingestion of fermentable carbohydrate, for example sucrose, the pH rapidly declines from the near-neutral, resting pH, to a more acidic pH (Stephan 1944). Furthermore, the magnitude of the decrease has been demonstrated to be a proportionate response to caries activity (Figure 1.11) (Stephan 1940; Stephan & Miller 1943). This decline is primarily due to the presence of acidogenic (acid-producing) oral bacteria producing organic acids as a result of fermentation. Decreases in pH favour the growth of aciduric bacteria, such as *S. mutans* and *L. casei*. These organisms are frequently highly acidogenic. Another effect of low pH which allows these organisms to thrive is the suppression of non-aciduric species and a resultant lack of competition. In the presence of high proportions of cariogenic (aciduric and acidogenic) bacteria combined with the intake of easily fermented carbohydrates, pH can rapidly fall to

below 5.0 (Cawson & Odel 2008), and as low as pH 4.5 (Brailsford et al. 2001). Then, over a period of between 15 and 40 min, the pH slowly returns to a resting pH approaching neutral (Stephan 1940; Stephan & Miller 1943; Raner et al. 2014).

The level of the decrease in pH is dependent on the carbohydrate source (Touger-Decker & Van Loveren 2003). Those microorganisms associated with health are able to tolerate short periods in acidic conditions, but are suppressed or killed by prolonged exposure. The fall in pH favours the growth of aciduric, cariogenic bacteria, such as *S. mutans* (Loesche 1986) and *Lactobacillus* spp. (Bowden 1990). At near neutral pH, potentially pathogenic microorganisms may exist at low levels, however they have little competitive advantage. When acid-sensitive microorganisms are killed, cariogenic species are able to thrive in the lack of competition (Marsh 2003). Fluctuations in pH result in a microbial shift to a more acidogenic, aciduric population. This means that, with subsequent exposure to fermentable carbohydrates the more acidogenic, aciduric population will produce more acid, resulting in lower pH levels and prolonging the time required to return to resting pH. The level below the critical pH, i.e. the level below which demineralisation of the dental hard tissue occurs, and time spent at these levels are increased. This further shifts the population towards a cariogenic population. Complex carbohydrates, such as starches, may require breakdown to allow further metabolism. Although starch is recognised to have a lower carcinogenicity than sugars such as sucrose, frequent consumption of starch has been shown to produce a large number of carious lesions (Lingström et al. 2015). This is because starch can be broken down to maltose by the enzyme in saliva called amylase. Maltose can then be further metabolised to acids, which in turn lead to demineralisation (Kashket et al. 1996).

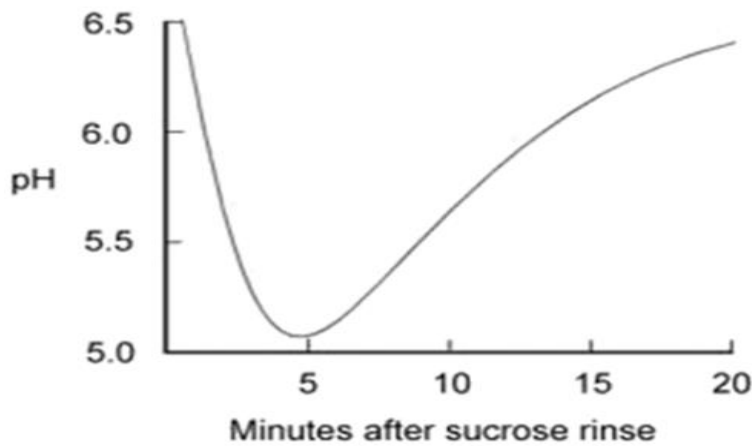


**Figure 1.10** The Stephan curve, an archetypal profile of pH with respect to time following exposure of dental plaque to fermentable carbohydrates (Stephan 1940).

### 1.5.1.1 Resting pH

In health, the resting pH of an individual is approximately neutral. The resting pH of an individual remains relatively stable and may do so over long periods of time (Sissons et al. 1998). This resting pH is significantly affected by caries activity and may approach or exceed the pH at which demineralisation occurs (critical pH) in an individual with marked or extreme caries activity (Figure 1.11).

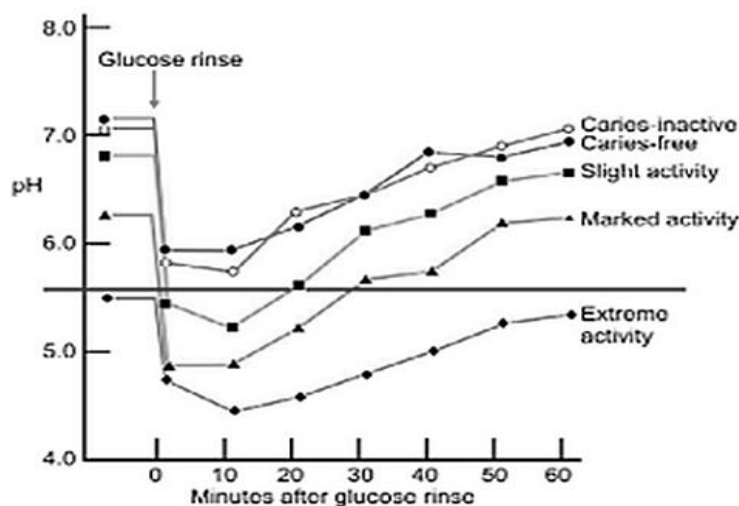


**Figure 1.11** Stephan curves demonstrating the differences in pH decreases in patients with different caries activity (Stephan & Miller 1943).

### **1.5.1.2      *Decrease in pH following ingestion of fermentable carbohydrates***

The role of readily-fermentable sugars, particularly sucrose, in the caries process is evident (Marsh 2003). The prevalence of dental caries in the industrialised world, where sucrose is often added to food and drink as a sweetener, exceeds that of the non-industrialised world (Moynihan & Petersen 2007). Also, the rate of dental caries increased significantly with an increase in the availability of readily fermentable carbohydrates (Stephan 1944). The major etiological factors for caries are considered to be high consumption of refined sugars (sucrose) and presence of an acidogenic flora in the dental plaque (Marsh & Nyvad 2003). Following the ingestion of readily fermentable carbohydrates, organic acids decrease the pH rapidly, reaching the lowest level approximately five to ten minutes after intake (Stephan 1940). This fall is primarily due to the production of lactic acid, while acetic and propionic acids being simultaneously lost from the plaque (Higham & Edgar 1989 b). The rate of pH decrease is, in part, due to the microbial composition of dental plaque. In early dental plaque consisting predominantly of non-acidogenic bacteria, the decrease is infrequent, mild and comparatively short in duration. As dental plaque matures and species diversity increases, fermentable carbohydrate ingestion results in a longer and larger decrease in pH (Marsh 2006). Dental plaque comprising greater proportions of aciduric, acidogenic bacteria leads to a more rapid drop in pH (Stephan 1944). The rate at which the carbohydrate is metabolised as well as the thickness and density of plaque plays a significant role in the rate of pH decrease. Less dense plaque can be penetrated more readily by saliva causing slower decreases due to the buffering capacity (Marsh 1994). In terms of pH change in plaque, the amount of a low pK acid, such as lactate, relative to higher pK acids, such as acetate, is of major importance (Higham & Edgar 1989 b). The high pK acids provide a buffering system because they can absorb the hydrogen ions generated by dissociation of the low pK acids such as lactate, formate and pyruvate (Vratsanos 1981; Vratsanos & Mandel 1982; Margolis & Moreno 1994). Many of the dental plaque bacteria prefer a pH in the proximity of neutral for optimum growth. As the pH moves from this neutral pH, metabolic activity and growth is suppressed. This allows aciduric species to gain a foothold and thrive in the lack of competition. The

result of frequent ingestion of fermentable carbohydrates also has an ecological effect on the microbial composition and its ability to maintain homeostasis. As time to return to a neutral pH is limited, non-aciduric species may become non-viable.

**1.5.1.3 Return to resting pH**

The gradual recovery of the plaque pH is influenced by various factors. These include the buffering capacity of saliva, whether fermentable carbohydrate remains in the mouth, the pH value within the plaque which may be unfavourable to bacterial enzyme systems, and the diffusion of acids from plaque into saliva or teeth. It is also influenced by base production in plaque. Ammonia, from the deamination of amino acids and breakdown of urea in saliva, are examples of reactions that contribute to the pH rise. These bases are important to neutralise acid when carbohydrate intake is moderate (Shu et al. 2007). The rise in pH may also be assisted by the removal of acids by bacteria that use lactate as a substrate metabolising it to less acidic products such as *Veillonella* spp. (Marsh & Martin 2009).

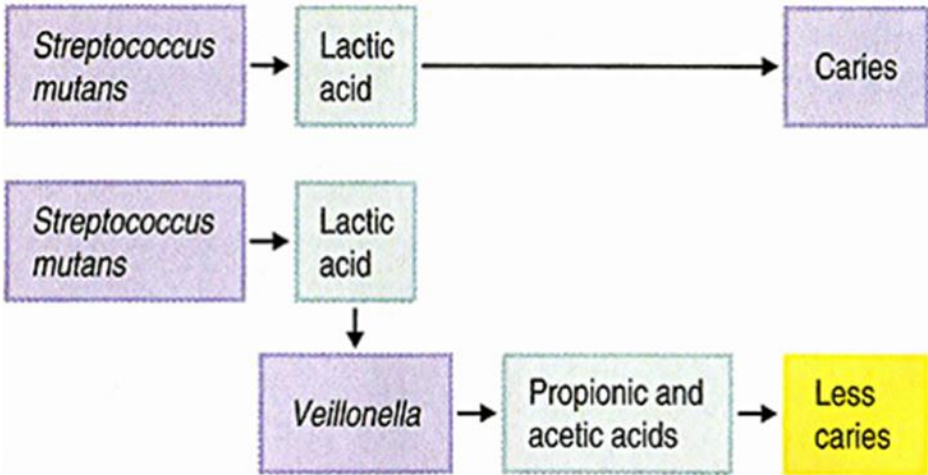


**Figure 1.12** Diagram of a basic food chain showing the effect of the presence and absence of *Veillonella* spp. (Marsh and Martin 2009).

#### **1.5.1.4     *The Concept of Critical pH***

The critical pH is the level at which saliva and the plaque bulk fluid is no longer saturated with calcium and phosphate. Below the critical pH, the inorganic hydroxyapatite in the enamel of the tooth begins to dissolve and demineralisation occurs. This level differs between individuals, however it is generally accepted to be pH 5.5 (Marsh & Martin 2009). However, due to the deposition of fluorapatite and fluorinated hydroxyapatite (Selwitz et al. 2007), which possesses greater resistance to demineralisation from acid attack, the critical pH of decreases as a results of fluoride (Dawes 2003; Lussi et al. 2012). The deposition of fluorapatite is dependent upon the presence of fluoride ions.

#### **1.5.1.5     *Frequency of carbohydrate intake***

Increased frequency of sugar intake results in an increased risk of the developing dental caries due to an extension in the duration at which the pH is below the critical pH. Therefore, demineralisation outweighs remineralisation (Marsh & Martin 2009). This is demonstrated in the diagrams below (Figure 1.13). In the example below it can be clearly seen that in A, increasing the frequency of eating and drinking increases the episodes when the pH of plaque falls below 5.5. Alternatively, in B, restricting between-meal snacks and drinking non-sugared drinks reduces the time that plaque pH falls below 5.5.

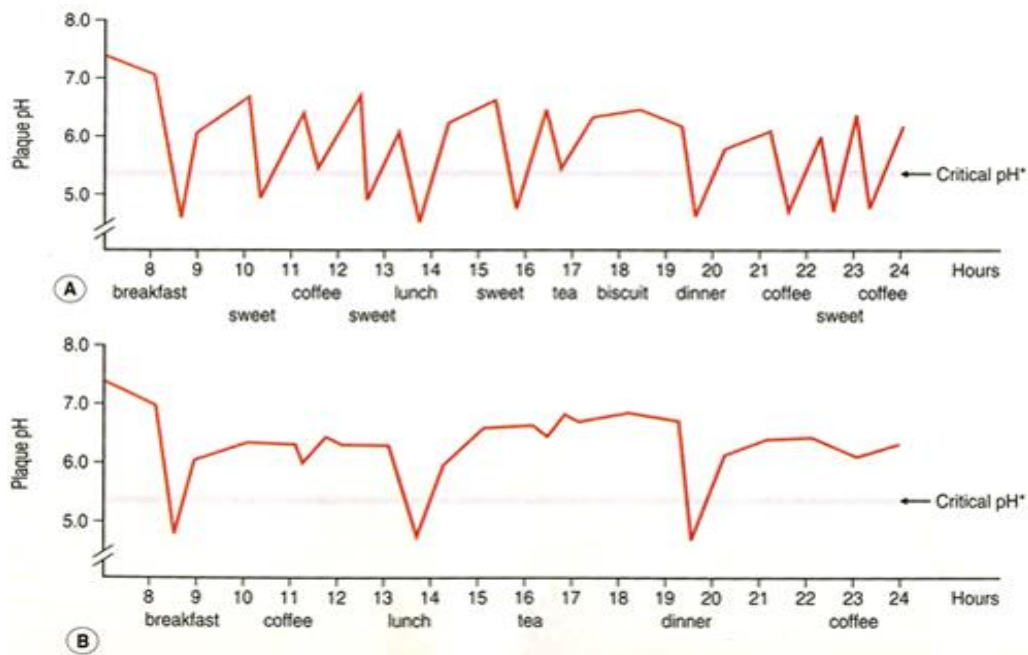


**Figure 1.13** Plots of dental plaque pH following (A) numerous and frequent carbohydrate exposures through diet and (B) limiting carbohydrate intake (Marsh & Martin 2009).

### 1.5.2 Oxygen Concentration and Oxidation-Reduction (Redox) Potential (Eh)

Availability of oxygen varies greatly from site to site in the oral cavity. This allows the growth of a wide range of species with different oxygen requirements (Marcotte & Lavoie 1998). In spite of the availability of oxygen, the majority of microorganisms that inhabit the oral cavity do not require oxygen for growth and few, if any, obligate aerobes are present (Kampoo 2011). Facultative and obligate anaerobes, in addition to microaerophilic and capnophilic microorganisms, thrive. More important for the colonisation of microorganisms are the production and metabolism of highly reactive oxygen species by both the bacteria and the host. These include superoxide radical ( $O_2^-$ ),  $H_2O_2$  and hydroxyl radical ( $OH^\cdot$ ) (Moons et al. 2009; Haussler & Fuqua 2013). Oxygen is the major electron acceptor encountered in the oral cavity (Marcotte & Lavoie 1998). As the plaque biomass increases, oxygen concentration decreases due to the consumption of oxygen by facultative species and the decrease of diffusion through the biomass (Takahashi 2005). Oral

streptococci possess the ability to metabolise oxygen and defend against the toxic products of oxygen metabolism through the production of protective enzymes, superoxide dismutase and NADH peroxidase (Marquis 1995). Although oxygen concentration is a major limiting factor for the growth of obligate anaerobes, redox potential (Eh) also regulates the growth of anaerobes. *“Bacterial metabolism requires hydrogen acceptors and results in the formation of “free” electrons which cause a fall in the Eh of the bacterial milieu. Therefore, the level of Eh will change as bacteria in dental plaque proliferate and such changes may affect the type of organisms present at various stages of plaque maturation.”* (Kenney & Ash 1969). Some anaerobes are able to grow in the presence of oxygen provided the Eh is sufficiently reduced. Also, some anaerobes are not able to thrive in environments where Eh is high even if oxygen is absent. As biofilm mass increases, redox potential decreases due to oxygen consuming species producing carbon dioxide and late colonisers producing hydrogen gas and other reducing compounds. In health, the Eh of the subgingival crevice is oxidised at around +70 mV, inhibiting the growth of anaerobic species. When inflammation occurs, the Eh may decrease to -50 mV in gingivitis and as low as -300 mV in advanced periodontitis. Microgradients in redox potential and oxygen concentration form, particularly in thick plaque. The Eh of supragingival plaque decreases significantly in the first few days of plaque development (Kenney & Ash 1969). As a result, the number of obligate anaerobes increases over time. Further to the production of organic acids by bacteria which lowers the pH, bacteria also excrete reduced metabolic end products which lower the redox potential and produce hydrogen peroxide.

### **1.5.3 Temperature**

In health, the resting temperature of the oral cavity remains relatively stable at between 35 and 36°C (33-37), although this varies from site-to-site (Moore et al. 1999). These temperatures provide ideal growth conditions for many of the mesophilic microorganisms that inhabit the oral cavity. Significant fluctuations occur with the consumption of hot or cold food and drink. In disease states, such as gingivitis and periodontitis, inflammation may cause the temperature of the

periodontal pocket to increase to 39°C (Haffajee et al. 1992). It has been shown that an increase in temperature to 39°C leads to an up-regulation of superoxide dismutase synthesis in *P. gingivalis*, which plays a major role in counteracting the toxicity of oxygen by catalysing the dismutation of  $O_2^-$  into  $O_2$  and  $H_2O_2$  (Amano et al. 1994). Therefore, temperature provides an additional selective pressure (Maiden et al. 1998; Haffajee et al. 1992).

#### **1.5.4 Nutrient Sources**

The oral cavity is a nutritionally-rich environment (Gibbons & van Houte 1975; Lappin-Scott & Costerton 1989; van 't Hof et al. 2014). The nutrient sources available to microorganisms in the oral cavity can be endogenous from the host in the form of saliva and gingival crevicular fluid and exogenous from the host's diet (Takahashi 2005). The main sources of nutrition for many of the bacterial inhabitants of the oral cavity is obtained from saliva (Wilson 2005). Other endogenous sources of nutrition include gingival crevicular fluid (GCF), substances secreted or excreted by the oral mucosa, and desquamated epithelial cells (Takahashi 2005). As the gateway to the digestive tract, the oral microbiota is also exposed to numerous nutrient sources as part of the hosts' diet. Growth within a biofilm facilitates the concentration of nutrients and other elements present within endogenous nutrient sources and helps to retain metabolites that might otherwise be lost from cells (Marquis 1995).

##### **1.5.4.1 Endogenous sources**

Saliva and GCF are the principal endogenous nutrient sources available to microorganisms (Beighton et al. 1986; Wilson 2005) but their breakdown requires coordinated effort (Bradshaw et al. 1994; Marsh & Bowden 2000). Saliva and GCF contain amino acids, proteins and glycoproteins (Wilson 2005). GCF also contains albumin, vitamins and glucose (Loesche 1988). Some black-pigmented obligate anaerobes such as *Porphyromonas gingivalis* and *Prevotella intermedia* require haemin, protoporphyrin IX containing a ferric iron ion with a chloride ligand, for

growth. This is derived from the host following the degradation of haemoglobin from erythrocytes. Nutrients can also be derived from metabolic products of other bacteria (Marsh & Bradshaw 1997). An example of these synergistic feeding interactions is the production of short chain fatty organic acids by *Streptococcus* spp. a result of sugar metabolism, which are utilised by *Veillonella* spp. (Mikx & Van der Hoeven 1975). Therefore, *Veillonella* spp. is unable to colonise the pellicle-coated tooth in the absence of *Streptococcus* spp. Another example is the stimulation of *T. denticola* growth by the isobutyric acid produced by *P. gingivalis* metabolism (Figure 1.9). As dietary intake varies greatly, members of the oral microbiota are not able to rely on a stable supply of exogenous nutrients. When available, the supragingival plaque is able to obtain nutrients from dietary sources. When these sources are not available, saliva acts as a nutrient source. Saliva is able to maintain the growth of major oral species in the absence of dietary nutrients (De Jong et al. 1986; De Jong & Van der Hoeven 1987).

#### **1.5.4.2 Exogeneous sources**

The mouth is the gateway to the digestive system and, consequently, the oral cavity is afforded a regular flow of exogenous nutrients in the form of diet. The host's diet provides a wide array of nutrients, none of which affect the ecology to the extent of fermentable carbohydrates. Of the carbohydrates, sucrose is considered the most cariogenic (Aires et al. 2006). Sucrose is a disaccharide, consisting of the monosaccharides glucose and fructose linked by an ether bond between the C1 of the glycosyl subunit and the C2 of the fructosyl subunit (Figure 1.14). This structure is metabolised to produce monosaccharides of glucose and fructans as well as fructose and glucans. These fructans and glucans are key components of the extracellular polymeric substance (EPS), and appear to promote the adhesion of bacterial species to plaque and may enhance the virulence of *S. mutans* through increasing the porosity of plaque resulting in greater acidification at the plaque-enamel junction (Zero 2004). Some bacteria produce glycosyltransferases and fructosyltransferases which break down sucrose to produce glucans and fructans. Glucans are associated with bacterial attachment. Fructans are associated with

energy storage and may prolong pH decreases. The presence of extracellular polysaccharides increases the porosity of dental plaque (Dibdin & Shellis 1988). It also maintains low pH values caused by bacterial metabolism (Zero et al. 1986). *Streptococcus mutans* is the only bacterium in which adhesion is stimulated in the presence of sucrose (Schachtele et al. 1976).

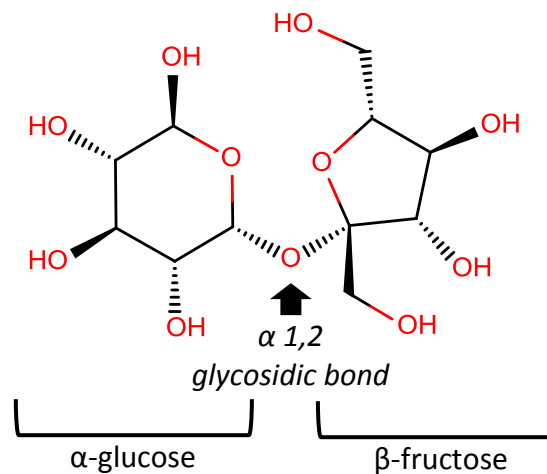


**Figure 1.14** Chemical structure of sucrose, showing a glucose molecule and a fructose molecule joined by a glycosidic linkage.

## 1.6 The Formation of Spatial Microgradients

An important feature of biofilms is the formation of physical, chemical, spatial and temporal microgradients (Hunter & Beveridge 2005). The differing bacterial composition and metabolism compounded by the limited diffusion through the extracellular matrix, leads to the formation of chemically diverse microgradients within close proximity. Within dental plaque, gradients develop in parameters of ecological significance, such as pH, redox potential and oxygen tension (Marsh 2004). These variations are constantly influencing the composition, growth rate and metabolic activity of microbial population. They provide differing conditions suitable for the growth and survival of microorganisms with a diverse spectrum of requirements. Under such conditions, no single bacterial species has a particular advantage and numerous species can co-exist. Many of the resident oral microbiota have fastidious nutritional requirements. Due to the close proximity in which the

microorganisms grow, transfer of genetic information is common. It also allows the growth of species that would not usually be able to grow. An example of this is the demonstration of obligately anaerobic microorganisms growing in aerobic environments when in close proximity to oxygen consuming species.

## 1.7 Dental Caries

Dental caries is a multi-factorial disease characterised by the localised dissolution of the dental hard tissues (enamel, dentin, cementum) as a result of organic acids of bacterial origin (Kidd & Fejerskov 2016). Dental caries however, differs from dental erosion where the consumption of foods or drinks with high acid content cause the pH to drop and leads to demineralisation, although this may have a minor effect in shifting the bacterial population. The caries process is a ubiquitous and natural phenomenon (Manji et al. 1991) however, dental caries should be considered a preventable infectious disease (Rugg-Gunn 2013; Balakrishnan et al. 2000). It is driven by the formation of dental plaque, a biofilm, forming on the surface of the pellicle-coated tooth. The site at which dental caries occurs is dependent upon the bacteria present at a particular site, and a continuous source of protective and/or harmful processes (Loesche 1996). When exposed to fermentable carbohydrates in the form of diet or in GCF, the bacteria produce organic acids through anaerobic fermentation. These acids decrease the local pH causing demineralisation of the tooth structure. The decrease in pH also suppresses the growth of microorganisms unable to tolerate the acid stress. This allows aciduric, and often acidogenic bacteria to thrive in the lack of competition. Of particular note, dental caries does not occur in the absence of bacteria (Orland et al. 1954). *In vitro* studies have demonstrated that, when growth media pH is reduced to pH 5, two organisms associated with dental caries, *S. mutans* and *L. casei* are capable of metabolism. This explains, at least in part, their common presence in caries lesions (Svensäter et al. 1997). This shift in ecology results in a population vastly different from the early, non-acidogenic microbiota. With each exposure to carbohydrates, the decrease in pH is both more severe and prolonged and the balance between remineralisation and demineralisation is shifted in favour of mineral loss. Over time, this results in a net

mineral loss from the tooth and initiation of dental caries. Therefore, the frequency of eating sugars is of greater importance than total sugar consumption (Bowen & Birkhed 1986). The formation of dental caries requires the presence of cariogenic bacteria and access to fermentable carbohydrates and is influenced by the constituent oral microbiota, susceptibility of the tooth, quality and quantity of saliva and time. In short, dental caries occurs when the net rate of demineralisation exceeds that of remineralisation. The mineralisation of the teeth is a pH-dependant balance.

Dental caries is one of the greatest contributors to tooth loss. Left untreated, dental caries can progress through the enamel to reach the cementum and dentine. Both of which can cause considerable discomfort. Progressing further still to the pulp can lead to tooth infections such as abscesses. Despite continuing developments in preventative measures, dental caries remains one of, if not the, most prevalent disease effecting man today. According to the World Health Organisation (WHO), dental caries affects between 60% and 90% of school-aged children and approaching 100% of adults (Petersen 2003). Dental pathologies, although rarely life-threatening, remain one of the greatest burdens on health services in developed countries due to their high prevalence and cost of treatment. In a 24-month period to September, 2013, 29.8 million patients underwent dental treatment. Of this number, 84.3% (25.1 million) were treatments in NHS Bands 1 & 2, which include the filling of cavitated teeth. £3.8 billion is expended by the NHS on dentistry annually, with a further £1 billion spent by private practice (Ramsay 2014). According to the American Dental Association, the annual expenditure in 2014 on dental services in the United States was \$113.5 billion (Wall & Vujicic 2015). Dental caries has a major effect on the health and well-being of the patient. Along with the considerable costs associated with the treatment of dental caries, sufferers of dental caries may experience effects on their self-confidence and quality of life (Moynihan & Petersen 2007). The teeth play an important role in communication through speech and emotional expression. They also play an important role in allowing a person to gain nutrition through a varied diet.

## **1.8 The Role of Fermentable Carbohydrates in Dental Caries**

The role of readily-fermentable sugars, particularly sucrose, in the caries process is evident. The prevalence of dental caries in the industrialised world, where sucrose is often added to food and drink as a sweetener, exceeds that of the non-industrialised world. Also, the rate of dental caries increased significantly with the introduction of readily fermentable carbohydrates. The major etiological factors for caries are considered to be high consumption of refined sugars (sucrose) and presence of an acidogenic flora in the dental plaque (Marsh & Nyvad 2003). Following the ingestion of readily fermentable carbohydrates, organic acids decrease the pH. In early dental plaque consisting predominantly of non-acidogenic bacteria, the decrease is infrequent, mild and comparatively short in duration. As dental plaque matures and species diversity increases, fermentable carbohydrate ingestion results in a longer and larger decrease in pH. Many of the dental plaque bacteria prefer a pH in the proximity of neutral for optimum growth. As the pH moves from neutral pH, metabolic activity and growth is suppressed. This allows aciduric species to gain a foothold and thrive in the lack of competition. The result of frequent ingestion of fermentable carbohydrates also has an ecological effect upon the microbial composition and its ability to maintain homeostasis. As time to return to a neutral pH is limited, non-aciduric species may become non-viable.

## **1.9 The Concept of Microbial Homeostasis**

In health, dental plaque exists in a dynamic equilibrium and remains relatively stable over time, despite regular exposure to environmental changes (Marsh 2006). This stability is termed microbial homeostasis and exists regardless of regular minor environmental stresses, e.g. oral hygiene measures, diet, host defences, changes in saliva flow rate (Alexander 1971, Bradshaw et al. 1989). This is achieved by a number of microbial interactions, both synergistic and antagonistic (Kuramitsu et al. 2007). These include conventional biochemical interactions such as those necessary

to catabolise complex host glycoproteins and to develop food chains, but in addition, subtler cell-cell signalling can occur (Schaudinn et al. 2007; Stoodley et al. 2002; Elias & Banin 2012; Steinberg 2015). This signalling can result in co-ordinated gene expression within the microbial community, and these signalling strategies have been regarded as potential targets for novel therapeutics (Kolenbrander et al. 2002; Suntharalingam & Cvitkovitch 2005). When environmental changes occur, for example a pH decrease as a result of the ingestion of fermentable carbohydrates, homeostatic mechanisms come into play and return the community to homeostatic stability. The ecological plaque hypothesis is based on the principle that oral disease results from disruptions to this microbial homeostasis (Marsh 1994). Earlier, the specific plaque hypothesis constituted the basis for the caries aetiology, and mutans streptococci were considered the 'arch-villain' for caries initiation and progression (Emilson & Krasse 1985). Later studies suggested that caries development is much more complex (Beighton 2005). Under the ecological plaque hypothesis, when environmental parameters are altered they affect the microbial composition of dental plaque, which in turn affects the environment in which they exist. Although mature plaque is afforded a degree of stability, the metabolically active constituent microorganisms react to changes in environmental parameters. The host tempers subgingival plaque by immune responses and low levels of gingival crevicular fluid. Microbial homeostasis may be disrupted by changes to the host responses by; accumulation of non-specific dental plaque, plaque-independent host factors such as immune disorders or hormonal irregularities (e.g. pregnancy, puberty and menopause) or environmental changes caused by diet or smoking (Zambon et al. 1996). Alterations to the environment such as inflammation, tissue degradation and increases in the flow rate of GCF may illicit a shift in microbial population and allow the establishment of periodontal pathogens, causing periodontal disease. Many of the early colonisers of dental plaque require a pH close to neutral to thrive (Marsh & Martin 2009). When fermentable carbohydrates are introduced, the metabolically active constituent microbiota metabolise the sugars producing strong organic acidic by-products, predominantly lactic acid. The production of these acidic by-products drives local decreases in pH. It has been shown that pH decreases rapidly before slowly returning to and approaching the resting pH (Stephan 1940).

Many of the microorganisms are able to withstand only short durations at low pH without detrimental effect. Provided that the decrease is not prolonged, they are able to return to normal growth rates as the pH increases. The non-mutans streptococci and *Actinomyces* are the key microorganisms within dental plaque responsible for the maintenance of microbial homeostasis (Takahashi & Nyvad 2008). Conversely, regular and prolonged intake of dietary carbohydrates causes recurrent declines in pH which suppresses growth of beneficial bacteria while allowing aciduric bacteria to thrive (Loesche 1986; Higham 2010; Caufield et al. 2015). The higher concentration of aciduric, acidogenic bacteria leads to more prominent decreases in pH and slower returns to resting pH. Disease-associated microorganisms may be part of the healthy oral microbiota, however are kept in check by interspecies competition during microbial homeostasis and host defences. Following changes in the local microenvironment, specific elements are able to overgrow and overwhelm host defences causing disease. The removal of the disease-inducing stimuli (host, microbial, environmental) will aid in the return to homeostasis. Targeting a specific pathogen may be less effective as the condition leading to the disease state may remain. Additionally, the space left by the removed pathogen may be filled by another pathogen not susceptible to the removing agent.

## **1.10 Plaque Hypotheses**

Dental plaque is essential for the development of dental pathologies. It has been shown in animal models that, in the absence of microorganisms, dental caries does not develop even in the presence of a high carbohydrate diet Current (Thonard 1966). In the past, dental pathologies have been considered to be caused by either specific pathogenic bacterial species (the specific plaque hypothesis) or through the collective action of the dental plaque as a whole (the non-specific plaque hypothesis). Current understanding has reconciled many of the key theories of the earlier hypotheses, focussing upon the shifts which occur within the microbial population as a result of environmental pressure (the ecological plaque hypothesis).

### **1.10.1 Specific Plaque Hypothesis**

The specific plaque hypothesis proposes that, out of the diverse collection of microorganisms comprising the resident microbiota, only a few particular species are actively involved in disease (Loesche 1976). Particular interest has been paid to *S. mutans* due to; its high acid tolerance and acidogenicity (Loesche 1986; Hamada & Slade 1980), consistent high correlation with disease and frequent isolation from cavitated lesions (Orland et al. 1954), low abundance in the absence of disease (Loesche 1986) and its ability to cause disease in animal models (Boyar et al. 1989). Also, *S. mutans* is physiologically adapted to causing dental caries. It readily metabolises dietary sucrose forming insoluble polymers of glucose (glucans) facilitating the colonisation of the tooth as well as the ability to produce surface antigens I/II. The formation of glucans promotes the adhesion of *S. mutans* to the tooth surface and to other bacteria (Hamada & Slade 1980). Howe and Hatch and McIntosh, James and Lazarus-Barlow found large quantities of *Bacillus acidophilus*, later reclassified as *Lactobacillus acidophilus* in carious dental plaque (Howe & Hatch 1917; McIntosh et al. 1922; Clarke 1924). Other species of interest include Lactobacilli and Actinomyces. Treatment centred on removal of these offending species with the use of targeted antimicrobials. Contrary to this hypothesis, disease occurs in the apparent absence of these putative pathogens, while these organisms may be recovered from healthy sites.

### **1.10.2 Non-Specific Plaque Hypothesis**

The non-specific plaque hypothesis proposes that all bacteria in the oral cavity have the potential to cause oral disease (Miller 1890). In his seminal paper, Miller termed the hypothesis 'the Chemo-Parasitic Theory of Dental Caries'. According to the hypothesis, dental pathologies form as a result of the accumulative effect of dental plaque producing copious amounts of noxious substances. These substances stimulate host defences and the action of the host defences causes dental pathologies. Interestingly, this hypothesis was outlined prior to any concept of the microbial diversity of the oral cavity (Loesche & Grossman 2001). It is the

production of acid by-products, by the oral bacteria which causes the destruction of the dental hard tissue leading to dental caries. Miller demonstrated, through his experiments, that the action of oral bacteria on carbohydrates could produce sufficient acid to damage the teeth (Miller 1890). As a consequence of the above hypothesis, the non-specific plaque hypothesis was proposed. This hypothesis proposes that disease is the outcome of the overall activity of the total plaque microbiota (Theilade 1986). In this way, a heterogeneous mixture of microorganisms could play a role in disease. Marsh stated, *"In some respects the arguments about semantics, since plaque-mediated diseases are essentially mixed culture (polymicrobial) infections, but in which only certain (perhaps specific!) species are able to predominate"* (Marsh 2006). The arguments then centred on the definitions of the terms specific and non-specific. If not actually specific, then the disease certainly shows evidence of specificity. The isolation of specific organisms was inconsequential as disease is driven by the overall bacterial population. Miller's work led to the hypothesis that the decalcification of the dental hard tissue as a result of the production of acid of bacterial origin following carbohydrate fermentation to be universally accepted.

### **1.10.3 Ecological Plaque Hypothesis**

The ecological plaque hypothesis reconciles the key elements of the earlier plaque hypotheses. The ecological plaque hypothesis proposes that disease occurs as a result of a shift in the balance of the resident microbiota due to a response to a change in the environmental conditions. A repeated cycle of low pH in plaque as a consequence of frequent sugar intake favours the growth of acidogenic and aciduric species which cause caries. Furthermore, the inflammatory response to dental plaque accumulation around the gums leads to increased flow of GCF, providing a source of various nutrients that favours the growth of the proteolytic and obligate anaerobes that predominate in periodontal disease. Importantly, therefore, prevention can be achieved not only by direct inhibition of the causative bacteria but also by the removal or neutralisation of the forces that drive the selection of these organisms (Kleinberg 2002; Xiao et al. 2012; Rugg-Gunn 2013). The ecological

plaque hypothesis proposes that the organisms associated with disease may also be present at healthy sites, but at levels too low to be clinically relevant (Marsh 2003). Dental caries has previously been described as an endogenous infection, due to the microorganisms associated with dental caries being part of the normal oral cavity microbiota (Marsh & Nyvad 2003). Endogenous infections are able to occur when certain members of the normal flora are able to gain a selective advantage over other species shifting the microbial population (Marsh & Martin 2009).

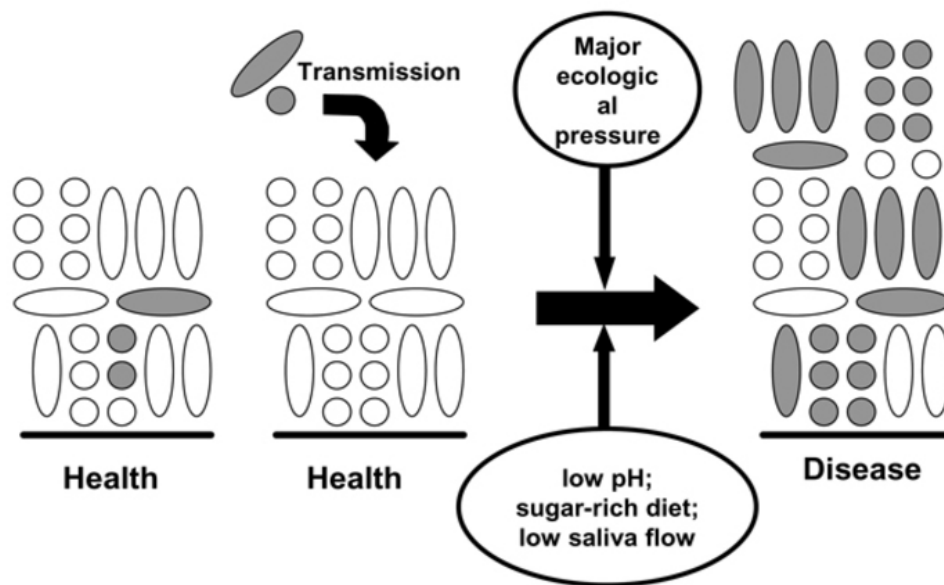


**Figure 1.15** Representation of the dental plaque composition and the transition from health to disease under ecological pressure. (Marsh 2009).

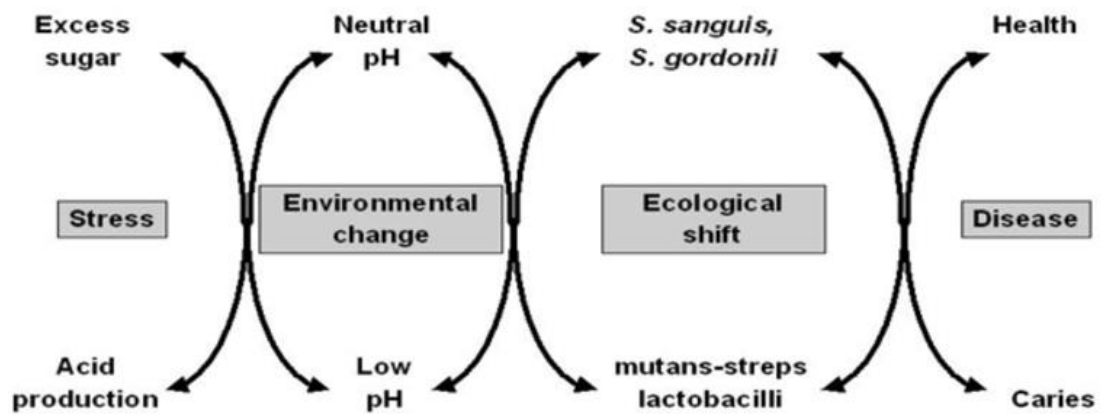


**Figure 1.16** The ecological plaque hypothesis, factors leading to the progression of dental caries and how control of these factors can reinstate oral health (Marsh 2003).

#### 1.10.4 Extended Ecological Plaque Hypothesis

As an extension to the ecological plaque hypothesis, the extended caries ecological plaque hypothesis was proposed. It states that the initiation and progression of dental caries occurs in three reversible steps (Takahashi & Nyvad 2011). According to Takahashi (2011); *“Environmental acidification is the main determinant of the phenotypic and genotypic changes that occur in the microflora during dental caries”* (Takahashi & Nyvad 2011). Early dental plaque microbiota consists predominantly of non-mutans streptococci and actinomycetes, and environmental acidification is mild and infrequent. The microbiota exists in a state of microbial homeostasis and the mineralisation balance is in equilibrium or may favour net mineral gain. These organisms are responsible for the maintenance of microbial homeostasis (Takahashi & Nyvad 2008). This stage is termed the dynamic stability stage. With an increase in intake of fermentable carbohydrates, environmental acidification increases and becomes moderate to frequent. The acidogenicity and aciduricity of the non-mutans streptococci may increase adaptively. Also, those species less acid-tolerant may be suppressed or killed during periods of low pH. This lack of competition allows the selective increase of low pH non-mutans streptococci. Over time this adaptation and selection destabilises the microbial homeostasis and shift the

mineralisation equilibrium towards net mineral loss. This leads to the initiation or progression of dental caries. This is the acidogenic stage. During periods of frequent and prolonged exposure to fermentable carbohydrates, acid-induced selection leads to an increase in the number of aciduric, acidogenic species. Mutans streptococci and lactobacilli predominate as well as low pH non-mutans streptococci, *Actinomyces* spp. and bifidobacteria. This stage is termed the aciduric stage. Therefore, the hypothesis takes into account that the progression towards disease is a result of an assault on the microbial homeostasis continually shifting the bacterial population and the environment in which they exist (Figure 1.17).

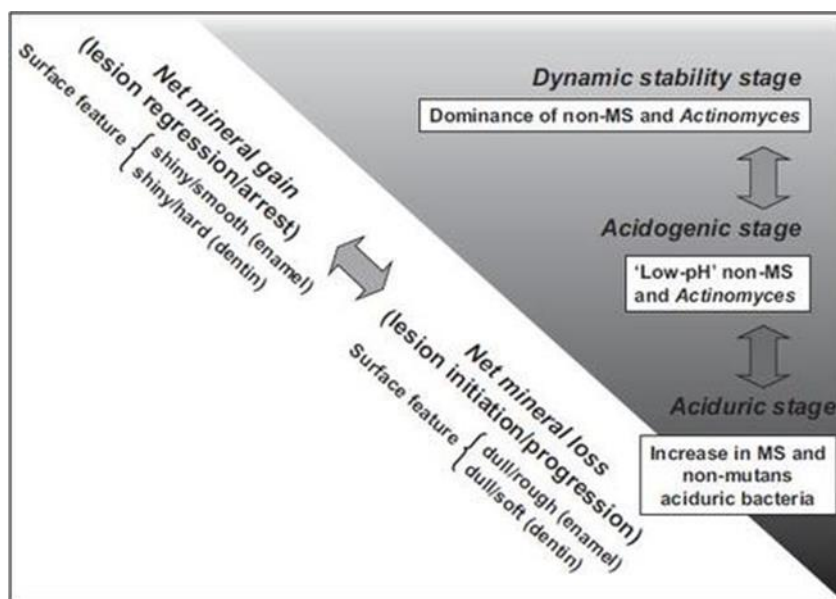


**Figure 1.17** The concept of the extended ecological plaque hypothesis, showing the various stages of disease progression (Takahashi & Nyvad 2008).

## 1.11 The Microbiota of the Oral Cavity

As the gateway to both the respiratory and gastrointestinal tract, microorganisms are constantly presented to the oral cavity from the exogenous environment (air, food, water). The microbiota of the oral cavity is diverse and abundant. This is influenced by a number of factors. The oral cavity provides a favourable environment for inhabitation of a wide range of microorganisms. It is warm, moist and has a steady supply of nutrients, both exogenous and endogenous. It also has a

great variety of environmental niches, each with distinct environmental constraints. Due to the wide diversity of these ecological niches and the nutrients that supply them; the number of resident microorganisms able to thrive within them is accordingly numerous. The oral microbiota is able to survive by forming biofilm and it is likely that many of the species could not survive outside these communities due to the reliance on inter-species metabolic interactions (Jenkinson & Lamont 2005). Therefore, many of the bacteria that inhabit the oral cavity are unique to this habitat. Metagenomics has demonstrated how many microorganisms are able to inhabit the oral cavity. The oral cavity is home to over 700 predominantly bacterial species (Kilian et al. 2016), of which approximately 35% are not currently cultivable in the laboratory and are only identified through molecular methods (Paster & Dewhirst 2009). In oral health, between 100 and 200 species may be present in the oral cavity, , each with a preferable niche in the oral cavity (Dewhirst et al. 2010). In disease, cultural diversity and richness increases (Paster et al. 2006).

The microorganisms that are able to thrive in this environment are able to do so by attaching to the surfaces of the oral cavity and forming biofilms. Many of these bacterial species have little or no detrimental effect on oral health and may provide a benefit to the host, providing protection by inhabiting the tooth surface and preventing colonisation of pathogenic species or affording assistance in the digestion of food. The indigenous microbiota also provide a range of vitamins (Capozzi et al. 2012; Masuda et al. 2012) and contributes to the hosts' immunity by the production of immunoglobulins (Hooper et al. 2012). On the contrary, members of the indigenous microbiota may be implicated in the progression towards disease states such as dental caries and periodontal diseases (Marcotte & Lavoie 1998). The bacteria which inhabit the oral cavity have a proclivity to colonise various environmental niches within the oral cavity. This is due to specific adherence, tissue tropism and biofilm formation. The bacteria utilise specific adhesins in the salivary pellicle, such as to bind to different surfaces. Specific receptors on the cell membrane facilitate adhesion. Bacteria also demonstrate tissue tropism, forming on surfaces as a result of available nutrients, pH, temperature and redox potential. The formation of biofilms, complex three-dimensional communities, also plays a

role. Some species can attach and form these communities whereas others are able to attach to these pioneer species and join the community. Age plays a significant role in the composition of the oral microbiota. At birth, the oral cavity is sterile and quickly becomes colonised from the environment and as a result of feeding. The method of feeding has been shown to have an effect on the oral microbiota (Holgerson et al. 2013). The eruption of the dental hard tissue in infancy applies results in a shift in the population. *S. salivarius* in the oral cavity of the edentate infant gives way to other streptococci which require the tooth surface to facilitate colonisation (Carlsson et al. 1970; Kreth et al. 2009). Through the formation of biofilm, they become extremely difficult to eradicate. The low Eh of the gingival sulcus provides a favourable environment for the colonisation of anaerobic organisms, such as *Porphyromonas gingivalis* and *Tannerella forsythia* (Kenney & Ash 1969; Marsh 1994). Bacteroides and spirochaetes colonise around puberty (Wojcicki et al. 1987). Fungi, parasites and viruses may also be present in the oral cavity.

### **1.11.1 The Microbiota Pertaining to Human Dental Caries**

It is generally accepted that the aetiology of dental caries is polymicrobial in nature. However, a number of organisms are consistently recovered from the caries lesion (Marsh 2003). Of particular interest are mutans streptococci and lactobacilli due to their acidogenic and aciduric traits.

### **1.11.2 The Oral Streptococci**

The oral streptococci are among the most prevalent constituents of the oral microbiota and are important primary colonisers. In the early years, the oral cavity is devoid of hard tissues consisting solely of mucosal surfaces. *S. salivarius* predominate in this environment (Carlsson et al. 1970). Upon eruption of the teeth, *S. sanguinis* and *S. mutans* colonise the oral cavity, requiring the hard tissue for colonisation (Kreth et al. 2009). Many of the oral streptococci are able to produce polysaccharides, a major component of the biofilm matrix, and have the ability to

act as a nutrient source. They consist of four groups; the mitis group, the salivarius group, the anginosus group, and the mutans group. These mutans streptococci are often associated with dental caries, due to their acidogenicity and aciduricity. The close relation between mutans streptococci and caries is explained by sucrose fermentation during which the bacteria produce lactic acid and insoluble polyglucans (Loesche 1986). Irreversible colonisation of the oral cavity can only occur in the presence of sucrose. *S. mutans* synthesise and excrete four extracellular enzymes, three glucosyltransferases (Gtf) and one fructosyltransferase (FtF). These function by splitting sucrose, a disaccharide of glucose and fructose, into fructose and glucans or glucose and fructans, respectively. A major factor in the association of *S. mutans* with dental caries is the ability for the organism to produce glucans from the metabolism of sucrose. Glucan-binding is an important element of the *S. mutans* infectious process which facilitates the adherence and accumulation of the organisms on the tooth (Quivey Jr. 2006).

### **1.11.3 The Oral Lactobacilli**

Lactobacilli are gram-positive, facultative anaerobic or microaerophilic organisms. The association between lactobacilli and dental caries was established over a century ago (Kligler 1915; Owen 1949; Caufield et al. 2015). They form a major portion of the clade of lactic acid bacteria, that is, they produce lactic acid as a metabolic end-product from the fermentation of carbohydrates. Only a number of the *Lactobacillus* genus are found in caries lesions, but they are rarely found in children free of dental caries (Caufield et al. 2000).

### **1.11.4 The Oral *Neisseria* spp.**

Commensal *Neisseria* spp. are abundant within the oral cavity and oropharynx (Liu et al. 2015). These species include *N. flava*, *N. subflava*, *N. sicca*, and *N. mucosa*. *Neisseria* spp. are among the earliest colonisers of the salivary pellicle-coated tooth (Liljemark & Gibbons 1971). The consumption of oxygen by commensal *Neisseria* spp. facilitates the attachment of obligate and facultative anaerobic bacteria (Marsh

2000). These species differ from the human pathogens *N. gonorrhoeae* and *N. meningitidis*, in their ability to grow on basic media in the absence of CO<sub>2</sub> supplementation.

## **1.12 Dental Plaque as a Microbial Community**

The term dental plaque is commonly used for biofilm that forms upon the tooth surface however dental plaque encompasses the biofilm which covers all surfaces of the oral cavity. Dental plaque consists of microorganisms encapsulated in an extracellular polysaccharide matrix attached to an underlying salivary pellicle (Takahashi & Nyvad 2008). With the use of confocal laser scanning microscopy, it has been shown that dental plaque has an open architecture, similar to other biofilms, with projections, channels and voids (Marsh 2004). The formation of dental plaque is a naturally-occurring process which benefits the host by preventing colonisation by exogenous species. Sites of stagnation afford the dental plaque with protection from removal forces and therefore dental plaque preferentially forms at these sites. The formation of dental plaque upon the soft tissues of the oral cavity is primarily limited by desquamation of the oral epithelium. Dental plaque is the major etiological agent of two dominant dental pathologies, dental caries and periodontal disease. By growing as a biofilm, microorganisms are afforded protection from factors, such as host defences and desiccation. Furthermore, spatial and temporal heterogeneity, in environmental factors such as pH and O<sub>2</sub>, enables fastidious organisms to survive and grow in apparent hostile environments. This can be observed when obligate anaerobes are able to grow in an overtly aerobic environment. The microbial community lifestyle also offers improvement in the efficiency of metabolism. Microorganisms unable to metabolise complex host macromolecules (e.g. mucins) may be able to, working in concert, metabolise the by-product of another inhabitants metabolism.

### **1.12.1 Genetic Exchange**

Many streptococcal species are able to exchange segments of genetic material through transformation, the uptake of DNA extruded by another. This however only occurs when the bacteria are in a state of competence generated through an extracellular peptide pheromone, competence-stimulating peptide (CSP). Low levels of CSP are excreted during growth, accumulating and reaching threshold levels before genes associated with CSP production and genes involved in the processes of DNA uptake and recombination are up-regulated.

### **1.12.2 Bacterial Communication and Regulation of Gene Expression**

Bacteria within a biofilm communicate with each other via a wide variety of chemical signalling molecules. For example, quorum sensing is the cell-dependent regulation of gene expression through production and excretion of an autoinducer signalling molecule. When a threshold concentration is reached, gene expression is altered in aid of the community. Bacteria are able to coordinate gene expression and therefore the behaviour of the entire community. The ever-changing environment of the oral cavity provides an impetus for bacteria to regulate gene expression in order to maintain optimal phenotypic properties (Jenkinson & Lamont 2006). Therefore, in order to survive, organisms must be able to sense and respond to the prevailing environmental conditions. Gene expression is also altered by the presence of sucrose. For example, sucrose has been shown to repress the expression of wall-associated protein A (WapA) which plays an important structural role affecting cell-cell aggregation (Qian & Dao 1993). Upon attachment to the salivary proteins within the pellicle, coordinated responses are observed causing the up-regulation of genes associated with adhesins and production of cell-cell signalling molecules, e.g. CSP, AI-2 (Marsh & Nyvad 2009). Furthermore, within mature biofilms, marked up-regulation of glucosyltransferases (gtfBC) by *S. mutans* is observed (Li & Burne 2001).

## 1.13 Acid Tolerance of Oral Bacteria

The majority of organisms within healthy dental plaque require a pH near neutral for growth, however, are subjected to continual cycles of acid shock as a result of organic acid formation following carbohydrate intake. Provided these decreases in pH are not prolonged, microbial homeostasis is able to restore the health-associated dental plaque. If a low pH environment is recurrent and prolonged, this microbial homeostasis can break down, causing population shifts and predisposing sites to disease (Marcotte & Lavoie 1998; Marsh 2003). It has been shown that, following the intake of sucrose, pH drops from a near-neutral resting pH to levels approaching pH 4 in a matter of minutes (Stephan 1944). Stephan showed that dental plaque in those with rampant caries, pH falls rapidly but also has a tolerance to remain at a prolonged decrease of pH (Stephan 1944). The aciduricity of bacteria which inhabit the oral cavity ranges from those which are unable to function at levels below pH 6 to those which are able to carry out glycolysis at pH values approaching pH 3 (Marsh & Martin 2009) (Figure 1.18). The acid tolerance within a single species may also vary considerably. Those species considered non-cariogenic are often non-aciduric and are only able to tolerate short periods of time at low pH conditions. Provided these periods of acidic conditions are short, they may be able to return to microbial homeostasis. If the level of duration is prolonged, the growth of these beneficial organisms are suppressed or killed leaving an environmental niche open to colonisation by cariogenic organisms due to the lack of competition. Opportunistic pathogens, such as *S. mutans* and lactobacilli, may be found within immature dental plaque, but at low numbers. At a neutral resting pH, they have little competitive advantage. In this situation, remineralisation is favoured. The supragingival dental biofilm constitutes an ecosystem of bacteria that exhibits a variety of physiological characteristics. In particular, the acid production resulting from carbohydrate metabolism by these bacteria and the subsequent decrease in environmental pH are responsible for the demineralization of tooth surfaces (Marsh and Nyvad, 2008). However, other physiological traits of the biofilm bacteria, such as base formation, may partly dampen the demineralization processes. This lead

Kleinberg to suggest that it is the proportions and numbers of acid-base-producing bacteria that are the core of dental caries activity (Kleinberg 2002).

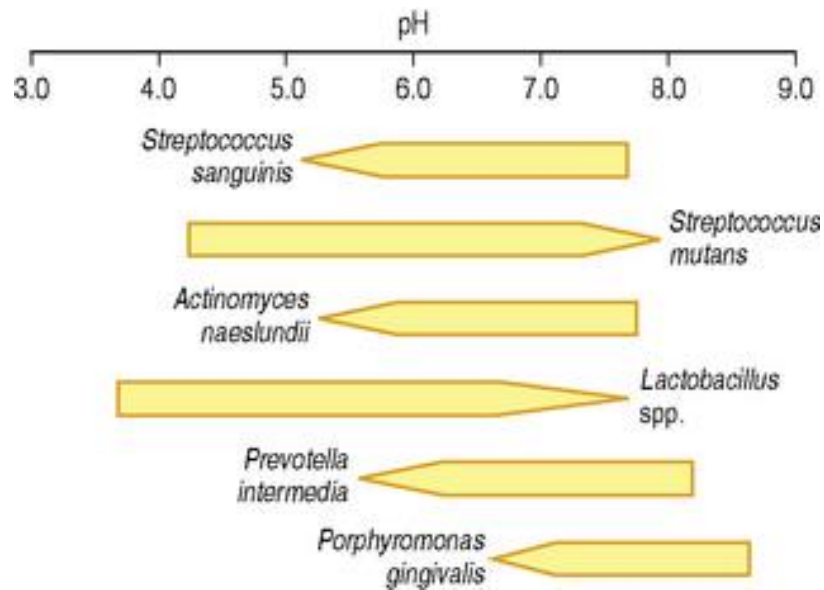


**Figure 1.18** A diagrammatic representation of the pH range for growth for some oral bacterial species (Marsh & Martin 2009).

## 1.14 Preventative Measures and Treatments of Dental Caries

The caries process is a ubiquitous and natural phenomenon (Manji et al. 1991) however, dental caries should be considered a preventable infectious disease (Balakrishnan et al. 2000; Rugg-Gunn 2013). When considering prevention of dental caries, true prevention pertains to the removal of predisposing factors which result in demineralisation. However, due to the complex nature and high prevalence of dental caries, early diagnosis and prompt treatment are needed to halt disease progression and, in the early stages of the caries processes, promote remineralisation and return to oral health. When dental caries has progressed, treatment may be focussed on removing and controlling the factors which maintain chronic disease. Measures for preventing dental caries can be divided into three groups; mechanical, chemical and nutritional. If good oral hygiene is maintained and

fluoride is supplied frequently, teeth will remain intact even if carbohydrate-containing food is frequently eaten (Van Loveren 2000).

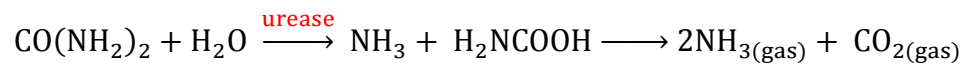
### **1.14.1 Mechanical Removal of Dental Plaque**

Dental caries is a multifactorial disease driven ultimately by the formation of dental plaque. It has been shown that, in the absence of dental plaque, caries cannot occur (Orland et al. 1954). Therefore, by removing the dental plaque, caries can be controlled. Measures of dental plaque removal include tooth brushing, the use of dental floss for interdental spaces and professional plaque removal in addition to scraping of the tongue, a reservoir for oral bacteria.

### **1.14.2 Chemical Control**

Dental caries is able to be controlled, by a number of actions, through the use of chemical agents. Of these, the most widely used is fluoride. Fluoride is added to drinking water in addition to dental hygiene products such as toothpastes and mouthwashes. The use of fluoride promotes the deposition of fluorapatite to the tooth stimulating remineralisation. The addition of fluoride to drinking water supplies has reduced the incidence of dental caries (Iheozor-Ejiofor et al. 2015), although one side-effect of overexposure to fluoride is fluorosis, a condition manifesting in discolouration of the teeth. Fluoride may also be applied topically. The use of fluoride has raised the threshold of sugar intake at which dental caries will progress to cavitation but fluoride has its limits and caries remains a serious problem for disadvantaged individuals in many industrialised countries and is a rising problem in many developing countries (Zero 2004). The disinfectant, chlorhexidine gluconate, is used extensively in the United Kingdom, both for treatment and prophylactically in the form of a mouthwash. It also has considerable antifungal properties and is used for the treatment of oral candidiasis in immunocompromised patients. It possesses an immediate bactericidal effect, particularly against gram-negative bacilli, in addition to a prolonged bacteriostatic effect as a result of adsorption upon the salivary pellicle-coated tooth (Scully 2013;

Jenkins et al. 1988). The non-ionic chlorinate bisphenol antiseptic, triclosan, has received considerable investigation (Jenkins et al. 1991). In addition to considerable antibacterial properties, triclosan also inhibits the formation of dental plaque, a property enhanced when used in conjunction with a copolymer or zinc citrate (Scully 2013). The use of urea and ammonia products in dental caries control has been shown to be effective. Urease in saliva converts urea to ammonia (Equation 1-5). Ammonia (NH<sub>3</sub>), has an alkali pH therefore acts to neutralise acidic by-products. Ammonium also has antibacterial properties. Positively charged molecules interact with the negatively charged phosphates on the cell wall disrupting the structure of the cell. This action is greater for gram-positive bacteria than gram-negative bacteria.



**Equation 1-5**

Antimicrobials, such as penicillin and erythromycin, have also been used to control specific bacteria or groups of bacteria considered as cariogenic. A consequence of broad spectrum antimicrobial, and to a similar extent targeted antimicrobial, use is that the healthy microbiota is disrupted causing an ecological shift. Other chemical approaches include antiseptics, such as chlorhexidine and alcoholic mouthwashes. A target response to dental caries may include the interference of bacterial growth or metabolism, interference with carbohydrate degradation through alteration of enzymes, alteration of the tooth surface or structure and targeted antibiotic-probiotic combination therapy to replace mutans streptococci with non-mutans streptococci, filling the gap left by disruption of the microbiota. The elimination of *S. mutans* from dental plaque has a significant effect in reducing other cariogenic species.

### **1.14.3 Nutritional Intervention**

Nutritional interventions include the restriction of readily fermentable carbohydrates from the diet or the use of non-fermentable, sugar alcohols (artificial

sweeteners) such as sorbitol and xylitol. Decreases in pH can be controlled through the elimination of snacks between meals. In particular, high carbohydrate confectionaries should be eliminated from the diet as they adhere to the tooth surfaces, especially at sites of stagnation and play a role in caries development. Regular intake of fermentable carbohydrates restricts the amount of time given for the pH to return to a resting pH. However, it has been recommended that by redirecting the focus from the elimination of sugar from the diet and towards oral hygiene and the use of fluoride toothpaste dental caries incidence would decrease (Konig & Navia 1995). This shows the importance of good oral hygiene and the use of fluoride.

#### **1.14.4 Beneficial Foodstuffs**

A number of foodstuffs have been shown to exhibit beneficial effects on the pH of the mouth. These include sugar substitutes such as the sugar alcohols xylitol and sorbitol, chewing gums, especially those containing sugar substitutes, dairy products, such as cheese and milk, shiitake mushrooms, and raspberries.

##### **1.14.4.1 *Sugar substitutes***

Sugar alcohols are hydrogenated carbohydrates and are typically composed of sugars and a polyol. Sugar alcohols include mannitol, sorbitol, xylitol and hydrogenated starch hydrolysates. They are not readily metabolised by bacteria (Tinanoff & Palmer 2000). Additionally, there is little to no production of extracellular polysaccharide (Van Loveren 2004). This makes them less cariogenic than dietary sugars, especially sucrose (Bradshaw & Marsh 1994). In addition to decreased fermentation and reduced cariogenicity, sugar alcohols possess other potential health benefits as they contain fewer calories, and therefore decrease glycemia and insulinaemia (Livesey 2017). It has, however, been noted that the used of sugar alcohols can contribute to retrogression of dental caries as the high acid content of the vehicle may promote dental erosion (Nadimi et al. 2011).

#### **1.14.4.2 Chewing gums**

The chewing of soft, cohesive substances, such as chewing gums and lozenges has been shown to stimulate the flow of saliva (Edgar & Geddes 1990; Dawes & Macpherson 1992; Fröhlich et al. 1992). Due to the fact that saliva is so beneficial in terms of buffering, much interest has been applied to agents that stimulate saliva flow (Edgar et al. 2004). Other substances which stimulate the flow of saliva include unflavoured materials, such as paraffin wax (Higham & Edgar 1989a). The flow of saliva assists in returning the pH of dental plaque to a resting pH by aiding the removal of cariogenic foodstuffs and their acid products, in addition to increasing the supply of bicarbonate (Section 1.2). Furthermore, the stimulation of saliva increases the availability of nitrogenous substrates, which are metabolised to alkali end products, increasing dental plaque pH. Both sugar-free gums and those containing sucrose are able to reduce the acid response, although sugar-free gums have a greater effect (Manning & Edgar 1993). Many gums are free of sugar, containing sugar alcohols, such as xylitol or sorbitol as a sweetener (Aguirre-Zero et al. 1993).

#### **1.14.4.3 Dairy products**

Dairy products such as cheese and milk have for a long time been considered beneficial to the health of bone and teeth as they contain high levels of calcium and phosphate (McClure & McCann 1960; Nizel & Harris 1964; Driessens et al. 1978). While sucrose has the potential to decrease plaque pH to below pH 5, the sugar in dairy, lactose, exhibits a lower pH potential with decreases in proximity to pH 6 and therefore a lower cariogenic potential (Telgi et al. 2013). Dairy products confer protection by counteracting the acidification by sucrose fermentation (Johansson 2002). Cheeses rich in nitrogenous compounds produce an increase in salivary pH due to the action of saliva, despite the acidic nature of the cheese (Manning & Edgar 1993). This may be due to the catabolism of casein and other cheese proteins, in addition to the fact that cheese increases the flow of saliva. Casein phosphopeptides, a group of peptides derived from casein, are part of the protein that occurs naturally in milk. Casein phosphopeptides stabilise calcium phosphate in

solution and significantly escalate the level of calcium phosphate in dental plaque (Reema et al. 2014). Furthermore, cheese raises the concentration of calcium and phosphate in the oral cavity and increase the chance of remineralisation (Higham & Edgar 1989a). Cheese is also a strong sialagogue, stimulating the flow of saliva (Higham & Edgar 1989a).

#### **1.14.4.4 Shiitake Mushroom**

Shiitake mushroom (*Lentinula edodes*), the most popular edible mushroom in Japan, has demonstrated significant anticaries properties (Shouji et al. 2000; Ciric et al. 2011). An extract from shiitake mushroom has been shown to inhibit the formation of water-soluble glucan from sucrose by crude glucosyltransferases of *S. mutans* and *S. sobrinus* (Zaura et al. 2011; Spratt et al. 2012).

#### **1.14.4.5 Raspberries**

Raspberries (*Rubus idaeus*) have been shown to inhibit the formation of biofilm in a number of bacterial species associated with both dental caries and periodontal disease (Spratt et al. 2012). Furthermore, the same study demonstrated that an extract from raspberries inhibits, to a large degree, the attachment of cariogenic species to hydroxyapatite (Spratt et al. 2012).

## **1.15 Methods for the Measurement of Hydrogen-Ion Concentration within Dental Biofilms**

Due to its involvement in the development of dental caries and numerous processes within dental plaque, hydrogen-ion concentration (pH) has been extensively studied. Numerous methods have been employed to determine pH within dental plaque. Each method possesses a number of advantages and disadvantages. These methods include the harvest method, the use of various microelectrodes and various optic techniques utilising fluorescent dyes. These methods may also be utilised for other parameters such as dissolved oxygen concentration, redox

potential and concentration of various ions such as calcium and fluoride. An ideal method for the determination of pH within dental plaque would possess the following characteristics; i) allow determination of pH without detrimental effect to the pH, the bacteria or the biofilm structure, which may affect the result obtained, ii) allow multidimensional (spatial and temporal) determination, iii) allow analysis within a natural, physiological and hydrated biofilm, iv) be simple to perform, and v) be cost-effective.

### **1.15.1 The Harvest Method**

The harvest method involves the scraping of dental plaque, predominantly from the gingival margins and dispersal in a diluent prior to testing with colourimetric indicators or pH electrodes (Jensen et al. 1982). Plaque harvesting is simple and cheap to perform and allows a great deal of access to the collected plaque. Patients usually refrain from dental hygiene measures for a period of time prior to testing. The major advantage of the harvest method is the plaque is grown in a physiological environment. The technique causes minimal discomfort to the patient and allows a wide range of patient parameters to be assessed. Patients may rinse or chew substrates prior to plaque harvest to test the effect of plaque pH. The harvest method does, however, have a number of drawbacks. The major disadvantage to the plaque harvesting method is the fact that, in collecting the plaque, the plaque is disturbed which may alter the metabolic activity within the plaque (Geddes 1981). Other disadvantages include the fact that plaque must be removed from accessible oral sites. Analysis is therefore limited by the amount of plaque collected which varies between individuals. This method can only be used to assess the bulk pH and does not provide information regarding pH at the plaque-tooth surface junction.

### **1.15.2 Microelectrodes**

The development of microelectrodes revolutionised the field. A microelectrode is considered an electrode with a tip with a diameter of less than 1 mm. The three most popular constructions for pH microelectrodes are; metal oxide, glass and

liquid-ion exchange (LIX) membrane pH microelectrodes. As with the harvesting method, touch electrode provides a cheap, facile and flexible method for plaque pH determination. Measurements are able to be made *in vivo* and therefore under physiological conditions. Less accessible plaque, such as interproximal and labial plaque and carious lesions may also be assessed, provided the tip diameter is sufficiently small. Although this approach provides information regarding the average pH within the plaque, it does not provide information regarding the pH values at the plaque-tooth surface interface. The major disadvantage of the use of microelectrodes is that inserting the electrode into the plaque alters complex metabolic processes, although not to the same extent as harvesting. Microelectrode systems require periodical recalibration due to calibration drift.

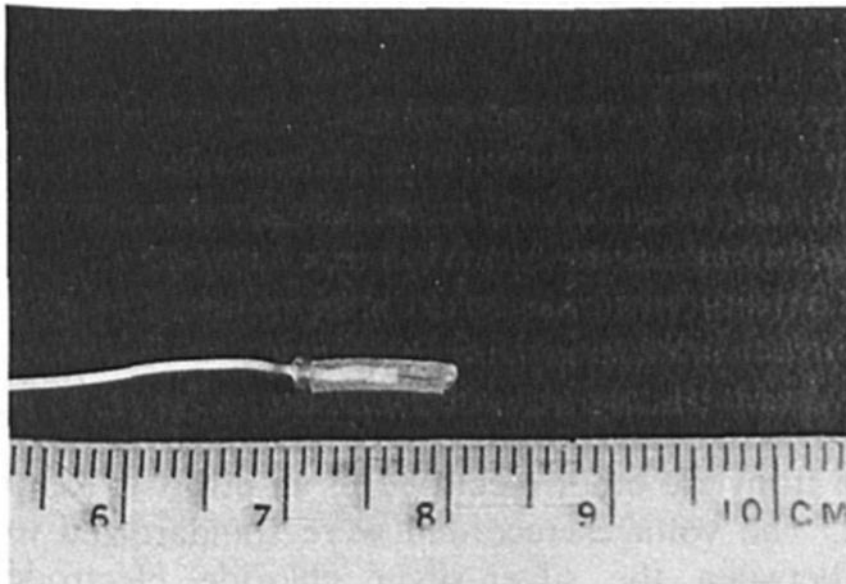


**Figure 1.19** An example of a pH microelectrode (Ewers & Greener 1985)

#### **1.15.2.1 Metal Oxides Microelectrodes**

The oxides of many noble metals, such as iridium, are sensitive to pH and can be used to make pH microelectrodes (VanHoudt 1992). They are straightforward to manufacture, with the major difficulty being in the oxidation of the metal as noble metals do not oxidise easily.

### **1.15.2.2 Antimony Microelectrodes**

Antimony electrodes have been fabricated from a solid piece of antimony or by electro-coating copper or platinum wire which allows the production of microelectrodes or purpose-shaped electrodes (Charlton 1956; Hassell 1971). These electrodes give accurate reading but are susceptible to increased lactate levels, the predominant acid produced within dental plaque during fermentation (Igarashi et al. 1981).

### **1.15.2.3 Glass Microelectrodes**

Glass pH microelectrodes are miniaturised versions of glass macroelectrodes. Construction is not difficult (Thomas 1978; Pucacco et al. 1986). The early glass microelectrodes were constructed from glass micropipettes. The micropipettes were heated until molten and stretched before filling with an electrolyte solution to conduct the electric signal (Ling & Gerard 1949). Subsequently, microelectrodes are pH-sensitive glass such as Corning glass #0150 within a 'lead glass' micropipette which acts as the shaft (Thomas 1978). The development of glass electrodes increased the accuracy of analysis (Jensen et al. 1982). Charlton concluded that the advantage of glass electrodes was that it was able to record the pH without being affected by other ions within complex biological systems and inert glass did not affect the system (Charlton 1956). The distinct disadvantage is the considerable length of the glass microelectrodes. Also, due to the small tip diameter, they are brittle and prone to breakage.

### **1.15.2.4 Liquid Ion Exchange (LIX) Membrane Microelectrodes**

LIX membrane electrodes utilise a liquid-ion exchanger that is held in place in an inert, porous hydrophobic membrane (Santegoeds et al. 1998). LIX membrane microelectrodes are simple to produce and use. They are comprised of ready-to-use constituents; an ion-exchanger, organic solvent and stabilisers which are applied to the tip by capillary action and salinised by immersing the tip in a salinising solution

before being baked at 200°C for 15min. The tips are prepared, used and then disposed of.

### **1.15.3 *In vivo* Prosthetic Devices Incorporating Electrodes**

*In vivo* prosthetic devices are devices which incorporate a power supply, electrode and reference electrodes mounted on removable partial dentures. As such, more typically caries-prone, younger, fully dentate individuals are often unable to be tested. Readings are collected by a lead from the prosthesis to a pH meter or by telemetry. Plaque pH is continually monitored which is advantageous to intermittent readings. Another advantage is that analysis is performed under physiological conditions. They allow the application of substrates to the oral cavity and the subsequent monitoring of pH changes, such as sucrose (Aires et al. 2006). The major disadvantage of the *in vivo* prosthetic devices is the fact that they are difficult to manufacture and have to be custom-made for each patient, thereby limiting the study population size. One major criticism of indwelling glass prosthetics is that pH is measured, not at a plaque-enamel interface, but at a plaque-glass interface. Therefore, plaque adherence and metabolic processes may be altered. Inherent issues with indwelling electrode systems include the possibility of protein-poisoning, failure of the plaque to cover the glass, restriction of saliva flow and increased food retention. Calibration of indwelling prostheses is also difficult and may not be completely accurate.

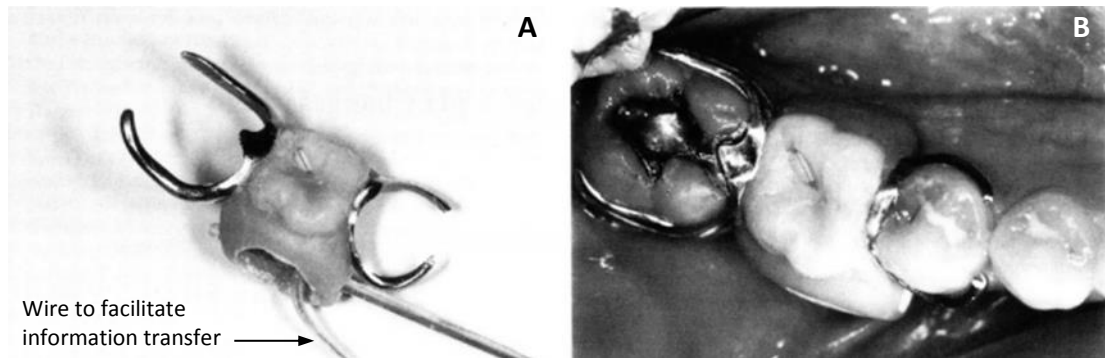


**Figure 1.20** An example of A) an in vivo prosthetic device incorporating a pH electrode and B) the device in situ, (Image credit: Mühlemann & de Boever 1970).

#### 1.15.4 Optical methods

Fluorescent dyes able to measure pH have been commercially available for some time. They allow measurement by changes either in intensity or wavelength of the emitted light (Figure 1.21 and Figure 1.22). They allow for the probing of local microenvironments with high spatial resolution, providing information that is difficult to obtain otherwise. The utilisation of pH-sensitive dyes has demonstrated the formation of pH microgradients throughout dental plaque (Schlafer et al. 2011).

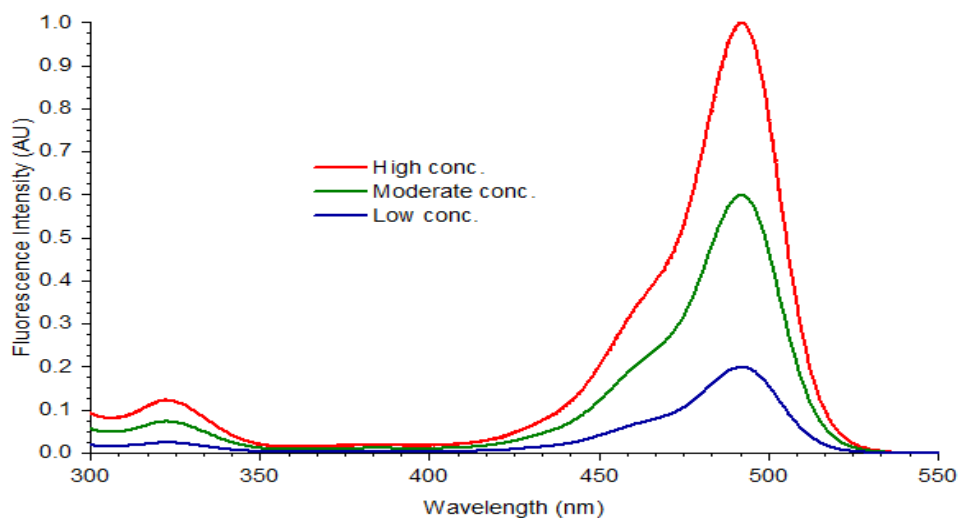


**Figure 1.21** Fluorescent emission shift with respect to changes in concentration.

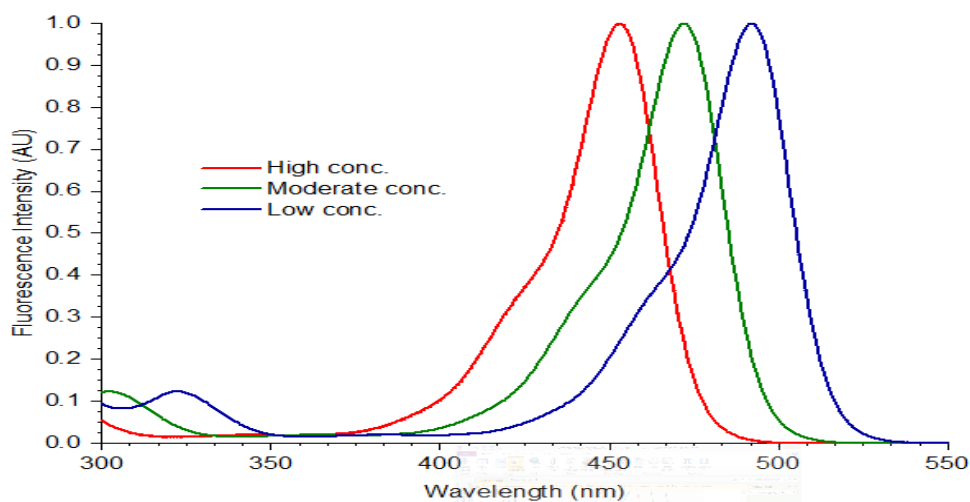


**Figure 1.22 Fluorescent wavelength shift with respect to changes in concentration.**

Advancements include the development of ratiometric dyes and sensors. Ratiometric dyes are dyes with dual-excitation wavelengths, dual-emission wavelengths or both. At one wavelength, changes in analyte concentration alters the intensity or wavelength of the incident light whilst at another wavelength the incident light remains stable despite changes in analyte concentration. The ratio of the sensitive to stable results is calculated and, following calibration, the ratio correlates to the analyte concentration. Nanoparticle sensors (nanosensors) consist of an inert backbone, such as polyacrylamide or silicon, to which a stable fluorophore and one or more sensitive fluorophores are incorporated into or covalently bound to the backbone. The major disadvantages in the use of nanosensors is the inherent cost of instrumentation (CLSM, MPE), the lack of commercial availability and their use is limited to those laboratories able to produce them.

## 1.16 Fluorescence

A fluorescent molecule at a relatively low energy state, or ground state, will not fluoresce. When electromagnetic energy strikes the fluorophore the molecule absorbs the energy. If the energy absorbed is sufficient the molecule reaches an excited electronic state. This process is known as excitation. The absorption of

energy occurs in the femtosecond scale ( $10^{-15}$  s). This duration corresponds to the time to travel one wavelength. There are multiple energy levels (excited states) which a fluorophore is able to attain, depending on the wavelength and energy of the light source. Since the fluorophore is unstable at high energy configurations it eventually adopts the lowest semi-stable energy state through non-radiative transition processes. During these processes, energy is lost in the form of heat. The energy of the excited state is unable to be maintained and, through release of energy, the molecule will return to its ground energy state in a statistical manner. If this energy is emitted in form of a photon, fluorescence occurs. This process is called emission. Fluorescence emission always occurs from the lowest vibrational level of the lowest excited state,  $S_1$  (Kasha 1950). The time taken to reach the excited electronic state is termed a quantum, likewise the time taken to return to the ground state. The energy in a quantum is expressed by Planck's Law (Equation 1-6), the equation of which is;

$$E = h\nu \quad \text{or} \quad E = hc/\lambda \qquad \text{Equation 1-6}$$

Where, **E** is energy, **h** is Planck's constant (approximately  $6.626 \times 10^{-35}$ ),  **$\nu$**  is frequency of light. The frequency of light can also be expressed as **c**, the speed of light, divided by  **$\lambda$** , the wavelength of light.

By examining Planck's Law, the energy of the absorbed photon is directly proportional to the wavelength. Therefore, incident light of shorter wavelengths possesses greater quantum of energy. Due to the loss of energy from the system during relaxation, the light released is typically of lower energy and, therefore a longer wavelength, to the incident light. Once the fluorophore has reached the ground state, provided it is intact, it is able to repeat the process. These processes are visualised in a simple electronic-state diagram (Jablonski diagram; Figure 1.23).

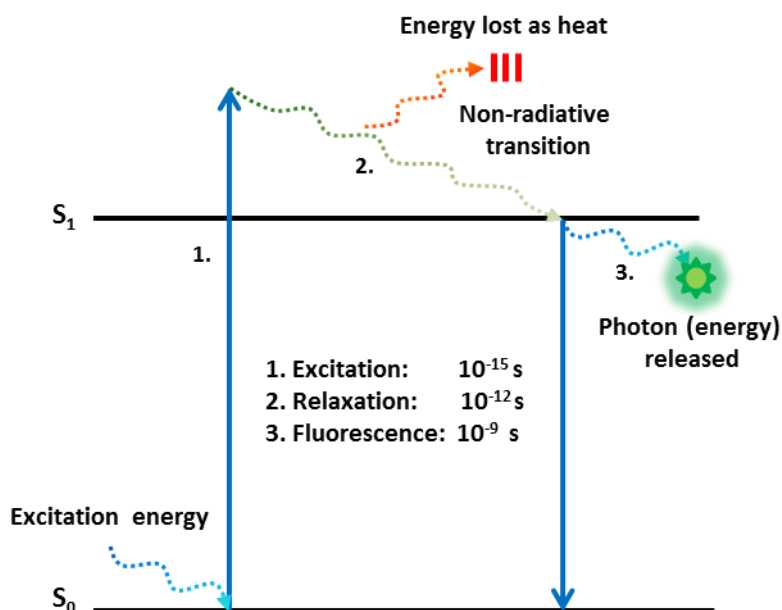


**Figure 1.23** A Jablonski diagram showing the various energy states that may be achieved following excitation by electromagnetic radiation and the consequential internal conversion (heat loss) and fluorescence emission (release of a photon).

### 1.16.1 The Fluorescence Spectra

The basic fluorescent properties of a fluorophore are often demonstrated as a line graph showing the likelihood of excitation and emission occurring at a particular wavelength. This line graph is referred to as the fluorescence spectrum. The fluorescence spectrum provides important information about the excitation and emission behaviour of the irradiated fluorophore. Each fluorophore will exhibit a specific fluorescence spectrum. A fluorophore is most efficiently excited at a particular wavelength, i.e. the excitation maximum or  $\lambda_{ex(max)}$ . Light of a wavelength either side of the excitation maximum may excite the fluorophore, but will do so less efficiently (Figure 1.24). Fluorescence emission behaves in a similar manner. The fluorescence output is most likely to occur at a particular wavelength, and will do so more efficiently. This wavelength is termed the emission maximum or  $\lambda_{em(max)}$ . Emission at wavelengths either side of the emission maximum can occur but will do so with less intensity. Only the intensity is affected, the range and shape of the

curve will not be altered. The emitted light is invariably of a longer wavelength, having less energy. This difference in wavelength is called the Stokes shift, after Sir George Gabriel Stokes (Stokes 1853). This shift is a result of a loss in energy during molecular vibrational relaxation lost as heat to surrounding solvent molecules as they collide with the excited fluorophore.

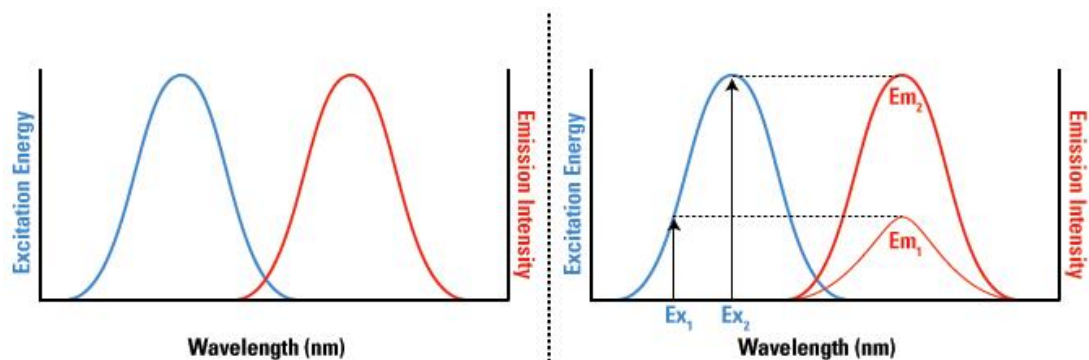


**Figure 1.24** An example of a fluorescence spectra showing excitation (blue) and emission (red) peaks. The right pane shows the effect of different excitation wavelength on emission intensity (Thermo Fisher Scientific CC BY 2.0).

### 1.16.2 Fluorescence Lifetime

Fluorescent molecules exhibit emission intensity and spectra. Furthermore, the fluorescent molecule exhibits a fluorescent lifetime. The fluorescent lifetime will differ between fluorescent molecules but will also vary based on the molecular environment the fluorophore exists in. Interactions that occur between the fluorophore and the local environment will have an effect on the fluorescent lifetime. When excited, the fluorescence produced by a fluorophore will exponentially decay over time. The fluorescence lifetime is the average time which an excited fluorophore remains in an excited state before returning to the ground state. This time is short-lived, lasting between  $10^{-15}$  and  $10^{-9}$  s. The process whereby the fluorophore returns to the ground state following excitation occurs in a first order kinetic process. The decay of the excited state of a fluorophore to the ground state can be expressed in the equation;

$$I_{(t)} = I_{(0)}e^{-t/\tau} \quad \text{Equation 1-7}$$

Where,  $I_0$  is the intensity of fluorescence at excitation,  $\tau$  is the fluorescence lifetime, and  $t$  is time. Fluorescence lifetime,  $\tau$ , is defined as the time for the initial fluorescence intensity,  $I_0$ , to decay by  $1/e$ , (approximately 36.8%). The excited fluorophore may return to the ground state by various and competing pathways of de-excitation (Noomnarm & Clegg 2009; Lakowicz 2006). These pathways include, but are not limited to fluorescence, non-radiative decay, quenching and Förster resonance energy transfer (FRET). Each pathway of de-excitation,  $s$ , exhibits an associated rate constant, or  $k_s$ . As such, the rate constant of each pathway is the probability per time unit that the molecule will return to the ground state through this pathway. As such, the fluorescence lifetime can be determined by the following equation;

$$\tau = \frac{1}{k_r + k_{nr}} \quad \text{Equation 1-8}$$

Where,  $k_r$  is the sum of the radiative processes, and  $k_{nr}$  is the sum of non-radiative processes. The fluorescence lifetime is an intrinsic molecular property and therefore unaffected by differences in concentration. However, the fluorescence lifetime may be influenced by the environment it exists in.

A major advantage of fluorescence lifetime imaging is that fluorescence lifetime will not change with variations in concentration of the fluorophore used and therefore, it is an ideal method for the detection of local environments within cells, including pH and other ion concentrations, redox potential, oxygen saturation and temperature. In fluorescence, following excitation, a small amount to the absorbed energy is dissipated as heat. The remaining energy is emitted as a photon. The fluorescent light exhibits a typical spectra but is also emitted with a characteristic time constant, i.e. the fluorescence will decay at a set rate (fluorescence decay rate) (Lakowicz 2006).

### **1.16.3 Fluorescent Molecular Probes**

The use of fluorescent molecular probes (fluorophores) in biomedical research is widespread and continues to gain popularity due to their sensitivity, versatility and quantitative capabilities. The fluorescent output of a fluorophore depends on the efficiency with which it absorbs and emits photons, and the ability to undergo repeated excitation/emission cycles.

## **1.17 Fluorescence-Based Microscopy Techniques**

Fluorescence, the emission of light following molecular excitation with light of a higher frequency, is an important tool in biological sciences. It is exceptionally sensitive, allowing detection of a single molecule. Although some specimens may possess autofluorescence as a result of their chemical composition, fluorescent probes (fluorophores) may be applied to facilitate fluorescence. Detection of fluorescence may be observed through the use of a number of microscopy techniques, each with its own applications. These fluorescent microscopy techniques include; epifluorescence microscopy, confocal laser scanning microscopy, two-photon molecular excitation-based imaging and fluorescence lifetime imaging microscopy.

### **1.17.1 Epifluorescence Microscopy**

Microscopy utilising fluorescence is one of the most widely used imaging techniques in biological sciences. Light of a specific wavelength is used to excite the specimen and fluorescence is observed either through the microscope's eyepiece or by a detector allowing visualisation on a computer monitor (Figure 1.25). The fluorescence emission is separated from the excitation light through the use of a spectral emission filter (Figure 1.26).

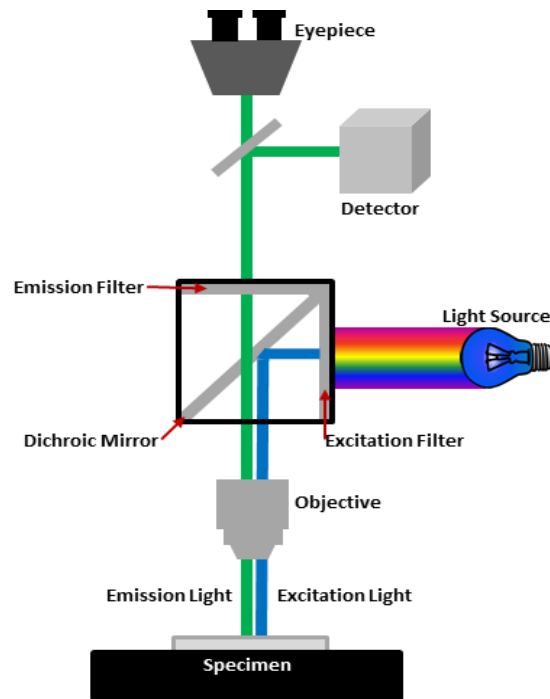


Figure 1.25 Schematic of a typical fluorescence microscope.

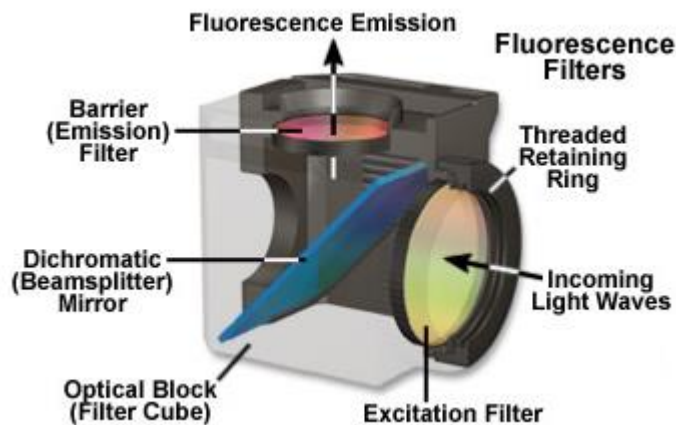
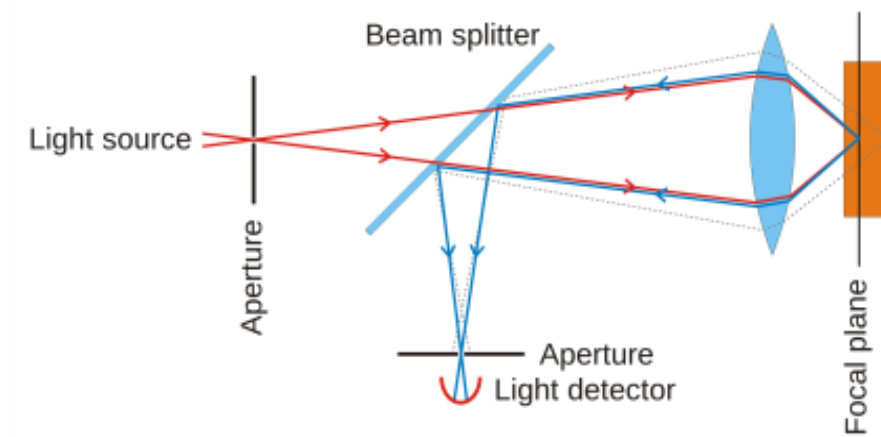


Figure 1.26 Cut away diagram of a filter cube used in fluorescence microscope (Leica Microsystems).

### 1.17.2 Confocal Laser Scanning Microscopy

Confocal laser scanning microscopy (CLSM) is an optical imaging technique which allows the acquisition of high-resolution images with depth penetration and selectivity (Pawley 2006). It often utilises fluorescence. An advantage of CLSM in the visualisation of biofilms is that they are able to be visualised in a naturally hydrated

state. In laser scanning microscopy, the laser is raster-scanned across the specimen at a particular plane. Confocal laser scanning microscopy allows depth discrimination and improves spatial resolution within the plane of focus. This is achieved by forming the image through the same scanning optics used for illumination. Additionally, a pinhole aperture placed in front of the detector acts as a spatial filter to select emission from the plane of focus and excludes out-of-focus emission from reaching the detector (Wilson 1984) (Figure 1.27). The fundamentals of fluorescence microscopy are; excitation of the specimen at the appropriate wavelength and selection of the emission light so that only emitted light is observed or detected.



**Figure 1.27** A schematic of a typical CLSM. Laser light (red line) travels through an objective aperture, which removes light of unwanted wavelength. The light continues through a dichroic mirror allowing light of the excitation wavelength (CC BY 2.0).

### **1.17.2.1 Point Scanning Illumination (Raster-Scanning)**

Raster scanning is a technique used to generate images by scanning in a line-by-line manner. To obtain each image, a laser light of the excitation wavelength is passed across the image in the x-axis before moving one position in the y-axis and travelling across the image again.

### ***1.17.2.2 Elimination of out-of-focus emitted light in confocal laser scanning microscopy***

As excitation light with sufficient energy to cause single-photon excitation travels through the specimen, molecular excitation will occur where that energy is achieved. This results in excitation in out-of-focus areas both above and below the point of focus (Figure 1.28). In order to obtain high-resolution images, elimination of the out-of-focus light is necessary. High-resolution images are obtained by acquiring emitted light from the focal plane and rejecting out-of-focus light (Figure 1.29). This can be achieved through the use of an adjustable pinhole aperture situated in front of the photodetector. The pinhole aperture is typically set to or slightly below 1 Airy unit, eliminating the diffraction rings and resolution-limiting wave interference. Due to the nature of single-photon fluorescence, excitation occurs along the light path creating a large amount of out-of-focus light. The pinhole aperture is used to eliminate out-of-focus emission and allow optical sectioning.

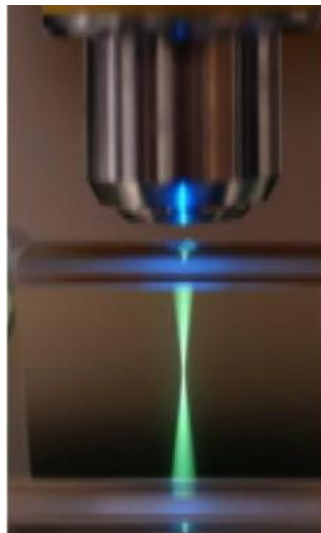


**Figure 1.28 Conventional (single-photon) molecular excitation demonstrating out-of-focus fluorescence emission. (Image credit: Steve Ruzin)**

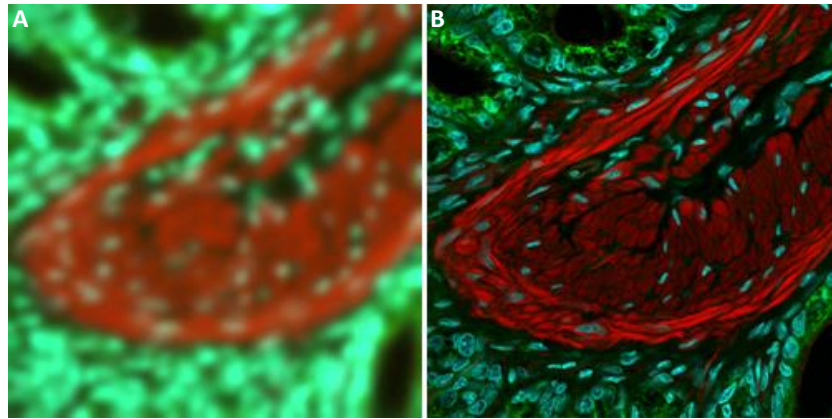


**Figure 1.29** Images demonstration a comparison of image resolution. A) shows a lack of resolution caused by out-of-focus fluorescence emission. B) shows an improvement to image resolution by blocking out-of-focus light through the use of a pinhole aperture (Image credit: University of Texas CC BY 2.0)

Light travels through the objective lens which focuses the light onto the specimen. Laser light is directed onto the specimen. Due to the nature of single-photon fluorescence, fluorescence occurs along the light path resulting in a large amount of out-of-focus light (Figure 1.27). The emitted fluorescent light and out-of-focus exits the specimen and is deflected by the dichroic mirror. Out-of-focus light is blocked by the pinhole aperture. The light is collected onto a sensitive photodetector, often a photomultiplier tube (PMT) or an avalanche photodiode (APD). The photodetector converts the light signal into an electronic signal. A dichroic mirror is a device that will allow light of a certain wavelength to pass while light outside of this wavelength is reflected away. As fluorophores are excited at one wavelength and emit at another they can be selected as appropriate.

### **1.17.2.3** *Optical sectioning*

One of the main capabilities of CLSM is the ability to obtain images at varying planes in the z-axis, a technique called optical sectioning. Following images being obtained at differing planes, a three-dimensional rendering of the specimen can be obtained through the computer modelling software.

#### 1.17.2.4 The Effect of Numerical Aperture

The ability to gather light and resolve fine specimen detail at a fixed object distance, through a specific medium, is referred to as the numerical aperture (NA) of an objective lens. Following excitation, image-forming light waves pass through the specimen and enter the objective in an inverted cone. A longitudinal slice of the cone of light shows the angular aperture, a value that is determined by the focal length of the objective (Figure 1.30).

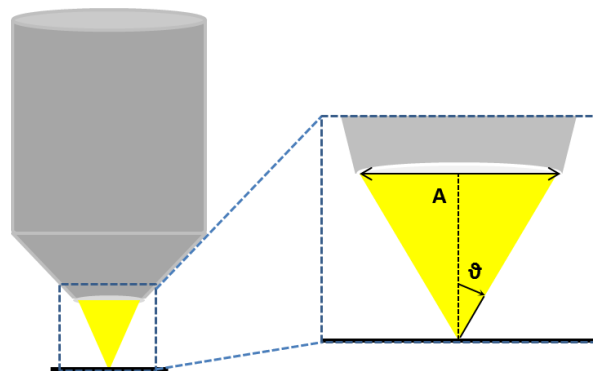


**Figure 1.30** The numerical aperture of an objective lens. **A** is the aperture of the objective lens and  $\vartheta$  is the one half the angular aperture.

$$NA = n \sin(\vartheta) \qquad \text{Equation 1-9}$$

Where, **NA** is the numerical aperture, **n** is the refractive index of the media through which imaging is occurring and  $\vartheta$  is  $\frac{1}{2}$  the angular aperture.

The shortest distance between two objects, able to be distinguished by an observer, recording device or detector as distinct entities is referred to as resolution, i.e. the two objects are resolved. The resolution of an optical system can be somewhat subjective as, at high magnification, two objects may not be clear but are able to be resolved. The resolving power of a microscope system is governed by the objective lens, specifically the numerical aperture (NA). The greater the NA of the objective, the greater the resolution. Resolution can be calculated from the following equation;

$$r = 0.61\lambda/NA \quad \text{Equation 1-10}$$

Where,  $r$  is the resolution,  $\lambda$  is the wavelength of the light, and  $NA$  is the numerical aperture. For example; the resolution of the objective lens with an  $NA$  of 0.80 and excitation wavelength of 488 nm will be limited to approximately 372 nm, and the same lens at 543 nm will be limited to approximately 414 nm.

#### 1.17.2.5 *The effect of diffraction on resolution*

The resolution of a microscope may be limited by a number of reasons including lenses imperfections or system misalignment. However, diffraction plays a fundamental role in the level of resolution of any optical imaging system (Born & Wolf 1999). The resolution of a system is dependent upon the wavelength of the light being observed, and the numerical aperture of the objective lens through which that light is being observed. The visualisation of structures with microscopes smaller than the wavelength of the incident light is difficult due to the Abbe diffraction limit. Light with wavelength,  $\lambda$ , traveling in a medium with refractive index,  $n$ , and converging to a spot with half-angle,  $\theta$ , will make a spot with radius  $d$ . In Equation 1-11, we see that the numerical aperture is equal to the refractive index,  $n$ , multiplied by the sine of the half-angle,  $\theta$ . Therefore;

Abbe resolution in the x,y-axis;

$$d_{x,y} = \frac{\lambda}{2NA} \quad \text{Equation 1-11}$$

Abbe resolution in the z-axis;

$$d_z = \frac{2\lambda}{NA^2} \quad \text{Equation 1-12}$$

### 1.17.3 **Two-Photon Excitation Microscopy**

Two-photon molecular excitation microscopy is possibly the most important advance since the introduction of confocal imaging in the 1980's (Diaspro et al.

2005). Similar scanning optics to confocal imaging systems is used for two-photon molecular excitation microscopy with the addition of an ultrafast pulsed laser. The femtosecond pulse obtained with newly developed laser systems has been used to improve the time-resolution of lifetime imaging (König et al. 1996; French et al. 1997; Sytsma et al. 1998; Straub & Hell 1998; Peter & Ameer-Beg 2004). The confinement of absorption to the focus in two-photon molecular excitation has also been exploited in photodynamic therapy (Bhawalkar et al. 1997; Fisher et al. 1997; Wachter et al. 1998; Kim et al. 2007). The first applications of two-photon molecular excitation to fluorescence microscopy were presented at the beginning of the 1990s by Denk and colleagues (Denk et al. 1990), who demonstrated that images with excellent optical sectioning, could be obtained with minimal detrimental effect on living cells. The development of commercially available mode-locked lasers, with high peak-power femtosecond pulses and repetition rates around 100 MHz was then the trigger for a fast uptake of the multi-photon method in biology (Spence et al. 1991; Curley et al. 1992; Fisher et al. 1997).

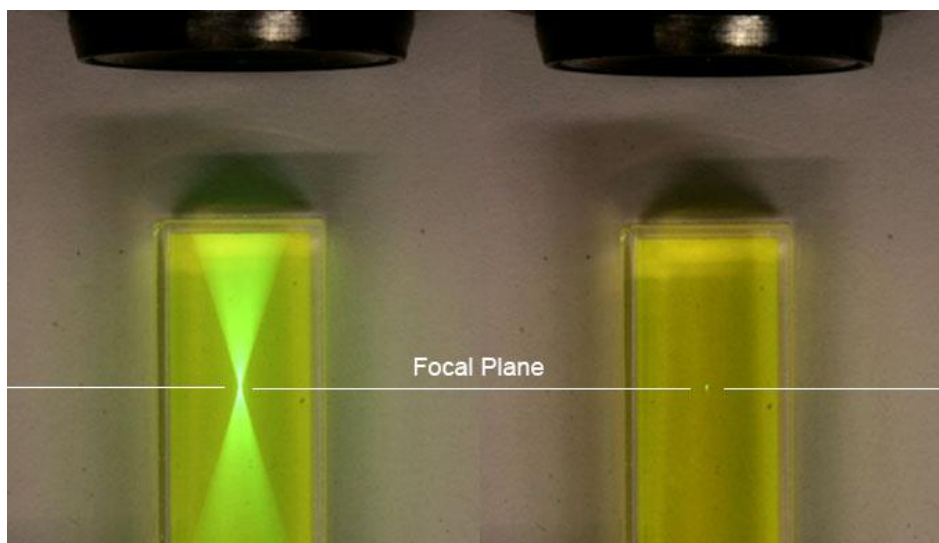


**Figure 1.31** Fluorescent emission as a result of single-photon excitation (left) and two-photon excitation (right) (Cornell University CC BY 2.0).

#### **1.17.4 Two-Photon Molecular Excitation Scanning Microscopy**

Two-photon molecular excitation scanning microscopy is a technique which incorporates multiphoton molecular excitation with scanning microscopy. It offers an alternative to confocal laser scanning microscopy and deconvolution microscopy with a number of distinct advantages. These include improved depth penetration allowing the visualisation of thick biological specimens. Also, as a result of the higher wavelength excitation light (near infra-red) cell damage is minimised. In fact, it has been demonstrated that, using the technique to visualise the development of hamster embryos, the embryos survived to reach full-term with no detrimental effect (Centonze 2002; Lin et al. 2003).

#### **1.17.5 Fluorescence-Lifetime Imaging Microscopy**

FLIM is an imaging technique in which the duration of the excitation event, and not the emitted fluorescence wavelength or intensity, is measured. Since the commercial introduction of FLIM in the 1990's, it has initiated a breakthrough in biomedical imaging (Gadella et al. 1993). FLIM shares many similarities with CLSM. Both offer optical sectioning capabilities, and use a laser to scan in a raster (line-by-line) pattern to produce an image. The fluorescence lifetime is determined at each spatial coordinate (x, y and z) of the specimen. The measurements are then built into an image based on the differences in decay rates. FLIM has been used for the mapping of fluorescence lifetimes of fluorophores in living cells (Y. Sun et al. 2011; Tadrous 2000; Lin et al. 2003) and tissues (Hille et al. 2008) in addition to biofilms (Gerritsen & de Grauw 2000; Hunter & Beveridge 2005). The major advantage of FLIM lies in the fact that, unlike in intensity-based measurements, the fluorescence lifetime is an inherent property and is unaffected by variations in fluorophore concentration, light path distance, sample thickness or photobleaching. Fluorescence lifetime may however be affected by the environment in which the fluorophore resides. When a fluorophore alters its structure as a result of changes in an environmental parameter, e.g. pH, the fluorescence lifetime may vary in a predictable manner. This allows the determination of that parameter. Therefore,

each fluorophore molecule within a heterogeneous environment will decay at a different rate. The differences in fluorescence lifetime are produced as a result of the transfer of energy between the excited fluorophore and its environment. These interactions result in predictable changes in the fluorescence lifetime (Lakowicz 2006). When a fluorescent molecule is excited, energy is lost through a variety of radiative (e.g. the emission of a photon,  $k_r$ , and non-radiative (e.g. vibrational relaxation or internal conversion,  $k_{nr}$ ), processes. Each of these processes occurs with a certain probability, characterised by the decay rate constant,  $k$ . The average duration ( $\tau$ ), referred to as average fluorescence lifetime or simply lifetime, for a set of molecules to decay from one state to another is inversely proportional to the rate of decay;

$$\tau = 1/k \quad \text{Equation 1-13}$$

As fluorescence decay is influenced by both radiative and non-radiative processes, this equation can further be expressed as;

$$\tau = \frac{1}{k_r + k_{nr}} \quad \text{Equation 1-14}$$

FLIM is particularly attractive when utilised in conjunction with multiphoton excitation. Multiphoton excitation is a non-linear process which occurs when two or more photons of lower energy, and therefore longer wavelength are simultaneously absorbed within a single quantum event (within  $10^{-16}$  s). The two photons provide a cumulative energy sufficient to raise the fluorescent molecule to an excited state. Each of the two photons possesses approximately half the energy required to excite the fluorophore. Two-photon excitation occurs at longer wavelengths than single-photon excitation, often in the near-infrared (IR) range, i.e.  $\lambda$  700 nm to 1 mm. Due to the greater energy required, the likelihood of the process occurring at visible wavelengths is rare (Denk & Svoboda 1997). Because two photons are absorbed during the excitation of the fluorophore, the probability for fluorescent emission from the fluorophore increases quadratically with the excitation intensity, such that;  $1P(\lambda_{ex}) \propto I$ ,  $2P(\lambda_{ex}) \propto (I)^2$ ,  $3P(\lambda_{ex}) \propto (I)^3$ , etc. Where,  $I$  is the fluorescence

excitation intensity. Therefore, a much greater amount of two-photon excitation is generated where the laser beam is tightly focused (Figure 1.31). This phenomenon is observed in Figure 1.31, where it is compared to single-photon molecular excitation and the generation of out-of-focus light.

#### **1.17.6 Time-Correlated Single Photon Counting**

The measurement of fluorescence lifetime is determined using one of two methods; time-resolved and frequency-resolved. In time-resolved fluorescence, the fluorescence lifetime is directly measured upon excitation of the sample with a short pulse of light. The intensity of the resultant emission decays exponentially over time. Time-correlated single-photon counting (TCSPC) is a sensitive technique used to determine fluorescence lifetimes. TCSPC is considered to be the most sensitive technique to determine fluorescence lifetime values. Measurements are unaffected by fluctuation in excitation source intensity. The technique measures the time between excitation and the detection of a single-photon with very high precision and picosecond resolution. TCSPC uses signals produced by high repetition rate optical signals and high gain detectors. TCSPC measures single emitted photons following a periodic and repetitive excitation. The process commences when the TCSPC module receives an excitation scan clock signal from the scanning unit attached to the microscope. In the event of fluorescence occurring, the measurement is ceased by a photon reaching the detector. The TCSPC module acquires information about the detection time and the detector channel (Figure 1.32). The expired times are recorded in the appropriate time 'bin' and possess discrete probability, Poisson distribution. The measurements are repeated numerous times, often in the 10,000's. The fluorescence lifetimes detected resemble an exponential decay curve for that fluorophore, within that environment displayed within the pixel of that image. From the exponential decay curve, the fluorescence lifetime can be calculated. This fluorescence decay, the decay for an excited fluorophore to return to its ground electronic state, follows the equation;

$$I_t = I_0 e^{-t/\tau} \quad \text{Equation 1-15}$$

Where,  $I_0$  is the intensity at excitation (time = 0) and  $\tau$  is the fluorescence lifetime. The fluorescence lifetime can be termed as the time for the exponential decay to reach  $1/e$ , or approximately 36.8% of the initial intensity.

A consideration when employing TCSPC is an effect termed 'photon pile-up'. When a detector detects a photon during an excitation incident the detector requires time to reset prior to detecting the next photon. This 'dead time' can be greater than the repetition rate of the excitation laser (Phillips et al. 1985). Therefore, in the unlikely event of greater than one photon is emitted in a single excitation event being detected in a single event, only the first photon is recorded. Furthermore, due to the dead time duration, a photon emitted in the next event to a photon being detected may also not be detected. These events may result in two outcomes; the average fluorescence lifetime may be falsely shorter and/or the mono-exponential decay curve may become bi-exponential, with a shorter component. However, this can be overcome by ensuring that the count repetition rate does not exceed approximately 10% of the excitation rate and the probability of detecting greater than one photon can be neglected (Becker et al. 2004).

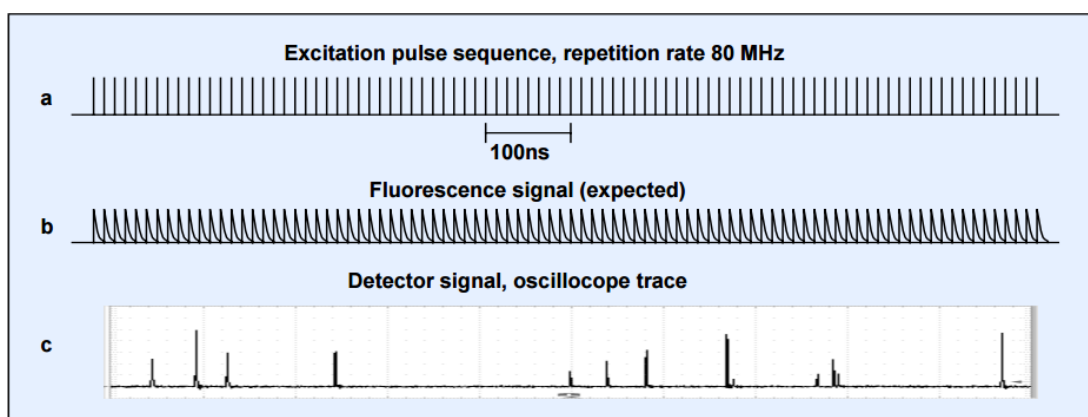


**Figure 1.32** Detector signal for fluorescence detection at 80 Hz laser pulse repetition rate. a) shows the excitation pulse sequence at 80 Hz. b) shows the expected fluorescence signal and fluorescence decay. c) shows the actual detector signal achieved.

The field of imaging using time-correlated fluorescence lifetime was revolutionised by Becker & Hickl when they introduced a technique whereby, not only the duration was recorded, but also the spatial origin. The technique was coined multidimensional TCSPC. The process is repeated numerous times and the number of photons with respect to time are plotted to resemble the fluorescence decay curve from which the average fluorescence lifetime can be calculated (Figure 1.33).

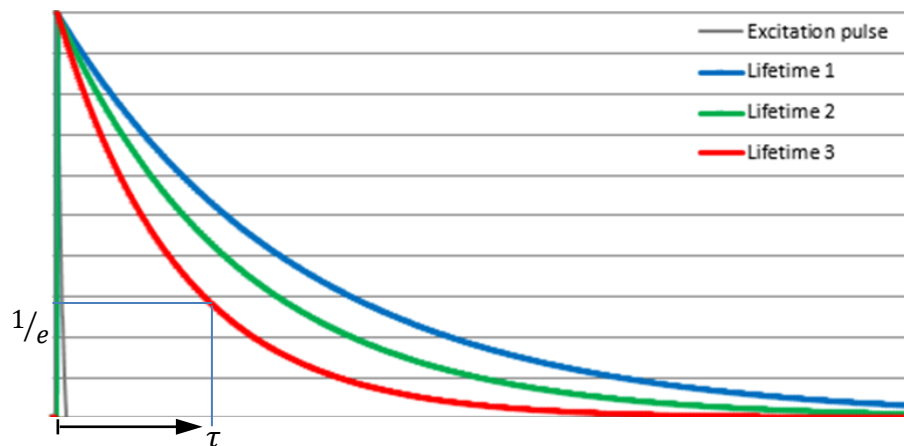


**Figure 1.33 Fluorescence exponential decay curve and determination of fluorescence lifetime.**

Electromagnetic radiation in the near-infrared range not only results in minimal scattering of light in tissues and biofilms but may also fail to excite background autofluorescence (Stutzmann & Parker 2005; Girkin 2003). As a result, background signal is strongly suppressed. Following excitation, the same pathways available to the molecule when excited by single-photon fluorescence are followed. These pathways include relaxation to the ground state with the release of a single-photon of light energy, fluorescence emission (Figure 1.23). However, unlike in single-photon excitation, the fluorescence emission is of a shorter wavelength than the excitation wavelength. Due to this localised excitation, there is no need for a pinhole aperture or any form of computation to remove out-of-focus light. Furthermore, crosstalk from lifetime values at different focal planes is circumvented (Duncan 2007). Two-photon excitation microscopy is considered a superior imaging technique to confocal microscopy as it possesses improved depth penetration, efficient light detection and reduced phototoxicity (Denk et al. 1990). The concept

of two-photon absorption was first described by Maria Göppert-Mayer in 1931 (Göppert-Mayer 1931). She proposed, as a consequence of the Heisenberg uncertainty principle, that one atom or molecule should be capable of absorbing two photons in the same quantum event within  $10^{16}$ – $10^{17}$  s. However, it was not observed until 1961 when Wolfgang Kaiser used laser excitation to excite europium-doped calcium phosphate ( $\text{CaF}_2\text{:Eu}^{2+}$ ) crystals (Kaiser & Garrett 1961). In a Fabry-Perot laser cavity, numerous longitudinal modes satisfy the resonance condition and oscillate independently. This will repeat in accordance with the round trip of the cavity (Figure 1.34). If the phases of each mode are random, the output intensity exhibits random fluctuations, like noise, detrimental to the output signal. The interference between phases may, in fact, be incapable of providing sufficient signal to illicit excitation.

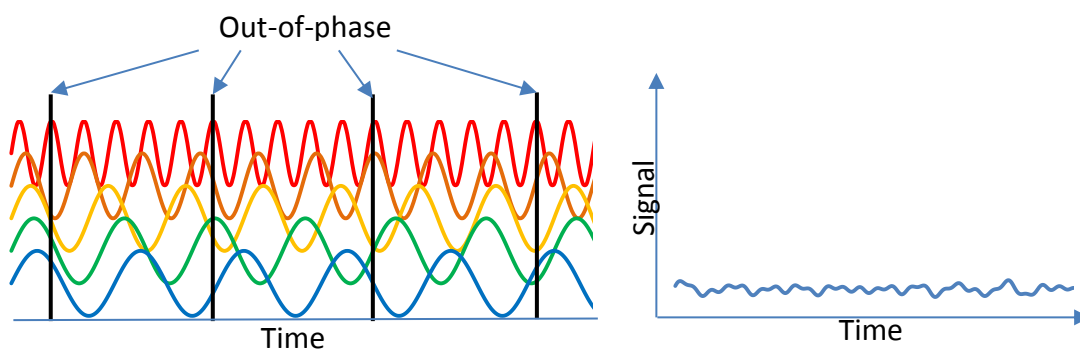


**Figure 1.34** Diagram demonstrating oscillation of random longitudinal modes within a laser cavity and the resulting output signal.

To permit this, a high flux of excitation photons is required generated through the use of a mode-locked femtosecond laser (Figure 1.35). Mode-locking is a method to obtain ultrafast pulses from lasers. By mode-locking, the longitudinal modes are locked. When signals occur in phase, the result is constructive interference occurring periodically such that a train of intense pulses occur with a regular interval rate corresponding to the cavity round-trip, i.e. a few femtoseconds (Figure 1.35). The use of FLIM to determine environmental parameters offers a number of advantages over fluorescence intensity-based imaging methodologies. These include the fact that the fluorescence lifetime is an inherent characteristic, unaffected by detrimental effects which affect fluorescent intensity measurements,

such as photobleaching and optical conditions experienced when using fluorescence intensity (Chen & Periasamy 2004) or the method of detection (Berezin & Achilefu 2010). Furthermore, the use of fluorescence lifetime measurements is not limited by a narrow dynamic range, experienced with fluorescence intensity fluorophores. A considerable amount of work has been conducted using FLIM to measure intracellular parameters, both ratiometric and full spectral measurements (Hakonen & Hulth 2008; Lin et al. 2003; Szmecinski & Lakowicz 1995; So et al. 2000).

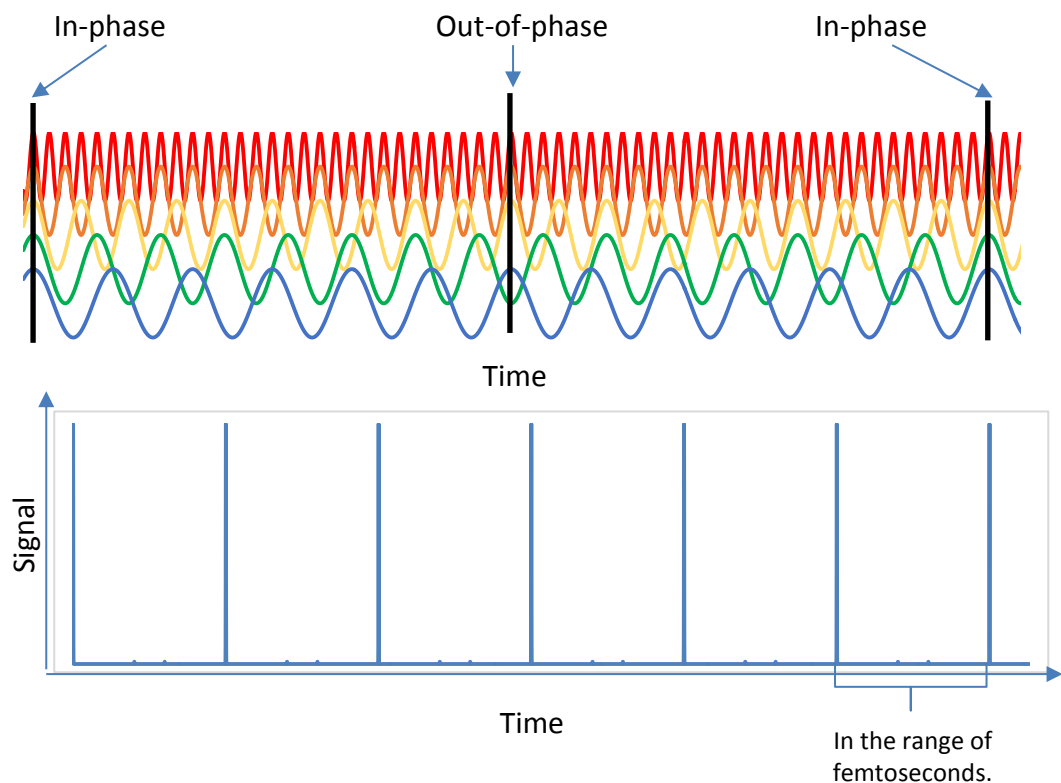


**Figure 1.35** Diagram demonstrating 'locked' longitudinal modes within a laser cavity and the resulting output signal, a train of intense and regular pulses.

## 1.18 Nanosensors

Nanosensors are nanoscopic transducers that detect an environmental measurement (chemical, such as concentration, or physical parameters, such as temperature) and convert this information into a signal that carries information.

Typically nanosensors range from 10 to 100 nm in diameter. One example of nanosensors is probe encapsulated by biological localised embedding (PEBBLE's). PEBBLE's encapsulate a fluorophore sensitive to changes in a specific analyte as well as a second fluorophore which remains unaffected by changes in the analyte of interest, within a biologically inert matrix, such as polyacrylamide (Clark et al. 1998; Lin 2000; Park et al. 2003; Koo Lee et al. 2009) (Figure 1.36). The combination of a sensitive and insensitive fluorophore allows a ratiometric methodology to be employed. In a typical construct, the sensitive fluorophore and the insensitive fluorophore are selected to be excited, and the fluorescence emission detected, at distinct wavelengths. In such a methodology, the ratio of the fluorescent emission intensity is determined. As the fluorescent emission intensity can be affected by differences in nanosensor, and consequently fluorophore, concentration it may be difficult to attribute differences in fluorescent emission to either consequence. The analyte is able to then be analysed using a fluorescent spectrophotometer, wide-field or confocal microscopy. PEBBLE's have been developed to determine a number of both intracellular and extracellular parameters, including pH (Clark et al. 1999b; Hidalgo et al. 2009; Chauhan et al. 2013), oxygen (Koo Lee et al. 2009), calcium (Clark et al. 1999b; Koo Lee et al. 2009), magnesium (Park et al. 2003), and potassium (Clark et al. 1998; Acosta et al. 2012). The matrix of the nanosensors protects biological components from the fluorophores, protects the fluorophores from cellular interferents, and allows the incorporation of multiple fluorophores or other components.

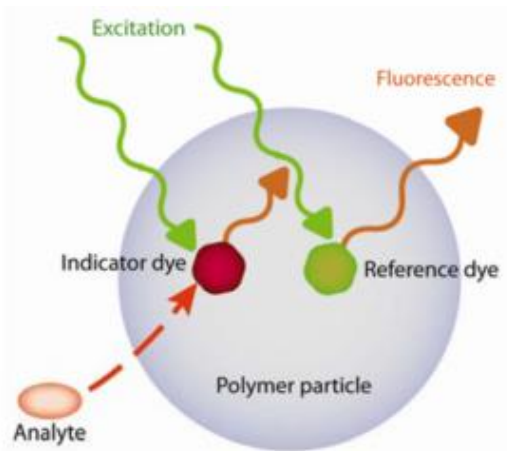


**Figure 1.36 Schematic of PEBBLE construct (Koo Lee et al. 2009).**

## 1.19 Benzo[c]xanthene Fluorescent Dyes

There are a number of commercially available pH-sensitive fluorophores which are able to be used in fluorescence lifetime analysis. These include the benzo[c]xanthene group of dyes, which include the seminaphthorhodafluor (SNARF) dyes and the seminaphthofluorescein (SNAFL) dyes, and 2',7'-bis-(2-carboxy-ethyl)-5-(and-6)-carboxyfluorescein (BCEFC). These pH-sensitive fluorophores possess a similar core structure, consisting of a number of aromatic rings, offering the molecule increased stability and an electron acceptor allowing protonation and deprotonation to occur in response to the presence of hydrogen ions. The chemical structures of the three classes are demonstrated in Figure 1.37.

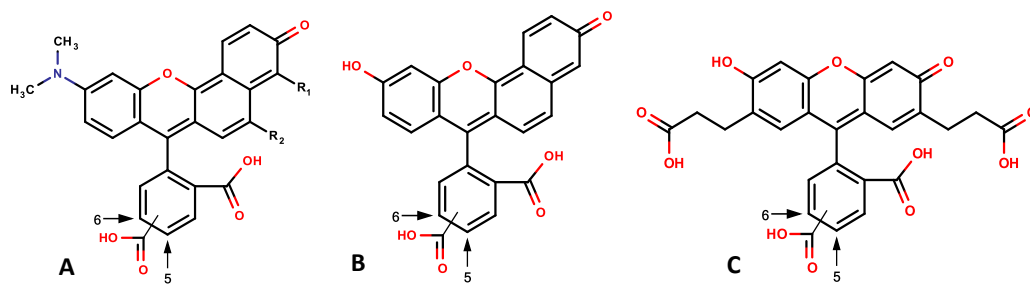
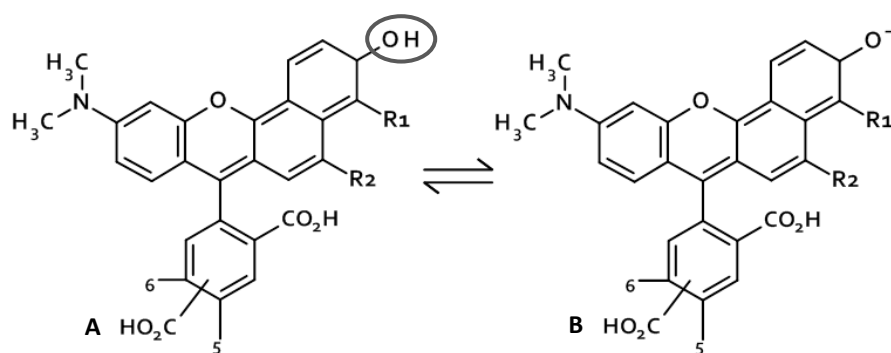


**Figure 1.37** Diagram demonstrating the similarity in chemical structure between A) SNARF B) SNAFL and C) BCEFC dyes.

The dyes exist in two forms, the acid (deprotonated) and base (protonated) forms. These dyes react to the presence of hydrogen ions by altering their emission properties. These altered forms demonstrate distinct fluorescent emission wavelengths. As such the ratio of the two forms produces a spectral shift associated with changes in pH and provides a 'signature' of the pH within the surrounding medium (Brasselet & Moerner 2000; Ribou et al. 2002). The fact that both the acid and base form of the dye is fluorescent permits their use as fluorescence lifetime probes. If only one form of the probe was fluorescent their lifetime would not change with pH, and fluorescence lifetime measurements would not be possible (Lakowicz 2006). However, it is important to recognise that lifetime measurements, like intensity ratio measurements, can be affected by interactions of the probes

with biological macromolecules. The protonation equilibrium equation for the SNARF dyes is demonstrated in Figure 1.38.



Name	R1	R2	pK <sub>a</sub>
Carboxy-SNARF-1	H	H	~7.5
Carboxy-SNARF-4F	F	H	~6.4
C Carboxy-SNARF-5F	H	F	~7.2

**Figure 1.38** Chemical structure of SNARF dyes. A) As pH decreases, protonation of the phenol group occurs. B) As pH increases, this is reversed. The site of protonation is indicated. C) indicates R groups and pK<sub>a</sub> values.

Benzo[c]xanthene fluorescent dyes are a family of dual emission, long-wavelength excitable, pH-sensitive fluorescent dyes which have been utilised in both excitation and emission ratiometric measurements (Whitaker et al. 1991). The family consists primarily of two groups; the seminaphthofluorescein (SNAFL) and the seminaphthorhodafluor (SNARF) dyes. Both families consist of a 'fused ring system'. It is the fused ring structure which actually fluoresces. In other fluorophores, e.g. fluorescein or rhodamine, it is also the fused ring system responsible for fluorescing. The fusion of rings delivers extensive conjugation and the fusion also decreases the chances of non-radiative decay by blocking the vibrational relaxation process. The chemical structure of the SNARF and SNAFL dyes are similar, differing in the substitution of the nitrogen in the 10 position with oxygen, respectively, as demonstrated in Figure 1.39. In their deprotonated state, the fluorophores exhibit a dianionic naphtholate group at the site of protonation. As the hydrogen-ion increases and pH decreases protonation occurs and the naphtholate is converted to

the monoanionic naphthol group (Hunter & Beveridge 2005) (Figure 1.40). The concentration of each form is dependent upon pH of the local microenvironment with protonation/deprotonation occurring at the  $pK_a$ . The protonated and deprotonated forms of both SNARF and SNAFL exhibit distinct fluorescent emission maxima wavelengths, allowing them to be utilised for the determination of pH, particularly through ratiometric applications (Whitaker et al. 1991). Furthermore, the fact that both protonated and deprotonated forms of the probe is fluoresce and demonstrate shifts in fluorescence decay rates allows their use as fluorescence lifetime probes. If only one form of the probe was fluorescent their lifetime would not change with pH, and fluorescence lifetime measurements would not be possible (Lakowicz 2006). However, it is important to recognise that lifetime measurements, like intensity ratio measurements, can be affected by interactions of the probes with biological macromolecules.

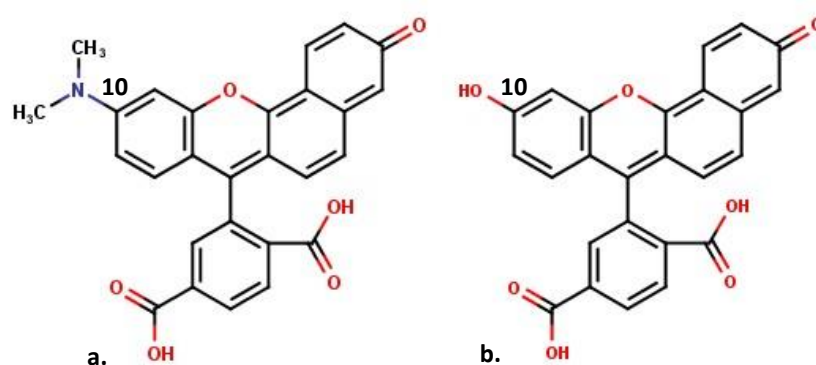
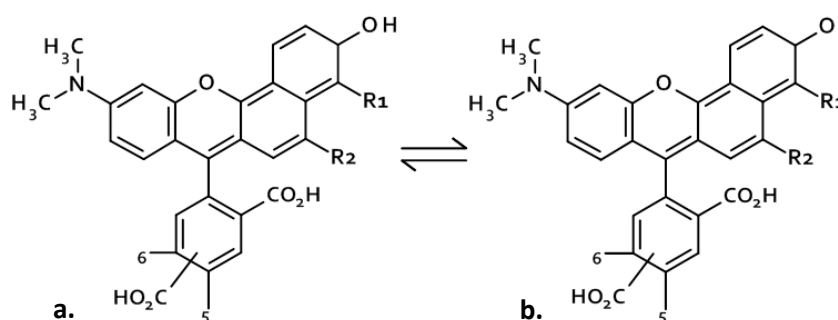


**Figure 1.39** Chemical structures of a. SNARF-1 and b. SNAFL-1, showing the substitution at the 10 position of nitrogen for oxygen, respectively.



Name	R1	R2	$pK_a$
Carboxy-SNARF-1	H	H	~7.5
Carboxy-SNARF-4F	F	H	~6.4
Carboxy-SNARF-5F	H	F	~7.2

c.

**Figure 1.40** Chemical structure of SNARF dyes, demonstrating a. the protonated (low pH) form, exhibiting a monoanionic naphthol group at the site of protonation (blue) and b. the deprotonated (high pH) form exhibiting the naphtholate group.

SNARF<sup>®</sup>-4F 5-(and-6)-carboxylic acid (SNARF<sup>®</sup>-4F) belongs to the seminaphthorhodafluor family of dyes (Whitaker et al. 1991). SNARF<sup>®</sup>-4F is a commercially available, pH-sensitive fluorophore which has been utilised to determine environmental pH through the use of ratiometric (Marcotte & Brouwer 2005; Hunter & Beveridge 2005; Schlafer et al. 2015) and fluorescence lifetime methodologies (Szmecinski & Lakowicz 1993; Szmecinski & Lakowicz 1995; Kaylor 2004; Burdikova et al. 2015). However, the utilisation of multiphoton excitation of the fluorophore, SNARF<sup>®</sup>-4F 5-(and-6)-carboxylic acid, is novel. Multiphoton excitation has been utilised for the closely related fluorophore, 5-(and-6)-carboxy SNARF-1 (Bestvater et al. 2002). This suggests that SNARF<sup>®</sup>-4F 5-(and-6)-carboxylic acid is able to be excited through multiphoton excitation and exhibit a shift in fluorescence lifetime in response to variations in environmental pH. The seminaphthorhodafluor (SNARF) family of pH-sensitive fluorophores were developed by Molecular Probes (Eugene, OR) (Johnson & Spence 2010). The family consists of three dyes. These are SNARF-1 and its fluorinated derivatives, SNARF<sup>®</sup>-4F and SNARF<sup>®</sup>-5F. All three dyes are excited in the visible spectrum and exhibit significant spectral shifts with changes in pH (Johnson & Spence 2010). The addition of a fluorine atom, and furthermore, the location of that fluorine atom significantly alters the pK<sub>a</sub>. The pK<sub>a</sub> of SNARF-1 is ~7.5 and SNARF-5F is ~7.2, which makes them ideal for the imaging of near neutral environments such as the environments in most living cells (Hille et al. 2008). However, the pH observed in dental plaque extends from near-neutral to as low as pH 3.0. Alternatively, SNARF<sup>®</sup>-4F has a pK<sub>a</sub> of ~6.4 which may make this dye more appropriate. One drawback to the use of the SNARF family of dyes is the relatively low quantum yield ( $\phi$ ) (Martinez et al. 2001;

Brasselet & Moerner 2000). The acid free form of SNARF dyes are membrane impermeable (Kaylor 2004). Although, a considerable amount of the work performed pertains to intracellular measurements. To allow this the molecules are conjugated to acetoxymethyl (AM) esters. This esterification protects the carboxylic groups of the dye molecule making the molecule charge neutral and able to cross the cell membrane. Once internalised, esterases cleave the acetoxymethyl groups reverting the dye molecule to anionic species of the fluorophore and entrapping them inside the cell (Silver 2003; O'Connor & Silver 2007). After consulting the literature, the two-photon excitation wavelength was not able to be determined. Imaging of murine kidney and small intestine cells was performed at a wavelength of 740 nm (Murtazina et al. 2007). Furthermore, it would be desirable to determine that the wavelength is optimal as this may vary from instrument to instrument. The two-photon excitation wavelength is, as a rule-of-thumb, approximately double the single-photon excitation maximum ( $\lambda_{ex_{max}}$ ).

## **1.20 Biofilm Models**

In the environment, bacteria rarely find the nutrient-rich utopia available in culture media and preferentially attach to surfaces and form biofilms. Bacteria growing in the biofilm lifestyle differ greatly from those growing as planktonic cells. Biofilms have an open, heterogeneous architecture with the formation of projections and interstitial channels through which bulk fluid can travel (Stoodley et al. 1994). This allows for the transport of nutrients and the removal of waste by-products to and from the biofilm microbiota (De Beer & Stoodley 1995; De Beer et al. 1996). The structure of biofilms can be affected by two factors; flow rate and nutrient supply (Stoodley et al. 1998). When bacteria form biofilm growth rate decreases, complex synergistic and antagonistic interactions occur and a considerable amount of genetic transfer occurs (Roberts & Mullany 2010). To better understand bacteria growing as biofilms, planktonic bacteria cannot provide appropriate information. Therefore, bacteria need to be grown as biofilms using an appropriate model which mimics the natural environmental and growth conditions. The desired outcomes of all biofilm models are; the ability to produce biofilms with minimal variability and to

enable appropriate analysis. This may require the removal of the test substratum to allow analysis (Jones & Bradshaw 1996). Dental plaque is a classic model of biofilm exhibiting projections and water channels. There are a number of well-established biofilm models in use for the study of dental biofilms. The choice of model system selected to produce dental biofilms is dependent on the intended investigation to be carried out. Many of the models available for the growth of biofilms allow for environmental parameters to be adjusted emulating in vivo conditions. Each biofilm model has advantages and drawbacks to their use so have to be selected with care. The use of flow cells allow visualisation and facilitates microscopy, provided that the substrata on which the biofilm is grown is transparent. The flow cell model also allows the effect of flow and sheer forces upon the biofilm to be analysed. Biofilms grown on semipermeable membranes applied to solid media provide a cheap, facile method for the growth of biofilms and allows easy removal for analysis however; the biofilms grown may not reflect natural biofilms. More complex models which emulate the oral cavity allowing the growth of appropriate biofilms include the constant depth film fermenter (CDFF) and artificial mouth. These complex devices allow the regulation of parameters to further mimic the natural environment. These parameters may include the gaseous environment, temperature, nutrient supply. The constant depth film fermenter also removes excess biofilm, much like the action of the tongue, to produce biofilm of adjustable, consistent, uniform depths.

### **1.20.1 Static Biofilms**

Polycarbonate and nitrocellulose membranes provide a flat, thin, smooth and biologically inert substratum upon which to grow bacterial biofilms (Merritt et al. 2005). They allow the diffusion of nutrients from the solid media support through the substratum to the bacterial colony. Nutrient sources are able to be replenished or changed simply by removing the membrane and depositing it on a fresh plate. They allow removal facilitate microscopy. By growing biofilms in this method simple biofilms are produced. Many biofilm systems involve the attachment of bacteria to a surface while bathed in a liquid media. In this method, the substratum upon which the bacteria attach themselves is also the avenue for meeting the nutritional needs

and removing waste. This method is more analogous to growing bacteria on plates than in broth. Colonies can grow much larger because they are periodically relocated to fresh plates and thus a fresh supply of nutrients. One advantage is that the biofilms formed are from clonal growth of the original population of bacteria deposited upon the membrane, i.e. genetically identical to common ancestor cell/s. Liquid cultures allow motile bacteria to invade an aggregation of cells. Attached bacteria have limited ability to detach and migrate or drift from the formed biofilm.

### **1.20.2 The Constant Depth Film Fermenter**

The constant depth film fermenter was developed by Peters and Wimpenny in 1988 (Peters & Wimpenny 1988) and has since been established as an excellent model for oral biofilms (Ready 2002; Hope et al. 2002; Pratten et al. 2003; Deng & ten Cate 2004; Dalwai et al. 2006; Hope et al. 2012; Pratten et al. 2015; Sousa et al. 2016). The CDFE facilitates the production of reproducible bacterial biofilms of a desired depth. It is a complex *in vitro* model providing close control over environmental parameters for the development and maintenance of biofilms. Environmental parameters that can be controlled include; temperature, gaseous environment, nutrient source, substrate and, if required, active ingredients such as antimicrobials. The fermenter consists of a glass housing and two stainless steel plates which are sealed under polytetrafluoroethylene (PTFE) seals (Figure 1.41). The housing has a number of inlet ports which facilitate the removal of pans for analysis, the introduction of inoculum, nutrients and gases and the removal of effluent. The biofilms are grown on a variety of substrata applied to each PTFE plug ( $\varnothing$ : 5 mm) inserted in a PTFE pan ( $\varnothing$ : 20 mm). A constant depth is established by recessing the plug at a defined and desired depth through the use of a precision stainless steel tool. Each pan sits in a turn table, set to be flush with the top of the turn table plate and held in place by a rubber O-ring. Each PTFE pan accommodates 5 plugs and the turn table accommodates 15 pans resulting in 75 individual and reproducible biofilms. Excess biofilm is removed by a set of spring-loaded PTFE scrapers as the plate rotates under the action of a motor. This action mimics the removal of biofilm

by mechanical shear force experienced in the oral cavity. Each pan has a threaded central hole with facilitates the removal of the pan for analysis.

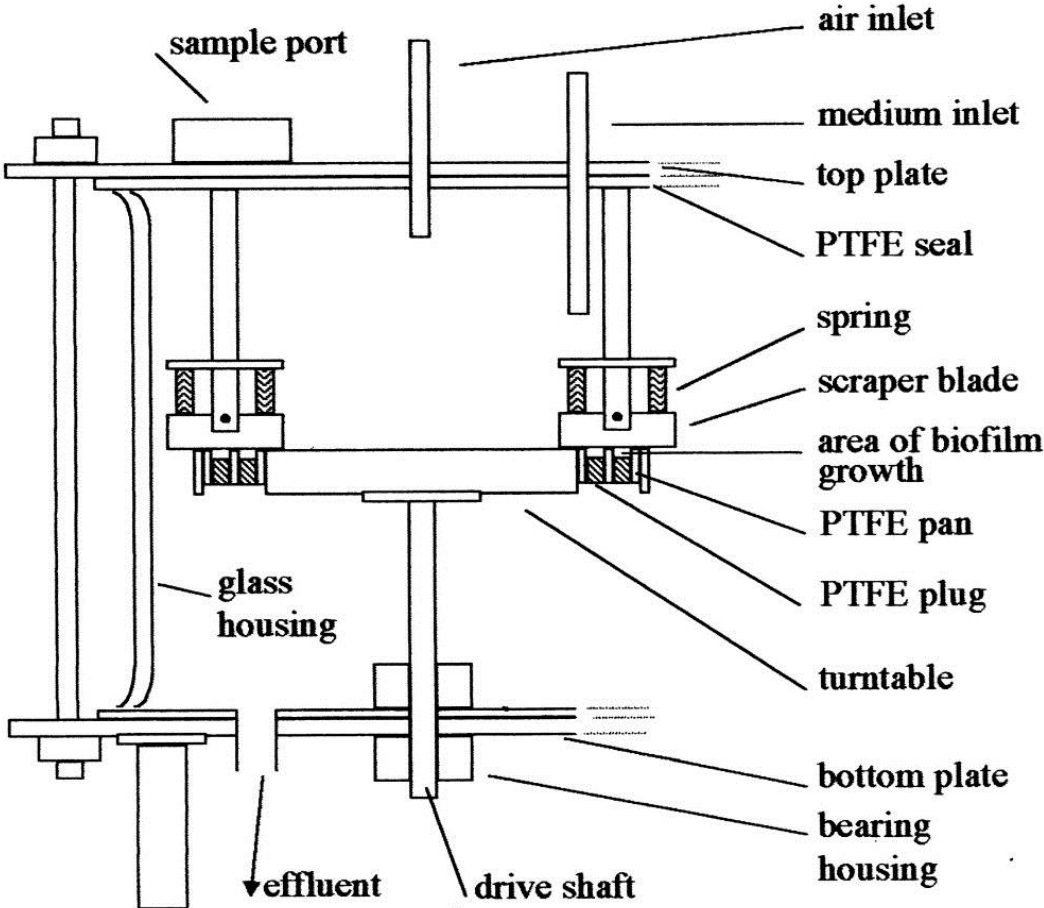
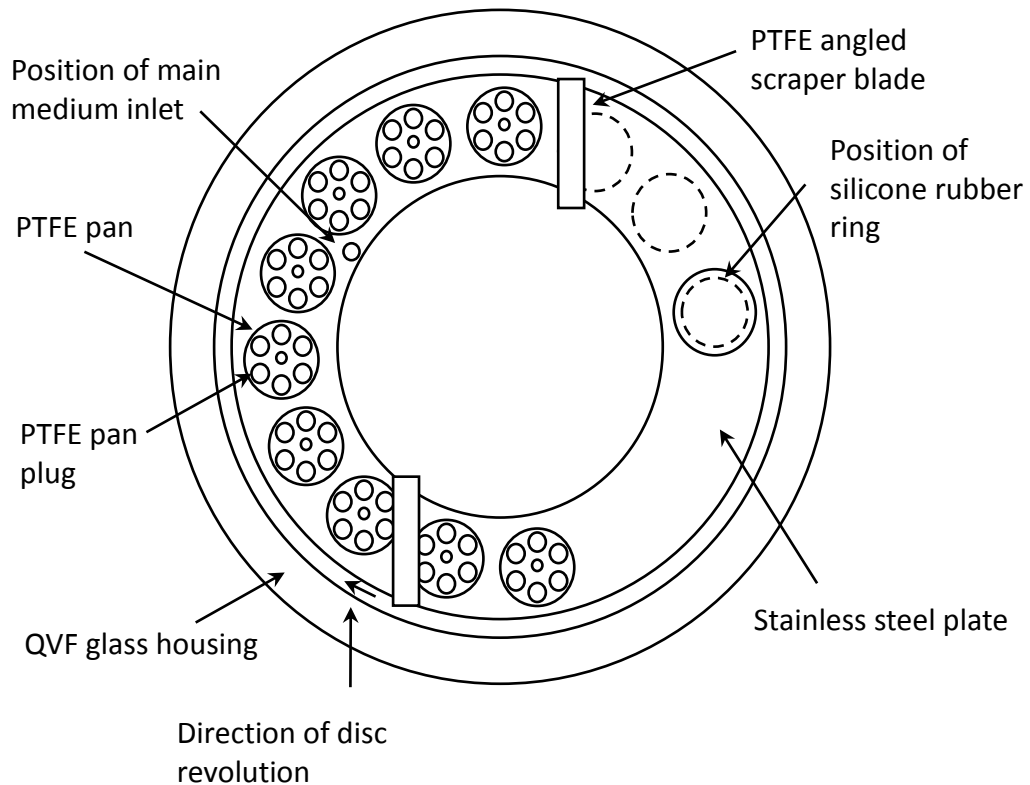


Figure 1.41 Side aspect view and components of the CDFF (Pratten & Wilson 1999).



**Figure 1.42** Top aspect of the turn table of the constant depth film fermenter (Adapted image, used with permission from J Pratten).

## 1.21 Rationale for the Study

Among the fundamental goals of microbial ecology is the development of methods that will enable the detection, identification and enumeration of the important microorganisms in nature, the determination of their physical and chemical microenvironments and the analysis of their metabolic processes and interactions (Revsbech & Jørgensen 1986). With respect to the oral cavity, this pertains to the microorganisms that inhabit that environment and the numerous environmental constraints upon them. These microorganisms are able to survive and thrive in the oral cavity by attaching to all the surfaces herein (Spratt & Pratten 2003), most significantly the dental hard tissues. Development of significant biofilm on sites other than the dental hard tissue is limited by desquamation. The biofilm that forms on the salivary-pellicle coated tooth is a naturally-occurring process providing a benefit to the host by preventing the colonisation of exogenous pathogenic species

(Marsh 1995). However, the production of acid by dental plaque as a result of carbohydrate fermentation has the ability to cause a shift in the microbiota. Extracellular pH is driven by the anaerobic metabolism of fermentable carbohydrates. Following fermentation growth of non-aciduric organisms are suppressed or killed. These microorganisms may be viewed as beneficial to the host. This suppression allows more acidogenic, aciduric organisms, e.g. *S. mutans* and *Lactobacilli* spp. to thrive in the lack of competition. A more cariogenic population results and, over time, a net dissolution of the enamel and the formation of dental caries lesions are established. Due to the complex structure and various metabolic rates and interactions, gradients develop in numerous environmental parameters. Therefore, the ability to measure and visualise hydrogen-ion concentration (or pH) would be highly advantageous to study dental plaque.

At present, the most widely used technologies for the determination of the microenvironments within dental plaque are microelectrodes and colorimetric methods following the removal of dental plaque. The inherent drawbacks of these methods include the fact that, in order to record measurements, the biofilm is, at least, partially disrupted and the course of action for measurement may directly or indirectly affect the result. Also, both methods lack resolution, looking at the biofilm as a whole or a minute portion of the biofilm. The recent development of optical methods has allowed the visualisation of a number of intracellular chemical parameters and may provide methods for the extracellular parameters of complex bacterial communities observed in biofilms. A simple, quantitative method to measure the extracellular pH may improve the study of complicated biological systems such as dental plaque. A majority of techniques currently employed for the determination of extracellular pH within biofilm tend to be invasive (e.g., microelectrodes). Limitations of the former techniques result from the inability to determine spatially-resolved pH gradients without significant damage to the specimen potentially having an effect on the readings. The most commonly used optical techniques use ratiometric fluorescence approaches. Fluorophores sensitive to pH such as SNARF<sup>®</sup>-4F, are excited by a single wavelength of laser light and the

emission measured at two wavelengths. The determination of pH is, following calibration, a result of the ratio of the two emission lifetimes. These values correspond to the discrete spectra of protonated (HA) and deprotonated (A<sup>-</sup>) in solution (bulk dental plaque fluid) (Marcotte & Brouwer 2005; Hunter & Beveridge 2005).

It is predicted that a methods which overcomes many of the drawbacks of the previously described methods would be highly advantageous. The technique would have relevance in industry allowing the assessment of products with desirable properties with respect to increasing or maintaining pH to be analysed on dental plaque in a natural state and without disruption. It may also be utilised to assess to pH potential of the oral microbiota of the patient, in conjunction of the population of the patients microbiota, to observe detrimental synergistic interactions pertaining to the formation of dental caries. The development of an optical technique may have a role in understanding the formation of dental caries lesions in individuals with an absence or low levels of those organisms typically associated with dental caries.

This thesis investigates two optical methods for the determination of pH and formation of microgradients in *in vitro* biofilms mimicking potentially cariogenic dental plaque. **Chapter 2** describes the general materials and methods employed throughout the experiments within this dissertation. **Chapter 3** investigates the acidogenicity of a number of bacterial species commonly found in the oral cavity, and therefore, to determine their cariogenicity. **Chapter 4** pertains to the design and production of a dual-fluorophore, ratiometric, pH-sensitive nanosensor capable of determining pH at levels consistent with those observed in the oral cavity, both at rest and during acid attack as a result of bacterial metabolism of fermentable carbohydrates. The physical and optical properties of the nanosensors are also assessed to ensure that the nanosensors produced possess the desired properties to allow the determination of pH. **Chapter 5** is an assessment of the suitability of the produced and characterised nanosensors for use in a bacterial biofilm model. The nanosensors are assessed for biocompatibility with the bacteria used in the biofilm model. The nanosensors response to changes in environmental pH is also

assessed and calibrated for the determination of pH. **Chapter 6** investigates the suitability of an alternative method for the determination of environmental pH and the formation of distinct microenvironments. A pH-sensitive fluorophore with properties suitable for the determination of pH in the desired range is investigated. Furthermore, an interesting optical technique, multiphoton molecular excitation time-correlated fluorescence lifetime imaging microscopy is employed to determine environmental pH. The fluorophore and technique combination, following optimisation, is evaluated for its response to changes in environmental pH and subsequently calibrated. The biocompatibility of the fluorophore with the bacterial species used is assessed. Moreover, a number of environmental factors which have the potential to have a detrimental effect upon the fluorophore and the technique are examined. **Chapter 7** investigates the application of the two techniques to determine environmental pH upon bacterial sediment and biofilms.

## **1.22 Aims & Objectives**

The aim of this project is to investigate, develop and apply fluorescent optical methods to facilitate the accurate and reliable determination of environmental, extracellular pH within biofilms, mimicking dental plaque. The techniques should be able to allow determination of pH in biofilms in a naturally-hydrated state, with minimal disruption, negating concentration-dependent effects, without detrimental effect upon bacterial inhabitants, and ideally in four-dimensions.

## **Chapter 2    General Materials and Methods**

### **2.1    Reagents**

All chemicals and reagents were purchased from the indicated suppliers and used without further purification or modification, unless otherwise stated.

### **2.2    Media**

All dehydrated media was purchased from LabM (Lancashire, UK) or Oxoid (Hampshire, UK) and reconstituted in deionised H<sub>2</sub>O in accordance with the manufacturer's instructions. Following reconstitution, media was autoclaved at 121°C for 15 min. Following sterilisation, agar was allowed to cool to 50°C. The agar was mixed and poured to sterile petri dishes under laminar flow to maintain sterility and allowed to solidify. With exception, Columbia blood agar was produced by reconstituting Columbia agar in deionised water and sterilising by autoclaving, as stated above. Once cooled, horse blood (E&O Laboratories, Bonnybridge, UK) was added to constitute 5% of the total volume. Each batch of media was assessed for sterility prior to use. Where selective or differential media was used, the media was assessed for appropriate results with control organisms.

### **2.3    Storage of Bacterial Isolates**

All bacteria isolates were obtained from the National Collection of Type Cultures (NCTC) (Public Health England, Wiltshire, UK) or the American Type Culture Collection (ATCC) (LGC Standards, Middlesex, UK). Upon receipt, the isolates were reconstituted and processed as per the provided instructions using sterile brain heart infusion broth (Sigma-Aldrich, Dorset, UK) and plated to Columbia agar (LabM, Lancashire, UK) supplemented with 5% horse blood (E & O laboratories, Bonnybridge, UK) (CBA), produced in house as previously described (Section 2.2). Plates were incubated overnight at 37°C in an aerobic environment, supplemented

with 5% CO<sub>2</sub> or an anaerobic environment (atmospheric gas mixture; 80% N<sub>2</sub>, 10% CO<sub>2</sub>, 10% H<sub>2</sub>), as appropriate. Following incubation, each culture was assessed for purity before inoculating into sterile BHI broth supplemented with 15% glycerol. 1.5 mL of each stock culture was transferred to a screw cap micro tube (Sarstedt, Leicester, UK) and stored at -80°C. Prior to each procedure, bacterial isolates were sub-cultured from stock cultures stored at -80°C onto either CBA or FAA. Inoculated plates were incubated overnight at 37°C in an appropriate atmosphere, as stated above. Cultures were sub-cultured as above for a further two days in order to minimise any detrimental effect of freezing.

## **2.4 Production of Citric Acid-Sodium Phosphate Buffer Solutions**

Citric acid-sodium phosphate buffers were selected as the buffers for these experiments due to the pK<sub>a</sub> of the acid and the range of measurements desired, i.e. the pH values likely experienced within the dental plaque during rest and under acid attack during fermentation of carbohydrates. The pK<sub>a</sub> of citric acid is 4.78 at 20°C (Mohan 2003), and therefore has a useful pH range of 2.6 to 7.6 (Dawson et al. 1986). This is in contrast to lactic acid, possibly a more suitable acid due to its occurrence in dental plaque during fermentation and its role in dental caries, which exhibits a pK<sub>a</sub> of 3.86 (Dawson et al. 1986). Therefore, the useful range is too low for the desired range. Stock solutions (1 L) of 0.1 M (21.01 g/L) citric acid monohydrate (C<sub>6</sub>H<sub>8</sub>O<sub>7</sub>·H<sub>2</sub>O) and 0.2M (28.40 g/L) sodium phosphate dibasic (Na<sub>2</sub>HPO<sub>4</sub>) (Both Sigma-Aldrich, Dorset, UK) were made in sterile dH<sub>2</sub>O. From the stock solutions, citric acid-sodium phosphate buffer solutions were produced for pH values ranging from pH 2.6 to 7.6 in 0.2 pH increments, as stated in Sigma-Aldrich Buffer Reference Centre (Dawson et al. 1986; Sigma-Aldrich © 2016). The buffers were monitored using a Cole-Parmer pH electrode (Cole-Parmer, London, UK) connected to a Corning pH meter 240 (Cole-Parmer, London, UK). The pH meter was calibrated prior to analysis, using 'Colourkey' buffers solutions (VWR, Leicestershire, UK), and the calibration checked following every 10 readings. The pH of the buffers

within 0.2 units of the appropriate pH was adjusted by microaddition of concentrated citric acid or sodium phosphate solution, as appropriate. For those outside this range, a new buffer solution was produced and the adjustment repeated. Over the course of the production of the solutions the buffer solutions were covered with aluminium foil to minimise exposure to light. Stock solutions and buffers were refrigerated and discarded within 1 month of production. The pH value of each buffer was tested prior to use.

## **2.5 Selection of Organisms to Mimic a Dental Caries Biofilm**

For the purpose of the population of the biofilm, the following organisms were selected; *S. mutans* (NCTC 10449), *S. sanguinis* (NCTC 7863), *N. subflava* (ATCC 49275) and *L. casei* (NCTC 13641). Each species is universally found within the oral cavity and in saliva (Marsh 2003; Aas et al. 2005) and have frequently been employed in *in vitro* dental plaque biofilm models (Marsh 1995; Sissons 1997; Lingström 2012). Furthermore, the species selected based on their acidogenicity. *S. mutans* is often referred to as the 'arch-villain' of the initiation and progression of dental caries (Bradshaw & Lynch 2013; Raner 2014). Likewise, *Lactobacillus* spp. has been associated with dental caries due to their high acidogenicity (Brailsford 2001; Takahashi & Nyvad 2011). In contrast, *S. sanguinis* is a primary coloniser binding to salivary receptors in the acquired salivary pellicle (Kolenbrander et al. 2010). *S. sanguinis* is considered a beneficial bacterial species (Jenkinson & Lamont 2005; Gross 2012; Holgerson et al. 2013), and is due to its role in inhibiting the colonisation of cariogenic *S. mutans* (Caufield et al. 2000). *Neisseria subflava* is a commensal of the human nasopharynx (Liu et al. 2015) and have been shown to be one of the predominant species of the hard palate (Aas et al. 2005). They possess low acidogenicity, and are also non-aciduric, unable to withstand pH levels below 4.5 (Bradshaw & Marsh 1998; Kolenbrander 2000). The selection of two acidogenic species and two species which exhibit reduced acidogenicity was to add contrast to

the images of biofilms following exposure to fermentable carbohydrates due to variations in acid production.

## 2.6 Preparation of Static Biofilms

The method was adapted from Growing and Analysing Static Biofilms, Current Protocols in Microbiology (Merritt et al. 2005). A colony biofilm was grown on a semipermeable membrane resting on a solid media. Organisms stored at  $-80^{\circ}\text{C}$  were sub-cultured to Columbia agar supplemented with 5% horse blood and incubated at  $37^{\circ}\text{C}$  overnight in 5%  $\text{CO}_2$ . Following incubation, isolates were checked for purity and subsequently sub-cultured for a further two days to minimise any adverse effects of freezing. Following the third incubation, isolated colonies were selected and inoculated into sterile isotonic saline (0.9% w/v NaCl in sterile  $\text{dH}_2\text{O}$ ). Bacterial suspensions were standardised to  $\text{OD}_{600}$  of 1.0, previously performed by establishing a standard curve of absorbance vs. colony forming unit (CFU) count. Suspensions were diluted 1:30 in physiological saline supplemented with 0.1 mg/mL of pH-sensitive nanoparticles. 50  $\mu\text{L}$  of the suspension was dispensed onto each 5 mm nitrocellulose discs upon a CBE plate and incubated at  $37^{\circ}\text{C}$  for 48 h in an aerobic environment supplemented with 5%  $\text{CO}_2$ . Using sterile forceps, single membranes were placed into sterile petri dishes. Each side of the membranes was sterilised by irradiation of UV light ( $\lambda 254$  nm) for 20 min. The stationary phase bacterial suspensions were diluted in fresh, sterile BHI broth to an  $\text{OD}_{600}$  of 0.5. If the nanosensors suspension was being added prior to incubation, the  $\text{OD}_{600}$  was doubled to 1.0 to allow for the addition of equal amounts of nanosensors. Using sterile forceps, an irradiated membrane was placed, with the shiny side up, onto the solid media. Up to 4 membranes were placed on each agar plate. 5  $\mu\text{L}$  of the diluted bacterial suspension was inoculated on to the centre of each membrane and allowed to dry. The plates were incubated overnight in the upright position, in the appropriate environmental conditions. Following overnight incubation, each membrane was gently removed and transferred to a fresh agar plate using sterile forceps. Plates were incubated further, as required. After the required incubation

period, each membrane was carefully removed and washed in sterile distilled water to remove any planktonic bacteria and debris.

## **2.7 Preparation of Microtitre Plate Biofilms**

The method was adapted from Growing and Analysing Static Biofilms, Current Protocols in Microbiology (Merritt et al. 2005) . Following incubation, isolates were inoculated into 3-5 mL of Brain Heart Infusion (BHI) broth and incubated to stationary phase (approximately 24 h). The liquid cultures were diluted 1:100 with fresh, sterile media. 100  $\mu$ L of the diluted suspension was transferred into each well of a 96-well microtitre plate. The microtitre plate was incubated at the optimal growth temperature for 24 h. Planktonic bacteria and waste were removed by carefully decanting off the supernatant and fresh, sterile media was replenished at 24 h intervals.

## **2.8 Set-up of the Constant Depth Film Fermenter**

The components of the CDFF were prepared in the following order; 1) selection of the appropriate growth conditions (gaseous environment, temperature, etc.), 2) preparation and sterilisation of the CDFF housing, 3) selection, preparation and sterilisation of the peripheral devices, 4) preparation and sterilisation of media (artificial saliva medium, inoculum), 5) set up of the CDFF, and 6) inoculation of the CDFF.

### **2.8.1 Selection of an Appropriate Environmental Temperature**

A temperature of 36°C, representative of the resting human oral cavity (Moore et al. 1999) was selected. The temperature was established by allowing the set up CDFF to acclimatise prior to pellicle and nutrient delivery through housing the device in a large incubator (Model BD 720, Binder, Tuttlingen, Germany). The CDFF was maintained at this temperature for the duration of the experiment, with minimal opening of the incubator.

## 2.8.2 Selection of an Appropriate Gaseous Environment

To reflect the oral environment and an appropriate environment for the growth of the bacterial species selected, an aerobic environment was selected. An aerobic gaseous atmosphere free from contaminants was established and maintained through exposure to the environment via 0.2  $\mu\text{m}$  HEPA-vent air filter (Whatman, Maidstone, UK) attached to the air inlet in the top plate.

## 2.8.3 Selection of an Appropriate Nutrient Source

To simulate human saliva, an artificial saliva medium (ASM) containing mucin was used as the principal nutrient source with porcine gastric mucin was used as the main carbon source. Mucins are large molecular weight glycoproteins characterised by carbohydrate sugars attached via O-glycosidic linkages to serine or threonine (Figure 2.1). These amino acids are the sites of O-glycosylation. A MUC protein backbone typically consists of an  $\text{NH}_2$ -terminal domain, one or more central domains with a high number of tandem repeat domains, and a  $\text{COOH}$ -terminal domain. Numerous O-glycans are attached to threonine or serine residues in the tandem repeat domains. O-glycans exhibit size heterogeneity, which may reflect incomplete biosynthesis during elongation and termination of O-glycans or differences in substrate preferences of various glucosyltransferases at specific serine or threonine sites (Rose & Voynow 2006). Porcine gastric mucin was used as a model substrate for saliva because this mucin possesses the highest similarity in oligosaccharide structure with human salivary mucin (Herp et al. 1979).

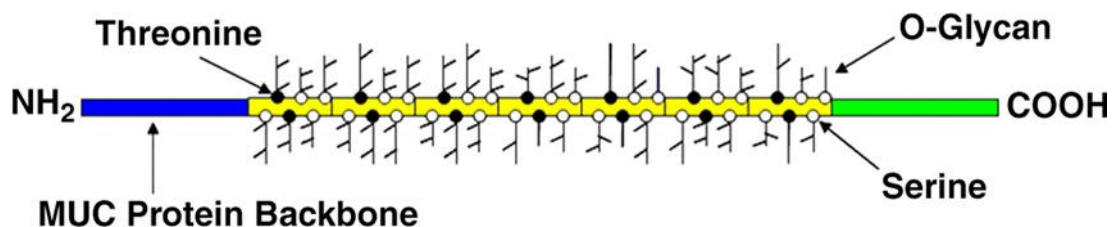


**Figure 2.1** Schematic drawing of a secretory mucin glycoprotein depicting a MUC protein backbone and its O-glycans.

#### **2.8.4 Selection of an Appropriate Biofilm Substratum for the Constant Depth Film Fermenter**

The organisms selected for biofilms growth in the CDFF growth model were selected to reflect dental plaque and were all typical resident dental plaque microbiota. To mimic a natural, physiological tooth surface, dental enamel (bovine dental enamel) may be a more appropriate substratum however, it is more difficult to obtain and discs of BDE would be costlier to produce. Therefore, hydroxyapatite was selected as an appropriate substratum for this model. Hydroxyapatite is an appropriate substitute for dental enamel (Wheeler et al. 1979; Rölla et al. 1977; Ciardi et al. 1977; Ciardi et al. 1987).

#### **2.8.5 Production of Hydroxyapatite Discs for Use in the Constant Depth Film Fermenter**

Hydroxyapatite powder ( $\text{Ca}_{10}(\text{PO}_4)_6(\text{OH})_2$ ) was purchased from Sigma-Aldrich (Leicestershire, UK). The powder was sieved using a vibratory sieve in a step-down manner (1 mm, 200  $\mu\text{m}$ , 150  $\mu\text{m}$ , 106  $\mu\text{m}$ , 75  $\mu\text{m}$ ) to a collection pan. In an attempt to standardise the disc thickness, 0.9 g of sieved hydroxyapatite powder was added to a 5.0 mm diameter pellet press die (GS03060, Specac, Orpington, UK) and the plug added. The powder was compressed to a pressure of  $1.5 \pm 0.2$  t before being extruded. The hydroxyapatite discs were then sintered at a temperature of 1300°C. The produced discs had a thickness of roughly 2 mm. Due to the time-consuming and labour-intensive nature of the process, hydroxyapatite discs (5 mm diameter, 2 mm thick) were purchased from Clarkson Chromatography Products Ltd. (Pennsylvania, USA).

#### **2.8.6 Preparation of the Peripheral Devices**

The peripheral devices include the nutrient source carboy, inoculum Erlenmeyer flask, HEPA-filters, grow back trap, effluent carboy, peristaltic pumps and all tubing and connectors required. To prepare the nutrient source and effluent carboy;

polystyrene tubing was applied to the inlets of the carboy lid and female automatic shut-off quick-connect coupling bodies were connected to the tubing ends. HEPA-filters were added to the air inlet and the tubing clamped to keep the filters dry during autoclaving. The coupling bodies were covered in foil and the effluent carboy was autoclaved at 121°C for 30 min. The nutrient source carboy was prepared as above, replacing the female coupling bodies with male bodies. Prior to autoclaving, the nutrient source (ASM) was prepared as described (Section 2.8.7). The carboy lid was left open, covered in foil and autoclaved at 121°C for 15 min. Following sterilisation, the carboy was removed and allowed to cool to room temperature. At room temperature, 1.25 mL per L of 40% w/v urea (syringe-driven 0.22 µm filter sterilised) was added. To prepare the inoculum Erlenmeyer flask; 500 mL of ASM was prepared (Section 2.8.7). HEPA-filters were added to the gas inlet and both opening (to the environment and the flask) were clamped to keep the filters dry during autoclaving. To the other inlet, a male tubing connector was applied. The rubber stopper was placed ajar to allow for penetration of steam during autoclaving and covered in foil. The tubing connector was covered in foil to maintain sterility following autoclaving. The inoculum bottle was autoclaved at 121°C for 15 min. Following sterilisation, the flask was removed and allowed to reach room temperature. At room temperature, 1.25 mL per L of 40% w/v urea (syringe-driven 0.22 µm filter sterilised) was added. To prepare the peristaltic pumps, ASM was prepared as previously described and run through three peristaltic pumps at a selected speed for a period of half an hour. The speed was adjusted until a flow rate of 30 mL per h was achieved. These pumps and the determined speeds were selected for all future experiments. To connect the components prior to setup, all components were transported to the incubator. A mist of 70% isopropanol was applied to the incubator and closed for a period of 5 min. The incubator was opened and 70% isopropanol was applied to gloves and all surfaces associated with connection. The components were situated to aid connection. The connections were brought together and covered in a Bio-Pure pre-moistened alcohol wipe (Sigma-Aldrich, Dorset, UK), the foil removed and the connection made. When set up, all clamps were removed, where appropriate. Immediately prior to set up completion, the inoculum was removed to a Class II flow hood and 5 mL of an

overnight culture of *S. mutans*, *S. sanguinis*, *N. subflava* and *L. casei* were added to the inoculum ASM, either as a single species or as a microbial consortium.

### **2.8.7 Preparation of an Artificial Saliva Medium Containing Mucin**

Lab-Lemco, yeast extract and proteose peptone were purchase from Oxoid, (Hampshire, UK). Sodium chloride, potassium chloride, calcium chloride and urea and hog gastric mucin (mucin from porcine stomach, type III, bound sialic acid 0.5-1.5 %, partially purified powder) were purchased from Sigma-Aldrich (Dorset, UK). The composition (per litre) of ASM was Lab-Lemco (1 g), yeast extract (2 g), proteose peptone (5 g), hog gastric mucin type III (2.5 g), sodium chloride (0.35 g), potassium chloride (0.2 g), calcium chloride (0.2 g). The dry reagents were weighed and added to the appropriate volume of deionised water and autoclaved at 121°C for 15 min. Following sterilisation, 1.25 mL of 40% w/v urea (syringe-driven 0.22 µm filter sterilised) was added. This formula has previously been used (Dalwai 2008; Wiecek 2015), and is modified from well-established artificial saliva media composition (Coulter & Russell 1975; Pratten et al. 1998).

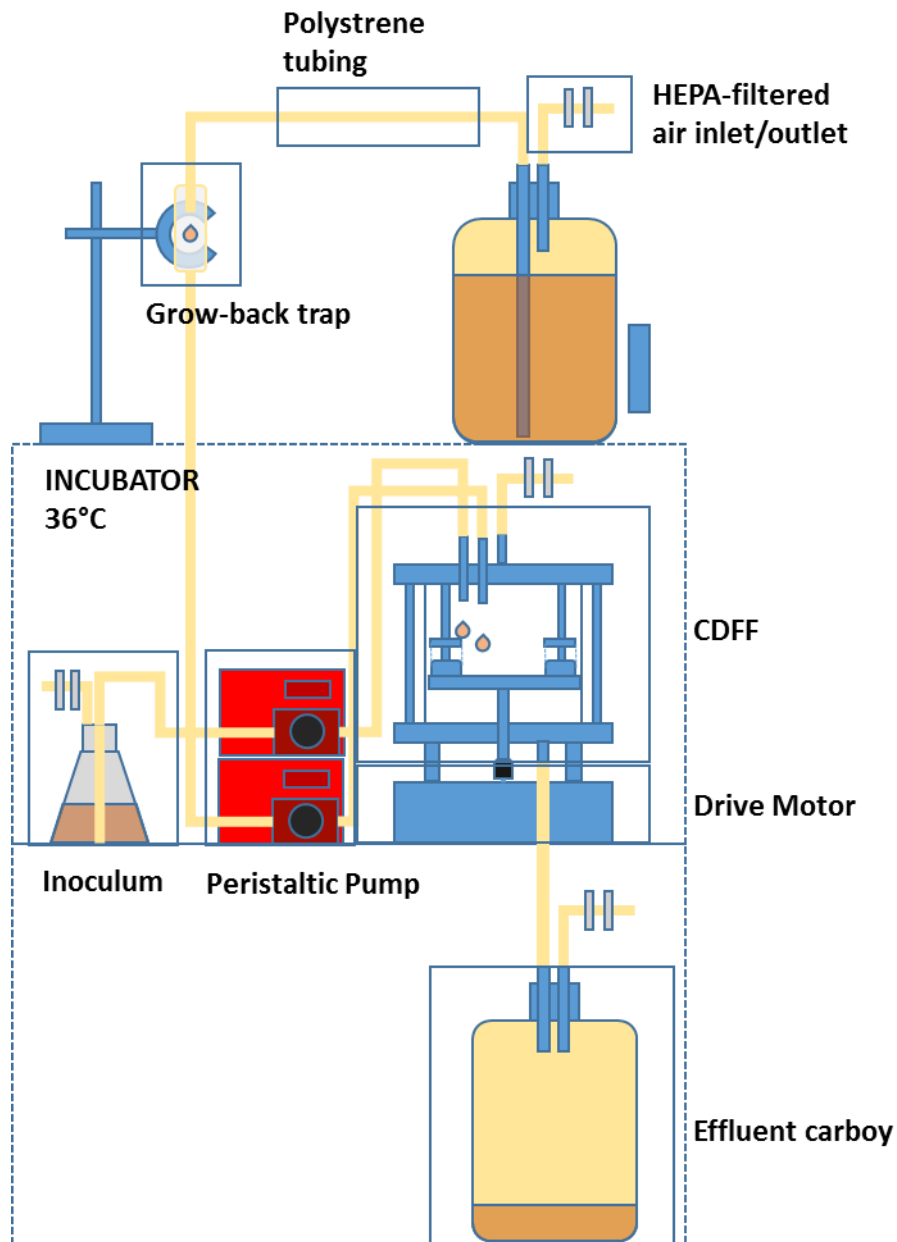


**Figure 2.2** Schematic diagram of the CDFD when set-up.

### 2.8.8 Calibration of the Peristaltic Pump

Approximately 720 mL of saliva are secreted into the oral cavity daily (Bell et al. 1980; Lamb 1991; Guyton 1991; Pratten et al. 1998; Dalwai et al. 2006; Dalwai et al. 2007; Dalwai 2008). In accordance with this amount the desired flow rate through the flow cell was 30 mL/h. To ensure that the flow rate within the system was consistent with the flow rate experienced in the oral cavity, the system was

calibrated. To perform this, the system was allowed to run with artificial saliva through it for a period of 2 h, the amount of waste measured and the flow rate, in rpm, adjusted to fall within the appropriate range. At a speed of 14.0 rpm the amount of effluent produced was 45 mL (22.5 mL per hour) and as such this speed was selected for future experiments.

### **2.8.9 Preparation of the Constant Depth Film Fermenter**

A small amount of high vacuum silicone grease (VWR, Leicestershire, UK) was applied to the top of each plug and PTFE plugs were placed into the pans. A hydroxyapatite disc (Clarkson Chromatography Products, Pennsylvania, USA) was situated upon each PTFE plug and pressure was applied until flush with the PTFE pan. The hydroxyapatite discs were recessed to desired depth of 300  $\mu\text{m}$  through the use of a stainless steel recession tool (Figure 2.3 c). This process is demonstrated in (Figure 2.4). The pans were added to the turn table and set flush through the use of a tamping tool (Figure 2.4). The 300  $\mu\text{m}$  recession depth was selected as representative depth of smooth surface plaque thickness (Main et al. 1984). High vacuum silicone grease was added to the bottom of the glass housing and the glass housing was placed over the turn table and on to the base plate, creating a seal. The above step was repeated with the top of the glass housing and the top plate was added. Two HEPA-filters were added to a length of polystyrene tubing and connected to the air inlet on the top plate. The sections of tubing before and after the filters were closed by a screw clip to facilitate autoclaving. Lengths of polystyrene tubing were added to the various inlets and a female automatic shut-off quick-connect coupling body (Z126519, Sigma-Aldrich, Dorset, UK) was connected. The coupling body was covered in foil and the tubing was clamped in preparation for autoclaving. Tubing was connected to the effluent outlet and a male automatic shut-off quick-connect coupling body (Z126543, Sigma-Aldrich, Dorset, UK). The sampling port was left slightly ajar and the CDF unit was autoclaved at 121°C for 30 min.



**Figure 2.3** CDFF tools including A) tamping tool, B) PTFE pan removal tool, and C) PTFE plug recession tool. (Wiecek 2015).

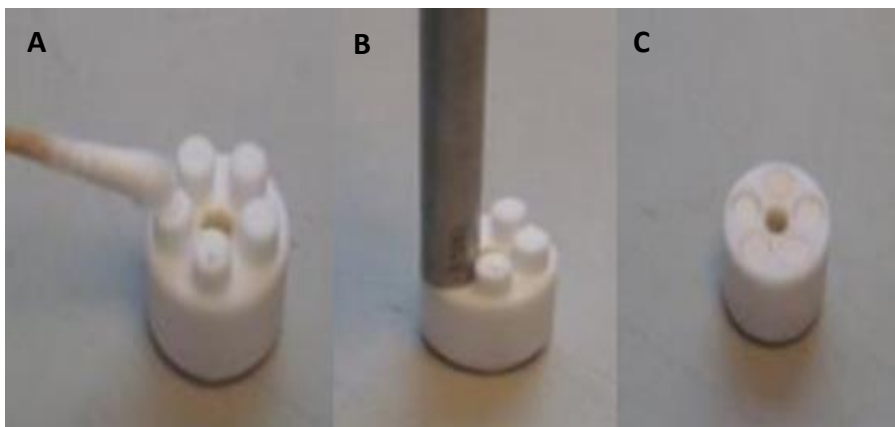


**Figure 2.4** Recession of PTFE plugs and substratum at desired depth using the PTFE plug recession tool (Wiecek 2015).

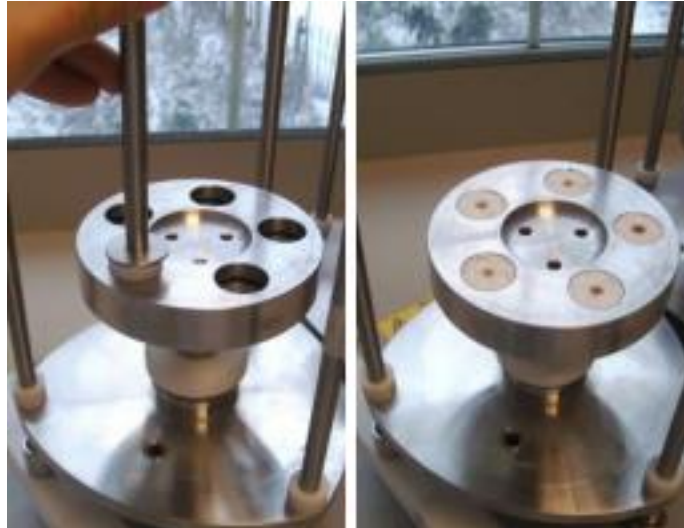


**Figure 2.5** Use of the tamping tool to situate the PTFE pans flush with the turn table (Wiecek 2015).

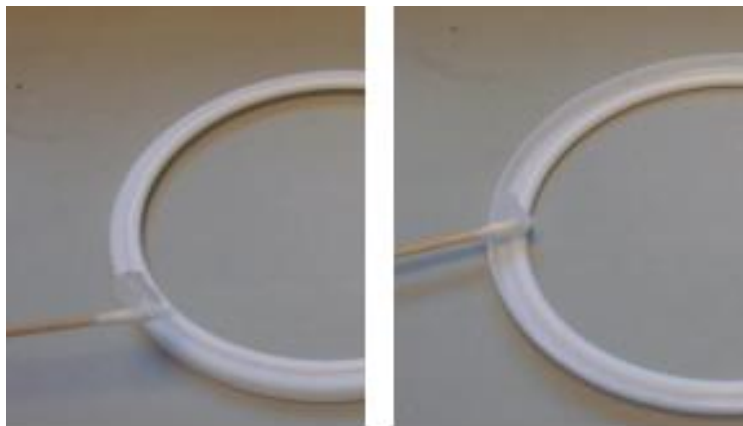


**Figure 2.6** Application of high vacuum silicone grease to each side of the PTFE seals (Weicek 2015).

### **2.8.10 Set-up of the Constant Depth Film Fermenter**

The PTFE pans were prepared by placing a PTFE plug in each hole. A small amount of high vacuum grease was applied to the top of each PTFE pan and a hydroxyapatite disc was placed on top of each plug. The discs were then recessed at the desired depth using the precision recess tool. The pan was placed in the turn table and set flush with a tamping tool. The bottom PTFE seal is applied on both sides with Dow Corning® high vacuum grease (Sigma-Aldrich, Dorset, UK), which

creates an airtight seal. The seal was placed on the bottom plate and the glass housing was placed on the seal. High vacuum grease was applied to both sides of the top PTFE seal and the seal applied to the top of the glass housing (Figure 2.6). The top plate was placed on top of the glass housing and screwed down to create a seal within the CDFF chamber. Silicone tubing was applied to the inlet ports.

### **2.8.11 Preparation of the Inoculum for the Constant Depth Film Fermenter**

BHI Broth (LabM, Lancashire, UK) was produced in accordance with the manufacturer instructions and sterilised by autoclaving at 121°C for 15 min. The media was inoculated with one of the following isolates; *S. mutans*, *S. sanguinis*, *L. casei* and *N. subflava*. The inoculated broth was incubated overnight at 37°C, in an aerobic environment supplemented with 5% CO<sub>2</sub> to an approximate cell concentration of 1 x 10<sup>8</sup> CFU/mL. 500 mL of ASM was prepared as previously described (Section 2.8.7). Immediately prior to set up completion, the inoculum and overnight cultures were transported to a Class II flow hood. 5 mL of an overnight culture of *S. mutans*, *S. sanguinis*, *N. subflava* and *L. casei* were added to the inoculum ASM, either as a single species or as a microbial consortium.

### **2.8.12 Inoculation of the Constant Depth Film Fermenter**

The inoculated ASM was connected to inlet port to the CDFF device, under sterile conditions, and the tubing was run through a peristaltic pump. Sterile nutrient source (ASM) was run for a period of 1 h to produce a salivary pellicle upon the hydroxyapatite substratum. Following the pellicle coating, the sterile artificial saliva flow was ceased by clamping the tube and the flow of the inoculated ASM was commenced by starting the peristaltic pump set to a continuous flow rate of 30 mL/h (0.72 L per day), representative of the normal flow rate of saliva (Bell et al. 1980; Lamb 1991; Guyton 1991; Pratten et al. 1998; Dalwai et al. 2006; Dalwai et al. 2007; Dalwai 2008). This was achieved through use of a peristaltic pump (Watson-Marlow, Cornwall, UK). The inoculum was allowed to run for a period of 2 h.

Following inoculation, the inoculum was disconnected using aseptic technique and the sterile nutrient source (ASM) was recommenced at a flow rate of 30 mL/h. The CDFE was allowed to run for a period of 7 days. Following growth of the biofilms, the biofilms were aseptically removed via the sampling port through the use of the PTFE pan removal tool (Figure 2.3 b) and analysed. After removal, the resultant biofilms were carefully washed with sterile isotonic saline to remove unbound CFU's. The biofilms were removed and placed in a small petri dish for analysis.

# Chapter 3 Investigation of Processes Which Effect the Microbial Ecology of Biofilms Formed in the Oral Cavity

## 3.1 Introduction

The bacteria which inhabit the oral cavity do so by forming biofilm called dental plaque. This dental plaque is associated with two diseases, dental caries and periodontal diseases, encompassing gingivitis and periodontitis. These diseases have both been attributed to shifts in the microbial population as a result of environmental pressure (Marsh 2003; Milicich 2009; Hajishengallis 2014). In the case of dental caries, pH plays a major role in the shift of the population from a 'beneficial' profile of pioneer species consisting predominantly of oral streptococci to a population predominated by acidogenic, aciduric species, such as *S. mutans* and lactobacilli. The beneficial bacteria are non-acidogenic, producing considerably less acid than those organisms associated with dental caries, and aciduric, so are unable to withstand overtly acidic environments or prolonged duration of high hydrogen-ion concentration. When organic acids are produced as a result of fermentation of carbohydrates, the growth of these organisms is therefore suppressed. Provided this acid attack is not prolonged or severe, the microbial homeostasis of the oral cavity is restored. Many of the bacteria that inhabit the oral cavity require a pH around neutral (i.e. pH 7.0) for optimum growth (Section 1.13). Changes in pH levels particularly affect bacterial enzymes (Humphrey & Williamson 2001). The growth of bacteria with respect to pH is defined by three particular points, the minimum and maximum values, at which below and above, respectively, the bacteria are unable to grow. The third point being the optimum level, at which the maximum growth rate is achieved. As a rule of thumb, most bacterial species have a range of growth of approximately 3 pH units. When you consider that pH is measured on a logarithmic scale, 3 pH units equated to a 1000-fold difference in hydrogen-ion concentration between each extreme. The proportions of bacteria are altered as a result of fluctuations of environmental pH (Marsh & Martin 2009). To

investigate the effect of environmental pressures on the oral microbiota, the effect of pH on a selection of organisms in co-culture was performed.

### **3.1.1 Aims and Objectives**

The aim of this chapter is to determine the acidogenic potential of a number of oral bacteria following exposure to fermentable carbohydrates in the form of sucrose.

## **3.2 Materials and Methods**

### **3.2.1 Preparation of Bacterial Suspensions for Fermentation Assays**

Following subculture and incubation, bacterial isolates (*S. mutans*, *S. sanguinis*, *L. casei*, and *N. subflava*) were suspended in sterile non-buffered isotonic saline (0.9 g/L NaCl in H<sub>2</sub>O). Suspensions were standardised to an OD<sub>600</sub> of 1.0.

### **3.2.2 Fermentation Assay 1**

A 500 µL volume of each suspension was added to the wells of a 96-well microtitre plate. A 500 µL volume of 0.2 M (68.46 g/L) sucrose solution was added to half of the cells while sterile non-buffered saline was added to the remaining wells. Plates were incubated for a period of 2 h at 37°C in an aerobic atmosphere. Following incubation, the pH of the suspensions was measured using a Shindengen pHBOY-P2 portable ISFET (ion-sensitive field-effect transfer) pH meter (Camlab, Cambridge, UK). The instrument was calibrated prior to use and the calibration checked following each group of experiment.

### **3.2.3 Fermentation Assay 2**

pH was measured through the use of a pH microelectrode (Lazar Research Laboratories, California, USA), connected to a portable pH/ORP pH meter (6360,

Jenco, California, US). The pH meter was connected to a computer loaded with pH plotter software (Lazar Research Laboratories, California, USA). Prior to analysis, the pH electrode and meter was calibrated using Colour key pH buffers (VWR, Leicestershire, UK). Five mL of a bacterial suspension was added to a sterile flat-bottomed flask, with a magnetic stirring bar in situ. A rubber stopper was applied to the flask. The pH microelectrode was inserted through the rubber stopper and into the bacterial suspension. The bacterial suspension was placed on a magnetic stirrer within an incubator at 37°C. The pH was allowed to settle. Five mL of a 0.2 M sucrose suspension was added to the bacterial suspension and the pH plotter software was started. The pH plotter software was left to record for a period of two hours, at which point the analysis was ceased. The data was exported and transferred to Microsoft Excel (2013) for analysis. pH values were averaged for each 5 s period. The average pH values were plotted with respect to time for the 4 microorganisms.

## **3.3 Results**

### **3.3.1 Fermentation Assay 1**

Four isolates were exposed to sucrose, with a final concentration of 0.1 M and the pH was measured over time. Figure 3.1 demonstrates the differences in pH between bacterial suspensions not exposed to a fermentable carbohydrate in the form of sucrose and those exposed to sucrose following 2 h incubation. When exposed to sucrose, *L. casei* showed the greatest difference in mean pH between those not exposed, and those exposed, to sucrose, at pH 6.51 to pH 4.03 respectively, a difference of 2.49 pH units. *S. mutans* and *S. sanguinis* showed changes from 6.50 to 4.46 (a difference of 2.03) and 6.45 to 5.21 (a difference of 1.24), respectively. *N. subflava* showed a minor decrease in pH when exposed to sucrose, with a difference of 0.3 pH units, from 6.60 to 6.30.

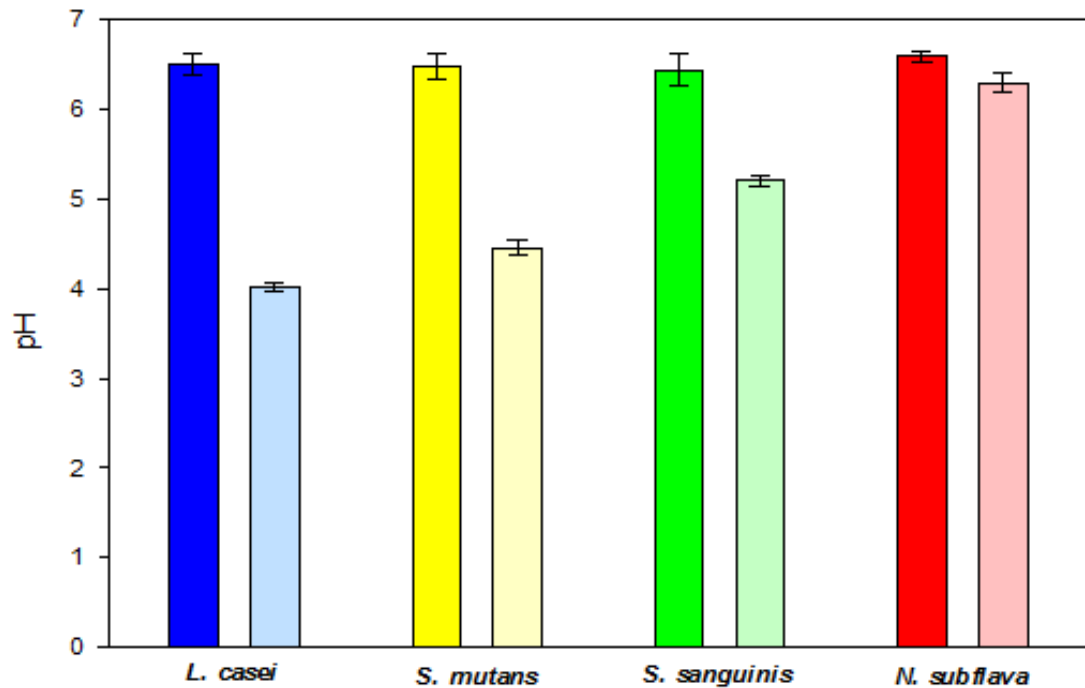


**Figure 3.1** Graph showing the average change in pH following after 2 hours of exposure to sucrose or non-exposed (saline). Lighter bars indicate those exposed to sucrose. The error bars shows 1 standard deviation, n = 12.

### 3.3.2 Fermentation Assay 2

Figure 3.2 shows pH with respect to time for *S. mutans*, *S. sanguinis*, *L. casei* and *N. subflava* following exposure to sucrose. *L. casei* has a starting pH of 6.68, reaching a pH of 4.07 after 2 h incubation. *S. mutans* has a starting pH of 6.78, reaching a pH of 4.41 after 2 h incubation. *S. sanguinis* has a starting pH of 6.73, reaching a pH of 5.17 after 2 h incubation. *N. subflava* has a starting pH of 6.84, reaching a pH of 5.23 after 2 h incubation. The pH values obtained reflect those seen in fermentation assay 1.

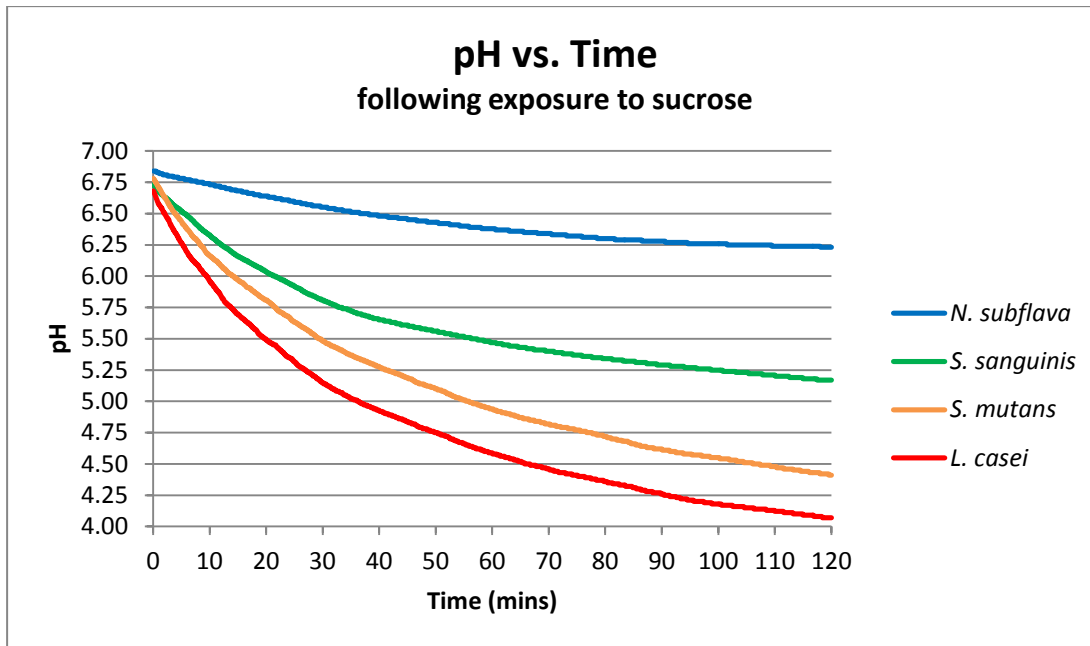


**Figure 3.2** Graph of pH with respect to time following exposure to sucrose. n = 1 for each isolate.

### 3.4 Discussion

The fermentation assays were performed to determine the acidogenicity of the bacteria tested and to ascertain the cariogenic potential of a variety of microorganisms commonly found in the oral cavity, including some often associated with dental caries. It should be noted that this is only a very small number of those bacterial microorganisms which make up the, approximately 700, microorganisms commonly which may make up the oral microbiome (Kilian et al. 2016). The choice of the microorganisms for the investigation of fermentation was selected as a result of their supposed acidogenic potential. The selection of these microorganisms has been previously discussed in Section 2.5.

Sucrose was chosen as the fermentable carbohydrate as it is considered more cariogenic (Minah et al. 1985). Sucrose is a disaccharide, consisting of a single glucose and a single fructose monosaccharide by a glycosidic bond between the C1 of the glucosyl subunit and C2 on the fructosyl subunit. Sucrose is metabolised by microorganisms, due to the action of invertase, into the constituent

monosaccharides. This is because sucrose is involved in the formation of extracellular polysaccharide (Li & Burne 2001; Paes Leme et al. 2008), more specifically the synthesis of glucans from sucrose, promoting accumulation of *S. mutans* (Zero et al. 1986), and the development of positive selective pressure to *S. mutans* and lactobacilli (Ellen et al. 1985; Minah et al. 1985; Filoche et al. 2008; Ribeiro et al. 2005). Sugars containing 6-carbons, e.g. glucose, and disaccharides containing 6-carbons, e.g. sucrose, may be fermented, with the formation of acid, by bacteria in the oral cavity. However, sucrose is particularly acidogenic under the action of *Streptococcus mutans* and *S. sanguinis*. The fermentation assay demonstrates production of acidic products as a result of fermentation. Based on the results of these experiments, sucrose was chosen as the fermentable carbohydrate source for future experiments. As expected, those isolates considered more cariogenic (*S. mutans* and *L. casei*) produced greater decreases in pH as a result of the fermentation of sucrose. It is also observed that there is a range of acidogenicity in the bacteria selected. This will likely add contrast to the imaging, as desired. When the pH is measured over time, through the use of a microelectrode, the rate of acid production is able to be visualised. Again, as expected, the cariogenic bacteria produced greater decreases in pH. Moreover, by monitoring the pH with respect to time over the duration of the experiment, the rate of acid production and decrease is also revealed. The pH of *L. casei* and *S. mutans* fall rapidly, *S. sanguinis* falls at a lesser degree, while the rate of increase is almost constant over the duration of the experiment. The pH values obtained reveal a similar decrease in pH over the same duration of both experiments. It should be noted that this analysis was performed to observe the potential differences in decrease of pH within the system. Variations in the bacterial concentration would likely change the values.

# Chapter 4 Design, Production and Characterisation of Dual-Sensitive Fluorophore, Ratiometric, pH-Sensitive Nanosensors

## 4.1 Introduction

An important feature of biofilms is the formation of spatial microgradients in physical and chemical parameters (Hunter & Beveridge 2005). The existence of these microenvironments has previously been demonstrated with the use of microelectrodes or fibre optic sensors (Schachtele & Jensen 1982; Wimpenny & Coombs 1983; Ewers & Greener 1985; Revsbech & Jørgensen 1986; VanHoudt 1992; Scheie et al. 1992; Küsseler et al. 1993). However, the use of microelectrodes and fibre optic sensors are not without their shortcomings. They have a relatively large size and relatively small volume of measurement and, when inserted into the biofilm, cause disruption to the biofilm structure which will inevitably effect results (Cullum and Vo-Dinh 2000).

Recent developments in optical technologies have allowed the visualisation of various spatial and temporal, physical and chemical parameters (Koo Lee et al. 2009). As such, optical methods may provide determination of ion concentrations microgradients within biofilms, such as dental plaque. A vast majority of these optical methods incorporate fluorescent probes in one form or another. A fluorescent probe, also known as a fluorophore, is a molecule which is able to emit light following excitation, a phenomenon known as fluorescence. They typically consist of combined aromatic groups, for example, benzene rings. Aromatic groups are particularly stable, resulting from delocalisation of  $\pi$  electrons (electrons shared between two atoms) above the  $C_6$  ring, and are therefore difficult to disrupt or react with other substances. Many fluorophores are commercially available and have been extensively used, including those which are sensitive to ions or other parameters of interest.

In general, fluorophores generate a fast, bright response and are able to be quantified through the use of fluorescent spectroscopy. These properties make them ideal for rapid, real-time measurements (Resch-Genger et al. 2008). Fluorophores sensitive to changes in environmental parameters typically shift either their emission intensity at a particular wavelength or shift their excitation maximum wavelength, corresponding to a change in analyte concentration (Section 1.15.4). When selecting the optimal fluorophore, certain properties of each fluorophore must be considered. These include the optimum excitation and emission wavelengths (fluorescent spectra), brightness, sensitivity, resolution, stability and the effective range of usefulness of the fluorophore. Due to their unique electronic conformation, fluorophores possess distinctive characteristics of absorption, pertaining to excitation, and emission. The fluorescence excitation and emission spectra demonstrate relative intensity of fluorescence at a particular wavelength (Figure 1.21). Therefore, the maximum excitation and emission wavelengths for a particular fluorophore can be obtained.

To obtain the fluorescence spectra, the fluorophore is excited with various wavelengths of light and the absorbance plotted with respect to wavelength. The emission spectra are obtained by measuring the fluorescence intensity when excited at the excitation maximum wavelength. One observation from the fluorescent spectra is the shift in wavelength between excitation maximum and emission maximum (Figure 1.22). This shift, referred to as the Stokes' shift, is as a result of vibration energy lost by the photon during fluorescence (Section 1.16.1). Another observation from the fluorescent spectra is that there is typically an overlap between the longer wavelengths of the excitation spectrum and the shorter wavelengths of the emission spectrum. In fluorescence microscopy, this overlapping light must be eliminated through considered selection of excitation source wavelength or excitation filters, a dichromatic beam splitter and emission filters. Failure to do so results in detection of the substantially brighter excitation light overwhelming the weaker fluorescent excitation, reducing contrast. Finally, the emission spectrum is typically observed as a mirror image of the excitation spectra.

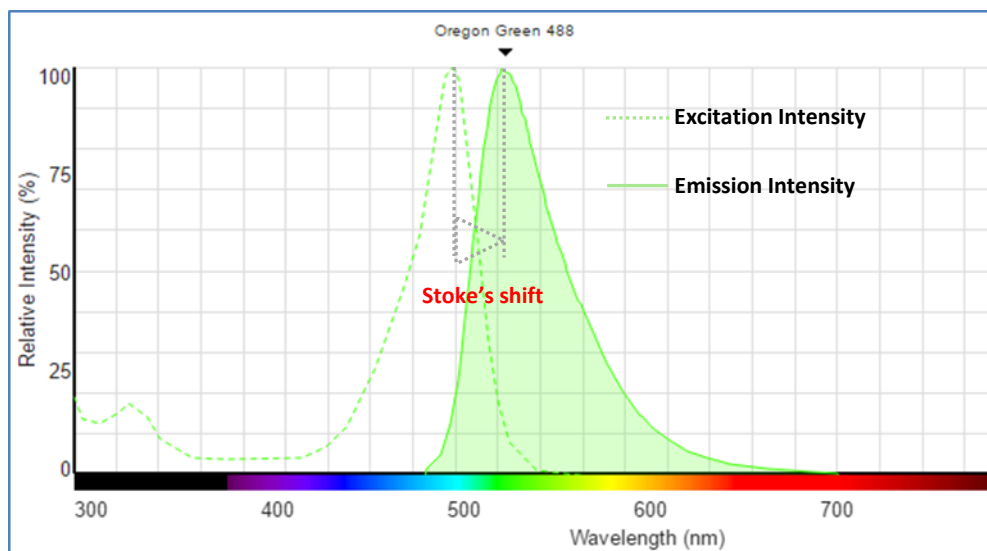


**Figure 4.1** An example of a fluorescence spectra, Oregon Green<sup>®</sup>-488, showing relative excitation and emission intensity and various wavelengths and the Stoke's shift (ThermoFisher Spectraviewer)

$$\phi = \frac{\# \text{ of photons emitted}}{\# \text{ of photons absorbed}} \quad \text{Equation 4-1}$$

The brightness of a fluorophore is calculated by the product of the molar extinction coefficient ( $\epsilon$ ) and the quantum yield ( $\Phi$ ) at a specific wavelength. The brightness is specific to each fluorophore. When observing the fluorescence spectra of a fluorophore, the intensity of the emission is usually of a lesser intensity than the excitation intensity. This is due to the amount of energy able to be absorbed by that fluorophore at a given wavelength, known as the molar extinction coefficient ( $\epsilon$ ), and the ratio of photons emitted to the number of photons absorbed, referred to as the quantum yield ( $\Phi$ ), (Equation 4-1). Quantum yield provides vital information about the efficiency of the fluorophore. The likelihood of the fluorescence being deactivated by non-radiative processes directly affects the quantum yield.

The sensitivity of a pH-sensitive fluorophore is difficult to define, due to the sensitivity changing through the fluorescence spectra. However, the sensitivity can be approximated to allow for comparison. An approximation of sensitivity is the change in signal between the minimal and maximal response within the dynamic

range. As such, the fluorophore sensitivity is proportional to the dynamic range. The simplest way of representing this is as a fold change ( $\Delta y/\Delta x$ ). Therefore, fluorophore sensitivity is inversely proportional to the dynamic range. The resolution of a fluorophore is the minimal change in pH required to produce a significant response. This is governed by the error in measurement from the fluorophore. For example, if the error in measurement for a given point is within  $\pm 0.5$  pH units, then any pH changes within 0.5 pH units will be insignificant. Hence, the resolution of the sensor is 0.5 pH units. Greater sensitivity reduces the probability of error, and therefore is likely to result in better resolution.

Photostability of a fluorophore refers to the ability to resist irreversible, light-induced alterations. These detrimental changes include photobleaching and changes in fluorescence lifetime. Photobleaching is a phenomenon in which a fluorophore is permanently rendered no longer able to fluoresce. The phenomenon is typically the result of cleavage of covalent bonds within the fluorophore or non-specific reactions with surrounding molecules. Changes in fluorescence lifetime (Section 1.16.2) can occur as a result of fluorescence quenching, affecting the brightness of the fluorophore.

The acid dissociation constant ( $pK_a$ ) of a fluorophore and pH are related and indicates what the fluorophore will do at a pH value with respect to acceptance or donation of a proton, i.e. protonation or deprotonation, respectively. pH refers to the concentration of hydrogen ( $H^+$ ) in an aqueous solution, more specifically pH is the negative of the logarithm to base 10 of the activity of hydrogen ion (Bates 1973), therefore the lower the pH, the higher the concentration of hydrogen.  $pK_a$  refers to the molecules proficiency to donate or lose a proton and the lower the  $pK_a$ , the greater that ability. The lower the  $pK_a$ , the stronger the acid. Lactic acid, with a  $pK_a$  of 3.86 (Dawson et al. 1986), is considered a weak acid, as are many of the acids found in the oral cavity; acetic, formic, propionic. These acids do not fully dissociate in water.

The effective range of usefulness, also referred to as the dynamic range, is the range of pH over which the fluorophore demonstrates detectable change

proportionate to changes in pH. This is a consequence of the fluorophores state of protonation and is typically limited to one pH unit either side of the fluorophore's  $pK_a$  (H. Sun et al. 2011). Generally, the  $pK_a$  of a fluorophore is the pH value at which the fluorophore exhibits half its maximum response. More importantly, the  $pK_a$  is the pH value at which the fluorophore shows its greatest sensitivity to changes in pH. As such,  $pK_a$  is a particularly important parameter when evaluating the fluorescent properties of a fluorescent probe.

Variations in fluorescent emission intensity may occur as a result of fluctuations in excitation source, detector sensitivity, light scattering and fluorophore concentration (Park et al. 2003). The final two points are particularly pertinent in complex structure and processes occurring within biofilms. These complications may be overcome through the use of ratiometric methodologies.

Through the use of a ratiometric methodologies accuracy of the measurements is enhanced (Desai et al. 2013). One method of ratiometric measurement is the use of a fluorophore which shifts its excitation or emission spectra with respect to changes in analyte concentration. By exciting the fluorophore or by measuring the emission at two separate wavelengths a ratio of the two emission measurements provides an accurate measurement of the analyte regardless of these fluctuations. Another method is to couple a pH-sensitive fluorophore with a pH-insensitive fluorophore, exciting and detecting emission of each fluorophore separately, facilitating ratiometric measurements. This may be facilitated by conjugating a pH-sensitive fluorophore, such as fluorescein, with a pH-insensitive fluorophore, such as tetramethylrhodamine (D1951, ThermoFisher Scientific). By plotting the fluorescent intensity ratio of the pH-sensitive fluorophore to the pH-insensitive fluorophore (pH-sensitive:pH-insensitive) with respect to pH, a standard pH titration curve can be obtained. Therefore, following calibration, the ratio provides a measurement of the pH value of the local environment.

Another option receiving considerable attention is the use of nanoparticle sensors. These are also referred to as nanosensors or PEBBLES (photonic explorer for bio-analysis with biologically localised embedding sensors). By combining the rapid,

real-time capability of fluorophores with the stable, inert properties of nanoparticles, fluorescent ratiometric nanosensors for real-time environmental analysis are able to be engineered. This is facilitated by the ability to engineer the physicochemical properties on the nanosensors to react to external stimuli. Fluorescent nanosensors are spherical optical probes, less than 1  $\mu\text{m}$  in diameter. They typically consist of an inert, non-toxic nanoparticle matrix such as polyacrylamide or silicon sol-gel (Clark et al. 1998; Sun et al. 2006). The inert matrix protects the cellular components from free fluorophores and protects the dye from cellular interferents (Aylott 2003). Free dyes have been shown to cause cellular damage by, for example, photoexcitation-induced toxicity (Hwang et al. 2012) or hindering cellular sensing by protein binding (Chauhan et al. 2011; Graber et al. 1986). Fluorescent nanosensors are relatively cheap and simple to produce and are able to be produced with traditional laboratory equipment. To this inert matrix, transducers in the form of fluorescent dyes are either encapsulated within or covalently bound. Polyacrylamide is a polymer able to be synthesised by cross-linking with the use of N,N'-methylenebis(acrylamide). Polyacrylamide is highly hydrophilic, forming a gel when hydrated. It is inert, porous and inexpensive to produce with standard laboratory equipment (Aylott 2003). These properties make it ideal for biological applications. Polymerisation of polyacrylamide typically produces nanoparticles in the range of 30 and 100 nm in diameter. They are composed of acrylamide (Figure 4.2 A) and a cross linker, N,N'-methylenebisacrylamide (Figure 4.2 B).

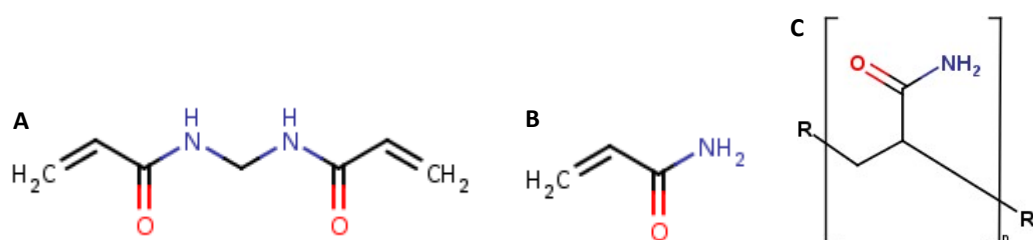


**Figure 4.2** Chemical structure of A) N,N'-methylbis(acrylamide), B) acrylamide and C) polyacrylamide

Like polyacrylamide, silica sol-gel nanoparticles are inert, hydrophilic, porous and inexpensive to produce. Silica sol-gel is also transparent, photostable and

thermostable (Aylott 2003). Silica sol-gel nanoparticles have a size distribution centred between 300 and 500nm diameter. Fluorescent nanosensors have been predominantly utilised for determination of intracellular parameters (Aylott 2003; Han & Burgess 2010; Shi et al. 2012; Desai et al. 2013). However, recently they have been utilised to determine extracellular environmental parameters (Schlafer et al. 2015). Through the incorporation of a second, insensitive fluorophore excited at a separate wavelength, the ratio of the measurement of the sensitive fluorophore to the insensitive fluorophore is utilised to obtain the environmental analyte concentration. The first fluorophore acts as the analyte-sensitive fluorophore in the same way as a non-ratiometric fluorophore, however, the second fluorophore acts as an analyte-stable fluorophore, unaffected by shifts in analyte concentration. As a result, the ratio of the fluorescent intensity of the two fluorophores (pH-sensitive:pH-insensitive) provides a measurement of the analyte concentration. This measurement is unaffected by fluctuations in in excitation sensitivity, detector sensitivity, light scattering and fluorophore concentration through the use of a ratiometric methodology. pH-sensitive ratiometric nanosensors incorporating a single sensitive fluorophore have previously been reported (Clark et al. 1998; Clark et al. 1999b; Park et al. 2003; Koo Lee et al. 2009), however limitations exists in the dynamic range and occurs as a result of the  $pK_a$  of the fluorophore. In order to overcome this limitation, it has been shown that, through the incorporation of a second pH-sensitive fluorophores the dynamic range can be extended (H. Sun et al. 2009; H. Sun et al. 2011; Chauhan et al. 2011) . For this to occur fluorophores must be selected which exhibit similar fluorescence spectra, but differ in their  $pK_a$  and therefore their dynamic range (H. Sun et al. 2009; H. Sun et al. 2011). At the acidic extreme of detection of the nanosensors, the fluorophore with the lowest  $pK_a$  is responsive to changes in the environmental parameter, while the second fluorophore essentially remains optically silent. As the concentration of interest increases, the responsiveness of the initial fluorophore diminishes and the response of the second fluorophore increases. This results in extension of the dynamic range and responsiveness of the nanosensor across the dynamic range of the fluorophores.

Once produced, the physical and optical properties of the nanosensors need to be analysed. Characterisation of the nanosensors involves analysis of the optical and physical characteristics on the nanosensors. Physical characteristics include the particle size, shape, electrokinetic potential, surface charge and stability of the nanosensors in a colloid. Depending on the construction of the nanosensors, size may be able to be determined by electron microscopy. Environmental scanning electron microscopy is typically used, as the dehydration of specimens required by other electron microscopy methods may cause deterioration of the nanosensor structure.

The ability to resolve two objects through the use of microscopy techniques is limited by diffraction of light by the object. As a result, the ability to resolve sub-wavelength structures is extremely problematic (Section 1.17.2.5). To overcome this, electron microscopy may be employed. Electron microscopy produces an image of a specimen through the use of a beam of electrons. The images produced possess exceptional magnification and resolution and as such electron microscopy is utilised prolifically in science. In transmission electron microscopy (TEM) electrons in the primary beam are transmitted through a specimen. In scanning electron microscopy (SEM) images are produced by detecting secondary electrons emitted from the surface due to excitation by the primary electron beam. In SEM, an electron beam is scanned across the surface of the specimen in a raster pattern, with detectors building up an image by mapping the detected signals with beam position. In both techniques, considerable preparation of the specimen is required. Also, the chamber is typically under vacuum to facilitate the travel of the electrons. Therefore, specimens are dehydrated. Environmental scanning electron microscopy (ESEM) allows the visualisation of wet specimens by allowing a gaseous environment in the specimen chamber. ESEM utilises a scanning electron beam, as per SEM, however there are some important requirements including the use of differential pumping, electron beam transfer, signal detection, sample charging, contrast and resolution and specimen transfer.

Nanosensor size, electrokinetic potential and surface charge are able to be determined through the utilisation of dynamic light scattering. Dynamic light scattering (DLS) is a technique which can be used to determine the size of particles as small as 1 nm dispersed in liquid. DLS correlates the size of particles to the rate of Brownian motion in a liquid. Brownian motion is the random movement of small particles suspended in liquid and occurs as a result of collisions with solvent molecules. When solvent molecules collide with larger particles the resulting movement will be inversely proportional to the size of the particle. When light is shone on a sample of particles in a liquid, the light is scattered. The intensity of the fluctuation of the scattered light provides information about the size of the nanoparticle. The diameter measured refers to how the particle diffuses in a liquid. It is therefore referred to as the hydrodynamic diameter. The hydrodynamic diameter is calculated from the translational diffusion coefficient based on the Stokes-Einstein equation;

$$d(H) = \frac{kT}{3\pi\eta D} \quad \text{Equation 4-2}$$

Where, **d(H)** is the hydrodynamic diameter, **D** is the translational diffusion coefficient, **k** is the Boltzmann's constant, **T** is the absolute temperature and **η** is the viscosity of the liquid phase. The diameter, calculated from this equation, is the equivalent diameter of a sphere with the same translational diffusion coefficient. The particle translational diffusion coefficient is also affected by the structure of the particle surface. The estimate of the width distribution is referred to as the polydispersity index.

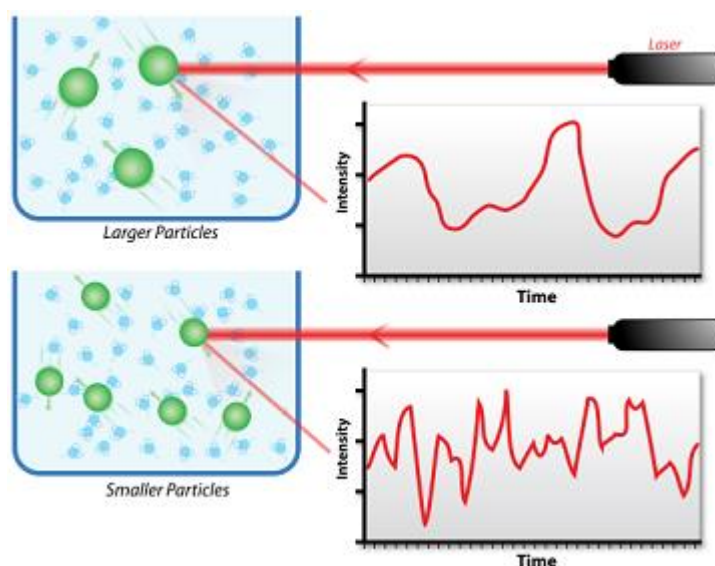


**Figure 4.3** The principle of obtaining nanoparticle size through the use of dynamic light scattering (Image credit Mike Jones CC BY 2.0)

When dispersed in solution nanoparticles form colloids, a homogeneous solution of solid in liquid in which the solid phase remains dispersed and are not separated by centrifugation or filtration. Nanoparticles possess a surface charge and as a result attract a thin layer of ions of opposite charge to the surface. This layer of strongly bound ions is referred to as the stern layer. The nanoparticle will possess an outer layer in which ions are less strongly bound, the diffuse layer. Within this diffuse layer there is a theoretical border within which ions form a stable entity. When particles move, those ions outside of the border transfer to the bulk fluid and those within remain with the nanoparticle. This boundary is referred to as the electrokinetic potential, or  $\zeta$ -potential. Determination of the  $\zeta$ -potential provides information about the potential difference between the dispersion medium and the stationary layer of fluid attached to the dispersed nanoparticle. Therefore,  $\zeta$ -potential is a key measure of the stability of a colloidal dispersion. The determination of  $\zeta$ -potential is an important measure of the state of the nanoparticle surface and predicts the long-term stability of the nanoparticle. This value is determined through the use of DLS. From the  $\zeta$ -potential measurements, the surface charge is able to be extrapolated.  $\zeta$ -potential provides the surface charge of a nanoparticle in the conditions of study. Therefore, parameters including pH, temperature and the ionic strength of the dispersion media will all affect the  $\zeta$ -

potential measurement. It will also depend on the viscosity of the dispersion media and the mobility of the nanoparticle in that dispersion media.

The optical characteristics of the nanosensors include the response of the fluorophores at different wavelengths and response to changes in pH (dynamic range). Response to different wavelengths is performed by exciting the fluorophores with a scanning range of wavelengths and measuring the fluorescent emission. This can be assessed through the use of a fluorescent spectrophotometer with the capability to scan at various wavelengths in the desired range. The dynamic range is assessed through applying the nanosensors to various pH environments of known values in the form of buffers.

It should be stated that, as the use of this construct of a nanoparticle construct which is pH-sensitive, has an extended dynamic range due to the use of two pH-sensitive fluorophores and the addition of a third pH-stable fluorophore to allow ratiometric determinations in biofilms is novel, this study is not a benchmarking exercise and is therefore an exploratory investigation.

Through review of the literature and thoughtful design, the nanosensors will be designed to overcome many of the shortcomings of previously employed methods. These include; i) the ability to overcome variations in fluorescence emission intensity caused by fluctuations in excitation sensitivity, detector sensitivity, light scattering and fluorophore concentration through the use of a ratiometric methodology, ii) the ability to maximise the dynamic range through the use of a dual sensitive fluorophore methodology providing the capability to measure pH across an appropriate range observed in dental plaque following exposure to fermentable carbohydrates, designated at a between pH 3.0 and 7.5, and iii) the ability to maximise quantum yield through covalent conjugation of the fluorophores to the nanoparticle matrix.

### 4.1.1 Aims and Objectives

The aim of this chapter is to investigate the capability to produce nanosensors able to determining local environmental pH in bulk extracellular fluid of biofilms. The objectives are to; i) design the nanosensors, with respect to the nanoparticle background, and fluorophores employed for conjugation and sensing, ii) production of the designed nanosensors, and iii) characterisation of the physical and optical properties of the produced nanosensors.

## 4.2 Materials and Methods

**Reagents:** Acrylamide (Fluka Analytical, Loughborough, UK), N,N'methylenebisacrylamide (Fluka Analytical, Loughborough, UK), N-(3-Aminopropyl)methacrylamide hydrochloride (APMA) (Polysciences Inc., Mannheim, Germany), polyoxyethylene (4) lauryl ether (Brij30) (Fluka Analytical, Loughborough, UK), dioctyl sulfosuccinate sodium (AOT) (Sigma-Aldrich, Dorset, UK), Ammonium persulphate (APS) (Sigma-Aldrich, Dorset, UK), N,N,N',N'-tetramethylethylenediamine (TEMED) (Sigma-Aldrich, Dorset, UK), Hexane (Fisher Scientific, Loughborough, UK), absolute ethanol (Fisher Scientific, Loughborough, UK), deionised water (18.2  $\Omega$ ), sodium tetraborate decahydrate (Sigma-Aldrich, Dorset, UK), 10,000 MW aminodextran (Thermo Fisher Scientific, Paisley, UK), citric acid (Sigma-Aldrich, Dorset, UK), sodium phosphate (Sigma-Aldrich, Dorset, UK).

**Fluorophores:** succinimidyl ester forms of Oregon Green<sup>®</sup>-488 (OG), 5-(and-6)-carboxyfluorescein (FAM), 5(and-6)-carboxytetramethylrhodamine (TAMRA). All fluorophores were purchased from Invitrogen (Thermo Fisher Scientific, Paisley, UK).

### 4.2.1 Design of Nanosensors

Dual pH-sensitive fluorophore ratiometric nanosensors were produced with the assistance of Dr. Veeren Chauhan and Prof. Jon Aylott (School of Pharmacy, University of Nottingham). Purely from a sensing perspective the most important

considerations are the dynamic range, sensitivity and resolution of the fluorophore. In order to clearly define these three parameters, it is helpful to consider them in the context of the relationship between pH and signal intensity. Most pH-sensitive fluorophores demonstrate a sigmoidal response to pH. In this context, the dynamic range is the range between the minimal and maximal response. This equates to the range in which the sensor produces a reliable measurement.

#### **4.2.1.1 Selection of Nanoparticle Matrix**

The options under consideration for the construction of the nanoparticles, due to availability and expertise, were polyacrylamide and silicon sol-gel. Both constructions are cheap to produce and are able to be produced with the use of standard laboratory equipment (Aylott 2003).

#### **4.2.1.2 Selection of Fluorophores**

To extend the dynamic range, a dual-sensitive fluorophore construct was selected. To facilitate this, two fluorophores which are sensitive to variations in pH and exhibit similar fluorescent spectra, but have different  $pK_a$ , required selection. To further permit ratiometric measurements a pH-stable, reference fluorophore also required careful consideration. This stable fluorophore is to act as the reference intensity for the purpose of comparison to facilitate ratiometric measurement. By exploiting the ratiometric nature of the nanosensor, the concentration of the nanosensors in the local environment is then inconsequential. This is particularly desirable in the complex structure of biofilm in which concentrations may fluctuate considerably. The reference fluorophore required stability across the pH spectra, as well as possessing a fluorescent spectrum different from those possessed by the sensitive fluorophores. This allows production of images from the fluorescent emission at two separate wavelengths without overlap. The fluorescent spectra of many commercially-available fluorophores are able to be analysed through the use of fluorescent spectra analysis software provided by the fluorophore suppliers, e.g. ThermoFisher Scientific Spectraviewer (Thermo Fisher Scientific). Following analysis

of the fluorescent spectra, the  $pK_a$  required analysis. The  $pK_a$  of a fluorophore is directly related to the pH range-of-usefulness (dynamic range); therefore in this case one fluorophore needed to be approaching neutral with the second in the acidic range. The further apart the  $pK_a$  values, the greater the dynamic range. However, the greater the dynamic range the poorer the sensitivity to variations in pH. Therefore, a balance must be struck between these two properties.

#### **4.2.2 Production of pH-Sensitive, Dual-Fluorophore Ratiometric Nanosensors**

Polyacrylamide nanoparticles were produced composed of acrylamide and the cross-linker, N,N'-methylbisacrylamide polymerised in the aqueous phase of an inverse water-in-oil microemulsion. The inverse microemulsion comprises a continuous hexane hydrophobic oil phase and a hydrophilic aqueous phase. The interfaces of the inverse microemulsion were stabilised with non-ionic surfactant, polyoxyethylene (4) lauryl ether (Brij 30®) and anionic surfactant, dioctyl sulfosuccinate sodium (AOT). Through careful control of the water, oil and surfactant ratio, a narrow distribution of nano-sized water droplets is created. The size of the water droplet directly affects the size of the nanoparticles produced. This occurs because acrylamide monomers are subjected to free radical polymerization within the water droplets. The polymerisation was accelerated with the use of a redox pair catalyst, ammonium persulfate (APS) and N,N,N',N'-tetramethylethylenediamine (TEMED). Ample hexane, sufficient to take into account evaporation, was deoxygenated under argon gas for 30 min. The needle supplying the argon gas was inserted through a rubber stopper and submerged in the hexane. A second syringe was inserted into the rubber stopper to gas pressure release. Following a short period of deoxygenation, a gas collection device was placed onto the gas pressure release needle and the device was allowed to fill with waste gas. The argon gas was turned off and the gas trap was monitored to assess leakages. If the gas collection device deflated, the leak in the system was rectified and deoxygenation was repeated. The conjugation of the dye to N-(3-

aminopropyl)methacrylamide hydrochloride (APMA) was adapted from Zen (Zen et al. 1992). The structure of APMA is observed in Figure 4.4.

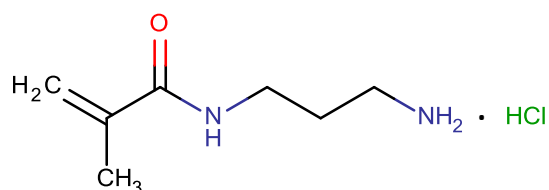


**Figure 4.4 Chemical structure of N-(3-aminopropyl)methacrylamide hydrochloride (APMA).**

The covalent incorporation of the fluorophores into the acrylamide matrix significantly enhances dye brightness, limited fluorophore leaching and photostability through increases in radiative fluorescence rate and decreases in non-radiative fluorescence rate, (Verbal communication with Veeren Chauhan). Succinimidyl esters of the three selected fluorophores (FAM and OG in a 1:1 ratio, and TAMRA) were conjugated to APMA ( $C_7H_{14}N_2O \cdot HCl$ , MW: 178.66) (Figure 4.4). To conjugate the fluorophores to APMA, a stock solution of APMA was produced by dissolving 5 mg (11.2  $\mu M$ ) of APMA in 2.5 mL of sodium tetraborate decahydrate buffer solution (50 mM at pH 9.5). 200  $\mu L$  of the APMA stock solution was added to 1 mg of each fluorophore (2  $\mu M$ ) in separate vials. To allow sufficient time for the conjugation to occur the suspension was stirred continually, initially at room temperature for 3 h and then for at least a further 21 h at 4°C. The conjugation reaction is observed in Figure 4.5. Aliquots of conjugate stock solutions were used for nanosensor synthesis.

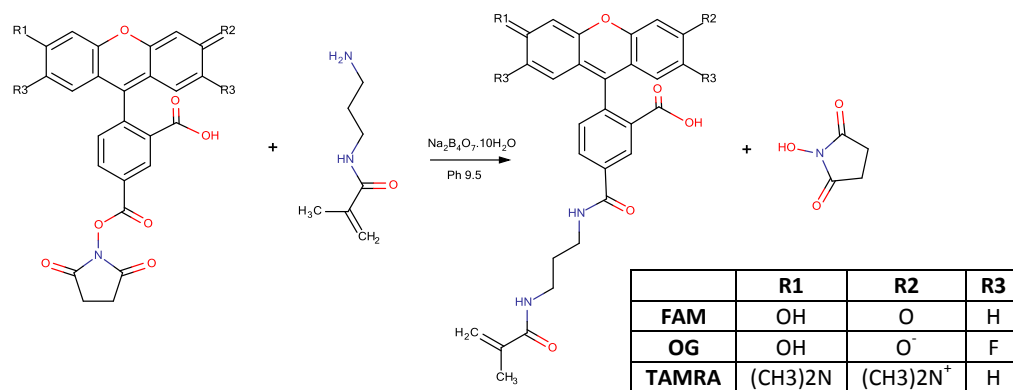


**Figure 4.5** Chemical reaction of conjugation of fluorophores to N-(3-aminopropyl)methacrylamide hydrochloride (APMA), in sodium tetraborate decahydrate ( $\text{Na}_2\text{B}_4\text{O}_7 \cdot 10\text{H}_2\text{O}$ , 50 nM at pH 9.5) buffer solution.

3.08 g (8.508 mM) of Brij® 30 (Polyoxyethylene (4) lauryl ether), a non-ionic surfactant, and 1.59 g (3.577 mM) of dioctyl sodium sulfosuccinate salt (AOT), an anionic surfactant were combined and deoxygenated under argon gas whilst stirring, as above. The solution was allowed to continue to stir for 10 min. 42 mL of deoxygenated hexane was added to the Brij®30/AOT suspension and stirred rapidly for 10 min to dissolve the Brij®30/AOT. 540 mg (7.579 mM) of acrylamide and 160 mg (1.307 mM) of N,N'methylenebisacrylamide were measured and added to deionised water and adjusted to a final volume of 2 mL. The suspension was then sonicated to promote adequate dispersal of the acrylamide in solution. Fluorophores were attached to polyacrylamide prior to synthesis. Fluorophores were attached to an acrylamide monomer containing a primary amine group (APMA). To synthesise acrylamide monomers conjugated to fluorophore, 15 µL of FAM-APMA, 15 µL of OG-APMA and 60 µL of TAMRA-APMA, (each 5 mg/mL), were added to the acrylamide solution. To facilitate conjugation, the fluorophore/acrylamide solution was added to the Brij® 30/AOT suspension and stirred for a further 10 min. A 10% w/v solution of ammonium persulfate (APS) was prepared. To initiate polymerisation, 30 µL of the APS solution and 15 µL of N,N,N',N'-tetramethylethylenediamine (TEMED) were added to the stirring Brij® 30/AOT mixture. The solution was allowed to mix for 2.5 h at room temperature

under argon gas. The hexane was then removed by rotary evaporation with the water bath set to 30°C. As much of the resultant pellet as possible, (light pink in colour, demonstrating successful incorporation of TAMRA), was collected into a centrifuge tube. This was performed by adding a small amount of ethanol to the round bottom flask and decanting the suspension into a centrifuge tube. This step was repeated a number of times to maximise yield. Ethanol was added to the centrifuge tube to a final volume of approximately 30 mL. The nanosensors were washed by centrifugation for 10 min at 4300 x g (~6000 rpm) and the supernatant was carefully removed. The particle pellet was resuspended in 30 mL of ethanol and centrifugation was repeated. This washing step was performed a total of ten times. Following the final wash, 5 mL of ethanol was added to the deposit and the deposit was transferred to a round bottom flask. The ethanol was removed by rotary evaporation, with the parameters as described above. The resultant yield was weighed. The expected yield is approximately 420-500 mg (based on 60%-70% of the starting amount of acrylamide and N,N'methylenebisacrylamide, and should not exceed the starting amount. The resultant pellet was then characterised. Prior to and following characterisation, the nanosensors were protected from light and stored at 4°C.

### **4.2.3 Characterisation of the Nanosensor**

Characterisation of the physical and optical properties allows the ability to determine the limits within which the nanosensors are able to be employed with accuracy. Characterisation of the nanosensors include analysis of the nanosensor fluorescence spectra, to determine the optimum fluorescence excitation wavelength and the best fluorescence emission filter to prohibit cross-talk of excitation light and other fluorescence processes, and determination of the size, through electron microscopy and dynamic light scattering.

#### **4.2.3.1 Analysis of Nanosensor Fluorescence Spectra**

Extended dynamic range pH-sensitive nanosensors were suspended in citric acid buffer solutions (1 mg/mL), ranging from pH 3.0 to 7.0, produced as previously described (Section 2.4). To ensure that the concentration of nanosensor was appropriate, a suspension was produced and imaged to ensure that sufficient fluorescence was observed for both the green and red fluorophores. An ideal concentration is one that will provide sufficient detectable fluorescence, however the higher the concentration, the higher the background fluorescence. Therefore an optimal concentration will possess the greatest ratio of fluorescence emission to background fluorescence. Analysis of the fluorescence spectra of the nanosensors was carried out using a Varian Cary® Eclipse™ fluorescence spectrophotometer (Aligent Technologies, Berkshire, UK). The pH-sensitive fluorophores, i.e. OG and FAM, were excited at 488 nm (excitation slit size 2.5 nm), and the emission spectrum was collected from 500 to 600 nm (emission slit size 5 nm). The pH-insensitive reference fluorophore, i.e. TAMRA, was excited at 540 nm (excitation slit size 2.5 nm), and the emission spectrum was collected from 550 to 650 nm (emission slit size 5 nm).

#### **4.2.3.2 Analysis of Nanosensor Size and Shape Using Environmental Scanning Electron Microscopy**

A suspension of nanoparticles (1 mg/mL) were spread and dried on 400 mm<sup>2</sup> mica placed on an aluminium scanning electron microscope stub (Agar Scientific, Essex, UK). The sample was platinum coated (90 s, 2.2 kV, 20 mA plasma current and 4x10<sup>-2</sup> mbar vacuum) using a Polaron Emitech SC7640 sputter coater (Quorum Technologies, East Sussex, UK). A Philips XL30 ESEM-FEG scanning electron microscope (Philips Research, Eindhoven, The Netherlands) was used to image dry nanoparticles (20 kV, 10.1 mm working distance). Nanosensor size was analysed with the use of ImageJ (Rasband 1997). Once the image was opened, the scale was set by selecting the rectangular marquee tool and measuring the size bar within the image. The scale was set and the length of the bar was correlated to the distance of the bar and the unit were added to the menu. The contrast threshold was set to

distinguish the background from the nanoparticles. The size and circularity settings were selected, as follows; size 20 to 100 nm and circularity was not adjusted (0.00-1.00). The sizes of the nanoparticles were then analysed. The mean diameter and standard deviation was obtained. The measured diameters were validated using dynamic light scattering.

#### **4.2.3.3 Analysis of Nanosensor Size Using Dynamic Light Scattering**

Dynamic light scattering was performed using a Malvern Zetasizer Nano ZS (Malvern, Worcestershire, UK) within the Department of Chemistry, University of Nottingham or the Department of Chemistry at UCL. The system was equipped with a 5 mW He-Ne laser source at 633 nm, operating at an angle of 173° (Malvern Instruments 2000). Extended dynamic range pH-sensitive nanoparticles were suspended in deionised water (1 mg/mL). Measurements (42 runs at 25 °C) were made using a disposable Sarstedt® polystyrene cuvette. The mean hydrodynamic diameter of the particles was computed from the intensity of the scattered light using Malvern Zetasizer software (v 7.03).

## **4.3 Results**

### **4.3.1 Design of the Nanosensors**

The major difference between polyacrylamide and sol-gel nanoparticles constructs is the size of the nanoparticles produced (Aylott 2003). Due to this comparative size between polyacrylamide and silicon sol-gel, polyacrylamide was selected. The fluorophores selected for conjugation to polyacrylamide nanoparticles for the production of pH-sensitive nanosensors were Oregon Green®-488 (OG) (Figure 4.6), 5-(and-6)-carboxyfluorescein (FAM) (Figure 4.7), and 5-(and-6)-carboxytetramethylrhodamine (TAMRA) (Figure 4.8). TAMRA exhibits little response to changes in pH and therefore acts as a reference dye to facilitate ratiometric imaging. The two remaining fluorophores both demonstrate significant response to changes in pH. Additionally, they also share similar excitation and emission spectra (Figure 4.9).

They, however, exhibit differing  $pK_a$  values and as a result demonstrate sensitivity to varying regions of the pH spectrum. FAM has a  $pK_a$  of 6.4, whilst Oregon Green<sup>®</sup> possesses a  $pK_a$  of 4.7. As a result FAM has a theoretical dynamic range of 5.4 to 7.4 and Oregon Green has a theoretical dynamic range of 3.7 to 5.7 (H. Sun et al. 2011).

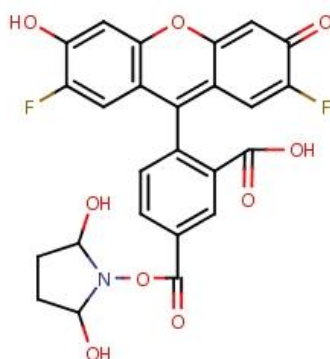


**Figure 4.6** Chemical structure of Oregon Green<sup>®</sup>-488, succinimidyl ester.



**Figure 4.7** Chemical structure of 5-(and-6)-carboxyfluorescein, succinimidyl ester

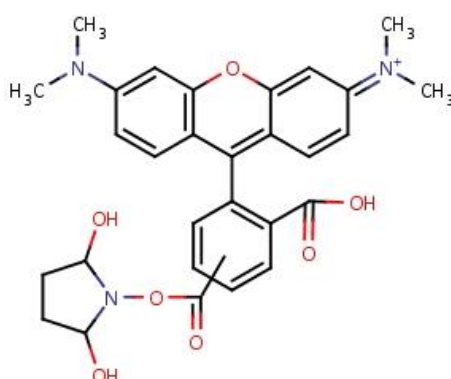


**Figure 4.8** Chemical structure of 5-(and-6)-carboxytetramethylrhodamine, succinimidyl ester

### **4.3.2 Analysis of the Fluorescent Spectra of Nanosensors**

Both pH-sensitive fluorophores, OG and FAM, are excited at a wavelength of 488 nm and demonstrate an overlapping emission peak at ~520 nm (Thermo Fisher Scientific) (Figure 4.9). This overlapping fluorescent excitation and emission spectra permits the use of a single excitation laser line and detection of the resultant fluorescent emission through the same detection channel. The pH-stable fluorophore, TAMRA, is excited at a wavelength of 540 nm and emits at a wavelength of ~577 nm (Thermo Fisher Scientific) (Figure 4.10). There is sufficient difference between the pH-sensitive fluorophores and that of the pH-stable fluorophore to use a second excitation laser line and detection channel, without fluorescent crosstalk.

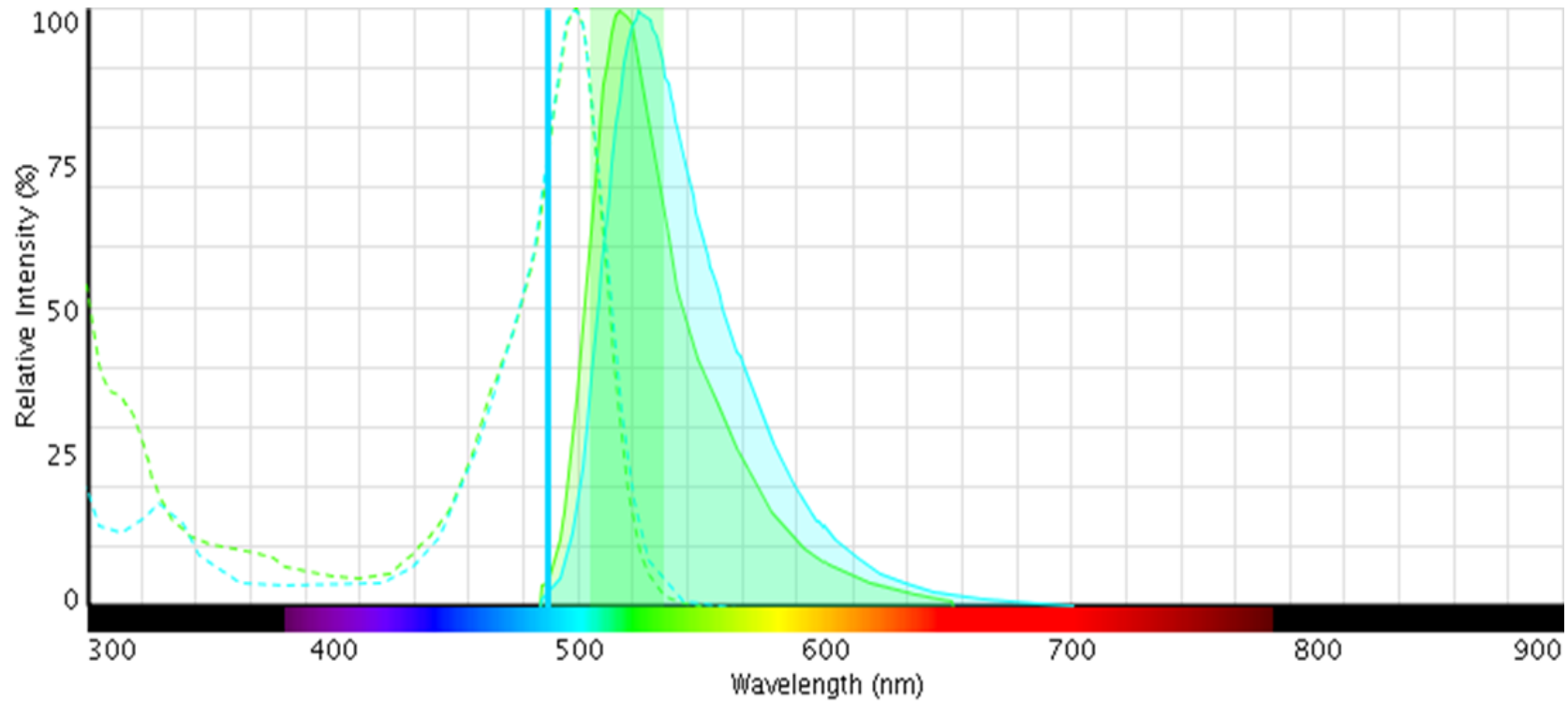


**Figure 4.9** Fluorescence excitation (dotted) and emission (solid) spectra for carboxyfluorescein (green line) and Oregon Green®-488 (blue line). The vertical blue line indicates the excitation laser line (488 nm) utilised throughout. The green bar indicates the emission filter (520/30 nm) applied

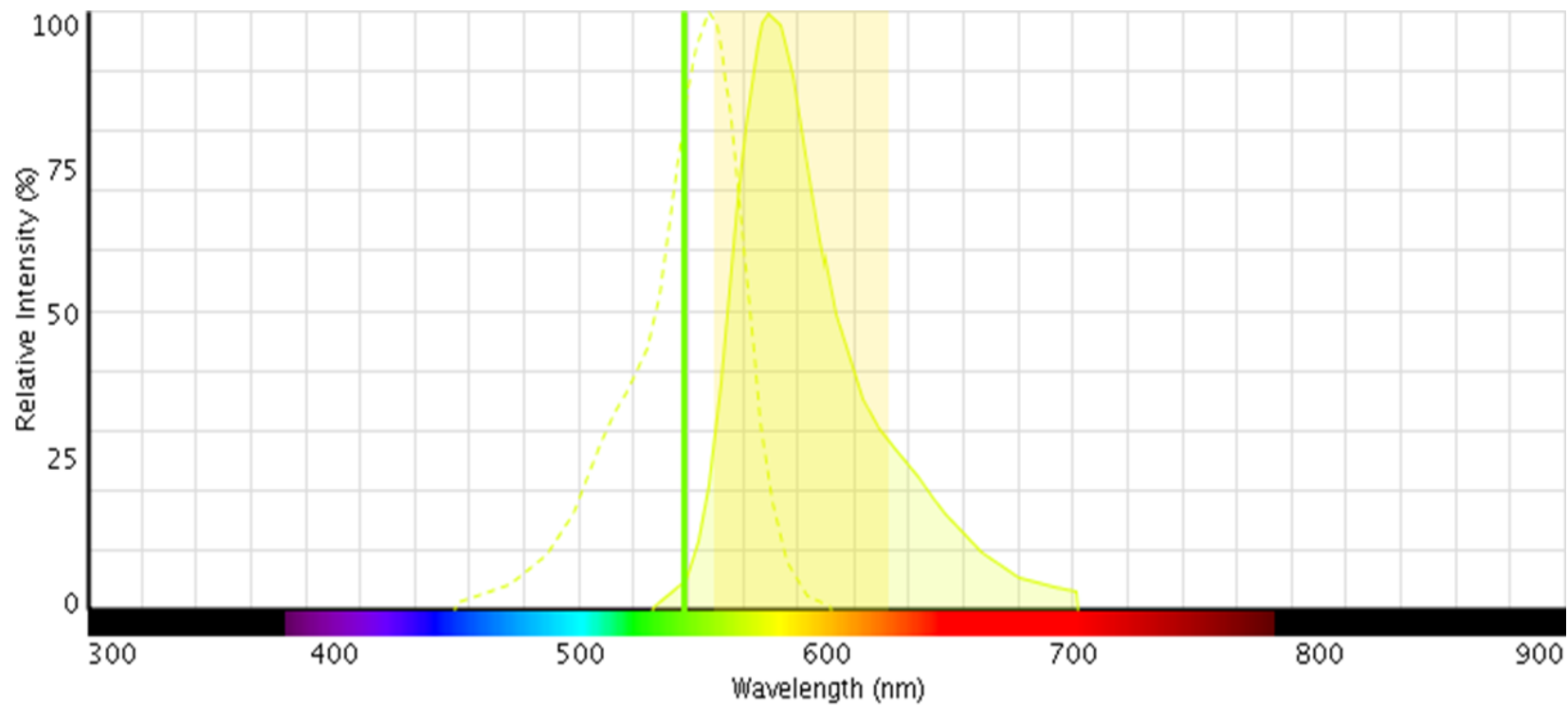


**Figure 4.10** Fluorescence excitation (dotted) and emission (solid) spectra for tetramethylrhodafleur (yellow line). The vertical blue line indicates the excitation laser line (543 nm) utilised throughout. The yellow bar indicates the emission filter (590/70 nm) applied

By utilising a ratio of 1:1, the dynamic range is able to be maximised (Clark et al. 1999a; Clark et al. 1999b; Chauhan et al. 2011) (Figure 4.11). Incidentally, when the ratio of fluorophores is adjusted, the dynamic range is able to be tuned (Chauhan et al. 2011). As a consequence of this adjustment, the dynamic range is decreased however; the sensitivity of the nanosensors is improved. This data was obtained in collaboration with Veeren Chauhan.

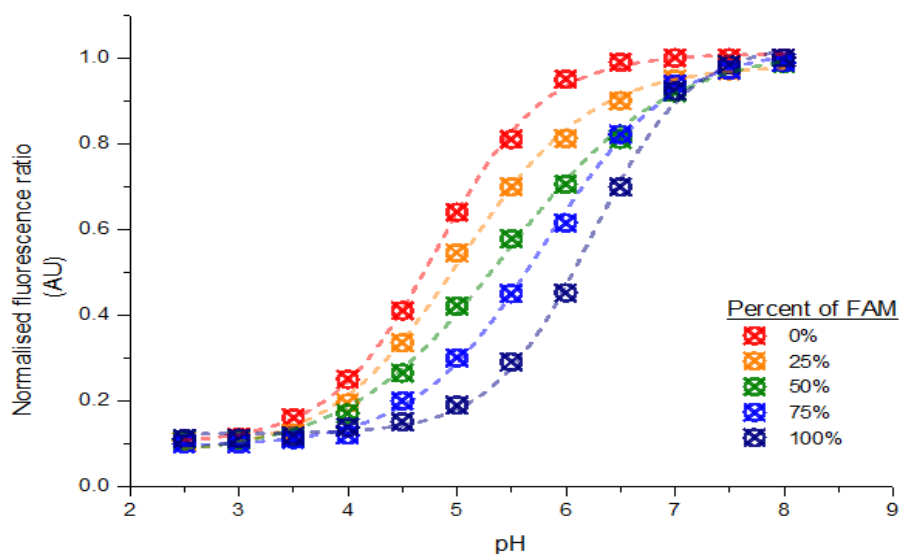


**Figure 4.11** Graphic representation of the dynamic range of nanosensors incorporating various ratios of FAM to Oregon Green. The extension of the dynamic range is visible when utilised in a 1:1 ratio.

### 4.3.3 Analysis of Nanosensor Size and Shape Using Environmental Scanning Electron Microscopy

When analysed using the 'Analyse Particles' functions in ImageJ, particle sizes were obtained. Analysis demonstrated nanoparticles with a mean diameter of  $43.06 \pm 8.98$  nm (Figure 4.12).

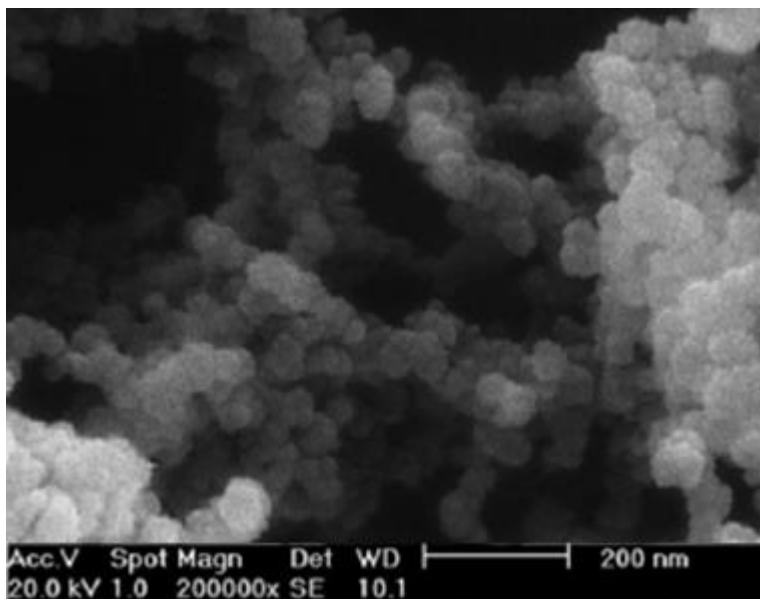


**Figure 4.12** Environmental scanning electron micrograph of the produced dual-fluorophore, ratiometric, pH-sensitive nanosensors.

#### **4.3.4 Analysis of Nanosensor Size Using Dynamic Light Scattering**

Figure 4.13 shows the resultant polyacrylamide nanoparticle distribution width determined through dynamic light scattering. These results were obtained with the assistance of Veeren Chauhan. The nanoparticles produced possess a narrow distribution width with an average nanoparticle diameter of approximately 40 nm. This corresponds with the diameter obtained through measurement of the environmental scanning electron microscopy of the nanoparticles.

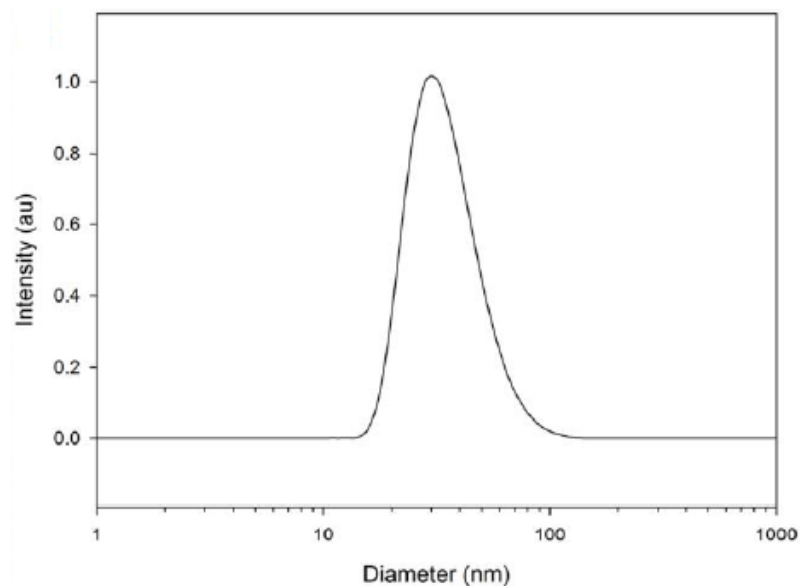


**Figure 4.13 Particle size distribution obtained through dynamic light scattering. (Image used with permission of V. Chauhan).**

#### **4.3.5 Analysis of Nanosensor Fluorescence Spectra**

Figure 4.14 shows the fluorescent emission intensities obtained plotted with respect to fluorescent emission wavelength. When the pH-sensitive fluorophores, Oregon Green and carboxyfluorescein, were excited at 488 nm the fluorescent emission peaked at approximately  $\lambda$ 524 nm. The pH-stable fluorophore was excited with a 543 nm laser and exhibited a peak fluorescent emission at  $\lambda$ 576 nm. As desired, the pH-sensitive fluorophores demonstrated significant difference in fluorescence intensity with respect to pH across the range of pH 7.0-3.0. In contrast, the pH-stable fluorophore, tetramethylrhodamine, remained considerably unaffected by changes in pH. Spectra between 497 and 550 nm shows the variation in fluorescence emission intensity with respect to pH for the pH-sensitive fluorophores. Spectra between 560 and 585 nm reveals the relative stability in fluorescence emission intensity across the pH range analysed.

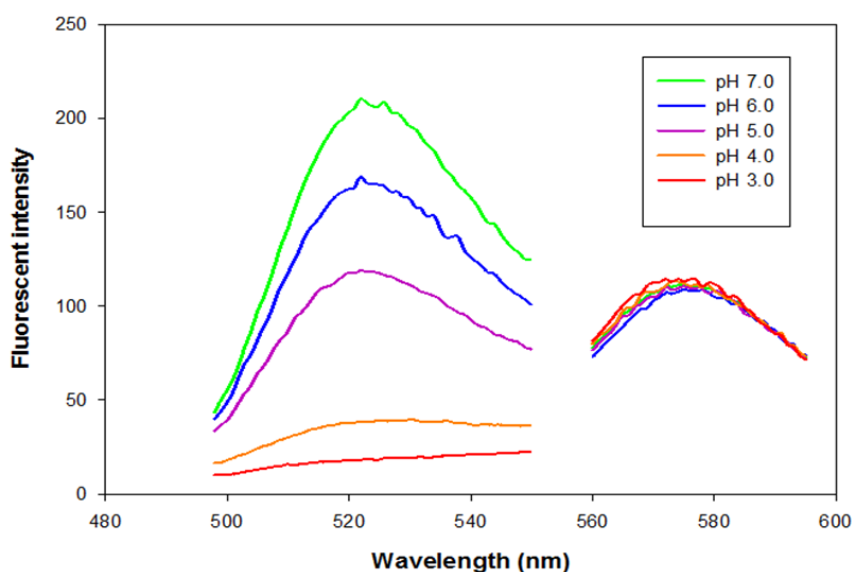


**Figure 4.14** The fluorescence emission spectra of dual-fluorophore, ratiometric, pH-sensitive nanosensors.

## 4.4 Discussion

The ability to produce particles in the nanometre range with the ability to functionalise them through the conjugation or incorporation of the fluorophores allows analysis of many parameters through the careful selection of those fluorophores (Chauhan et al. 2011; Wang et al. 2014; Wolfbeis 2004). One of the drawbacks of using a single fluorophore is the effect of concentration of the fluorophore which can affect fluorescent intensity and therefore the measurement. One benefit of the use of functionalised nanoparticles is the ability to conjugate or incorporate more than one fluorophores. Therefore, this concentration-dependent intensity can be overcome through the use of a ratiometric protocol with the use of a sensitive fluorophore in co-operation with a fluorophore unaffected by the parameter of interest. This does not, however, overcome the limitations of the sensitive fluorophores range of usefulness, also referred to as dynamic range. This is limited to the  $pK_a$  of the fluorophore which is typically the point at which the fluorophore shows maximum response to changes in the parameter of interest. As a rule of thumb, dynamic range is limited to one pH unit either side of the

fluorophores  $pK_a$ . One method for extending the dynamic range is through the careful selection and addition of more than one pH-sensitive fluorophore. One negative effect of increasing the dynamic range through the use of a dual-fluorophore nanosensor is that sensitivity decreases. Here, a polyacrylamide nanoparticle backbone was selected due to the diameter of the nanoparticles produced. To this polyacrylamide backbone, a pH-sensitive fluorophore (TAMRA) was conjugated. This allowed a stable point of reference across the pH range of interest and therefore facilitation of a ratiometric method. The ratiometric protocol was used to overcome the effect of variations in nanosensor concentration. Two pH-sensitive fluorophores were selected, following careful consideration, and conjugated to the nanoparticle matrix. The reasons for the selection of the fluorophores selected was that they shared a similar fluorescent excitation and emission profile, however, significant differences in each fluorophores  $pK_a$  results in the ability to extend the dynamic range. An advantageous effect of this dual-fluorophore protocol is that, through adjustment of the fluorophore ratios, the dynamic range can be altered increasing sensitivity. As the pH levels experienced in dental biofilms as a result of fermentation of carbohydrates in particularly wide, the dynamic range was maximised through the incorporation of the two pH-sensitive fluorophores in a 1:1 ratio. The nanosensors have been produced, characterised and calibrated for the ability to determine pH across much of the range likely to be observed in dental plaque following exposure to fermentable carbohydrates. This range was designated to be from a resting pH to values below pH 4, possibly approaching pH 3. With such a relatively wide range, the priority was to increase the dynamic range regardless of the decrease in sensitivity. The method described here was selected as it is likely to overcome a number of the shortcomings of previously described methods. Through the use of a dual-sensitive fluorophore construct, the dynamic range could be extended to allow measurement across a wider range of pH values. This is particularly important when considering the wide range of values experienced within dental plaque following exposure to fermentable carbohydrates, such as sucrose. Through further incorporation of a pH-insensitive fluorophore, in the form of TAMRA, it allowed a ratiometric methodology to be used. By employing a ratiometric methodology it allowed

measurements to be accurately recorded regardless of variations in nanosensor concentration. Nanosensor concentration may vary greatly as a result of the heterogeneous structure of the biofilm. Through characterisation we have demonstrated that the nanosensors are able to be produced which incorporate three fluorophores, two sensitive to pH and one insensitive to variations in hydrogen ion concentration. The resultant nanoparticles have a mean diameter of approximately 40 nm, as determined by ESEM and dynamic light scattering. The nanosensors have a narrow width distribution. The fluorescent spectra of the nanosensors demonstrate that the pH sensitive fluorophores react to variations in pH while the reference fluorophore remains stable allowing ratiometric measurements to be obtained.

#### **4.4.1 Summary**

Nanosensors were able to be produced which incorporate three fluorophores, two sensitive to variations in pH and a pH-insensitive fluorophore. This configuration allows ratiometric imaging negating variations in fluorophore concentration, excitation intensity, detector sensitivity and light scattering. By incorporating two pH-sensitive fluorophores with similar fluorescence spectra, but with differing  $pK_a$  the dynamic range was increased approximately two-fold. This increase, however, was at the expense of resolution. The produced nanosensors possessed a narrow distribution width and an average diameter of approximately 40 nm. Analysis of the fluorescence spectra demonstrated that the green (pH-sensitive) fluorophores exhibited a considerable difference in fluorescence intensity with respect to variations in pH with maximum fluorescence emission intensity at approximately 520 nm. The pH-insensitive fluorophore exhibited little variation in fluorescence emission intensity with respect to pH with a maximum fluorescence emission intensity observed at approximately 575 nm. The nanosensors have been designed and produced. They demonstrate the desired properties with respect to fluorophore excitation and emission spectra, ratiometric analysis, and dynamic range the fluorophores require calibration in order to be utilised in the determination of pH.

# Chapter 5 Investigation of Suitability and Calibration of Dual-Fluorophore, Ratiometric, pH-Sensitive Nanosensors for the Determination of pH

## 5.1 Introduction

Following production and characterisation of the nanosensors, an important aspect to consider is the biocompatibility of both the nanoparticle matrix and the nanosensors which needs to be assessed in order to determine whether there is any detrimental effect upon the bacteria being studied through their use. Furthermore, it is important to know whether any detrimental effect observed is dose-dependent. Analysis of detrimental effect was performed utilising two methods; live/dead staining using a commercial kit, and colony counting following serial dilution. LIVE/DEAD<sup>®</sup> BacLight™ Cell Viability Stain (Life Technologies, UK) was utilised for live/dead staining. The kit consists of two fluorescent dyes; SYTO<sup>®</sup> 9 green-fluorescent nucleic acid stain and propidium iodide red-fluorescent nucleic acid stain. Each stain differs in their ability to penetrate the cell membrane of healthy cells. When used exclusively, SYTO<sup>®</sup> 9 green-fluorescent nucleic acid stain will stain all bacteria, regardless of cell membrane permeability. When used in conjunction with propidium iodide, a cell-impermeant dye, the propidium iodide only has the ability to penetrate cells with a disrupted cell membrane (dead cells). Therefore, only when the cell membrane is disrupted will the propidium iodide gain access to the nucleus. When the cell membrane is damaged propidium iodide penetrates the cell and decreases the fluorescence of the SYTO<sup>®</sup> 9. As a result, live cells which possess an intact cell membrane display green fluorescence while dead cells with a disrupted cell membrane fluoresce red.

Once biocompatibility is established, the nanosensors require calibration to correlate the response of the sensor to changes in the analyte concentration. Correlation to responses to changes in pH also allows analysis of the usable limit of

determination (dynamic range) of the sensor. As the nanosensors investigated possess both pH-sensitive and pH-insensitive fluorophores, they allow a ratiometric methodology to be employed. Ratiometric methodologies alleviate the requirement to have knowledge of the fluorophore concentration. Changes in concentration will have a direct effect upon the fluorescence emission of a single pH-sensitive fluorophore. By using ratiometric measurements, that is the ratio of a pH-sensitive to a pH-insensitive fluorophore, concentration is negated. Through the use of image analysis software, ratios of the image intensities at each different wavelength were obtained. The fluorescence intensity values were able to be plotted with respect to pH. Through regression analysis, the line-of-best-fit and the corresponding equation of that line were obtained. This equation is then used to determine the pH value of unknown measurements. It is also essential to ensure that there is no detrimental effect to the microorganisms under investigation. In order to determine that there was no detrimental effect to the bacteria, cell viability following exposure to the nanosensor was analysed. This was performed by live/dead cell viability staining and by culture following serial dilution to analyse that there was no dose-dependent effect on cell viability.

### **5.1.1 Aims and Objectives**

The aim of this chapter is to analyse the suitability of dual-fluorophore, ratiometric, pH-sensitive nanosensors to determine variation in environmental pH without detrimental effect upon bacteria.

The objectives are to; i) determine if there is any detrimental effect upon cell viability due to exposure to both the polyacrylamide nanoparticle matrix and functional nanosensors, ii) determine if any detrimental effect observed is dependent upon the concentration of the nanoparticle components of functional nanosensors containing conjugated fluorophores, iii) calibrate the nanosensors to environmental hydrogen-ion concentration, and iv) determine the useful range of measurement (dynamic range) of the nanosensors.

## **5.2 Materials and Methods**

### **5.2.1 Analysis of Bacterial Cell Viability Following Exposure to Polyacrylamide Nanoparticles**

#### **5.2.1.1 *Bacterial isolate preparation***

Sterile BHI broth was prepared, in 20 mL aliquots, as previously described (Section 2.2). Bacterial isolates, stored at -80°C were subcultured and prepared as previously described (Section 2.3).. Isolates were harvested and inoculated into aliquots of sterile BHI broth and incubated overnight at 37°C in an aerobic atmosphere supplemented with 5% CO<sub>2</sub> to produce monocultures. Following incubation, the purity of each culture was assessed by subculture. Bacterial suspensions were standardised to an OD<sub>600</sub> of 0.5.

#### **5.2.1.2 *Plate Set-up***

A 16 g/L suspension of polyacrylamide nanoparticles without conjugated fluorophores, referred to as naked nanoparticles, was produced in sterile deionised water. The suspension was sonicated for 2 min to ensure separation and aid dispersal. The suspension was added to the first column of a 96 well plate and double diluted (1:1) with sterile deionised water to produce final concentrations, following the addition of bacterial suspension, ranging from 8 g/L to 7.813 mg/L. One mL of each bacterial suspension was mixed thoroughly and added to each well of a 96 well plate, such that each isolate was in two rows. Therefore, each concentration-bacterial species combination was analysed in duplicate. In column 12, 1 mL of sterile deionised water was added, replacing nanosensor suspension, to act as a negative control. The layout of the 96 well plate is demonstrated in (Figure 5.1). The plate was incubated overnight in 5% CO<sub>2</sub> at 37°C. Following incubation, cell viability was studied by two methods.

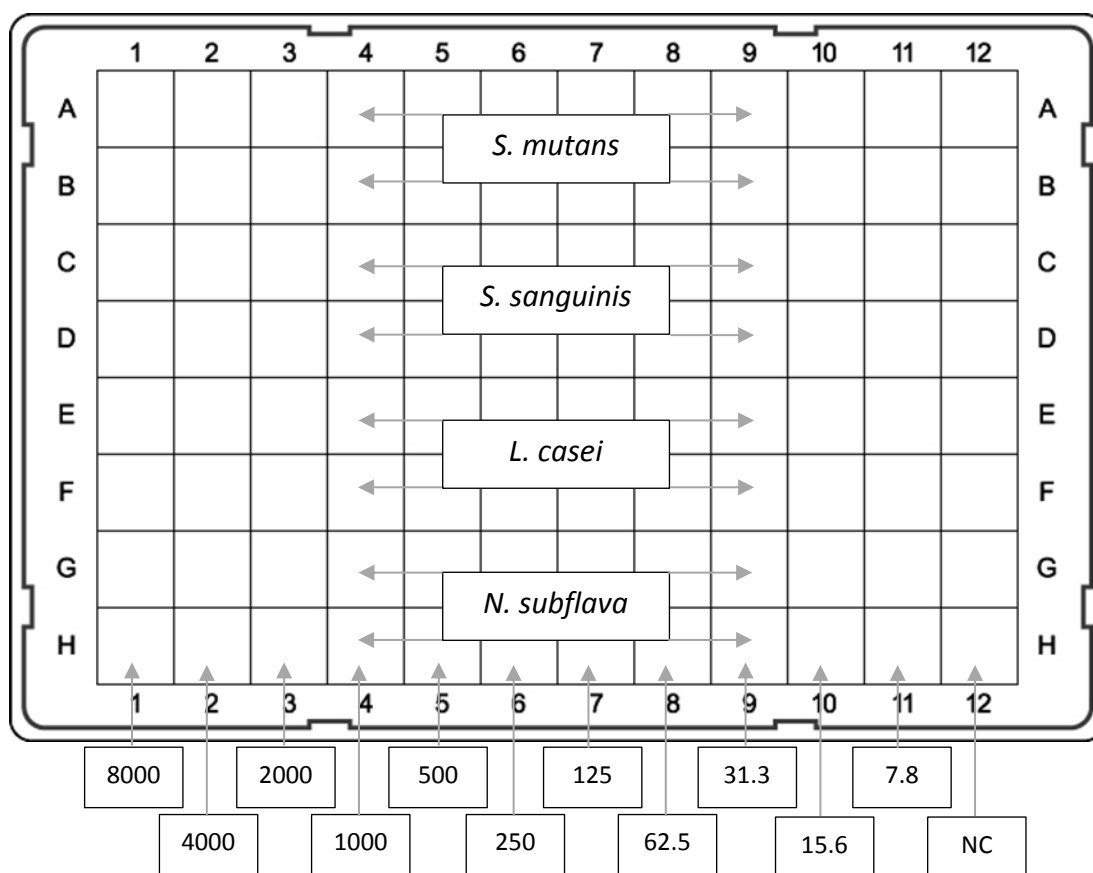


**Figure 5.1** Diagram of 96 well plate layout, showing concentration of nanoparticles, in mg/L, for each column. NC refers to the control well in which nanoparticles were replaced with sterile dH<sub>2</sub>O.

### 5.2.1.3 Analysis of nanoparticle biocompatibility through live/dead cell viability staining

Following incubation, 1 mL of each bacterial suspension exposed to naked nanoparticles from each well was aliquoted to a sterile 1.5 mL screw cap microcentrifuge tube. One  $\mu$ L of both SYTO<sup>®</sup> 9 nucleic acid stain and propidium iodide stain (LIVE/DEAD<sup>®</sup> BacLight™ Cell Viability Stain, Life Technologies, UK) was added to each tube. The tubes were allowed to incubate in the dark at room temperature for 15 min. The tubes were centrifuged for 2 min at 50 g, the supernatant removed and the pellet was resuspended. Fifteen  $\mu$ L of each broth was applied to a cavity well glass slide. A 22 x 22 mm coverslip was carefully applied to ensure that no bubbles were added. As a control, 500  $\mu$ L of methanol was added to

500 µL of a bacterial suspension. The slides were visualised on a BioRad CLSM system using an Olympus UPlanApo x20/0.7 NA water immersion objective. The slides were excited with 488 nm laser line and emission filters were set to 530/30 nm for green fluorescence (live) and 630 nm Long Pass emission filter for red fluorescence (dead). The pinhole was set to 3.0 Airy units, gain 15.0 and offset 0.0. Images were collected. The images obtained in both the green (live) and red (dead) channels were opened in the ImageJ image analysis software package. The images were falsely coloured and merged to produce a single image with the live bacterial cells exhibiting green colouring and dead bacterial cells exhibiting red colouring. To obtain the ratio of live cells to dead cells, 'the multi-point' tool was selected and each green bacterial cell was counted (Figure 5.2). The total was recorded. The process was repeated for red cells, recorded and the ratio of the two calculated. To visualise and analyse the results, the ratios were plotted with respect to nanoparticle concentration.

#### **5.2.1.4 Cell viability by serial dilution and colony counting**

A 500 µL volume of bacterial suspension from each well was transferred to a sterile 1.5 mL screw cap microcentrifuge tube. Each suspension was serially diluted to  $10^{-8}$ . A 100 µL volume of each suspension was applied to a BHI plate and incubated for 48 h at 37°C in aerobic atmosphere supplemented with 5% CO<sub>2</sub>. The protocol was repeated as outlined above. However, isolates were exposed to varying concentrations of nanosensors ranging from 8 g/L to 7.8125 mg/L by doubling dilutions.

#### **5.2.1.5 Colony counting**

Following incubation, plates were analysed to find a dilution factor with between 20 and 200 colonies per plate. The plates were photographed. To accurately count the colonies, ImageJ image analysis software package was used. The images were opened within the program. To aid colony visibility, the image was either inverted or a 'look-up table' was applied. The 'multi-point' tool was chosen and each colony

was selected to obtain the number of colonies (Figure 5.2). To convert the counts to CFU/mL, the colony count was multiplied by 20 to convert the number in 50  $\mu$ L to mL. This number was then multiplied by the dilution factor to convert to the cell concentration in the neat specimen.

#### 5.2.1.6 Data Analysis

The mean of the colony counts for those exposed and those not exposed were calculated for each microorganism. These colony-forming unit counts values were plotted for each organism. The standard deviation from the mean for each set of values was calculated. Error bars showing the standard deviation were applied to the bars. To determine whether there was a significant difference between those exposed to the nanoparticles and those left unexposed, a one-tail T-test was performed. The significance level was set at 0.05 ( $p < 0.05$ ) and  $p$  values were calculated. For the concentration dependent biocompatibility, the cell concentration was plotted with respect to nanoparticle concentration. Once plotted, the mean of the colony counts was calculated. Values two standard deviation from the mean were determined, approximately equivalent to 95% values within a standard distribution. To further determine whether a concentration-dependent effect upon cell viability is observed, a trend line was applied to the values.

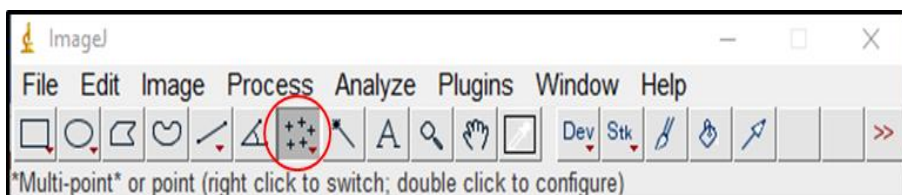


**Figure 5.2** Diagram demonstrating the location of the 'multi-point' tool utilised for counting in the ImageJ image analysis software package.

## **5.2.2 Calibration**

In order to calibrate the nanosensors, a pH titration curve was produced. Citric acid-sodium phosphate buffer solutions were prepared as previously described (Section 2.4). One mg of nanosensors was added to each buffer. The buffers were stored out of light until imaging. Each buffer was imaged using confocal laser scanning microscopy. The pH-sensitive fluorophores were excited using a 488 nm laser line. Fluorescence emission was collected through a 520/30 nm emission filter was applied. Therefore, emitted photons were detected between 505 and 535 nm. The pH-stable fluorophore was excited using a 543 nm laser line and an emission filter (590/70 nm) was applied.

### **5.2.2.1 Preparation of buffered nanosensors solutions**

Citric acid – sodium phosphate buffer solutions were prepared as previously described (Section 2.4). One hundred  $\mu\text{g}$  of nanosensors was added to 10 mL of each buffer. Buffered nanosensor solutions were sonicated for 1 min to ensure adequate separation and dispersal. An extra pH 7.6 buffered nanosensor solutions was prepared to aid optimisation.

### **5.2.2.2 Imaging Optimisation**

The fluorophores selected for the construction of the nanosensors were 5-(and 6)-carboxyfluorescein (FAM), Oregon Green<sup>®</sup>-488 (OG) and tetramethylrhodamine (TAMRA). The excitation and emission spectra for these fluorophores were obtained and analysed through the use of Fluorescence SpectraViewer (Thermo Fisher Scientific 2015). Both FAM and Oregon Green<sup>®</sup>-488, the pH-sensitive fluorophores, possess a maximum excitation wavelength of approximately 498 nm. The instrument used possesses laser lines at 488 and 543 nm. Therefore, in selecting the 488 laser line as the excitation source, the relative intensity can be expected to be between 73% and 83% of the maximum intensity at 498 nm (Figure 4.9). The maximum emission wavelengths for the two dyes vary slightly with FAM possessing a fluorescence emission maximum of 516 nm, while Oregon Green<sup>®</sup>-488 has a

fluorescence emission maximum of 524 nm. To this end, an emission filter was applied with a bandwidth of 520/30 nm, allowing photons emitted between wavelengths of 505 and 535 nm to be detected (Figure 4.9). The pH-stable fluorophore, TAMRA, possesses an excitation maximum at a wavelength of 552 nm. Therefore, the 543 nm laser line was selected to excite the pH-stable fluorophore. The fluorescence emission maximum for TAMRA is 576 nm. A fluorescence emission filter with a bandwidth of 590/70 nm was selected (Figure 4.10). The 590/70 nm fluorescent emission allows emitted photon with a wavelength between 555 and 625 nm to be detected. To analyse the excitation and emission spectra further, spectral analysis was performed. To maximise the fluorescence emission intensity, the 'set high' filter was applied from the lookup table. The 'set high' filter demonstrated the level of saturation of each pixel. The gain was then adjusted to slightly lower than saturation using the pH 7.6 buffer solution with nanosensors added. The pH 7.6 buffer solution was selected as the highest amount of fluorescence emission was greatest at higher pH values. This process was repeated for the pH-stable fluorophore using this sample, as fluorescence emission intensity should be stable over the pH range. By optimising the laser power, the likelihood and level of photobleaching is minimised.

### **5.2.2.3 Imaging**

A 100  $\mu$ L aliquot of each suspension was transferred to a cavity well glass slide (Brunel Microscopes Ltd., Wiltshire, UK). Images were obtained on an Olympus BX51 microscope equipped with a BioRad CLSM system using an Olympus UPlanApo x20/0.7NA water immersion objective lens. The focal plane was determined and set using the z dimension motor control. Images were obtained by raster scanning in the xy dimension. The pH-sensitive fluorophores (FAM and Oregon Green<sup>®</sup>-488) were excited using an Argon 488 laser set to 25.0% power. Fluorescence emission was collected using a HQ520/30 emission filter. Pinhole was set to 2.0 Airy units, gain 20.0 and offset 2.0. TAMRA was excited using a Green HeNe 543 nm laser set to 41.3% power. Emission was collected using a HQ590/70 emission filter, gain 50.0 and offset 2.0. The scan speed was set to 166 lines per second. Zoom was set to

1.0x. Images were collected using a Kalman filter set (linear quadratic estimation) to N:3 F:1. The resolution of the images was set to 512 x 512 pixels.

#### **5.2.2.4 *Image analysis***

Images obtained were analysed with the use of ImageJ Image Analysis Software Package (Rasband 1997). The intensity values at each pixel location, for each channel, were transferred to Microsoft Excel (2013) and the average fluorescence intensity value was plotted with respect to the pH value of the buffered nanosensor solution. Calibration curves were generated by plotting a ratio of the peak fluorescence intensities ( $R = \lambda_{em} 520 \text{ nm} / \lambda_{em} 577 \text{ nm}$ ), using peak emission spectra from three different suspensions of nanosensors. Variations in the red channel were corrected by normalisation. Fluorescence intensity should remain constant across the pH range and variations would likely be due to the optics. To perform the normalisation; the inverse of the fluorescence intensity in the red channel was calculated for each reading. The fluorescence intensity in the red channel was then divided by the inverse to produce a red channel value of 1. The inverse value was also applied to the corresponding green channel fluorescence intensity.

### **5.2.3 *Imaging of the Buffered Nanosensor Suspensions***

#### **5.2.3.1 *Image Analysis***

Images were analysed using ImageJ (Rasband 1997). Average intensity measurements for each pH were obtained and separated by channel. The ratio of the intensities was plotted with respect to pH and the calibration curve obtained.

#### **5.2.3.2 *Normalisation of the pH-insensitive Fluorophore Fluorescence Emission***

Due to visible variations in the intensity of the pH-stable red channel intensity values, the average fluorescence emission intensity of the red channel was normalised. The normalization value for the red channel was then applied to the green channel of the respective pH value. In order to normalise the calibration

curve; the inverse of the values obtained for each buffer in the red channel were calculated by Equation 5-1.

$$I_{V_{\text{red}}} = \frac{1}{O_{V_{\text{red}}}} \quad \text{Equation 5-1}$$

The normalised value for the red channel was applied to the green channel value, calculated by Equation 5-2;

$$N_{V_{\text{green}}} = O_{V_{\text{green}}} \times I_{V_{\text{red}}} \quad \text{Equation 5-2}$$

The values for the red channel were thereby given equal weighting and the calculation was applied to the green channel values and the normalised curve was produced.

## **5.2.4 Determination of pH Changes in Planktonic Bacteria Using Dual-Fluorophore, pH-Sensitive, Ratiometric Nanosensors**

### **5.2.4.1 Sample Preparation**

Following incubation, bacterial isolates were inoculated into sterile, non-buffered saline to an OD<sub>600</sub> of 1.0. A 1 mL aliquot of each bacterial suspension was added to the well of a 24-well microtitre plate. A 20 g/L nanosensors suspension was produced as previously described. To each well, 1 mL of the nanosensor suspension was added.

### **5.2.4.2 Image Acquisition**

The resting pH of the bacterial suspension with the nanosensors was imaged using a fluorescent microscope in both the green and red channels. Following imaging of the resting pH of the bacterial suspensions containing nanosensors, the plate was removed and 500 µL of 0.1 M sucrose was added. The plate was allowed to

incubate for 30 min at room temperature. Following incubation, the plate was imaged using the same parameters. The process was repeated for all four bacterial suspensions.

#### **5.2.4.3 Image Analysis**

The collected images were analysed using ImageJ (Rasband 1997). The images were separated by channel and the average intensity measurements of each channel obtained. The results were cross-referenced with those of the calibration to determine the pH values.

## **5.3 Results**

### **5.3.1 Analysis of Bacterial Cell Viability Following Exposure to Polyacrylamide Nanoparticles**

The analysis of the viability of bacterial cell following exposure to polyacrylamide nanoparticles was performed by live/dead fluorescent staining and by serial dilution and colony counting.

#### **5.3.1.1 Live/Dead Staining**

Figure 5.3 shows two images of bacteria (*N. subflava*) stained with live/dead stain (SYTO<sup>®</sup> 9 and propidium iodide). Green cells demonstrate cell viability while red cells with a disrupted cell membrane are non-viable. Image A shows a suspension not exposed to polyacrylamide nanoparticles while image B demonstrates the bacterial suspension following exposure to the nanoparticles.

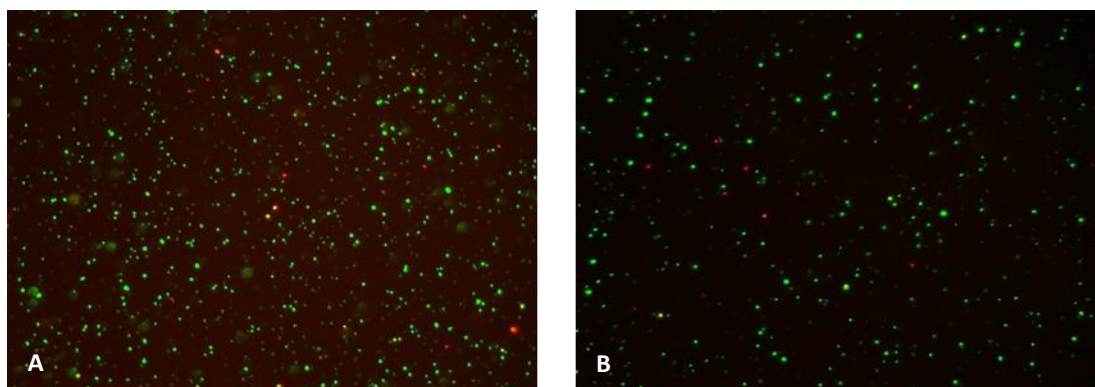


**Figure 5.3** Live/dead images of a suspension of *N. subflava*. A) Not exposed to nanoparticles B) Exposed to nanoparticles.

#### **5.3.1.2 Serial Dilution**

Figure 5.4 shows a comparison of the number of colony-forming units per mL of a number of bacterial suspensions unexposed to polyacrylamide nanoparticles to the same bacterial suspension following exposure to the nanoparticles. Statistical analysis (two tailed t-test) demonstrated the differences in cell viability for each organisms are not statistically significant (Figure 5.4 and Table 5-1). Not only was there minimal cell non-viability observed in those suspensions exposed to the naked nanoparticles, there was no increase in cell non-viability between the control suspensions and those exposed to the naked nanoparticles. Colony-forming unit counts obtained following serial dilution showed a maximum difference of 3.87% (average: 2.88%). The naked polyacrylamide nanoparticles had minimal detrimental effect on the cell viability of those bacteria tested.

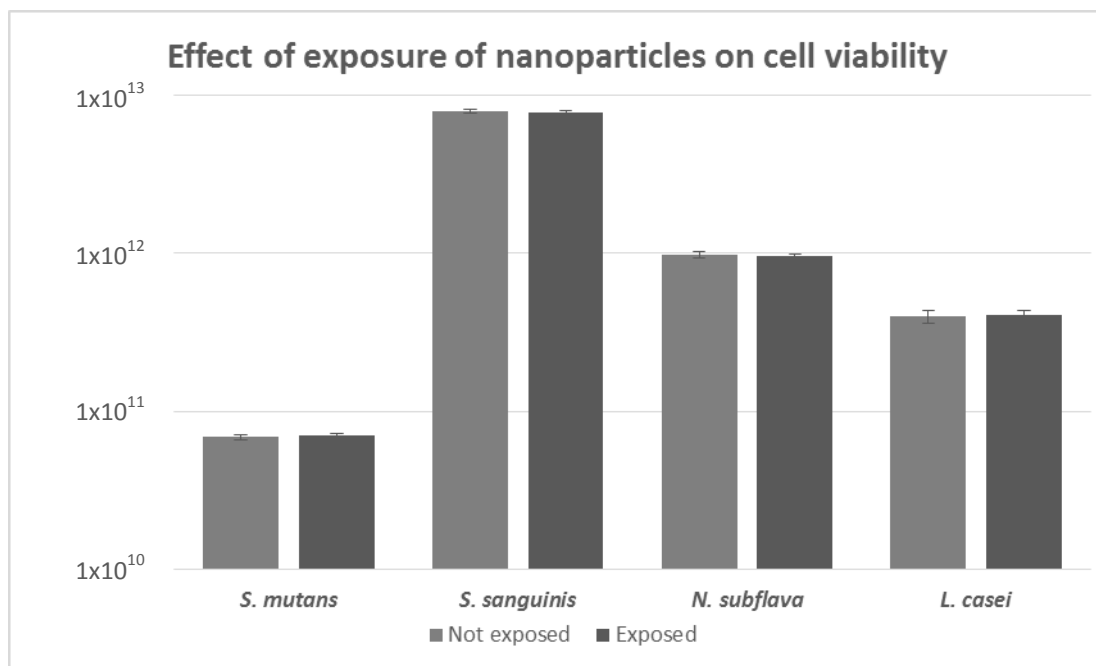


**Figure 5.4** A comparison of cell viability, determined by colony-counting, following exposure to polyacrylamide nanoparticles. Error bars show standard deviation from the mean. n = 3.

	<i>S. mutans</i>	<i>S. sanguinis</i>	<i>N. subflava</i>	<i>L. casei</i>
<b>p value:</b>	0.152	0.237	0.280	0.322
<b>(at p &lt; 0.05)</b>	Not significant	Not significant	Not significant	Not significant

**Table 5-1** Statistical analysis of the colony counts of exposed and not exposed to sucrose.

Figure 5.5 shows the relative proportions of viable to non-viable cells for each organism, at each concentration. When compared to the control, which was not exposed to the nanoparticles, no discernible difference was seen across all concentrations.

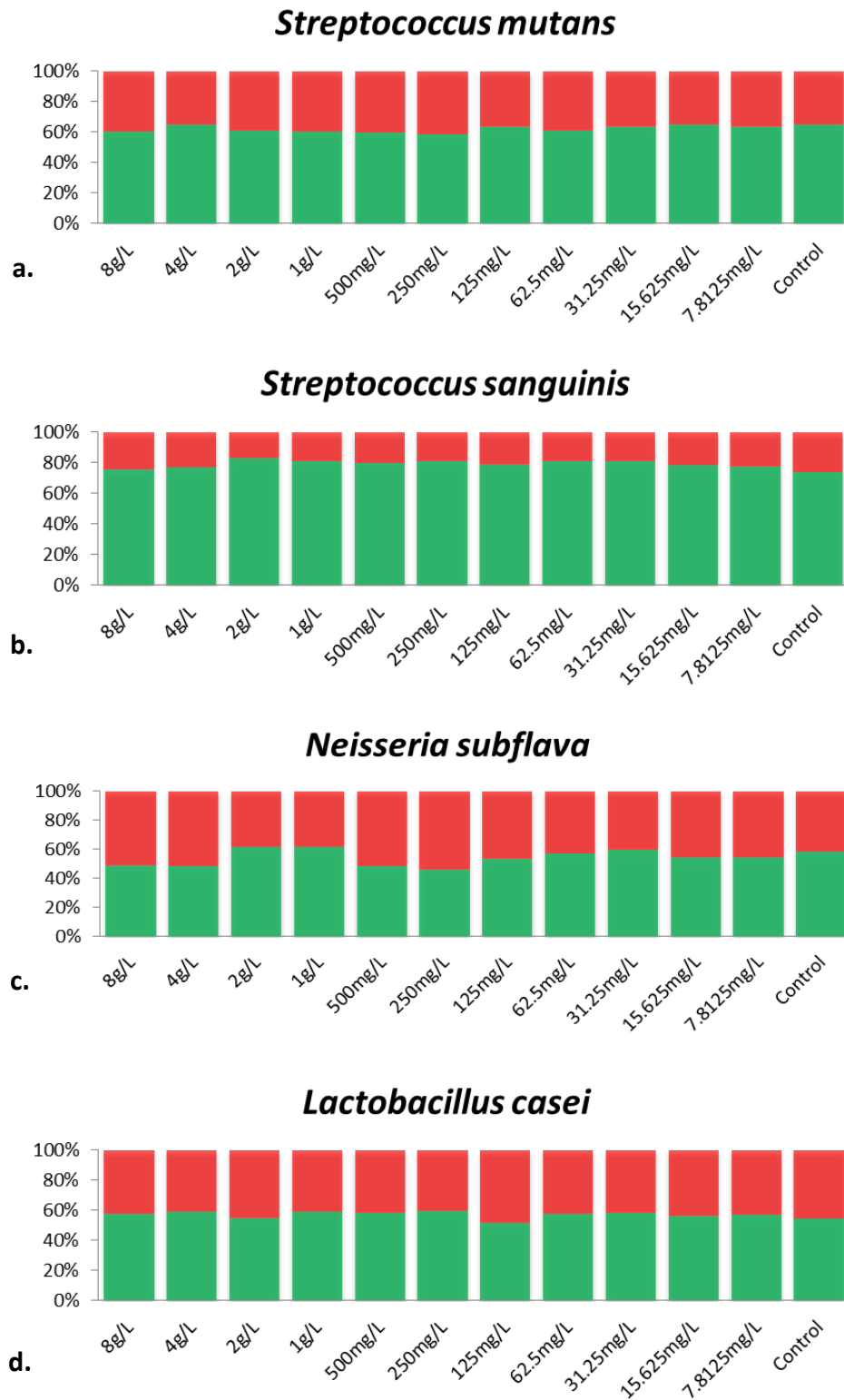


**Figure 5.5** Relative proportions of live (green) and dead (red) bacteria following exposure to nanosensors for 24 h for a.) *S. mutans*, b.) *S. sanguinis*, c.) *N. subflava*, and d.) *L. casei*. n = 1.

### 5.3.2 Serial Dilution

Figure 5.6 shows the number of colony-forming units obtained from bacterial suspensions when exposed to varying concentrations of polyacrylamide nanoparticles, incubated overnight and serially diluted. The green dotted lines demonstrate the mean bacterial number across all concentrations while the red dotted line represents 2 standard deviations from the mean. All bacterial counts fall, except for one within 2 standard deviations of the mean (*S. sanguinis*; 125 mg/L). This value falls above the upper limit indicating that the effect is not detrimental to cell viability. Therefore, detrimental effect can be excluded. A possible, yet unlikely, effect of nanoparticle exposure is promotion of growth. The variation observed across the different concentrations of polyacrylamide nanoparticles exposed to *S. sanguinis* demonstrates that this is unlikely. Furthermore, across the other organisms tested, no promotion of growth is observed. To further ensure that no effect upon growth was provided this nanoparticle concentration-organism combination was re-tested. Following this, the bacterial count fell within the upper 2 SD limit ( $2.98 \times 10^9$  CFU/mL). Furthermore, only small variation is observed in trend (yellow solid line) across the different concentrations. This variation is proportional to the concentration to which the bacteria are exposed. If a concentration-dependent detrimental effect was to be observed, this trend would be inversely proportional to the nanoparticle concentration. All, except one, of the bacterial counts were in excess of the control unexposed to nanoparticles. Statistical analysis revealed no statistical significance in variation of bacterial concentration at various concentrations of nanoparticles. Minor variation is observed in trend (yellow solid line) across the different concentrations. This variation is proportional to the concentration to which the bacteria are exposed. Again, if a concentration-dependent detrimental effect was to be observed, this trend would be inversely proportional to the nanoparticle concentration. Statistical analysis revealed no statistical significance in variation of bacterial concentration at various concentrations of nanoparticles. Statistical analysis revealed no statistical significance in variation of bacterial concentration at various concentrations of nanoparticles for these two organisms.

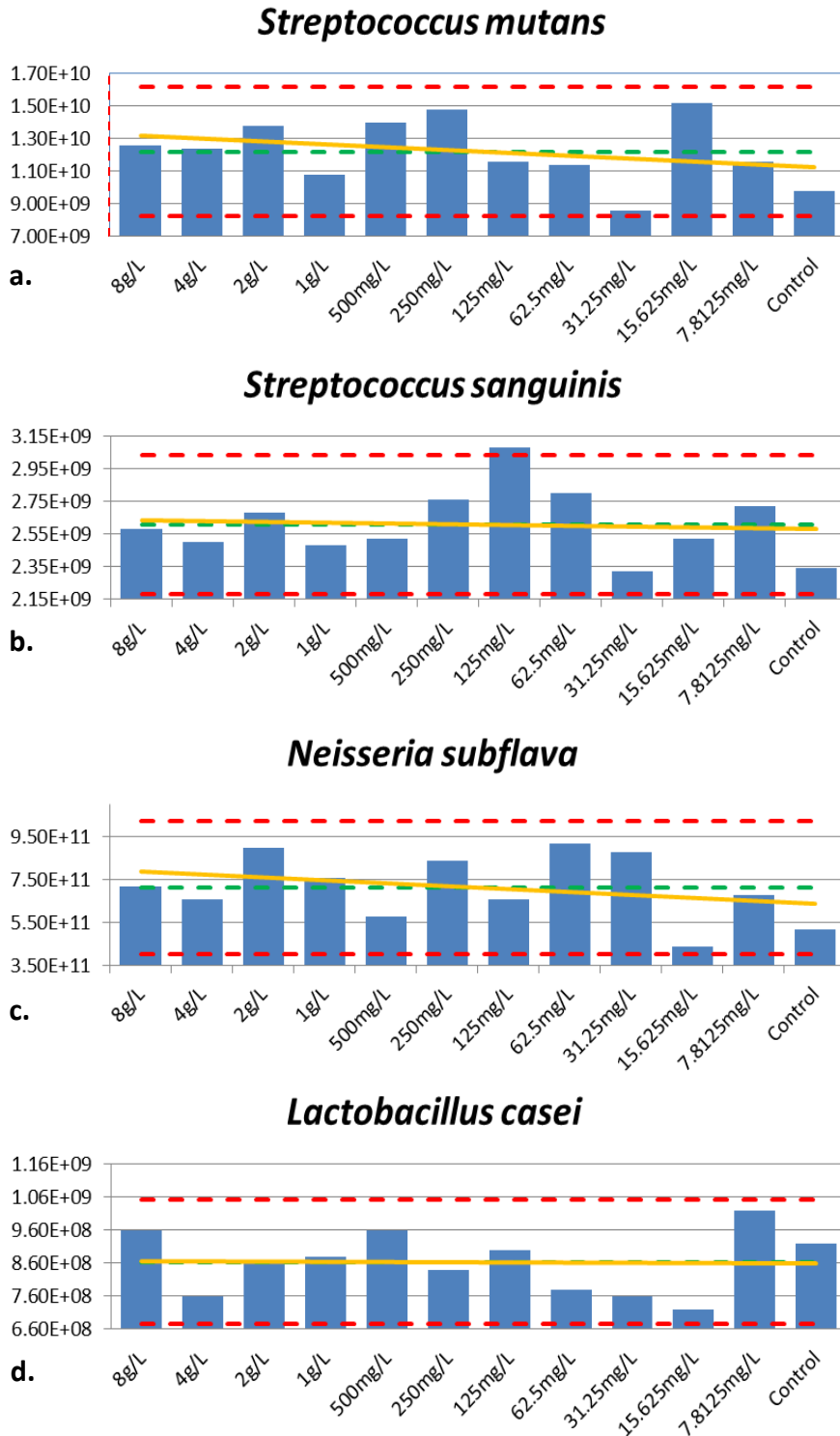


**Figure 5.6** Plot of CFU/mL following exposure to varying concentration of polyacrylamide nanoparticles for a.) *S. mutans*, b.) *S. sanguinis*, c.) *N. subflava*, and d.) *L. casei*. The green dotted line represents the mean bacterial concentration and the red dotted lines represent 2 standard deviations from the mean across the varying nanoparticle

**concentrations. The yellow solid line shows the trend in bacterial concentration values across the varying nanoparticle concentrations.**

### **5.3.3 Calibration**

Figure 5.7 shows an array of images obtained of dual-fluorophore, ratiometric, pH-sensitive nanosensors in buffered solutions at varying pH values. The pH-sensitive fluorophores were excited using the 488 nm laser line and emitted photons were collected, through a 520/30 nm emission filter, in the green channel (505 - 535 nm). The pH-stable fluorophore (TAMRA) was excited using the 543 nm laser line and emitted photons were collected in the red channel through a 590/70 nm emission filter (555 - 625 nm). The images obtained in each channel, at each pH, were merged in a third channel (Figure 5.7). The images obtained in the green channel demonstrate a visible increase in intensity with respect to pH from pH 2.5 to pH 8.0. This is also reflected in the colour of the merged images demonstrating the ratiometric nature of the nanosensors. Images obtained in the red channel remain relatively stable, although demonstrate small visible deviations, across the pH spectrum (Figure 5.7).

When the fluorescent emission intensities were plotted with respect to pH to produce titration curves fluorescent intensities in the green channel (pH-sensitive) demonstrated a response proportionate to increases in pH. When plotted, the variation in the red channel (pH-stable) become apparent (Figure 5.8 a). To negate the effect of this variation, the red channel fluorescent emission intensities were normalised. The fluorescent emission intensities in the green channels were adjusted to be normalised to the red channel for each pH. Following normalisation, the plot of the green channel fluorescent emission intensities followed a more sigmoidal response proportionate to increase in pH (Figure 5.8 b). Therefore, intensities obtained from the green channel provide a distinguishable value of pH. Further to this, the ratio of the fluorescent emission intensities in the green channel (pH-sensitive) to the red channel (pH-stable) was plotted with respect to pH. This produced the ratiometric calibration curve observed in Figure 5.9.

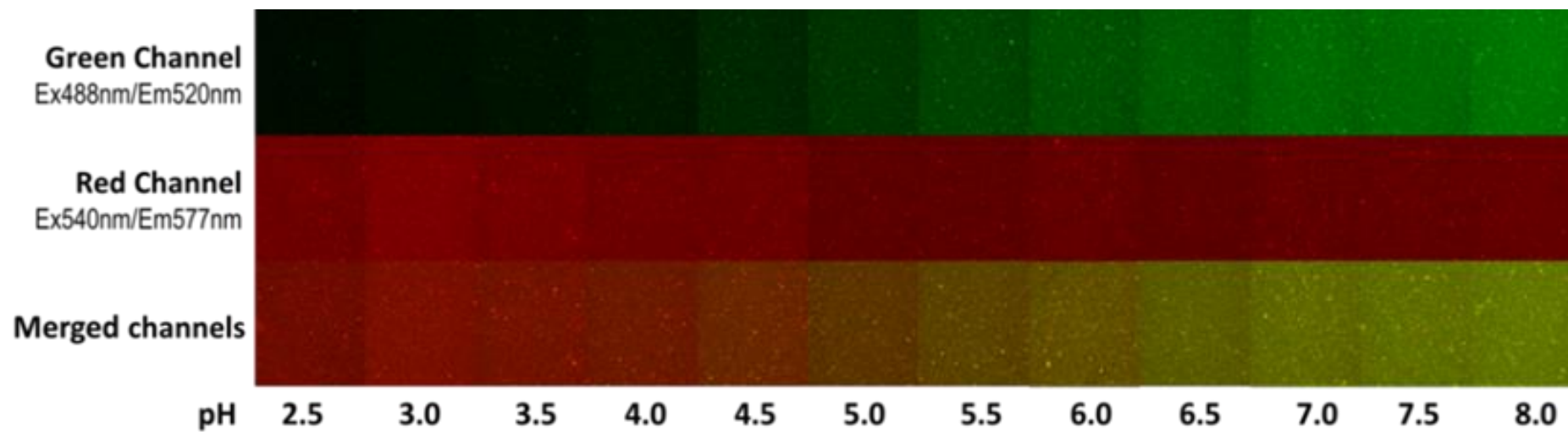
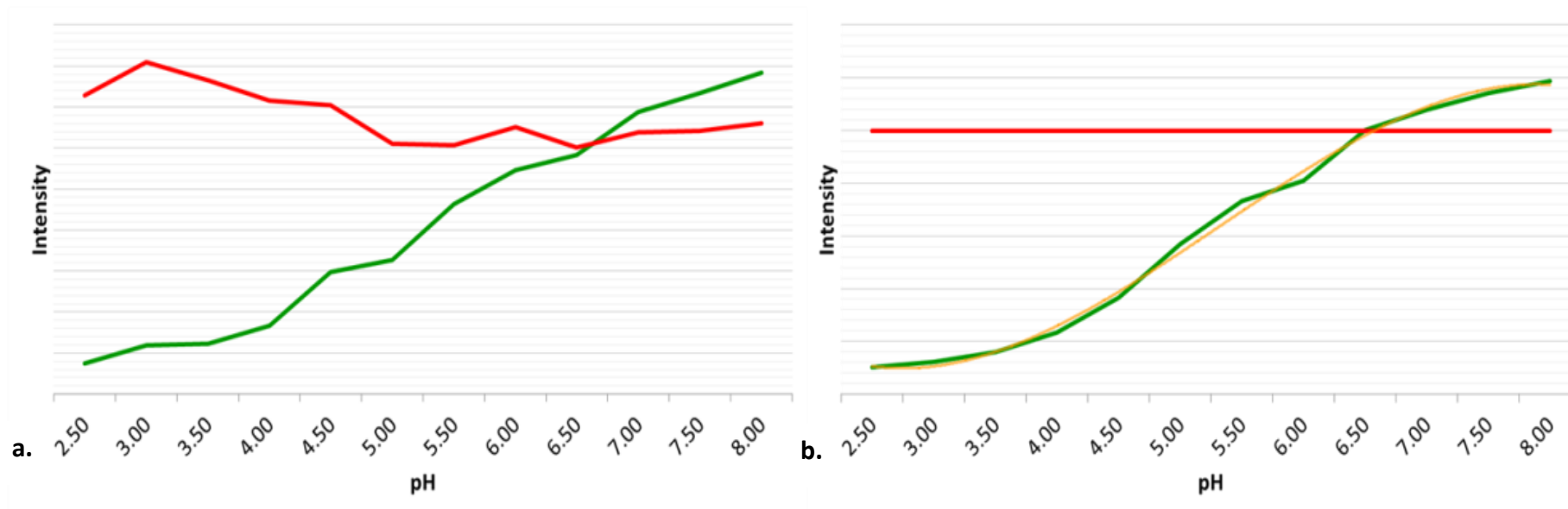
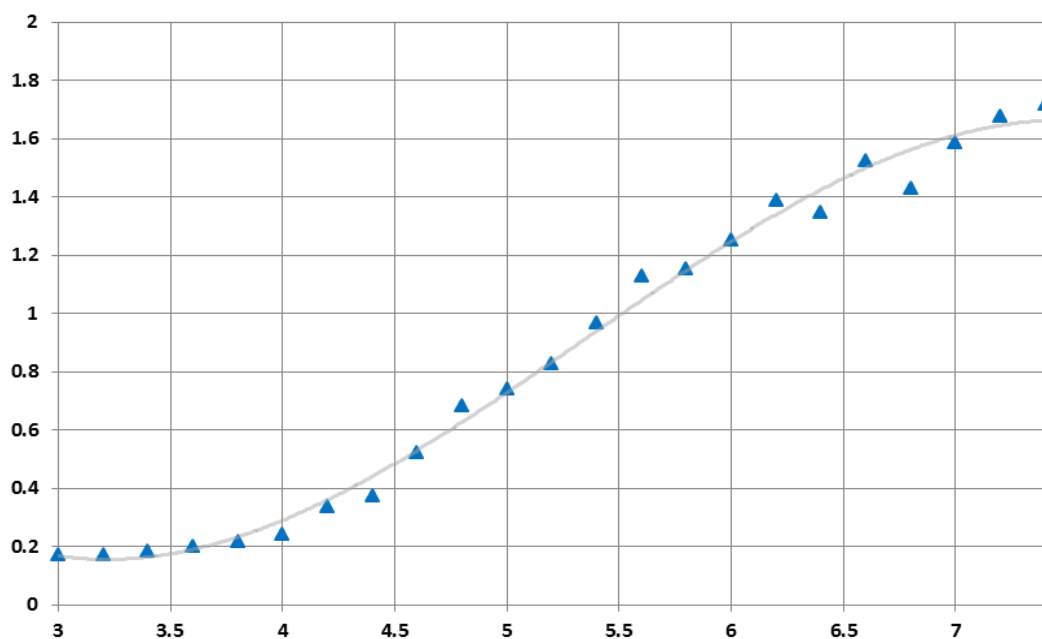


Figure 5.7 Matrix of images of nanosensors in buffers of varying values, showing separate images and merged images



**Figure 5.8** Graphic representation of obtained intensities with respect to pH. A) Intensities obtained prior to normalisation. B) Intensities following normalisation. The red line represents fluorescence intensity values in the red channel, while the green line represents fluorescence intensity values in the green channel. The yellow line represents the line-of-best-fit and represents the calibration curve.

## Normalised calibration curve



**Figure 5.9** Calibration curve of pH-sensitive nanosensors in pH buffer solutions ranging from pH 3.0 to 7.4, and the residual values

## 5.4 Discussion

Following initial analysis of the use of dual-fluorophore, ratiometric, pH-sensitive nanosensors, the use of these nanosensors appear to alleviate many of the drawbacks of currently-used and previously utilised methods to determine and monitor pH microgradients within biofilms. The potential improvements include; the minimisation of structural disruption and the potential effect upon results, decreased sensor size, the ability to analyse a larger volume and the ability to analyse a biofilm in a naturally hydrated state. Other advantages include the fact that the nanosensors are relatively inexpensive and relatively simple to produce. The pH-sensitive fluorophores used in the production of dual-fluorophore, ratiometric, pH-sensitive nanosensors; carboxyfluorescein and Oregon Green<sup>®</sup>-488, were selected as they are sensitive to changes in environmental pH and they possess a similar fluorescence excitation and emission spectra. The fact that they possess similar fluorescence spectra allows both fluorophores to be excited through

the use of a single laser line (in this case, 488 nm) and furthermore, the fluorescence emission can be detected at the same wavelengths. However, they possess significantly different  $pK_a$ . The  $pK_a$  is of particular significance to pH-sensitive fluorophores as it is the point at which the fluorophore demonstrates the greatest fluorescence emission change to alterations in pH.

In order to effectively use the nanosensors, it was imperative to ensure that the nanosensors demonstrated biocompatibility with the bacterial species being investigated. This was performed using two methods; BacLight LIVE/DEAD® Cell Viability Assay kit and colony counting following serial dilution. Although the nanosensors have previously been used to visualise pH within the free-living nematode, *C. elegans* (Chauhan et al. 2013), biocompatibility with bacteria has not been analysed. Nanoparticles of similar composition have been employed to determine intracellular parameters in bacterial biofilms (Hidalgo et al. 2009) and tissue cells (Aylott 2003; Han & Burgess 2010; Shi et al. 2012; Desai et al. 2013). The bacteria used in the formation of biofilms mimicking dental plaque were exposed to varying concentrations of the polyacrylamide nanoparticles without the fluorophores conjugated. Various concentrations were analysed to evaluate whether any observed detrimental effect was concentration-dependent. It was assumed that no detrimental effect would be observed as a result of fluorophore conjugation as all three fluorophores have been used extensively in the analysis of bacteria. When exposed to varying concentration of polyacrylamide nanoparticles, no statistically significant effect was observed by either cell viability technique. Calibration of the nanosensors is required to correlate the response to environmental pH. The calibration of the nanosensors was performed using a confocal laser scanning microscope. Confocal microscopy facilitates optical sectioning, through the use of a pinhole aperture which negates out-of-focus emitted light, allowing imaging not just in the x,y dimensions, in addition to the z dimension. This capability is of particular value when investigating microgradients in the three-dimensional structure of biofilms. The system used also allows multiple laser lines to be utilised simultaneously, producing each image in a timely manner. The nanosensors were able to be calibrated demonstrating a sigmoidal response to

increases in hydrogen ion concentration. As previously described, currently employed methods are limited by their considerable drawbacks. Therefore, it is imperative to investigate methods for determining environmental pH which alleviate these drawbacks. The use of nanosensors appeared to address many of the drawbacks of other techniques for the determination of extracellular pH in bacterial biofilms. These advantages include the ability to analyse and observe bacterial biofilms in their naturally-hydrated state, the ability to observe high-resolution extracellular pH microgradients in a number of spatial and temporal dimensions, no disruption of the biofilm structure which may affect the results obtained and no need for the knowledge of the sensor concentration due to the ratiometric nature of the nanosensors. The nanosensors show great promise in the determination and visualisation of bacterial biofilms. Due to the significance of pH plays in driving the dissolution of the dental hard tissue and the formation of the dental caries lesion, the determination of extracellular pH is of particular scientific interest. However, currently employed methods do not provide this information without drawbacks. The method investigated here is not without drawbacks itself. Therefore, the search for a method which allows the determination of extracellular pH of biofilms, in a naturally hydrated state, without disruption to the biofilm structure, continues

#### **5.4.1 Summary**

Through the use of two methods, it was determined that dual-fluorophore, ratiometric, pH-sensitive nanosensors, and the fluorophore-free nanoparticle cause no significant detrimental effect upon the bacteria used.

The pH-sensitive nanosensors were able to be calibrated allowing determination of environmental pH in buffer solutions.

# Chapter 6 Analysis of Seminaaphthorhodafluor (SNARF) Dyes to Determine Hydrogen-Ion Concentration

## 6.1 Introduction

Fluorescence-lifetime imaging microscopy (FLIM) is an imaging technique in which the duration of the excitation event, and not the emitted fluorescence wavelength or intensity, is measured. The major advantage of FLIM lies in the fact that, unlike in intensity-based measurements, the fluorescence lifetime is an inherent property and is unaffected by variations in fluorophore concentration, light path distance, sample thickness or photobleaching. In fluorescence-lifetime imaging, a technique called multiphoton excitation (or two-photon excitation in this case) is often employed. Multiphoton excitation arises when two (or more) photons with a combined energy sufficient to cause molecular excitation are absorbed within a single quantised event, resulting in excitation. Since the energy of a photon is inversely proportional to the wavelength of the light, the excitation wavelength must have wavelength of approximately double that of the single excitation wavelength. The single-photon excitation wavelengths for the fluorophores selected here are easily obtained from the literature. However, the two-photon are unable to be found. The optimum two-photon excitation wavelengths therefore require determination. Multiphoton excitation provides localised excitation at the point of focus and therefore no absorption occurs above or below the point of focus. This localised excitation removes the effects of photobleaching and phototoxicity above and below the point of focus and therefore makes the technique ideal for live cell imaging. Furthermore, this localised excitation and increase penetration of the excitation light improves depth penetration and removes the requirement for the pinhole aperture used in confocal imaging to block out-of-focus light as this does not occur.

Fluorescence-lifetime values are able to be determined in either the time-domain or the frequency-domain. In the time-domain, the duration of time between excitation

and emission is detected and placed in 'bins'. Each photon detected is added to the respective bin and the plot of the number of photons with respect to the time point reveals an exponential decay curve from which the fluorescence-lifetime can be calculated. This approach is rather intuitive. In frequency-domain measurements, the change in frequency between the excitation and emission light reveals the fluorescence-lifetime. The specimen is excited with an oscillating wave with the desired wavelength and, upon excitation, will emit light at the same frequency but with a different wavelength (a decrease in amplitude, demodulation), corresponding to the change associated with Stokes shift. The light will also be delayed corresponding to the fluorescence-lifetime event. The fluorescence-lifetime is able to then be calculated from the shift in phase and the demodulation. This works well for mono-exponential decay, however variation in the phase shift and modulation occur in bi-exponential decay. To determine fluorescence-lifetime values in the time-domain, time-correlated single photon counting (TCSPC) can be used.

The benzo[c]xanthene fluorophores of the seminaphthorhodafluor group have previously been employed for determination of intracellular pH in living cells when used in the cell-permeable acetoxymethyl ester form. With this in mind the cell-impermeable non-ester form appear to be an ideal choice to investigate extracellular pH. Upon further inspection of the properties, the  $pK_a$  of each member shows that seminaphthorhodafluor-4F 5-(and-6)-carboxylic acid (SNARF-4F) has the lowest and most appropriate  $pK_a$  for the pH values expected in dental plaque during fermentation. The optimal concentration requires determination. The concentration needs to be sufficient to allow excitation to two-photon to occur in appropriate conditions and with the employed instrumentation, and not too high to introduce noise from background emission. The fluorophore also requires the determination of changes in fluorescence-lifetime with respect to environmental pH and subsequently calibration by correlation of the fluorescence-lifetime to pH. When a fluorophore alters its structure as a result of changes in an environmental parameter, e.g. pH, the fluorescence lifetime may vary in a predictable manner. This allows the determination of that parameter. By utilising a single fluorophore that is

affected by the environmental parameter of interest, the difference in the fluorescence lifetime conveys information about the local environment.

The previous considerations are focussed on optimising the system; i.e. the fluorophore selected and the instrumentation; however other factors may have a detrimental effect upon the experiments and require consideration. Having previously been employed in live cell imaging with little to no detrimental effect, it is suspected no detrimental effect would be observed in the bacteria used, however this required assessment. Therefore, the bacteria used need to be exposed to increasing concentrations of the fluorophore to determine any detrimental effect. The choice of substrata for biofilm growth may produce fluorescence and therefore affect or mask the fluorescence of the fluorophore within the biofilm. Therefore the fluorescent properties of various substrata require analysis. Finally, the complexity of the biological system needs to be addressed. It is clear that fluorescence-lifetime changes with respect to pH, however other factors may affect the fluorescence-lifetime. Other factors within the biofilm may produce a diminishing effect on the fluorescence-lifetime values, and include physical factors (temperature, redox-potential), as well as chemical factors, (proteins and glycoproteins).

### **6.1.1 Aims and Objectives**

The aim of this chapter is to investigate the use of SNARF dyes to determine environmental pH through the use of multiphoton molecular excitation, time-correlated single-photon counting to determine fluorescence-lifetime values, and fluorescence lifetime imaging microscopy.

The objectives are to; i) determine the optimal two-photon excitation wavelength for SNARF<sup>®</sup>-4F 5-(and-6)-carboxylic acid, ii) optimise the excitation laser, emission and detection parameters and the instrument settings, iii) determine whether various substrata there effect fluorescence lifetime, iv) determine whether there are any detrimental effects upon measurements from other environmental parameters which may be experienced in the oral biofilm, such as variations in redox potential, temperature, protein and glycoproteins concentrations, and v)

calibrate the SNARF dyes in order to correlate fluorescence lifetime measurements with environmental pH.

## **6.2 Materials and Methods**

### **6.2.1 Instrumentation**

The laser system consisted of a mode-locked femtosecond/picosecond Ti:sapphire Tsunami (Spectra-Physics, Mountain View, CA) synchronously pumped by a Millennium VII (Spectra-Physics) diode-pumped high power solid-state CW laser. The laser was capable of producing 8.5W of green light at an output of 532 nm. The Tsunami laser was tunable in the range of 700 nm and 1000 nm and consistently produced pulses 80 fs between 840 and 920 nm. Pulse repetition rate was recorded as 80.7 MHz through the use of a Startek 1350 frequency counter (Startek International, Fort Lauderdale, FL). To continually monitor the average laser power reaching the objective at varying frequencies, part of the transmitted beam was reflected onto a photodiode detector (Thorlabs, Cambridgeshire, UK) and registered through the use of a Spectra-Physics 407a power meter (Spectra-Physics). Identification of the wavelength was performed using an IST laser spectrum analyser (Mirion Technologies (IST), Hampshire, UK) paired to a TDS 210 oscilloscope (Tektronix, Berkshire, UK). The Tsunami laser output was fed to an electro-optical modulator (OEM) (LIV20 Digital Pulse Amplifier, Linos, Göttingen, Germany) before reaching the confocal microscope instrument. This allowed the laser intensity control and optimisation of the microscope to be achieved. The instrument used was a Leica TCS SP2 multiphoton confocal laser scanning system (Leica, Milton Keynes, UK) coupled to a DMRE upright microscope (Leica). Upon entering the instrument, the Tsunami laser beam was expanded and focused through the objective lens to an estimated beam diameter of 0.14  $\mu\text{m}$  ( $\lambda_p = 880 \text{ nm}$ ). Emitted photons were collected through the same objective lens, separated from the excitation light by a dichroic mirror (Thorlabs, Cambridgeshire, UK). The lens used throughout the experiments was a Leica HCX APO L 40x/0.80

water-immersion objective. The light reflected was collected by an R6357 programmable photomultiplier tube (PMT) (Hamamatsu Photonics, Shizuoka, Japan). The average power of the laser irradiation after the microscope was measured with the aid of a PM140 thermopile digital optical power meter (Gentec Electro-Optics, Quebec, Canada).

## **6.2.2 Determination of Optimal Two-Photon Excitation Wavelength**

The number of photons being detected is reliant upon the two-photon excitation wavelength. In order to ensure that the optimal number of photons is being detected, the optimum excitation wavelength was investigated. To do this, a specimen of the dye was excited at near-infrared wavelengths and the numbers of emitted photons were detected. In order to obtain the optimal two-photon excitation wavelength for SNARF<sup>®</sup>-4F 5-(and-6)-carboxylic acid, the number of photons detected was collected at wavelengths between 760 and 940 nm, in increments of 10 nm. To select the desired wavelength, the laser wavelength was selected on the digital display and tuned, initially with the slit wavelength selector and then with the prism dispersion compensation control to the desired wavelength. This process of tuning the laser wavelength visible on the oscilloscope is known as 'walking the laser'. The laser power was then optimised by carefully adjusting the vertical high reflector and output coupler (blue) followed by the horizontal high reflector and output coupler (green) (Figure 6.1, Figure 6.2). Power output was read on Newport optical power meter (Model: 407A, Newport, Oxfordshire, UK). To ensure the equivalent laser power is delivered to the sample at various wavelengths, the laser power was optimised by adjusting the relative minimum and maximum transmission of the IR 2 photon laser. When the wavelength of the excitation source is adjusted, consequently, the polarisation of the IR light changes. The light is passed through two crystals that act as polarisers, within a piece of equipment called the Electro Optical Modulator (EOM). The crystals are independently moved by the pulse mode or offset mode switches. The gain switch controls one of the crystals and the offset controls the other crystal.

These are used to find the relative  $0^\circ$  position, indicating maximum transmission, and/or  $90^\circ$  polarisation, indicating minimum transmission, for any given laser wavelength. Therefore, the specimen was excited and the low setting was selected on the EOM apparatus. The gain was adjusted to lowest image intensity by sight. The switch was returned to the normal setting and the offset control was adjusted to the highest visible image intensity. The specimen was imaged using these settings for the selected wavelength. Image files were saved. The number of photons detected was determined by analysing each image using SPCImage software package. The number of photons per pixel was plotted with respect to the corresponding excitation wavelength.



**Figure 6.1** The Spectra-Physics Tsunami Ultra-fast tuneable Ti:sapphire oscillator

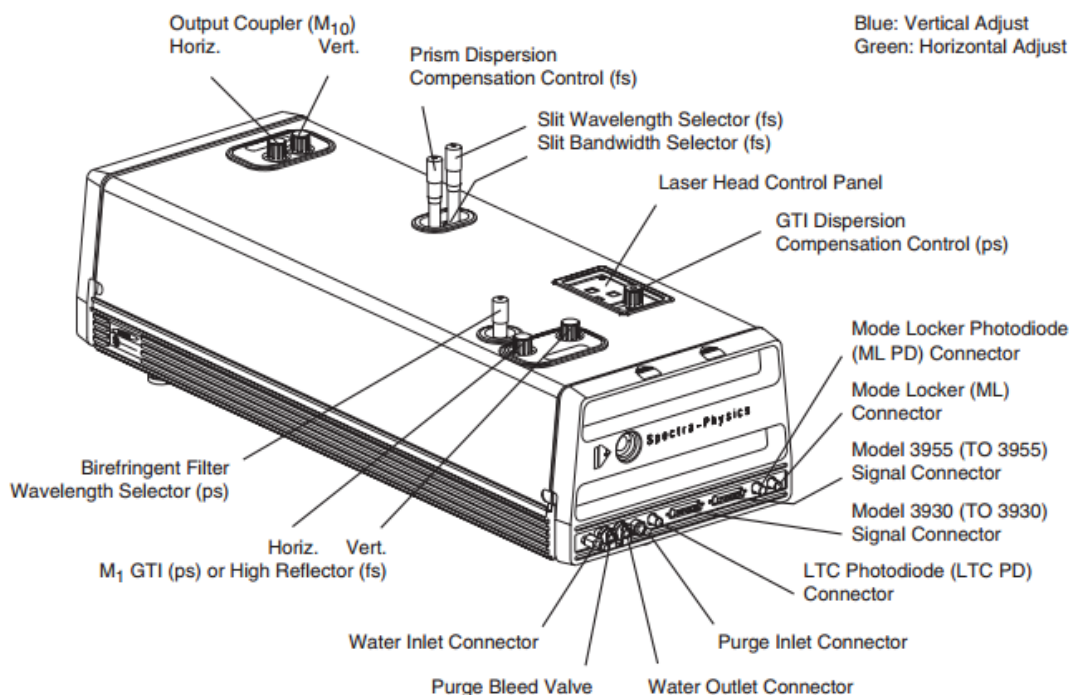


**Figure 6.2** Layout of the Spectra-Physics Tsunami Ti:sapphire oscillator

### 6.2.3 Preparation of SNARF<sup>®</sup>-4F 5-(and-6)-Carboxylic Acid Dye

SNARF<sup>®</sup>-4F 5-(and-6)-carboxylic acid was purchased (Life Technologies, Paisley, UK) as 1 mg aliquot. The dye was reconstituted in 10.61 mL of sterile deionised water to a concentration of 200  $\mu$ M, (MW: 471.44). The reconstituted dye was separated to 500  $\mu$ L aliquots. Aliquots of the fluorophore were stored at  $-20^{\circ}\text{C}$  prior to use.

### 6.2.4 Investigation of Detrimental Effect of SNARF<sup>®</sup>-4F 5-(and-6)-Carboxylic Acid upon Bacteria

*S. mutans*, *S. sanguinis*, *N. subflava* and *L. casei* were inoculated to sterile BHI broth and incubated overnight at  $37^{\circ}\text{C}$  in 5%  $\text{CO}_2$ . The broth was diluted to an  $\text{OD}_{600}$  of 1.0, equivalent to approximately  $1 \times 10^8$  CFU/mL. The bacterial suspension was diluted 1:10 with sterile BHI broth. Suspensions of SNARF<sup>®</sup>-4F 5-(and-6)-carboxylic acid were produced to concentrations of 100, 80, 60, 40, 20, 10, 5 and 2.5  $\mu$ M. A 1 mL volume of SNARF<sup>®</sup>-4F 5-(and-6)-carboxylic acid of each concentration was

added to two well of a 24-well plate. A 1 mL volume of the bacterial suspension was added to each well. Sterile saline was added to two wells in addition to the bacterial suspension to act as a positive growth control. Sterile BHI broth was added to two wells to act as a negative (contamination) control. The 24-well plate was incubated at 37°C for 48 h. Following incubation, the broth from each well was serially diluted, plated to BHI agar plates and incubated at 37°C in 5% CO<sub>2</sub> for 48 h. Cell concentrations were determined by colony counting and calculation. Cell concentrations were individually plotted with respect to SNARF<sup>®</sup>-4F 5-(and-6)-carboxylic acid concentration to determine detrimental effect upon the bacterial isolates and if any detrimental effect was concentration dependent.

### **6.2.5 Preparation of Citric Acid – Sodium Phosphate Buffer Solutions**

Citric acid buffers were prepared as previously outlined, ranging from pH 2.6 to 7.6, in increments of 0.2 pH units (Section 2.4).

### **6.2.6 Production of Reduced Transport Fluid**

To produce reduced transport fluid (RTF); 100 mL of a 25 g/L stock solution of magnesium sulphate and 10 mL of an 80 g/L sodium carbonate solution, both in deionised water were produced. Stock solution 1, consisting of 0.6 g/L of potassium phosphate dibasic in 100 mL of deionised water. Stock solution 2, consisting of 1.2 g of potassium chloride, 1.2 g of ammonium sulphate, 0.6 g of potassium phosphate monobasic and 1 mL of the magnesium sulphate stock, in 99 mL of deionised water. A 4 g/L solution of dithiothreitol (DTT) was produced in deionised water. Excess stock solutions were stored at 4°C. To produce the RTF; 7.5 mL of Stock 1, 7.5 mL of Stock 2 and 0.5 mL of the sodium carbonate solution were mixed and 80 mL of deionised water added. The solution was sterilised by autoclaving at 121°C for 15 min. The solution was allowed to cool at room temperature and 5 mL of 4 g/L DTT (0.22 µm filter-sterilised) was added. The RTF was refrigerated when not in use and used within one week.

### **6.2.7 Instrument Set-Up and Optimisation**

SNARF<sup>®</sup>-4F 5-(and-6)-carboxylic acid was added to each buffer solution to a final concentration of 20  $\mu$ M. 4 mL of each buffer solution was added to a small petri dish and imaged. Images were obtained using an Leica HCX APO L 40x/0.80 water-immersion objective.

### **6.2.8 Imaging a Specimen**

The specimen was excited with a repetition pulse rate of 80 Hz. Following this excitation event, in some instances photon emission occurred. Scanning of a specimen involved two pieces of equipment; the Leica TCS SP2 microscope and the SPC-803 TCSPC module. Under the control of the TCS software, the TCS SP2 microscope scans the specimen. Emitted photons are detected by the TCSPC module and processed. The TCSPC module is controlled by the SPCM software. The acquisition of data by the TCSPC module is synchronised with the scanning by two scan clock signals.

### **6.2.9 Obtaining the Fluorescence Emission Spectra of SNARF<sup>®</sup>-4F 5-(and-6)-Carboxylic Acid**

A 200  $\mu$ M solution of SNARF<sup>®</sup>-4F 5-(and-6)-carboxylic acid was produced and added to citric acid buffer solution at pH 7.0, to a final concentration of 20  $\mu$ M. The solution was added to a small petri dish and imaged using a Leica HCX APO L 40x/0.80 water-immersion objective. Following excitation at 840 nm, the number of photons detected by lambda scanning between approximately 330 and 850 nm, were recorded. Data was processed using Avantes spectrometer software package (v7.5.1, AvaSoft, Surrey, UK).

### **6.2.10 Calibration of SNARF<sup>®</sup>-4F 5-(and-6)-Carboxylic Acid With Respect to pH**

Initially, five buffer solutions containing SNARF<sup>®</sup>-4F 5-(and-6)-carboxylic acid were chosen to cover pH values between 4 and 7.6. A 4 mL volume of each buffer was added to a small petri dish, excited at a two-photon excitation wavelength of 840 nm and images obtained. As multiphoton molecular excitation was employed during collection of fluorescence lifetime images, the pinhole aperture was opened to the maximum diameter permitted of 600  $\mu\text{m}$ . Photon emission was detected through the use of a photomultiplier tube (PMT) to a TCSPC module via a  $\lambda 650/40$  nm emission filter. Histograms were produced and fluorescence lifetimes were calculated for each pixel of the image by SPCImage software (v 5.5). Fluorescence lifetimes were converted to colour and the image constructed within the software package. Histograms were analysed to evaluate the number of photons per pixel. The binning parameter was set to three, increasing the number of photons per pixel, however at a cost of image resolution. The  $\chi^2$  value was analysed to evaluate the fit of the exponential decay. The average fluorescence lifetime values of each image were plotted with respect to the pH of the buffer to evaluate the response of the dye to variations in pH. The process was later repeated with a range of buffers in increments of 0.2 pH units. To produce the calibration curve, the average fluorescence lifetime values were plotted with respect to the buffer pH.

### **6.2.11 Investigation of Fluorescence Emission of Various Biofilm Substrata**

Autofluorescence of the substrata may occur resulting in interference with imaging. To ensure that this did not occur, a variety of substrata were analysed. Discs of hydroxyapatite, polytetrafluoroethane (PTFE) and titanium were analysed. Discs measuring 5 mm in diameter and 2 mm in thickness (1 mm for titanium) were placed within a small petri dish. A small amount of sterile deionised water was added to the disc to aid the use of the water objective lens. The discs were located

using the light microscope and switched to FLIM. The discs were excited at 840 nm and imaged using TCSPC.

### **6.2.12 Investigation of Factors Which May Influence Fluorophore Accuracy**

A number of environmental factors were investigated for their effect on fluorophore accuracy. These factors include redox potential, temperature, protein concentration and glycoprotein concentration in the form of mucin. These factors were selected for investigation as variations in these parameters are experienced within both dental biofilms and biofilms being investigated.

#### **6.2.12.1 Redox**

Prior to analysis, a suspensions of SNARF<sup>®</sup>-4F 5-(and-6)-carboxylic acid, and reduced transport fluid (RTF), were produced as described above. To determine if any detrimental effect of redox upon the number of photons detected, and therefore the ability to determine fluorescence lifetime values, SNARF<sup>®</sup>-4F 5-(and-6)-carboxylic acid was added to deionised water and RTF to a final concentration of 20  $\mu$ M, immediately prior to analysis. The suspensions were imaged. Due to the fluorescence lifetime changing with respect to pH, the fluorescence lifetime was not measured for redox potential.

#### **6.2.12.2 Temperature**

SNARF<sup>®</sup>-4F 5-(and-6)-carboxylic acid was added to citric acid-sodium phosphate buffer at pH 7.0 to a final concentration of 20  $\mu$ M. The pH of the solution was checked using a Shindengen pHBOY-P2 portable ISFET pH meter (Camlab, Cambridge, UK). The solution was imaged at room temperature. The temperature of the buffer was measured at approximately 24°C. The chamber encasing the microscope was attached and the incubator was set to 37°C. The buffer was allowed

a period of time to reach the appropriate temperature. The temperature was measured at approximately 36°C and the buffer was imaged.

#### **6.2.12.3 Protein**

SNARF<sup>®</sup>-4F 5-(and-6)-carboxylic acid was added to citric acid-sodium phosphate buffer at pH 7.0 to a final concentration of 20 µM. The pH of the buffer solution was checked using a Shindengen pHBOY-P2 portable ISFET pH meter (Camlab, Cambridge, UK). Bovine serum albumin (BSA) was added to concentrations of 20, 10, 5, 2.5, 1.25 and 0.625 mg/mL. A buffered solution containing no bovine serum albumin was also imaged as a control. The pH of the solution was checked using a Shindengen pHBOY-P2 portable ISFET (ion-sensitive field-effect transfer) pH meter (Camlab, Cambridge, UK) prior to imaging.

#### **6.2.12.4 Glycoproteins**

SNARF<sup>®</sup>-4F 5-(and-6)-carboxylic acid was added to citric acid-sodium phosphate buffer at pH 7.0 to a final concentration of 20 µM. Mucin (from porcine stomach, type III, bound sialic acid 0.5-1.5%, partially purified powder) (Sigma-Aldrich, Dorset, UK) was added at concentrations of 20, 10, 5, 2.5, 1.25 and 0.625 mg/mL. A buffer solution containing no bovine serum albumin was imaged concurrently as a control. The pH of the solution was checked using a Shindengen pHBOY-P2 portable ISFET (ion-sensitive field-effect transfer) pH meter (Camlab, Cambridge, UK) prior to imaging.

## **6.3 Results**

### **6.3.1 Determination of the Optimal Two-Photon Excitation Wavelength for SNARF Dyes**

The optimal two-photon excitation wavelength, that is the wavelength at which the most number of photons were detected per pixel, was 840 nm. Therefore, this

wavelength was selected for all experiments. When plotted, the optimum mean number of photons per pixel was observed at a wavelength of 840 nm (Figure 6.3), with similar number observed at 800 nm. The optimum wavelength for two-photon excitation was determined to be 840 nm. The rationale for this was that; due to the laser power produced being at its maximum at 800 nm, greater efficiency was achieved at 840 nm and, as photon energy decreases proportionate to wavelength, phototoxicity is decreased. When excited at a wavelength of 840 nm, the maximum number of photons was detected at a wavelength of approximately 646 nm (Figure 6.4).

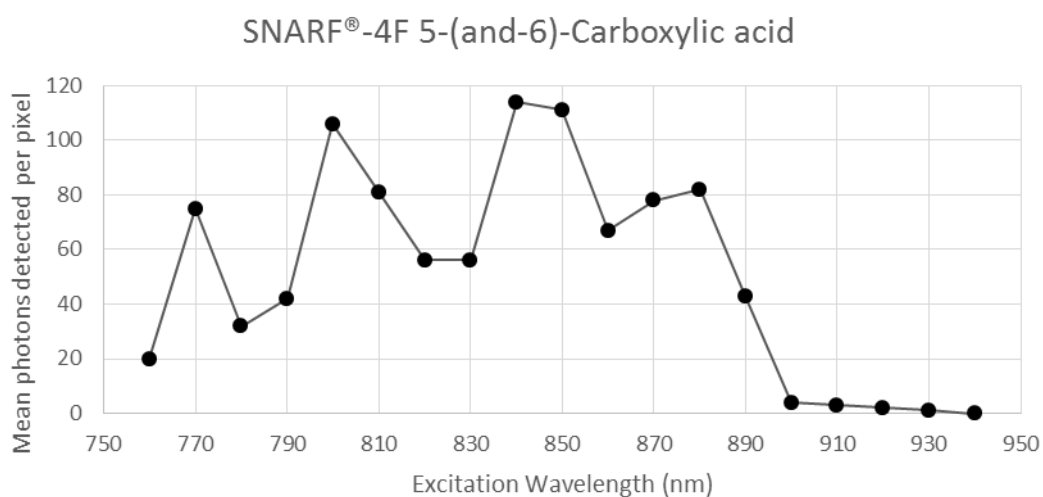


**Figure 6.3** Mean number of photons per pixels generated by two-photon excitation between 760 and 940 nm

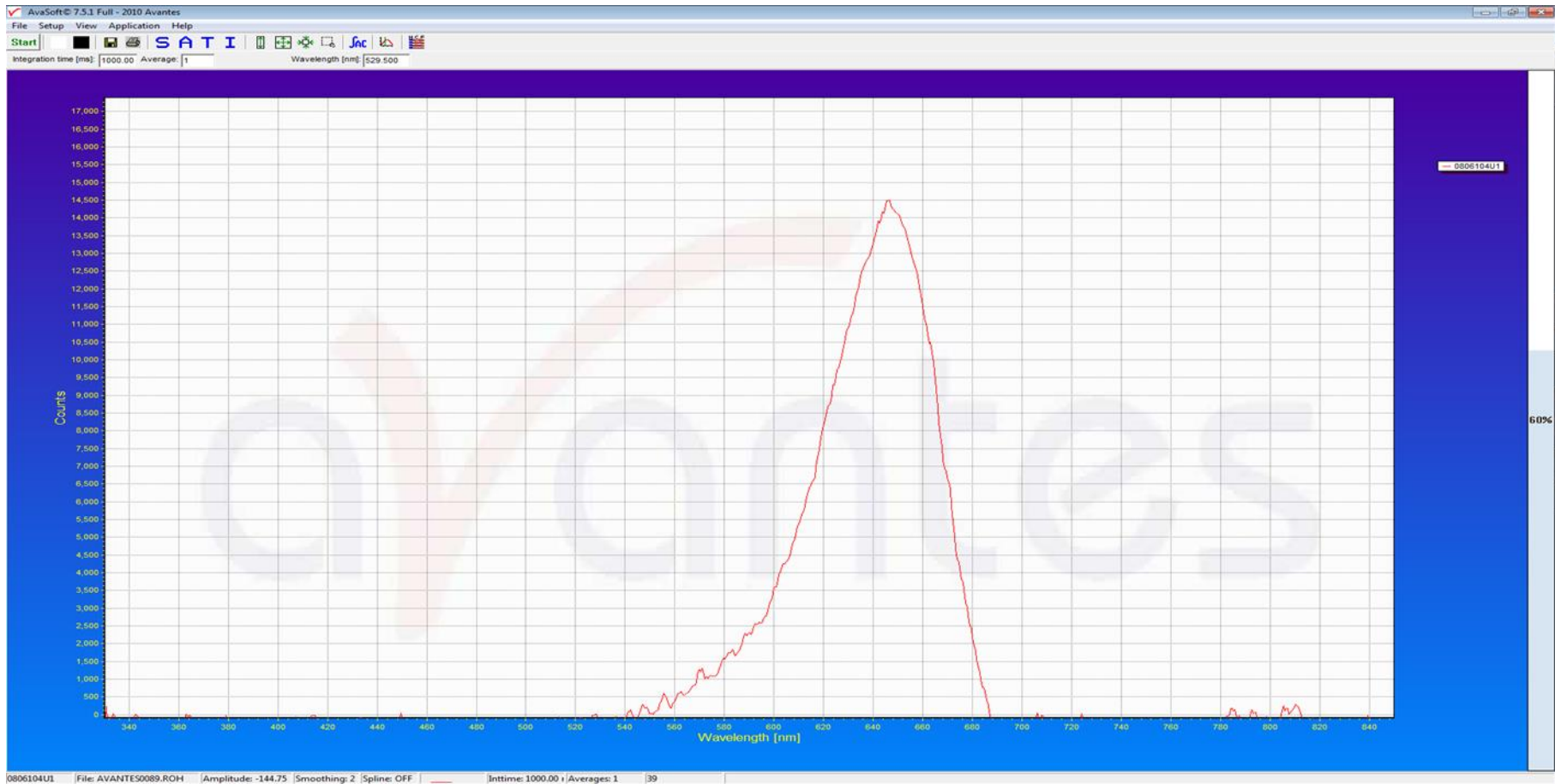
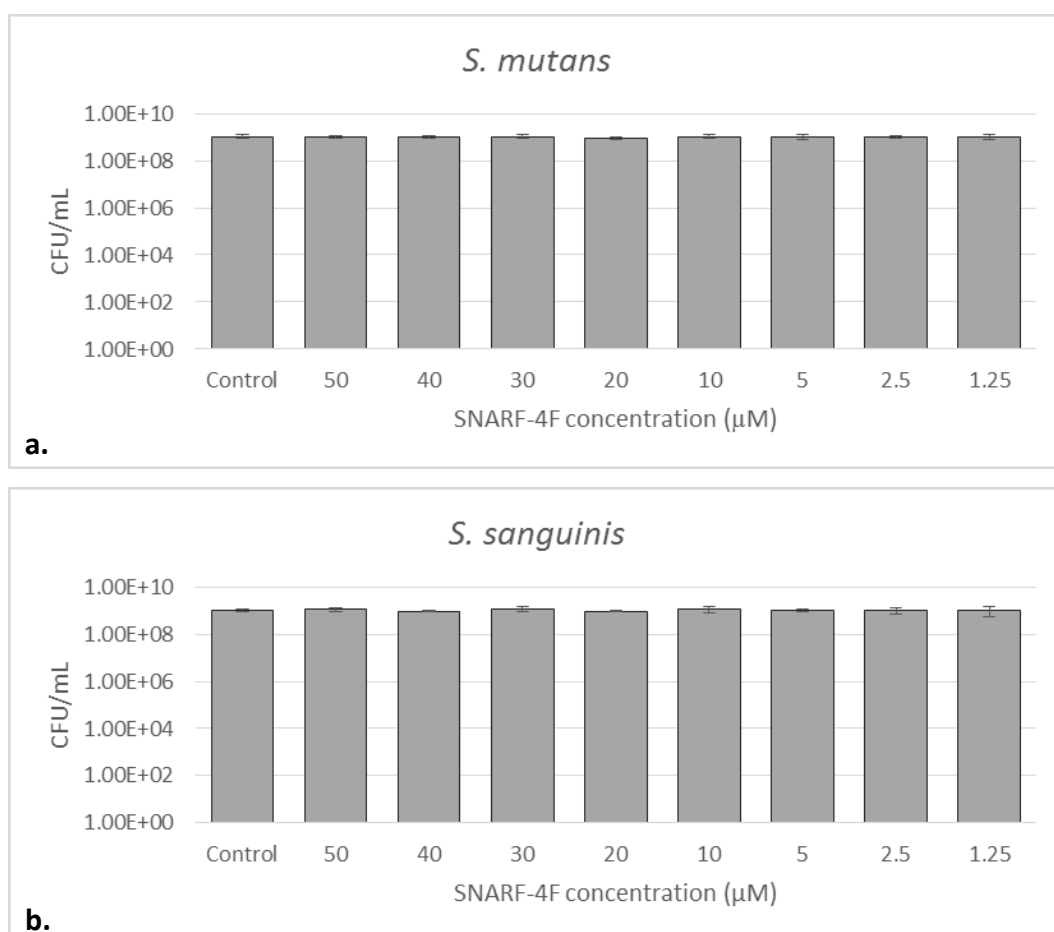
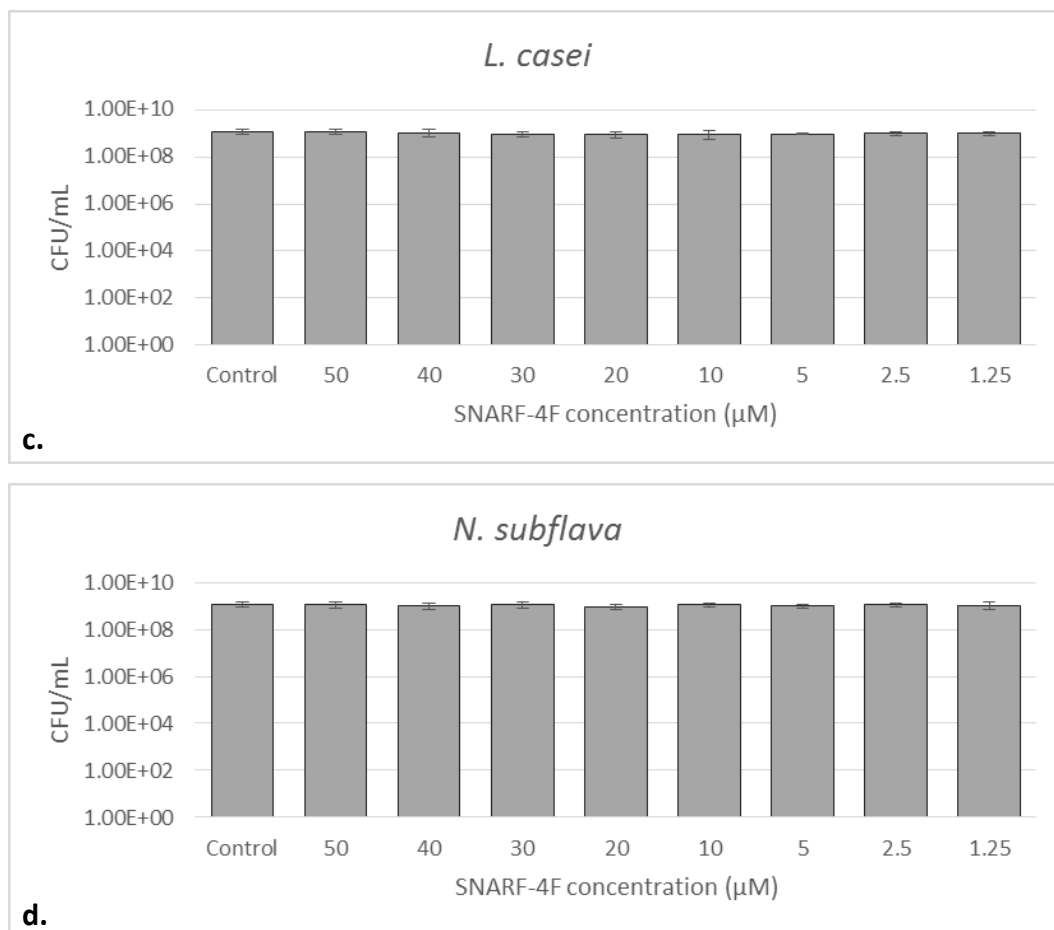


Figure 6.4 Fluorescence emission spectrum when excited at  $\lambda 840$  nm showing an emission peak maximum at approximately  $\lambda 646$  nm

### 6.3.2 Investigation of Detrimental Effect of SNARF<sup>®</sup>-4F 5-(and-6)-Carboxylic Acid upon Bacteria

Figure 6.5 reveals the effect of SNARF<sup>®</sup>-4F 5-(and-6)-carboxylic acid upon each species in a dose-dependent manner, in comparison to a bacterial suspension unexposed to the fluorophore. For all four organisms, the counts fell within two standard deviations of the mean for that organism demonstrating no statistical significance as a result of exposure to various concentrations of SNARF<sup>®</sup>-4F 5-(and-6)-carboxylic acid.





**Figure 6.5** Cell concentrations following exposure to various concentrations of SNARF<sup>®</sup>-4F 5-(and-6)-carboxylic acid for a) *S. mutans*, b) *S. sanguinis*, c) *L. casei*, and d) *N. subflava*. Error bars represent standard deviation from the mean, n = 3.

### 6.3.3 Calibration of SNARF<sup>®</sup>-4F 5-(and-6)-Carboxylic Acid for Two-Photon Excitation Fluorescence Lifetime Imaging Microscopy

Figure 6.6 shows a series of fluorescence lifetime images obtained at various pH environments through the utilisation of citric acid buffers. At each pixel of the image, the fluorescence lifetime is converted to colour across a spectrum. Through comparison of the images, an evident shift in fluorescence lifetime corresponding to variations in pH is evident.

Figure 6.7 shows the result of plotting the mean fluorescence lifetime values for the set of images at each pH with respect to the buffer pH. Regression analysis revealed a linear relationship between fluorescence lifetime and pH with a R2 value of 0.9945 with residual values from the calibration curve represented in Figure 6.7. A more intense calibration, with smaller intervals between buffer pH, revealed a linear relationship between fluorescence lifetime and pH with a R2 of 0.994. The line-of-best-fit and residual values of the calibration curve are represented in Figure 6.8. This calibration allowed the determination of pH from the obtained fluorescence lifetime values.

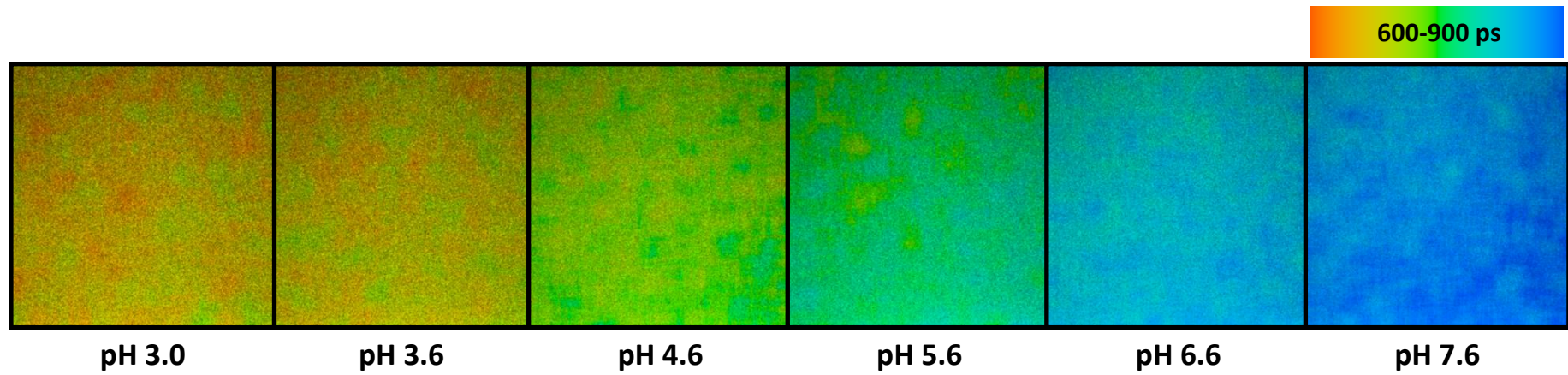
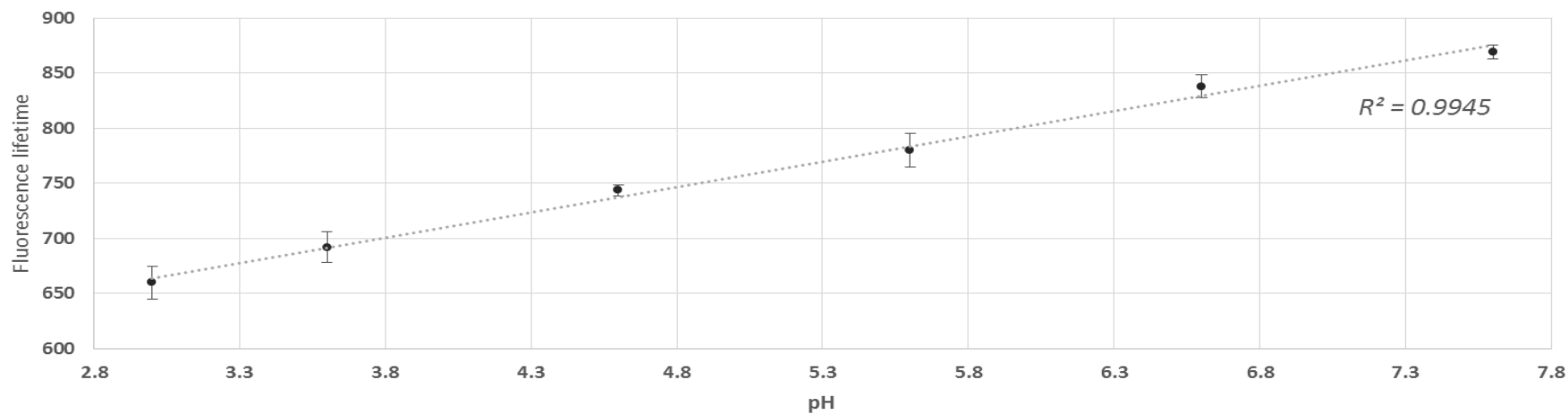


Figure 6.6 Matrix of colour-coded fluorescence lifetime images at various pH values.

### Calibration of SNARF<sup>®</sup>-4F 5-(and-6)-Carboxylic acid



### Plot of Residuals



**Figure 6.7** Calibration curve of fluorescence lifetime values for the calibration of SNARF<sup>®</sup>-4F 5-(and-6)-carboxylic acid in citric acid-sodium phosphate buffer and the residual values. The plot of residuals represents the variation between the observed values and the line-of-best-fit.

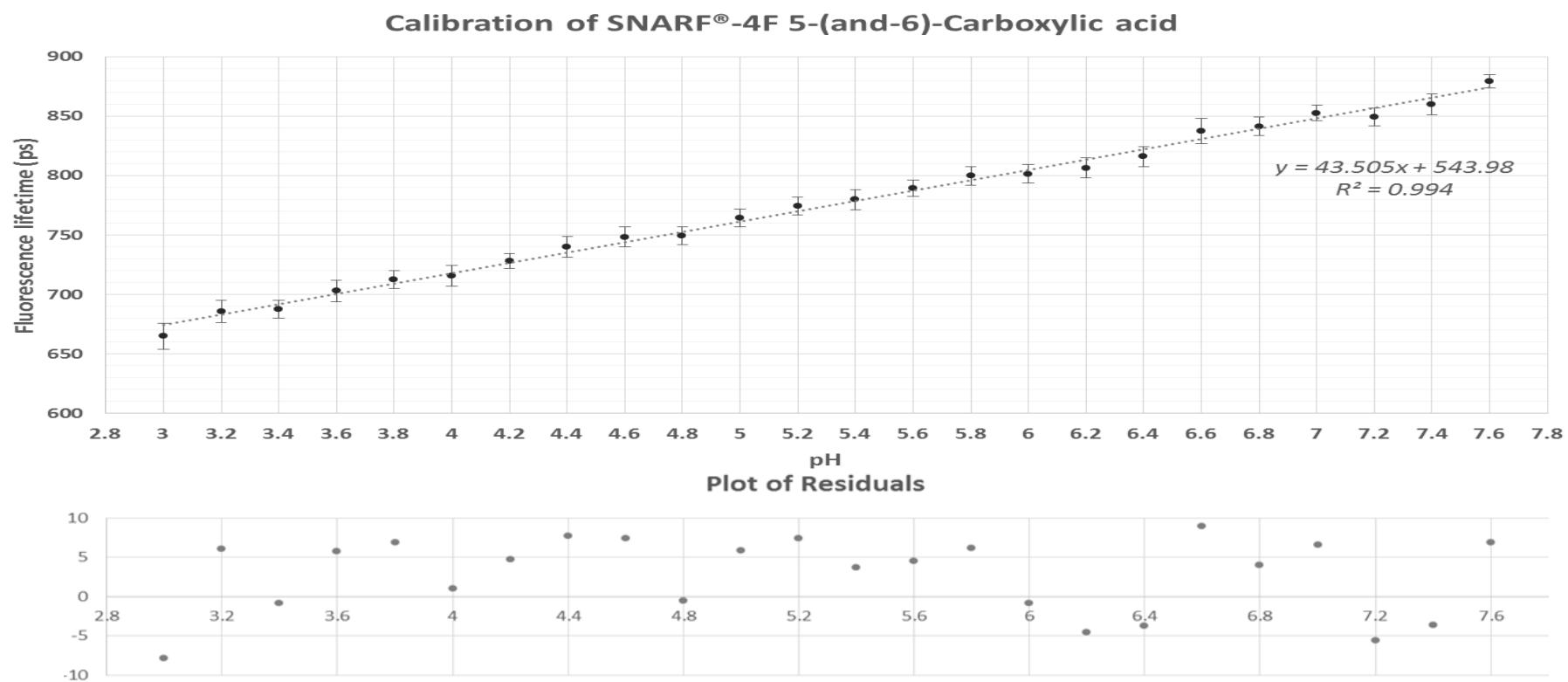


**Figure 6.8** Calibration curve for of SNARF®-4F 5-(and-6)-carboxylic acid in citric acid-sodium phosphate buffers and the residual values. The plot of residuals represents the variation between the observed values and the line-of-best-fit.

### 6.3.4 Investigation of Factors Which May Influence Fluorophore Accuracy

#### 6.3.4.1 Redox Potential

Figure 6.9 shows the mean number of photons detected per image in deionised water and in a reduced liquid media (reduced transport fluid). Little variation is observed and analysis demonstrates that this variation is not statistically significant. It is not possible to observe any detrimental effect upon fluorescence lifetime as the pH of the two media varied, resulting in fluorescence lifetime changes being pH dependent.

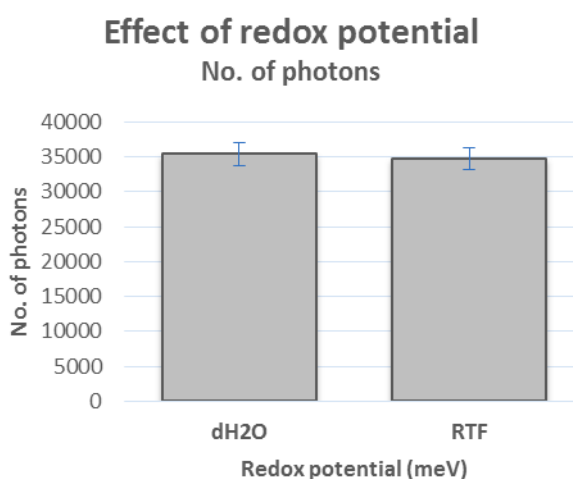
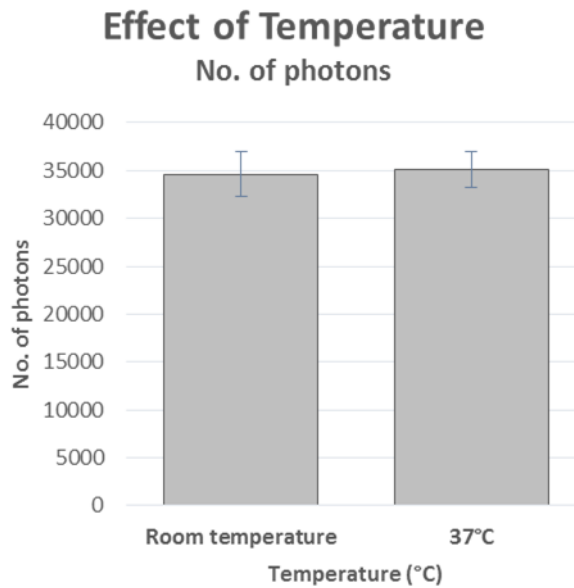
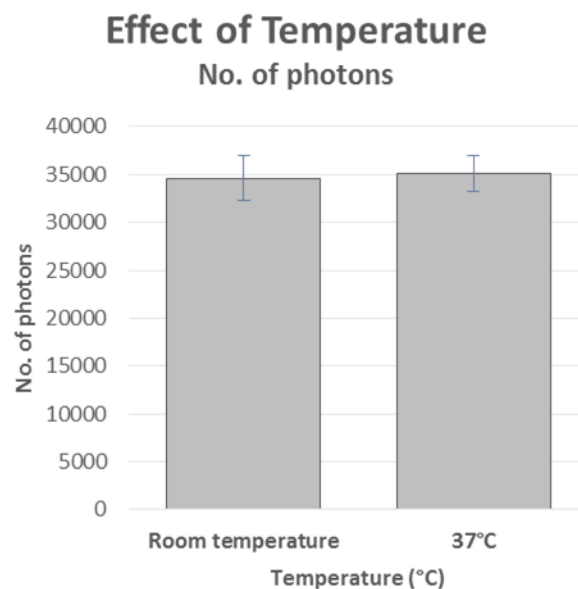


Figure 6.9 Plot of the number of photons obtained under differing redox potential environments. Error bars represent standard deviation from the mean



### 6.3.4.2 Temperature

Figure 6.10 shows the mean number of photons detected per image in deionised water and in a reduced liquid media. Little variation is observed and analysis demonstrates that this variation is not statistically significant. Figure 6.11 shows the fluorescence lifetime values at various temperatures. Little variation is observed between the fluorescence lifetimes within each solution. The two-tailed p value was 0.8277 and is determined to be statistically insignificant.



**Figure 6.10** Plot of the number of photons obtained under differing temperatures. Error bars represent standard deviation from the mean

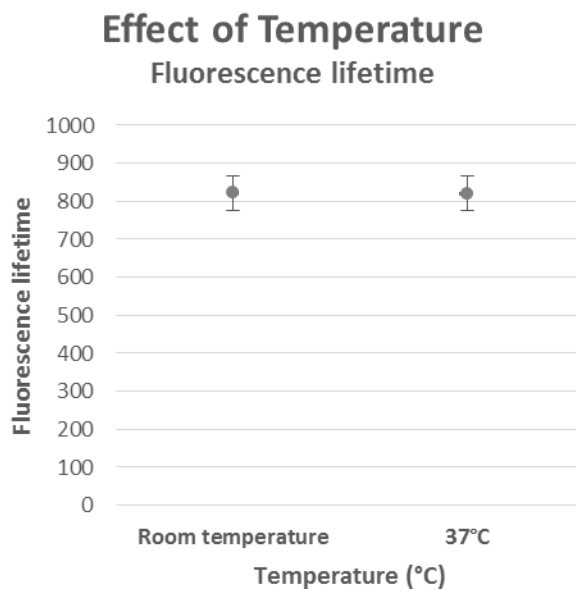


**Figure 6.11** Mean fluorescence lifetimes at various temperatures. Error bars represent standard deviation from the mean

**6.3.4.3 Protein**

Figure 6.12 shows the mean number of photons detected per image in solutions of various concentrations of protein in the form of bovine serum albumin. Little variation is observed and analysis demonstrates that this variation is not statistically significant.

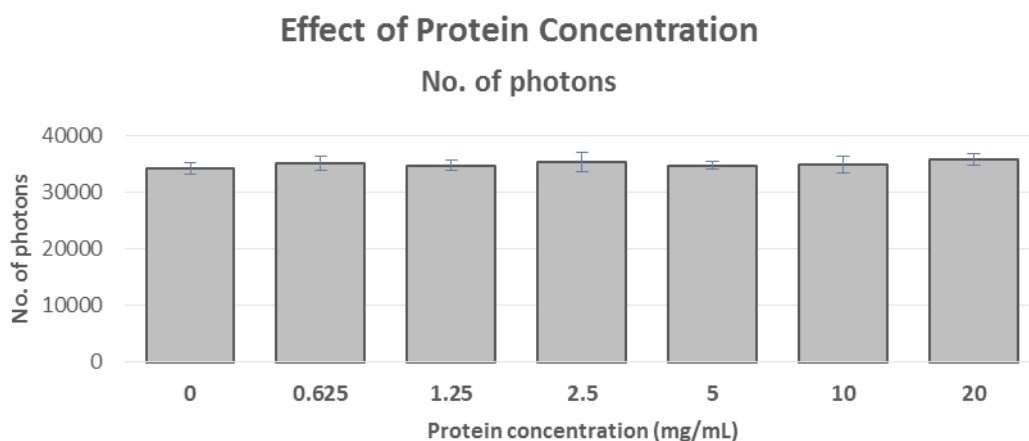


**Figure 6.12** Number of photons detected at various protein concentrations. Error bars represent standard deviation from the mean

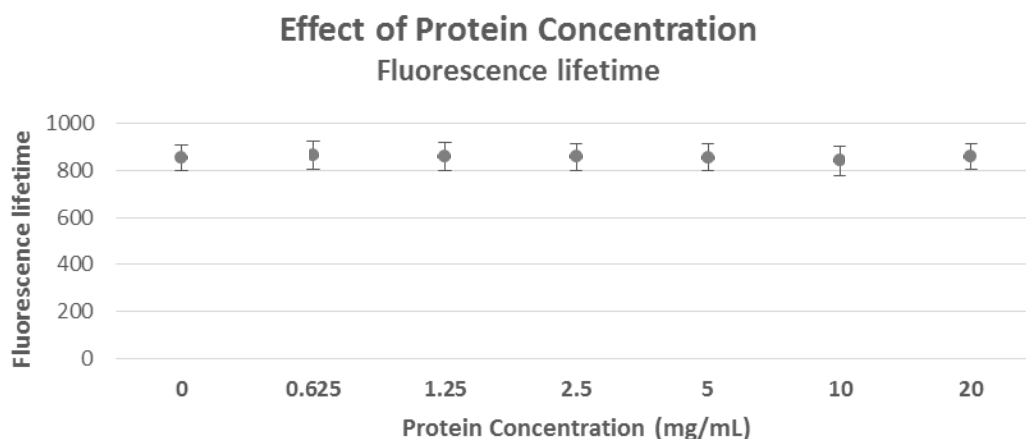
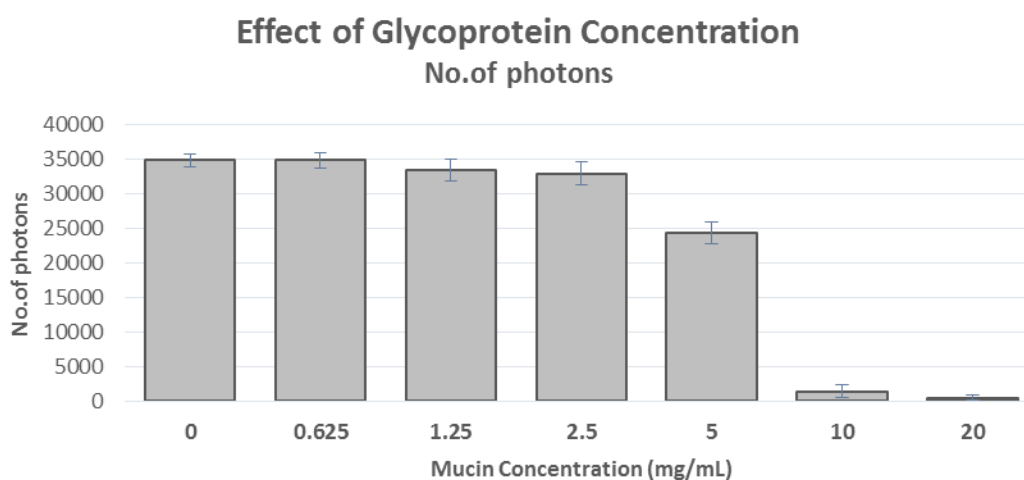


**Figure 6.13** Mean fluorescence lifetimes at various protein concentrations. Error bars represent standard deviation from the mean

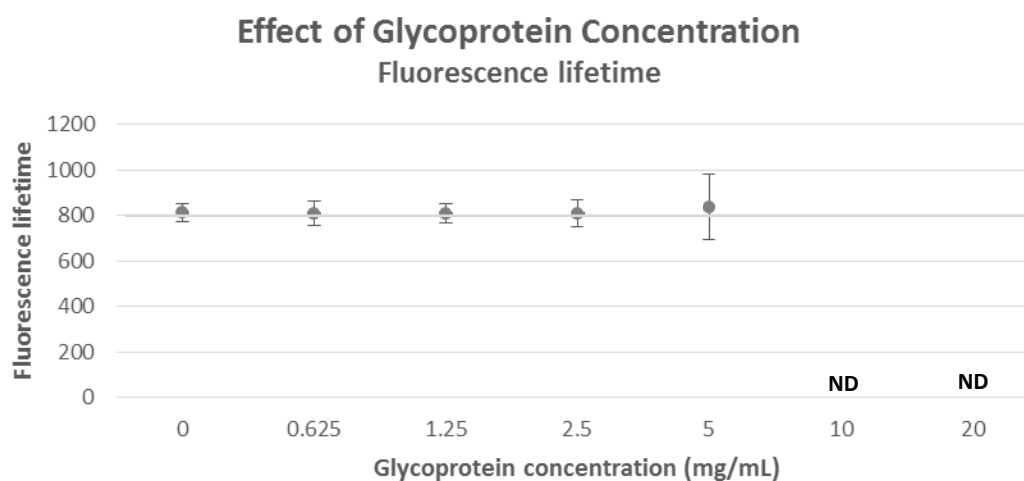
#### **6.3.4.4 Glycoproteins**

Figure 6.14 shows the mean number of photons detected per image in solutions of various concentrations of glycoprotein in the form of mucin. Little variation is observed and analysis demonstrates that this variation is not statistically significant.

Figure 6.15 shows that the mean fluorescence lifetime obtained for solutions of various concentrations of glycoprotein, in the form of mucin. Little variation in fluorescence lifetime is observed between 0 and 2.5 mg/mL. Some variation is observed at concentrations of 5 mg/mL, likely as an effect of the decrease in detected photons at this concentration. At concentrations of 10 and 20 mg/mL, it was not possible to determine the fluorescence lifetime values as a result of the lack of photons detected.



**Figure 6.14** Number of photons detected at various glycoprotein concentrations



**Figure 6.15** Mean fluorescence lifetimes at various glycoprotein concentrations. Due to a lack of photons detected, fluorescence lifetime values were not able to be determined at 10 and 20 mg/mL.

## 6.4 Discussion

The aim of this chapter was to investigate the use of SNARF dyes to determine environmental pH through the use of multiphoton molecular excitation fluorescence lifetime imaging microscopy. Due to the complex and dynamic

structural and chemical nature of biofilms, it is desirable that the method to determine environmental pH microgradients are obtainable unaffected by variations in concentration, which may vary greatly and be difficult to determine. Furthermore, it is desirable that determinations are obtainable in a naturally-hydrated environment as desiccation may affect the results and the structure of the biofilm. Unlike steady-state fluorescence emission intensity measurements, which may be affected by numerous variables such as; fluorophore concentration, light path distance, sample thickness or photobleaching, fluorescence lifetime measurements, which are intrinsic molecular properties, provide an absolute measurement and allow a dynamic representation of the fluorescence. The fluorescence lifetime may, however, be affected by variations in environmental parameters resulting to measurable changes in fluorescence lifetime. This makes fluorescence lifetime imaging microscopy a convenient tool for imaging environmental parameters. Time-resolved fluorescence lifetime measurements are unaffected by variations in excitation source intensity. Time-correlated single-photon counting (TCSPC) is considered the most sensitive technique for determining fluorescence lifetimes (Horiba Scientific, Technical Note TRFT-1). Two-photon excitation (2PE) offers the following advantages; 2PE only occurs where sufficient photons are allowing excitation therefore only where the beam of photons is focussed. This negates the need for a pinhole aperture to block out-of-focus light. Due to the near-infrared wavelengths of the excitation light, photon energy is decreased and therefore phototoxicity is minimised. It was established that it is possible to excite the pH-sensitive fluorophore SNARF<sup>®</sup>-4F 5-(and-6)-carboxylic acid through multiphoton excitation and that two-photon excitation occurs with maximum efficiency at 840 nm. Although, similar numbers of photons were observed at 800 nm, this corresponded to the maximum power output of the laser and therefore 840 nm laser light offered greater efficiency. Following optimisation of the excitation wavelength and the instrument, and exciting the fluorophore at 840 nm, it was possible to obtain fluorescence lifetime images. When excited at 840 nm, SNARF<sup>®</sup>-4F 5-(and-6)-carboxylic acid emitted fluorescence with a maximum emission intensity at a wavelength of approximately 656 nm, in the red region of the visible light spectrum. An advantage of this method is that it appears to enable

the imaging of biofilms in a hydrated state, without the disruption to the biofilm structure, and inevitable effect upon measurements, observed with microelectrodes. Early analysis indicated that SNARF<sup>®</sup>-4F 5-(and-6)-carboxylic acid exhibited changes in fluorescence lifetime in response to variations in environmental pH. Through measurement of fluorescence lifetime values in buffers of known pH and correlation of those values to buffer pH a calibration curve was formed. Calibration demonstrated a linear relationship between environmental pH and the fluorescence lifetime of SNARF<sup>®</sup>-4F 5-(and-6)-carboxylic acid. This calibration allowed localised environmental pH to be calculated from the fluorescence lifetime values using SNARF<sup>®</sup>-4F 5-(and-6)-carboxylic acid. Due to the numerous chemical and physical environments which occur within biofilms, it was essential to ensure that variations in these other environmental parameters had no detrimental effect upon fluorescence lifetime values or the number of photons detected. This experiment provides proof that fluorescence lifetime is not significantly affected by variations of temperature, redox potential and protein concentrations. However, the number of photons detected appears to be affected by the presence of glycoproteins. It also appears that this phenomenon is concentration dependent. Fluorescence quenching, leading to a reduction in the fluorescence emission intensity, can arise as a result of a number of processes. Processes causing quenching may occur due to the formation of complexes during rest (prior to excitation) or during excitation. During static quenching, a reversible molecular interaction occurs when the fluorophore exists in its ground state. This may account for the concentration-dependent reduction in fluorescence emission intensity observed here. Dynamic quenching (also referred to as collisional quenching) may be observed when the fluorophore interacts with other molecules in solution. The fluorophore may undergo electron transfer, spin-orbit coupling or inter-system crossing to the triplet state, resulting in deactivation of the fluorophore and return to the ground state. This may be of significance when imaging biofilms mimicking dental plaque grown in the CDFF. This may arise as a result of the biofilms being grown with an artificial saliva medium containing mucin as the main nutrient source. Salivary mucins, the principal components of mucus, are large glycoproteins with a major role in forming and providing a protective

coating upon the oral surfaces (Slomiany et al. 1996). The role of artificial saliva is to provide a representative nutrient source for the oral biofilms. However, due to the detrimental effect upon imaging it may be possible, and in fact pertinent, to remove mucin from the artificial saliva medium to facilitate fluorescence lifetime imaging microscopy. Variations in redox potential and temperature exhibited negligible effect upon the number of photons detected during fluorescence lifetime measurements. Variations in protein concentration, in the form of bovine serum albumin, had no significant effect upon the number of photons detected and the fluorescence lifetimes obtained. A significant decrease in the number of photons was observed, in a dose dependent manner, with increasing concentrations of glycoproteins in the form of mucin. This may have an effect on fluorescence lifetime measurements of biofilms mimicking dental biofilms by using artificial saliva containing mucin as a nutrient source. No fluorescence was detected from the variety of substrata tested. Therefore, as hydroxyapatite most closely resembled the mineralised tissue of the tooth, this substratum was used for the growth of biofilms.

#### **6.4.1 Summary**

SNARF<sup>®</sup>-4F was able to be excited through multiphoton molecular excitation and produces a maximum number of photons at an excitation wavelength of 840 nm. No fluorescence was detectable from a variety of substrata available for biofilm growth. These substrata included discs of hydroxyapatite, PTFE and titanium. The number of photons detected during fluorescence lifetime imaging microscopy was affected, in a concentration-dependent manner, by glycoproteins in the form of mucin. Negligible effects were observed in variations of temperature, redox potential and protein. Calibration demonstrates a linear relationship between environmental pH and fluorescence lifetime, allowing calculation of pH from fluorescence lifetime values by imaging.

# **Chapter 7 Application of Dual-Fluorophore, Ratiometric, pH-sensitive Nanosensors and SNARF<sup>®</sup>-4F 5-(and-6)-Carboxylic Acid Dye to Bacteria to Visualise pH Microgradients**

## **7.1 Introduction**

A majority of bacterial studies are carried out on planktonic phenotypes (single-celled and freely suspended) (Donlan 2002). Culture media provides microorganisms with excess nutrients and the optimum environmental conditions for growth, such as temperature and gaseous environmental constituents are afforded. Rarely in the natural environment are microbes provided with such utopian conditions as experienced in the culture flask. Outside the laboratory, microorganisms preferentially grow as part of a matrix-encased, highly-integrated, three-dimensional microbial community called a biofilm (Hunter & Beveridge 2005). Biofilms consist of microorganisms enclosed in a matrix of extracellular polymeric substance (EPS), produced by the microorganisms, and attached to a surface. Although each biofilm is unique (Tolker-Nielsen & Molin 2000), they possess some common structural characteristics. Biofilms consist of microcolonies which form projections and interstitial water channels which allow the exchange of nutrients and waste, (Figure 7.1) (Stoodley et al. 1998; Stoodley et al. 1999). Within these complex and dynamic structures, gradients in chemical and physical parameters are experienced, which can vary significantly over even a few micrometres (Hunter & Beveridge 2005). Despite the fact that the formation of microgradients is widely-accepted, the dynamic spatial and temporal complexity makes the determination of local environmental parameters challenging and problematic. Furthermore, the ability to understand how the development of these microenvironments affect microbial ecology and processes (Hunter & Beveridge 2005) are highly desirable. Consequently, the need to develop well characterised and robust methods to determine these environmental parameters with sufficient resolution, both spatially and temporally, is highly desirable.

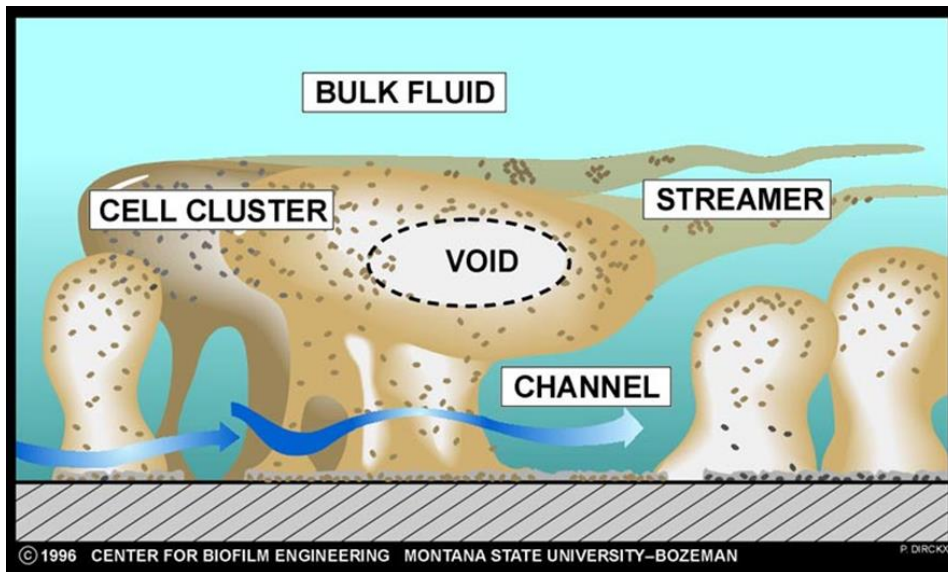


**Figure 7.1** Diagram demonstrating the structural heterogeneity of biofilms. The diagram displays projections and interstitial water channels facilitating the exchange of nutrients and waste products (Image credit: Peg Dirckx, Image used with permission)

The shortcomings of previously utilised methods include; the partial or full disruption of the biofilm structure as a consequence of measurement subsequently affecting the results obtained, limitations of resolution, multidimensional determination or dynamic range, the effect of sensor concentration for optical methods and the detrimental effect of the sensor upon the metabolically-active inhabitants of the biofilm. The two optical methods described here appear to overcome many of these drawbacks. The first method: imaging through the utilisation of single-photon molecular excitation and confocal laser scanning microscopy with the aid of dual-fluorophore, ratiometric, pH-sensitive nanosensors to determine pH. The second method: through the use of multiphoton molecular excitation and the utilisation of time-correlated single-photon counting to determine fluorescence lifetimes of SNARF<sup>®</sup>-4F 5-(and-6)-carboxylic acid correlated to pH. Dual-fluorophore, ratiometric, pH-sensitive nanosensors were produced incorporating three commercially available fluorophores, two pH-sensitive (carboxyfluorescein and Oregon Green<sup>®</sup>-488) and one pH-insensitive fluorophore (tetramethylrhodamine) conjugated to a polyacrylamide nanoparticle backbone. The integration of two pH-sensitive fluorophores extended the dynamic range of

the nanosensors allowing measurement of environmental pH across a greater range. The incorporation of the pH-insensitive fluorophore allowed a ratiometric methodology to be used, whereby the ratio of the fluorescent intensity produced by the pH-sensitive fluorophores to that of the pH-stable fluorophore is determined. This methodology negates the effect of variations of sensor concentration affecting fluorescence intensity in intensity-based measurements. The nanosensors were characterised and calibrated by correlating the response of the fluorophores to environmental pH in buffers. This calibration allows the determination of environmental pH extrapolated from the ratio of fluorescence emission intensity of the pH-sensitive fluorophores to the pH-insensitive fluorophore. It is anticipated that, through the use of these pH-sensitive nanosensors, it will be possible to determine extracellular environmental pH within laboratory-grown biofilms incorporating four species commonly found in dental plaque. SNARF<sup>®</sup>-4F 5-(and-6)-carboxylic acid is a commercially available, pH-sensitive fluorophore which has been utilised to determine environmental pH through the use of ratiometric (Marcotte & Brouwer 2005; Hunter & Beveridge 2005; Schlafer et al. 2015) and fluorescence lifetime methodologies (Szymanski & Lakowicz 1993; Kaylor 2004; Burdikova et al. 2015). The use of multiphoton molecular excitation has been utilised for the closely related fluorophore, SNARF-1 5-(and-6)-carboxylic acid (Bestvater et al. 2002). However, to my knowledge, the use of multiphoton molecular excitation of the fluorophore, SNARF<sup>®</sup>-4F 5-(and-6)-carboxylic acid, to obtain fluorescence lifetime measurement correlated to pH remains novel. The two methods were applied to bacterial biofilms designed to mimic dental plaque grown on nitrocellulose membranes or grown within a CDF. To minimise autofluorescence, fluorophore concentration should be as high as possible. However, high probe concentration may result in alterations of the fluorescence lifetime due to self-quenching, which shortens the fluorescence lifetime, or reabsorption of the emitted light, which increases the fluorescence lifetime. The near-infrared light spectrum is that light with a wavelength between 750 nm and 1400 nm. This light has photon energy of between 0.89 and 1.65 eV. As a comparison, light in the visible light spectrum within the blue spectrum (between 380 and 450 nm) has photon energy of between 2.5 and 2.75 eV and orange

(between 590 and 620 nm) has photon energy of between 2.0 and 2.1 eV. As such, light in the near-infrared spectrum has lower photon energy and therefore yields less phototoxicity to the living cells of the biofilm.

### **7.1.1 Aims and Objectives**

The aim of this chapter is to investigate the utilisation of dual-fluorophore, ratiometric, pH-sensitive nanosensors and SNARF<sup>®</sup>-4F 5-(and-6)-carboxylic acid to visualise pH microgradients within biofilms through four spatial and temporal dimensions.

The objectives are to; i) evaluate the use of dual-fluorophore, ratiometric, pH-sensitive nanosensors and SNARF<sup>®</sup>-4F 5-(and-6)-carboxylic acid to determine hydrogen-ion concentration within bacterial sediments, ii) ensure that the hydrogen-ion concentration determined through the use of each method correlates with those obtained through the use of the currently utilised method for pH determination, pH electrodes, iii) apply each sensor to the biofilms and image to determine localised extracellular microgradients in hydrogen-ion concentration through the use of confocal laser scanning microscopy (pH-sensitive nanosensors) or multiphoton molecular excitation fluorescence lifetime imaging microscopy (SNARF<sup>®</sup>-4F 5-(and-6)-carboxylic acid), and iv) analyse images and use calibration data to correlate the acquired information to determine localised extracellular microgradients in hydrogen-ion concentration within the biofilms, both prior to and subsequent to the addition of fermentable carbohydrates.

## **7.2 Materials and Methods**

### **7.2.1 Preparation of the Nanosensor Suspension**

Dual-fluorophore, ratiometric, pH-sensitive nanosensors were prepared as previously described (Section 4.2). pH-sensitive nanosensors were prepared in sterile deionised water at a final concentration of 20 mg/mL. The nanosensor

suspension was sonicated for 5 min to ensure adequate dispersal of the nanosensors in suspension. The nanosensor suspension was sterilised by passing the suspension through a syringe-driven 0.22 µm filter prior to use.

### **7.2.2 Application of Nanosensors to Biofilms**

Biofilms were grown in a constant-depth film fermenter and consisted of four bacterial species; *S. mutans*, *S. sanguinis*, *L. casei* and *N. subflava*, as previously described (Section 2.5). These species were selected as they possess different acidogenicity profiles. *S. mutans* and *L. casei* are considerably acidogenic, producing organic acids as a product of the metabolism of fermentable carbohydrates. *S. sanguinis* and *N. subflava* are less acidogenic (Section 3.3.1). It is envisaged that the difference will add contrast to the images. Mature biofilms were extracted from the CDFF by removal of one of 15 PTFE pans. Each PTFE pan houses 5 PTFE plugs allowing the growth of 5 individual biofilms. The hydroxyapatite discs were removed from the PTFE plugs and transferred to a 35 mm petri dish resting on a small amount of high vacuum silicon grease to minimise movement. A 5 mL volume of the nanosensors suspension was applied to each biofilm. The biofilms were transported to the confocal laser scanning microscope for imaging.

### **7.2.3 Growth of Biofilms Incorporating Nanosensors**

To incorporate nanosensors within biofilms during growth, the CDFF was set up for the growth of biofilms. To facilitate the addition of nanosensors within the biofilm during growth, a 2-into-1 tubing connector was used in order to introduce the inoculum and a 20 mL suspension of nanosensors at a concentration of 10 g/L into the CDFF housing. The nanosensor suspension was clamped for a period of 1 h to allow the inoculum to be introduced. After an initial 1 h period, the nanosensor suspension was unclamped and added during inoculation at a flow rate of approximately 15 mL/h. Mature biofilms were removed from the CDFF, transported and imaged as previously described (Section **Error! Reference source not found.**).

#### **7.2.4 Preparation of SNARF<sup>®</sup>-4F 5-(and-6)-Carboxylic Acid Suspension**

Stock aliquots of SNARF<sup>®</sup>-4F 5-(and-6)-carboxylic Acid were produced at a concentration of 200  $\mu$ M and stored at a temperature of approximately -20°C, as previously described (Section 6.2.3). Prior to use, an aliquot was removed from the freezer and allowed to thaw, protected from light, at room temperature.

#### **7.2.5 Preparation of a Suspension of *Streptococcus mutans***

An aliquot of *S. mutans* (NCTC 10449), stored at -80°C, was removed from the freezer and allowed to thaw at room temperature. Approximately 10 $\mu$ L of the aliquot was inoculated to a BHI agar plate and incubated overnight at 37°C in an aerobic atmosphere supplemented with 5% CO<sub>2</sub>. Following overnight incubation, the culture was assessed for purity and subculturing of a single colony to a sterile BHI agar plate was performed and incubated as previously described, to minimise the effects of freezing. To produce a bacterial suspension, *S. mutans* was inoculated to sterile BHI broth and incubated overnight.

#### **7.2.6 Determination of pH in Bacterial Sediment Exposed to Sucrose**

To produce bacterial sediment, 10 mL of the overnight *S. mutans* broth culture was transferred to a 35 mm petri dish. The petri dishes were centrifuged at 500 g for 10 min. The supernatant was removed by careful pipetting. The bacterial sediments were covered with sterile isotonic saline and the dish lid was applied to ensure no bubbles were present which may disrupt the bacterial sediment during transport. A 200  $\mu$ M aliquots of the SNARF<sup>®</sup>-4F 5-(and-6)-carboxylic acid was thawed at room temperature and diluted 1:5, to a concentration of 40  $\mu$ M. Following transport, the isotonic saline was removed by careful pipetting and 2 mL of the SNARF<sup>®</sup>-4F 5-(and-6)-carboxylic acid suspension was added to the bacterial sediment. The surface of the bacterial sediment was located using light microscopy before transferring to the

FLIM component with the excitation wavelength set to 840 nm. The bacterial sediment was imaged. A 2 mL volume of 28mM sucrose was added to the suspension and the fluorescence lifetime images recorded approximately every 3 min. In parallel, pH measurements were collected using a glass pH microelectrode (Sigma-Aldrich, Dorset, UK) connected to a Jenco 6350 pH meter (Jenco, CA, USA). pH values were monitored and collected with the use of pH plotter software (Lazar Research Labs, CA, USA).

### **7.2.7 Determination of pH in Bacterial Biofilm Exposed to Sucrose**

*S. mutans* (NCTC 10449) biofilms were produced in a CDFF, as previously described (Section 2.8**Error! Reference source not found.**). The PTFE pans were removed from the CDFF with the aid of the stainless steel extraction tool and biofilm-attached hydroxyapatite discs were removed and transferred to a 35 mm petri dish. The biofilms were overlaid with sterile isotonic saline to ensure no bubbles were present which may disrupt the biofilm structure during transport. Following transport, the isotonic saline was removed and SNARF<sup>®</sup>-4F 5-(and-6)-carboxylic acid was added at the produced biofilms to a concentration of 40 $\mu$ M. A 1 mL volume of 28 mM sucrose was added to the biofilm and the fluorescence lifetime images recorded. Images were analysed using Becker-Hickl SPCLImage software (v 5.5). The fluorescence lifetime values obtained at each pixel were transferred to Microsoft Excel (2013). The fluorescence lifetime values were converted to pH through the use of the equation of the line-of-best-fit obtained from the calibration data. The pH values were then assigned a colour value within appointed pH ranges.

## **7.3 Results**

### **7.3.1 Dual-Fluorophore, Ratiometric, pH-sensitive Nanosensors**

The dual-fluorophore, ratiometric, pH-sensitive were applied to biofilms, both following growth and prior to growth as part of the inoculum. The biofilms were imaged using CLSM.

#### ***7.3.1.1 Imaging of biofilms with nanosensors added after growth***

The apex of the biofilm was able to be located using light microscopy. When switched to fluorescence excitation imaging, only the periphery of the biofilm is able to be visualised. As the 'z' axis was moved and the distance between the objective lens and the biofilm was decreased to a deeper optical section of the biofilm, this periphery widened and followed the contours of what is suspected to be the biofilm structure. It is suspected that, following the addition of nanosensors after the growth of the biofilms, the nanosensors are unable to penetrate the structure of the biofilm and are attaching to the EPS. It may be possible to alleviate this phenomenon by adding the nanosensors to the biofilm by addition to the bacterial suspension used to inoculate the biofilm and therefore allow incorporation during growth.

#### ***7.3.1.2 Imaging of biofilms with nanosensors added prior to growth***

The apex of the biofilm was located through the use of light microscopy. When switched to fluorescence excitation imaging, it became evident that the issue experienced when the nanosensors were added after growth has not been alleviated and only the periphery of the biofilm is able to be visualised.

### **7.3.2 Imaging of Planktonic Bacterial Sediment of *S. mutans* using SNARF<sup>®</sup>-4F 5-(and-6)-Carboxylic Acid and Two-Photon Molecular Excitation Fluorescence Lifetime Imaging**

Colour-coded fluorescence lifetime images were obtained prior to the addition of a fermentable carbohydrate, in the form of sucrose, and subsequently at intervals of approximately 3 min over a period of 1 h. Figure 7.2 shows the fluorescence lifetime images of a resting *S. mutans* biofilm and following exposure to a fermentable carbohydrate, in the form of sucrose, at a concentration of 14 mM. The first image predominantly consists of blue and blue-green, consistent with longer fluorescence lifetime values and concurrently, higher pH values approaching neutral. Following exposure to sucrose and incubation, it is clear to see that the image shifts from the blue-green dominating the resting biofilm to an increase in yellows and oranges demonstrating a decrease in the local pH within those pixels and throughout the image. It also becomes apparent that pH values differ from those even a short distance away. These variations demonstrate the existence of microgradients in pH within the bacterial sediment. When this experiment was repeated with determination of fluorescence lifetime values at 3 min intervals, the shift in fluorescence lifetime, corresponding to decrease in local pH, becomes apparent. This is demonstrated in Figure 7.3.

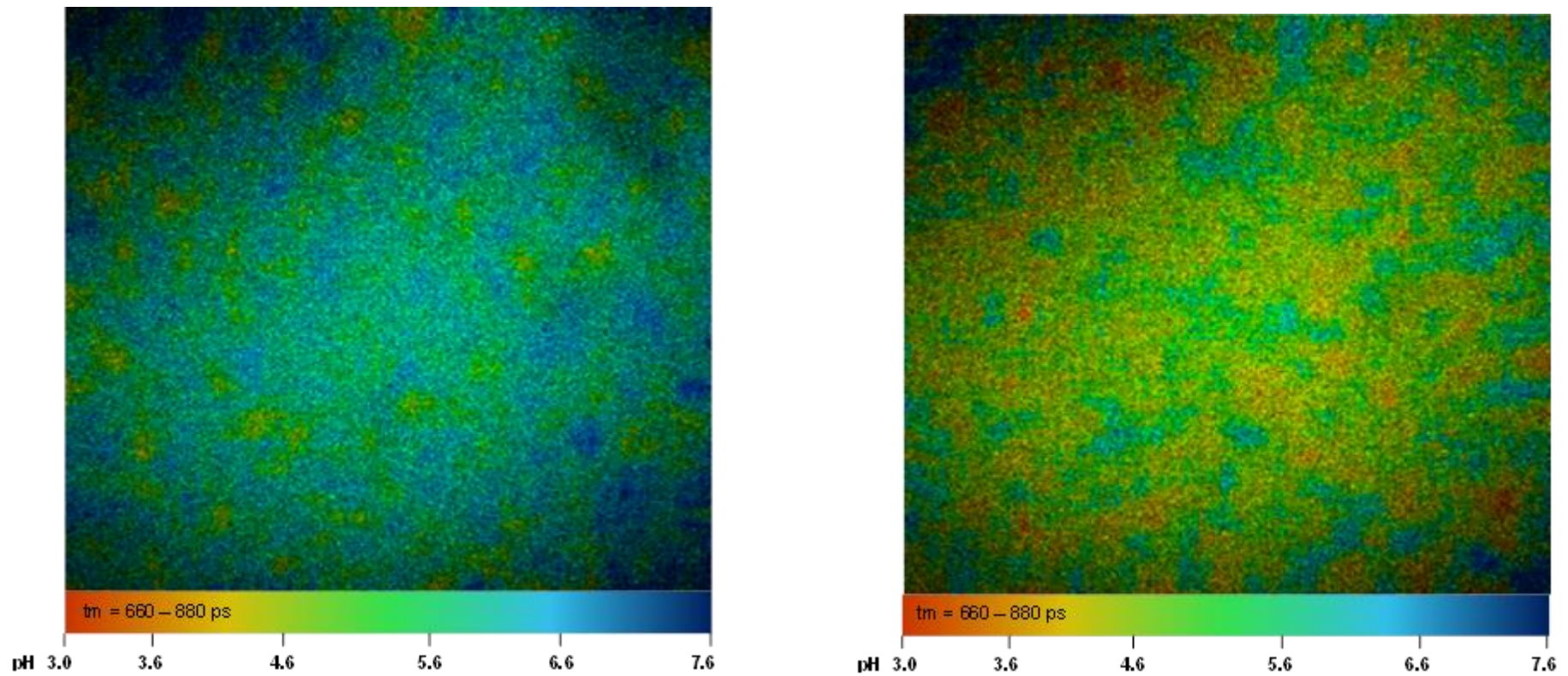


**Figure 7.2** Colour-coded fluorescence lifetime images of a bacterial sediment of *S. mutans* using SNARF<sup>®</sup>-4F 5-(and-6)-carboxylic acid. Images demonstrate fluorescence lifetime prior to sucrose (left), and 15 min post-exposure (right).

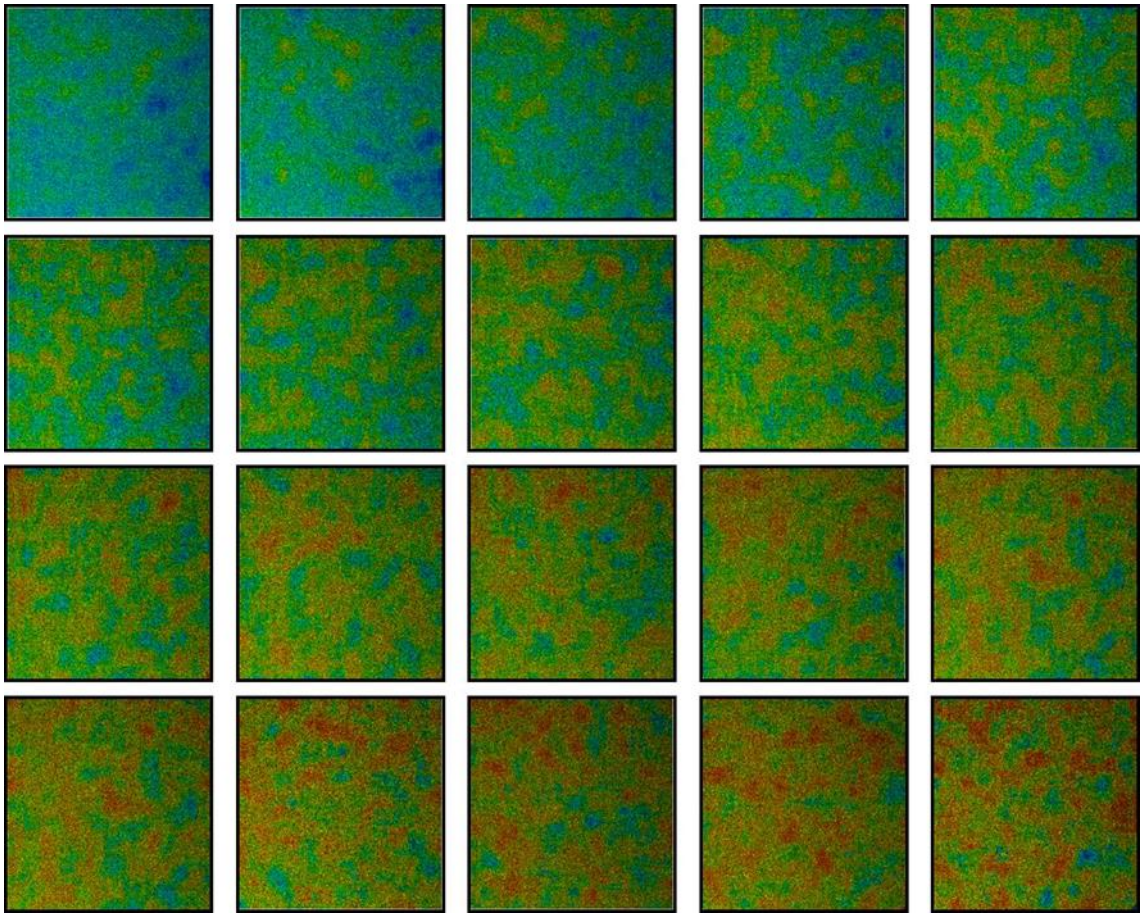


**Figure 7.3** Matrix of colour-coded fluorescence lifetime images over time following exposure to fermentable carbohydrates, in the form of sucrose. The images are taken at introduction of fermentable carbohydrate and subsequently at intervals of approximately 3 min over a period of 1 h.

### **7.3.3 Comparison of pH Values Determined Through the Use of a pH Microelectrode to SNARF<sup>®</sup>-4F 5-(and-6)-Carboxylic Acid Imaged Through the Use of Two-Photon Molecular Excitation Fluorescence Lifetime Imaging Following Exposure to a Fermentable Carbohydrate**

To evaluate the ability to determine extracellular pH through the use of SNARF<sup>®</sup>-4F 5-(and-6)-carboxylic acid imaged through the use of two-photon molecular excitation fluorescence lifetime imaging, it was compared to the currently utilised

methods, pH microelectrode. A comparison of the two methods was performed on the same bacterial suspension with the same concentration and amount of fermentable carbohydrate source. Figure 7.4 shows the pH values, averaged over the period of a minute, with respect to time. The plot demonstrates a sharp decrease from approximately pH 7 to below pH 6.5 within the initial 5 min. The rate of decrease in the pH slows, and that rate remains relatively constant over the next 45 min, declining from just below pH 6.5 to above pH 5.0. The rate then slows further, before reaching a pH slightly below pH 5.0 at the hour mark. Figure 7.5 shows the average fluorescence lifetime values of the suspension of *S. mutans* following exposure to sucrose with respect to time. In contrast, the rate of decrease of the fluorescence lifetime values appears relatively constant over the duration of the experiment. The initial average fluorescence lifetime value is approximately 764 ps before decreasing to a final average fluorescence lifetime of 696 ps. pH values were calculated through the utilisation of the calibration equation from the average fluorescence lifetime values. These pH values were then plotted with respect to time and are demonstrated in Figure 7.6. These values were converted to pH through the use of the calibration curve line-of-best-fit equation and plotted with respect to time. When compared, the values and the profile of pH determined through the utilisation of a glass electrode and pH meter (Figure 7.4) and SNARF<sup>®</sup>-4F 5-(and-6)-carboxylic acid imaged through the use of two-photon molecular excitation fluorescence lifetime imaging (Figure 7.6) exhibit similarity.

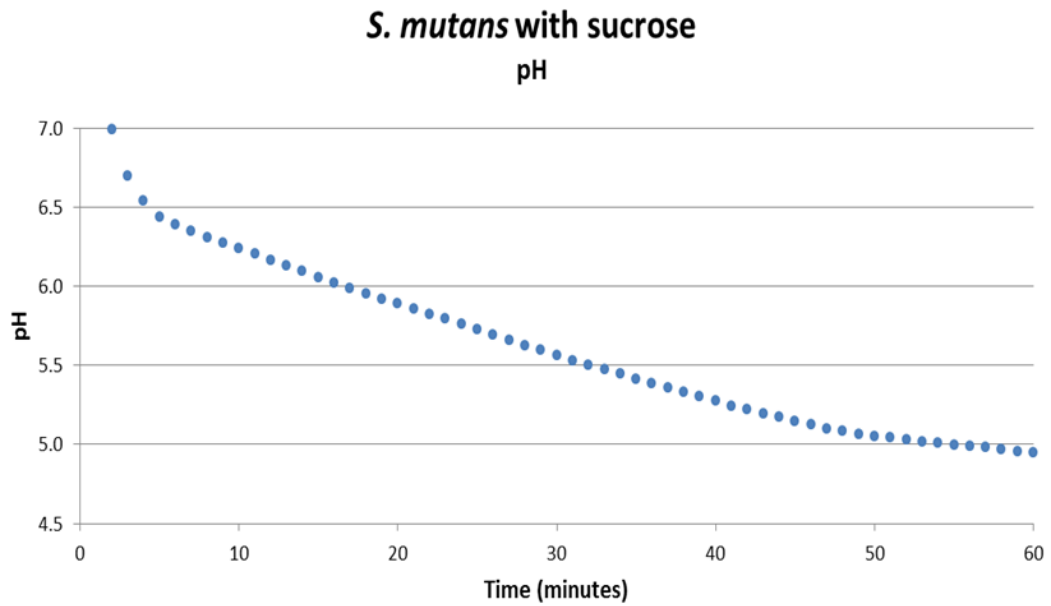


**Figure 7.4** Plot of pH values determined using a glass microelectrode, pH meter and plotting software package, with respect to time. Points correspond to the average pH values recorded every second over the period of a minute.

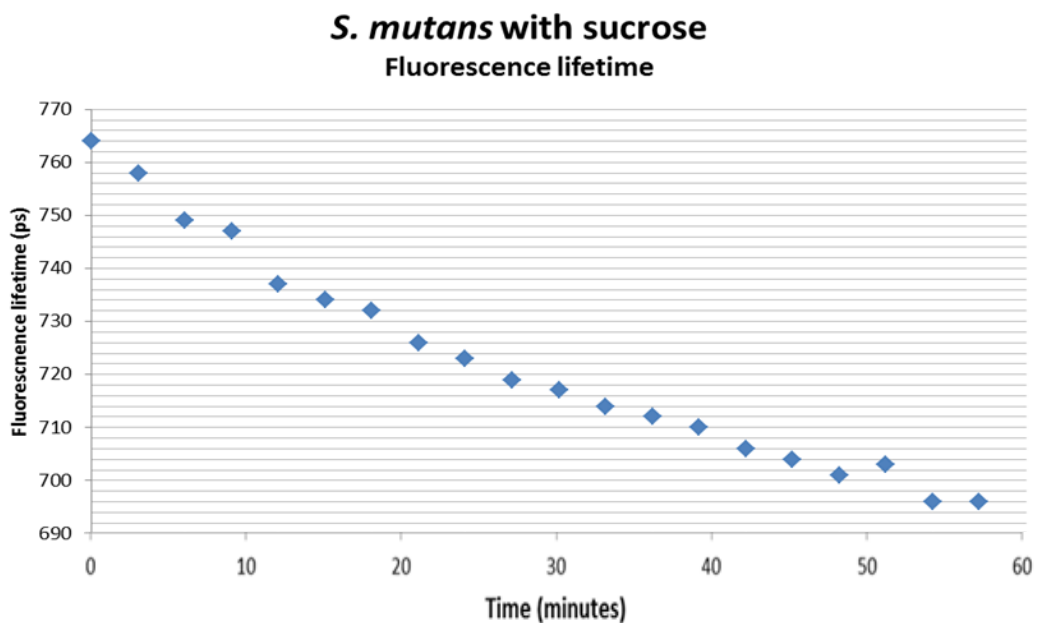


**Figure 7.5** Plot of average pH values determined through the use of SNARF<sup>®</sup>-4F 5-(and-6)-carboxylic acid excited through the utilisation of two-photon molecular excitation fluorescence lifetime imaging microscopy, with respect to time. Images were collected every 3 min and are observed in Figure 7.3.

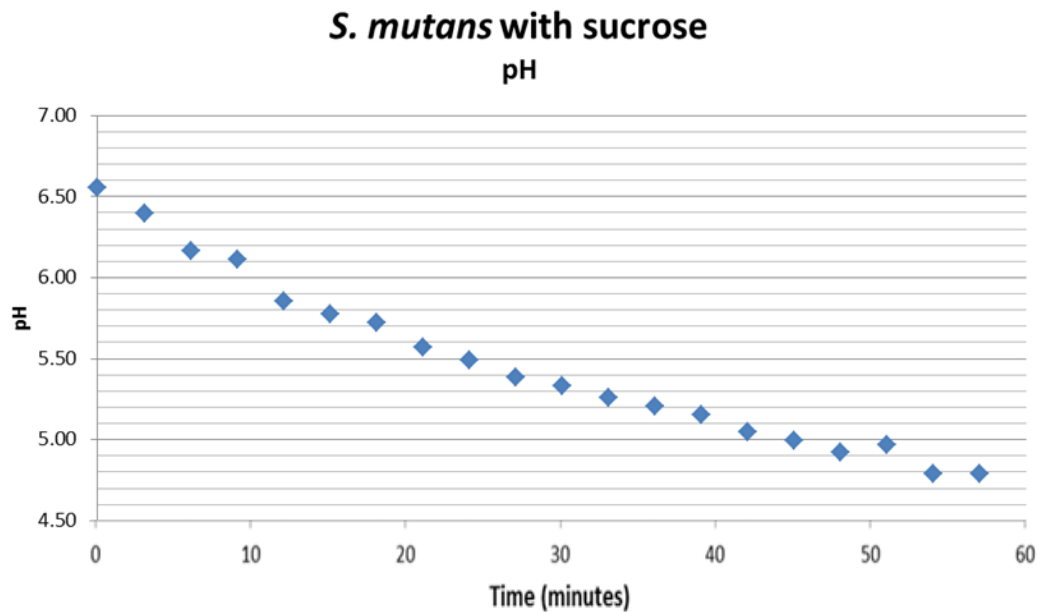


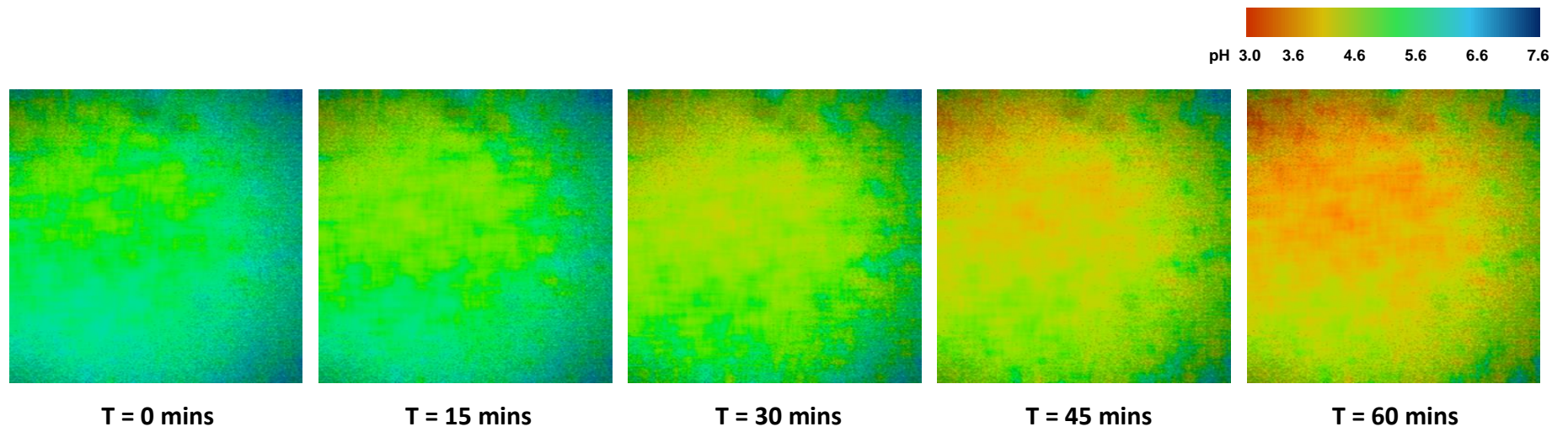
**Figure 7.6** Plot of pH values with respect to time extrapolated from the average fluorescence lifetime values and the calibration data for SNARF<sup>®</sup>-4F 5-(and-6)-carboxylic acid.

### **7.3.4 Imaging of *S. mutans* Biofilm using SNARF<sup>®</sup>-4F 5-(and-6)-Carboxylic Acid and Two-Photon Molecular Excitation and Fluorescence Lifetime Imaging**

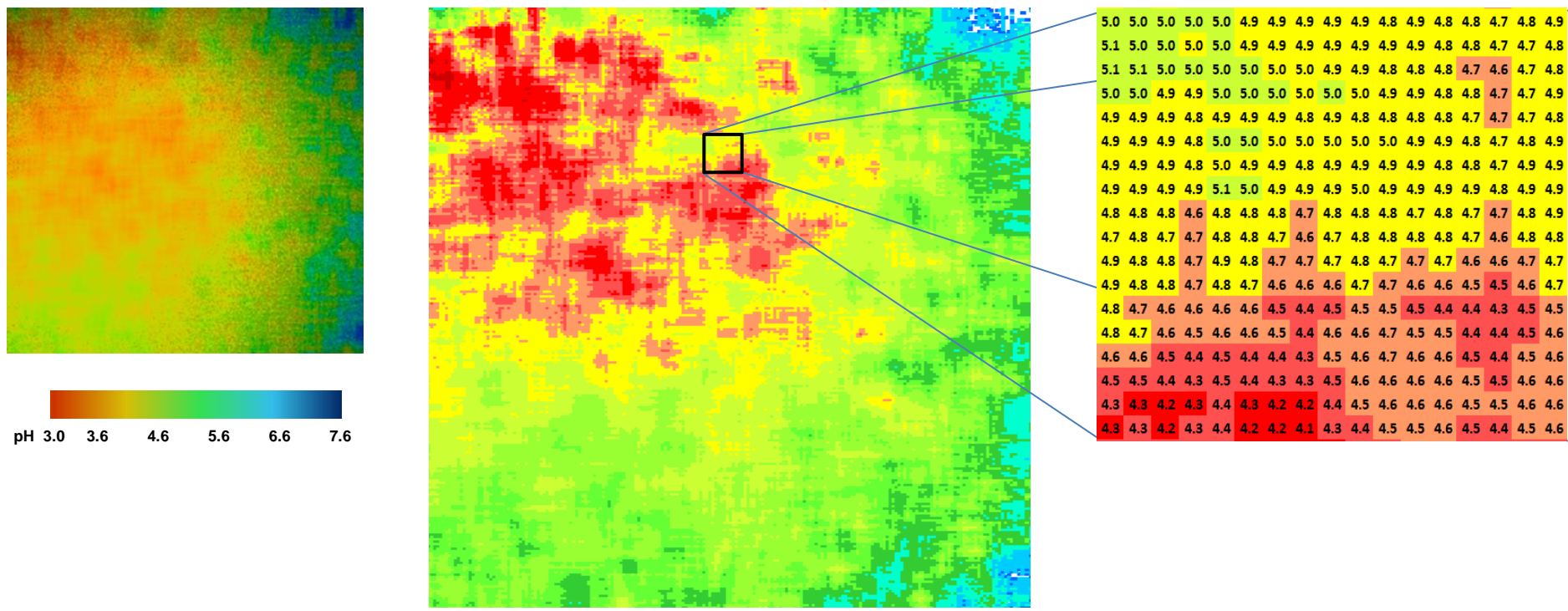
When SNARF<sup>®</sup>-4F 5-(and-6)-carboxylic acid is applied to *S. mutans* biofilms, it is possible to obtain fluorescence lifetime images through the application of two-photon molecular excitation and utilisation of a time-correlated single-photon counting procedure to determine the fluorescence lifetime values.

Figure 7.7 illustrates the fluorescence lifetime values observed in a *S. mutans* biofilm prior to exposure to a fermentable carbohydrate, in the form of sucrose, and following incubation for duration of 1 h, in 15 min increments. The shift in colour towards the orange end of the spectrum corresponds to a decrease in fluorescence lifetime and calibration demonstrates that this corresponds to a

decrease in pH. Furthermore, the shift to a decrease in pH appears to radiate from a defined origin.



**Figure 7.7** Colour-coded fluorescence lifetime images of *S. mutans* biofilm in 15 minute increments following exposure to sucrose



**Figure 7.8** Colour-coded fluorescence lifetime image following 1 hour incubation in the presence of sucrose. Fluorescence lifetime values of each pixel obtained from the Becker-Hickl SPCImage software are converted to pH through use of the calibration equation and converted colour using Microsoft Excel.

## 7.4 Discussion

The aim of this chapter was to investigate the application of two optical fluorescence-based sensors to biofilms mimicking dental plaque. The two methods were; dual-fluorophore, ratiometric, pH-sensitive nanosensors imaged through use of CLSM, and fluorescence lifetime correlated to pH using SNARF<sup>®</sup>-4F 5-(and-6)-carboxylic acid, TCSPC and FLIM. The two methods described have been well characterised and calibrated to correlate response with changes in environmental pH. Due to their optical nature, they appear to offer the ability to visualise environmental pH in three spatial dimensions, imaged through optical sectioning technologies, such as CLSM and two-photon molecular excitation FLIM. Both methods allow biofilms to be investigated in a naturally-hydrated state. The ability to respond to changes in pH also allows determination in the temporal dimension through time-lapse experiments. Through the use of ratiometric methodologies (pH-sensitive nanosensors) and FLIM (SNARF<sup>®</sup>-4F), environmental pH is able to be determined without measurements being affected by variations in fluorophore concentration, excitation source intensity or specimen thickness. This is advantageous as, in the complex structure of the biofilm; fluorophore concentration would vary greatly at various locations within the biofilm. Dual-fluorophore, ratiometric, pH-sensitive nanosensors were initially applied to biofilms grown on nitrocellulose membranes. Upon imaging, it appears that only the periphery of the biofilm structure was able to be obtained. This was suspected as i) the apex of the biofilm was first located using light microscopy before changing to fluorescence to image through confocal laser scanning microscopy, where a small and thin ring of excitation was observed, ii) this circular image widened as the distance between the objective lens and the specimen decreased, iii) the fluorescence excitation was observed in both channels and iv) the fluorescence excitation intensity was lesser than that observed during calibration. The possible explanations for this include; poor nanosensor penetration within the extracellular polymeric matrix or as a result of removal of the nanosensors from the biofilm through active or passive transport processes during growth. Biofilms grown in this way are known to have a more

closed structure than biofilms grown in, for example, a flow cell or system such as the CDFF (Merritt et al. 2005), which may account for an inability of the nanosensors to penetrate the biofilm structure. The extracellular polymeric substance produced by the biofilm may also result in the adhesion of the nanosensors to this structure. The nanosensors may also have an inherent charge and may be repelled by the charge of the biofilm structure. In an attempt to overcome this, the nanosensor suspension was added to the bacterial suspension prior to membrane inoculation. As the possibility of detrimental effect upon the bacteria has been determined to be minimal (Section 5.3.1), the concern was that biofilm structure could possibly be affected. The nanoscale of the nanosensors is not likely to have a significant effect. This, however, produced a similar result. It is therefore suspected that the lack of intensity in the depths of the biofilms is due to poor light penetration into the biofilm. This theory is less likely as light penetration may have been increased by increasing the laser power. When the laser power was increased the fluorescence intensity of the ring increased but did not increase in thickness. This suggests that increase in penetration was observed or increased penetration did occur but the presence of nanosensor at greater depths within the biofilm was lacking. With the most likely explanation being the absence of nanosensor penetration and the possibility of poor excitation source penetration, other microscopic methods were evaluated. Additionally, the use of visible light as an excitation source was evaluated, however a significant amount of photobleaching of the pH-sensitive fluorophores (carboxyfluorescein and Oregon Green®), but not in the pH-insensitive red fluorophore (tetramethylrhodamine), was observed. Photobleaching resulted in the decrease in fluorescence intensity in the green detection channel (530/30 nm). Due to the ratiometric nature of the methodology, an effect upon one of the fluorescence intensities will affect the ratio and therefore inaccuracies arise. The pH-sensitive nanosensors, to this end, have proven to be ineffective for the mapping of microgradients in environmental pH which occur in biofilms. Improved depth penetration is likely to be achieved by employing multiphoton molecular excitation microscopy. Depth penetration may increase by as much up to 10-fold (Vroom et al. 1999; Stutzmann & Parker 2005; So et al. 2000; Centonze 2002). Although this capability was not available at the

current site, collaboration with a group off-site provided the possibility to evaluate this technology. Furthermore, the microscope offering two-photon excitation microscopy was capable of fluorescence lifetime imaging microscopy (FLIM). Calibration of fluorescence lifetime values obtained by two-photon molecular excitation and time-correlated single-photon counting of SNARF<sup>®</sup>-4F 5-(and-6)-carboxylic acid in citric acid buffers demonstrated a fitted, linear relationship between fluorescence lifetime and environmental pH. Two-photon molecular excitation fluorescence lifetime imaging microscopy of SNARF<sup>®</sup>-4F 5-(and-6)-carboxylic acid on planktonic bacteria exposed to sucrose demonstrated a visible shift in the fluorescence lifetime corresponding to a decrease in environmental pH. Furthermore, when compared to pH values of the same bacterial suspension exposed to the same amount and concentration of sucrose determined through the utilisation of a glass microelectrode demonstrated that, over the same time period, the profile appeared similar. When applied to a biofilm, fluorescence lifetime values were able to be determined through the use of time-correlated single-photon counting. These fluorescence lifetime values were converted to local environmental pH using the equation from the line-of-best-fit from the calibration data. The biofilm, exposed to sucrose, demonstrated a visible decrease in fluorescence lifetime as time progressed. This fluorescence lifetime was translated to localised pH from the calibration equation. To aid this conversion, the fluorescence lifetime for each pixel was transferred to a spreadsheet (Microsoft Excel) where the calibration equation converted fluorescence lifetime values of each pixel to pH. Fluorescence lifetime values were assigned colours, within certain ranges, to greater visualise areas of various pH values. It appears that pH decreases radiating from a point-of-origin. Although these two optical methods offer a number of advantages, including the ability to not only determine localised pH but to also visualise those localised pH values and therefore the formation of environmental pH microgradients, they are not without their disadvantages. One of the key disadvantages of the methods is cost and as a consequence, access to advanced microscopy techniques, such as two-photon excitation fluorescence lifetime imaging microscopy and, to a lesser extent, confocal laser scanning microscopy. Furthermore, both optical methods require considerable training to obtain images

and extensive training to gain expertise. Additionally, considerable knowledge of the production of nanoparticles is needed as the nanosensors are not currently commercially available. Imaging of biofilms using confocal laser scanning microscopy and dual-fluorophore, ratiometric, pH-sensitive nanosensors was unable to provide determination of microgradients of extracellular pH. This is hypothesised to be as a result of inadequate nanoparticle penetration, active transport of the nanosensors during growth or insufficient excitation light penetration. Imaging of planktonic bacteria through the use of fluorescence lifetime imaging microscopy and the commercially available fluorophore, SNARF<sup>®</sup>-4F 5-(and-6)-carboxylic acid, demonstrated a decrease in fluorescence lifetime corresponding to a decrease in pH following the addition of sucrose. This decrease, measured through fluorescence lifetime imaging microscopy exhibits a profile consistent with that measured by a pH microelectrode. Imaging of biofilm through the use of fluorescence lifetime imaging microscopy and the commercially available fluorophore, SNARF<sup>®</sup>-4F 5-(and-6)-carboxylic acid, demonstrated that localised environmental pH was able to be determined and visualised over time following exposure to a fermentable carbohydrate. It appears that this technique may provide a method to determine environmental pH within biofilms.

# Chapter 8 General Discussion

## 8.1 Project Background

The overall aim of this project was to investigate novel and improved methods for the determination of pH within biofilms mimicking cariogenic dental plaque. The ability to determine high resolution spatially-resolved pH in the z-axis, with minimal disruption to the biofilm structure, in a naturally-hydrated state, and the ability to visualise the changes in pH as a direct result of metabolism, was also highly desirable. The determination of pH microgradients within biofilms may elicit important information about the microbial ecology that disrupts the microbial homeostasis, driving progression from oral health to dental diseases such as dental caries. It appears that the methods described and investigated here possess a number of advantages over previously used and studied methods, however, are not without some drawbacks themselves. The advantage that optical methods such as these provide is that they allow measurement independent of fluorophore concentration. This is particularly pertinent within the complex structure of the biofilm. Another advantage is that they allow determinations in a naturally hydrated state, without disruption of the biofilm structure. A disadvantage of optical methods is that they can only be used on in vitro biofilms. It is possible with the aid of complex methods of biofilm growth, such as the CDFP which allow exceptional control of the various parameters to produce biofilms mimicking a number of dental pathologies, including dental caries (Zaura et al. 2011), periodontal disease (Wiecek 2015) and peri-implantitis (Sousa et al. 2016).

Two optical methods for the rapid determination of spatial and temporal gradients of  $pH_e$  in the bulk phase of laboratory-grown dental plaque were investigated. The first method was the use of dual-fluorophore, ratiometric, pH-sensitive nanosensors imaged through the use of confocal laser scanning microscopy. The nanosensors were produced, calibrated and applied to both planktonic and biofilm phenotypes. The nanosensors caused no determinable effect upon the viability of the bacteria tested. However, the nanosensors were deemed not suitable for such

measurements due to a number of issues experienced. The nanosensors did not facilitate imaging within the biofilm, both following the addition after growth and prior to growth. This issue may be as a result of poor light penetration of the excitation laser source, poor nanosensor penetration or removal of the nanosensors during growth. Another issue that arose during the analysis of the nanosensors resulted from photobleaching of the pH-sensitive fluorophores, but not the pH-insensitive. This photobleaching alters the fluorescence intensity of the pH-sensitive fluorophores and, therefore, the ratio of pH-sensitive to pH-insensitive fluorophores. Due to these issues, and an inability to overcome these issues, investigation of the pH-sensitive nanosensors was ceased and alternative methods were investigated. The second method investigated was the use of the pH-sensitive fluorophore, SNARF<sup>®</sup>-4F 5-(and-6)-carboxylic acid and the use of two-photon excitation fluorescence lifetime imaging microscopy. Fluorescence lifetime values were determined through the use of time-correlated single photon counting.

## 8.2 Summary of Main Findings

The aim of **Chapter 3** was to determine the acidogenic potential of a number of oral bacteria following exposure to fermentable carbohydrates in the form of sucrose. This was achieved through application of sucrose to suspension of the selected species and measurement of the pH over time. This demonstrated that each of the species selected fermented the carbohydrate and produced acid by-products, reflected in a decrease in pH. It also revealed that each of the species produced a decrease in pH at different rates resulting in differences in the final pH. One of the desired properties of the selected bacterial species was this observable difference in rate and level of pH, as it was suspected that these differences would add contrast to the images obtained during microscopy.

The aim of **Chapter 4** was to investigate the capability to produce nanosensors able to determining local environmental pH in bulk extracellular fluid of biofilms. Nanosensors were designed; polyacrylamide was selected as the nanoparticle matrix, a number of fluorophores were selected with desired properties and the

preference of conjugation over incorporation was decided. This was performed with the assistance of Dr. Veeren Chauhan and Prof. Jon Aylott at the University of Nottingham. The fluorophores selected included two pH-sensitive fluorophores; 5-(and-6)-carboxyfluorescein (FAM) and Oregon Green<sup>®</sup>-488 (OG), which are excited, and emit, at similar wavelengths. This allowed the use of a single excitation source for both fluorophores and detection through the same emission filter. The crucial difference between the two fluorophores was the  $pK_a$ , the pH at which each fluorophore produced the greatest response to change in environmental pH. By utilising a 1:1 ratio of the two fluorophores, the dynamic range was extended to its maximum. The third fluorophore selected was the pH-insensitive fluorophore, tetramethylrhodamine, or TAMRA. TAMRA is excited by, and emits at, different wavelengths to the two pH-sensitive fluorophore. The fact that TAMRA is pH-insensitive provides a reference and allows ratiometric measurements, alleviating variations in concentration of the nanosensor which would otherwise result in changes in fluorescence intensity. The nanosensors were produced, and the physical and optical properties were determined. The nanosensors were characterised and found to have an approximate diameter of 40 nm through environmental scanning electron microscopy, corroborated through the use of dynamic light scattering. Dynamic light scattering also reveals particles with a narrow distribution width. The fluorescent spectra of the nanosensors confirmed that the pH-sensitive fluorophores revealed changes in fluorescence emission intensity with respect to localised environmental pH, while the pH-stable, reference fluorophore remained relatively unaffected by differences in environmental pH. This allowed a ratiometric methodology to be employed. Furthermore, by employing a 1:1 ratio of the pH-sensitive fluorophores in the nanosensor construct, each with a distinct  $pK_a$ , the dynamic range was extended.

The aim of **Chapter 5** was to analyse the suitability of dual-fluorophore, ratiometric, pH-sensitive nanosensors to determine variation in environmental pH without detrimental effect upon bacteria. The bacteria selected were exposed to the nanoparticles to determine if there was any detrimental effect on viability. Differing concentrations of the nanoparticles were used to determine if any detrimental

effects were concentration dependent. The functionalised nanoparticles were also assessed for detrimental effects upon the viability of the bacteria. The nanoparticle matrix was exposed to a number of bacterial species and no detrimental effect upon those species. No detrimental effect was observed for both the nanoparticles and the functionalised nanosensors. The response of the nanosensors to variations in pH was determined and correlated with pH to allow calibration of the nanosensors. The nanosensors were calibrated in citric acid buffers, and a calibration curve was produced. This calibration produced a linear relationship and allowed the use of the nanosensors to determine environmental pH. Finally, the dynamic range of the nanosensors was determined. It was determined that the dynamic range of the nanosensors was between approximately pH 4.0 and pH 7.0.

The aim of **Chapter 6** was to investigate the use of SNARF dyes to determine environmental pH through the use of multiphoton molecular excitation, time-correlated single-photon counting to determine fluorescence-lifetime values, and fluorescence lifetime imaging microscopy. A number of pH-sensitive fluorophores were investigated for the ability to resolve extracellular pH. These fluorophores included 5-(and-6)-carboxy-seminaphthofluorescein (SNAFL) dyes, 5-(and-6)-carboxysemnaphthorhodafluor (SNARF) dyes, and 2',7'-bis-(2-carboxyethyl)-5-(and-6)-carboxyfluorescein (BCECF). Following examination, the benzo[c]xanthene dye SNARF<sup>®</sup>-4F 5-(and-6)-carboxylic acid (SNARF<sup>®</sup>-4F), a fluorinated derivative of SNARF-1, was selected due to its comparatively low pK<sub>a</sub>. The use of fluorescence lifetime imaging was investigated and selected for imaging. This was due to fluorescence lifetime being an intrinsic property unaffected by differences in fluorophore concentration within the complex structure of biofilms. Additionally, this technique provides improved depth penetration, particularly useful when examining biofilms. To facilitate fluorescence lifetime imaging microscopy, two-photon molecular excitation was employed. To acquire fluorescence lifetime images, time-correlated single-photon counting was employed. A search of the literature did not reveal the optimum two-photon molecular excitation wavelength. This was determined to be 840 nm through determining the number of photons detected at wavelengths between 760 and 940 nm. Exposure of SNARF<sup>®</sup>-4F to a

number of bacterial species did not elicit any detrimental effect on viability (Section 6.2.4). This was to be expected as SNARF<sup>®</sup>-4F has previously been employed in live cell imaging. The optimal two-photon excitation wavelength for SNARF<sup>®</sup>-4F 5-(and-6)-carboxylic acid in this system was determined to be 840 nm. The single-photon excitation wavelength for SNARF<sup>®</sup>-4F is observed between 500 and 550 (Marcotte & Brouwer 2005), with many exciting at 488 nm with satisfactory emission. However, this would indicate that the two-photon excitation wavelength would be in the region of 1000-1100 nm, wavelengths that this system was not capable of. It should be noted that a smaller absorption peak is observed at approximately 410 nm and this would correlate with the maximum number of photons being detected in the region of 840 nm. The instrumentation was optimised for the experiments including, excitation laser, emission filter settings and the detection parameters. Various substrata had no detrimental effect on the fluorescence obtained. It was determined that variations in temperature and redox-potential had little effect upon the number of photon detected and the fluorescence-lifetime values of those photons detected. Chemical properties considered having a possible effect upon the number of photons detected and the fluorescence-lifetime were proteins and glycoproteins. Protein, in the form of bovine serum albumin, had little detrimental effect, however glycoproteins, in the form of hog gastric mucin, produced a concentration-dependent decrease in the number of photons detected. This is of particular notice as hog gastric mucin constitutes a large portion of the artificial saliva media used as the primary nutrient source during biofilm growth in the CDFF. It is unclear whether the concentrations found within the biofilm will be greater than those which have demonstrated an effect upon photon numbers. The fluorescence-lifetimes obtained with respect to pH demonstrated a pH-dependent variation. Correlation demonstrated a linear relationship with respect to pH, allowing calibration. Another consideration with respect to the use of this fluorophore is that Richter states that the *“separation of 5'- and 6'-carboxy-SNARF reveals a variation in pK<sub>a</sub> of 0.15, calling into question pH measurements with the commercially available mixture used here”* (Richter et al. 2015).

The aim of **Chapter 7** was to investigate the utilisation of dual-fluorophore, ratiometric, pH-sensitive nanosensors and SNARF<sup>®</sup>-4F 5-(and-6)-carboxylic acid to visualise pH microgradients within biofilms through four spatial and temporal dimensions. Dual-fluorophore, ratiometric, pH-sensitive nanosensors were evaluated for the determination of extracellular environmental pH within biofilms. Unfortunately, the nanosensors did not provide the information desired. The main issue with the application of the nanosensors appears to be a result of poor penetration. The nanosensor size (~40 nm) suggests that size would not play a major role in penetration, although aggregation may play a role by increasing this size. This may be due to a lack of penetration into the biofilm structure, adhering to the sticky extracellular polymeric substance or being actively or passively expelled from the biofilm structure. From the images obtained, it appears that the nanosensors were aggregating upon the surface of the biofilm structure. Another consideration was that closed structure of the nitrocellulose-supported biofilms. Although many of the drawbacks of other optical sensors for pH were overcome through the nanosensor design, the lack of penetration has led to the nanosensors being unusable for determining environmental pH in biofilms. Another possibility is the removal of the nanosensors from the biofilm through active or passive transport processes during growth. A final possibility considered is poor excitation light penetration into the biofilm structure. However, this was discounted due to the ability for the laser to penetrate biofilms grown within the same model when stained for live:dead analysis by fluorescence with the same excitation laser lines, that is 488 and 543 nm.

An alternative was sourced and SNARF<sup>®</sup>-4F 5-(and-6)-carboxylic acid was evaluated to determine hydrogen-ion concentration within bacterial sediments, and biofilms. Initially, the fluorophore was applied to bacterial sediment and imaged. Fluorescence-lifetime values were able to be obtained. To correlate this with pH changes, sucrose was applied and the sediment was imaged over time. This demonstrated detectable changes in fluorescence-lifetime. The fluorescence-lifetime values were correlated to pH through the use of the calibration data. To determine the accuracy of this method, average pH values determined through the

fluorescence-lifetime when compared to pH values determined through the use of a pH microelectrode. The pH average pH values determined through fluorescence-lifetime correlated well with those obtained through the use of the microelectrode, demonstrating the appropriateness of the technique. This shows that the technique could be used to determine environmental pH from the fluorescence-lifetime using SNARF<sup>®</sup>-4F 5-(and-6)-carboxylic acid. Both sensor were applied to biofilms and imaged in order to determine localised extracellular microgradients in hydrogen-ion concentration through the use of confocal laser scanning microscopy (pH-sensitive nanosensors) or multiphoton molecular excitation fluorescence lifetime imaging microscopy (SNARF<sup>®</sup>-4F 5-(and-6)-carboxylic acid). Issues arose when using the nanosensors, and the pH values were not able to be determined. This may be due to the nanosensors adhering to the extracellular polymeric substance, or active or passive removal from the biofilm, regardless of addition during or following biofilm formation. This may require further consideration to overcome. The use of SNARF<sup>®</sup>-4F 5-(and-6)-carboxylic acid allowed the imaging of pH microgradients within a bacterial sediment of *S. mutans*, and further the analysis of these microgradients over time during fermentation following exposure to sucrose. It was also possible to image a single planar view of a *S. mutans* biofilm. Due to time constraints, it was not possible to image the biofilm through multiple depths of the biofilm structure to observe these pH microgradients through the z-axis. Further to this, it was not possible to determine the pH over a time period. However, it should be stated that it is likely that these omissions appear to be possible.

### **8.3 Challenges and Difficulties**

Determination and visualisation of pH microenvironments was not possible through the utilisation of dual-fluorophore, ratiometric, pH-sensitive nanosensors. Upon imaging biofilms cultivated on nitrocellulose membranes, it appears that only the periphery of the biofilm structure was able to be obtained. This was suspected as i) the apex of the biofilm was first located using light microscopy before changing to fluorescence to image through confocal laser scanning microscopy, where a small and thin ring of excitation was observed, ii) this circular image widened as the

distance between the objective lens and the specimen decreased, iii) the fluorescence excitation was observed in both channels and iv) the fluorescence excitation intensity was lesser than that observed during calibration. The possible explanations for this include; poor nanosensor penetration within the extracellular polymeric matrix or as a result of removal of the nanosensors from the biofilm through active or passive transport processes during growth. Biofilms grown on nitrocellulose or polycarbonate membranes are known to possess a more closed architecture than those cultivated in other models. This plays a significant factor in nanosensor penetration. In an attempt to overcome possible nanosensor penetration issues, nanosensors were added to the inoculating bacterial suspensions. The addition of nanosensors to the bacterial suspension prior to growth of the biofilms produced a similar outcome. It is therefore suspected that this is due to the removal of the nanosensors from the biofilm through active or passive transport processes during growth. Another consideration is that this is due to poor excitation laser penetration, even with an increase in laser power. However this was discounted due to the ability of the laser to penetrate biofilms, grown within the same model, when stained for live:dead analysis by fluorescence with the same excitation laser lines, that is 488 and 543 nm.

The microscope for the study of SNARF<sup>®</sup>-4F 5-(and-6)-carboxylic acid was located off-site. Although this was not an issue during analysis and calibration, it did become an issue when analysing biofilms. Biofilms removed from the CDFF required transport to the microscope causing disruption to the structure, including desiccation and partial or complete separation from the substratum which diminished the number of biofilms able to be analysed. Biofilms removed from the CDFF were transferred to small petri dishes prior to being transferred to the microscope. This led to considerable dehydration of the biofilms and therefore significant detrimental effect upon analysis. To alleviate this, moistened absorbent paper was added to the transport vessel and desiccation continued to occur. Transport of biofilms in a hydrated state was attempted however due to the movement of the surrounding fluid, this resulted in disruption. To minimise this, biofilms were transferred to small petri dishes and flooded with sterile isotonic

saline. The lid was situated in a manner to ensure no bubbles were present which may cause disruption. The petri dishes were sealed prior to transport to the microscope. This alleviated the issue to some extent, however disruption to the biofilm was still observed. The set-up of the instrument was extremely complex and sensitive. On one occasion the instrument was out-of-service for an extended period making analysis impossible.

## 8.4 Future Work

Pertaining to dental caries, the desire is to determine extracellular pH. The ability to determine and visualise the location of the microorganisms and remove their presence within the image would allow differentiation of cellular and extracellular components. This could be accomplished through the use of fluorescent proteins, such as green fluorescent protein (GFP), however GFP requires molecular oxygen for fluorescence to develop (Tsien 1998). However, oxygen availability varies greatly within the structure of the biofilm (De Beer et al. 1994), and this may lead to an inability to determine the location of microorganisms transfected with GFP at greater depths within the biofilm. An alternative to the use of GFP is the use of flavin mononucleotide (FMN)-based fluorescent protein (FbFP) developed by Jena Bioscience (Jena, Germany). These proteins are similar to green fluorescent protein (GFP), however they do not require the presence of oxygen for fluorescence to develop. It is envisaged that FbFP would allow visualisation of the biofilm structure. The most predominant isolate will be transfected with a plasmid carrying a flavin mononucleotide (FMN)-based fluorescent protein (FbFP) (Jena Bioscience, Jena, Germany). These proteins are similar to green fluorescent protein (GFP), however they do not require the presence of oxygen. It is envisaged that FbFP will allow visualisation of the biofilm structure.

Another method for the visualisation and differentiation of the microbial composition of the biofilm community is the use of peptide nucleic acid - fluorescent *in situ* hybridisation, (PNA-FISH). Each species could be stained with species-specific stain allowing visualisation and differentiation within the biofilm

structure. Multiplex PCR, metagenomics and transcriptomics analysis could also be considered for analysis of species presence and prevalence and gene expression, respectively.

Once the pH values are able to be spatially and temporally mapped, investigation of the changes which occur following exposure to a series of fermentable carbohydrates and sugar alcohols could be analysed. Initial investigations have focused on acidic pH. It would be desirable to investigate the limitations of SNARF®-4F 5-(and-6)-carboxylic acid, or the alternative use of a fluorescent dye with a higher  $pK_a$ . This may allow a focus on alkali generation and its role in other dental pathologies (gingivitis and periodontal disease).

Fluorescent dyes for other environmental parameters may also be investigated. These may include temperature, redox potential, oxygen concentration and ion concentrations, such as fluoride, calcium and phosphate. Methods which may manipulate these processes and inhibition the progression from health to disease will be hypothesised and tested.

The further investigation of SNARF®-4F 5-(and-6) carboxylic acid and other fluorescent dyes for the determination of pH microgradients in CDFF grown biofilms mimicking dental plaque may be continued in the future.

Methods which may manipulate the production of pH within dental plaque and inhibition the progression from health to disease may be hypothesised and tested.

## **8.5 Conclusion**

Despite continual research and development, dental caries remains one of the most prevalent diseases affecting man today. Dental caries is characterised by the localised dissolution of the dental hard tissues as a result of organic acids produced during metabolism of fermentable carbohydrates by the microbial inhabitants of the oral cavity. Dental caries may lead to considerable pain and suffering to the individual, influence nutritional intake, have considerable bearing on the ability to

communicate effectively and significantly impact self-esteem and self-confidence. Furthermore, it is of huge economic burden to healthcare providers worldwide.

The role of pH in dental caries is well established however, the determination of pH within biofilms has primarily been performed through the utilisation of electrodes and microelectrodes. The drawbacks of such methods have been discussed. As a result, there is a requirement for novel methods to evaluate pH within biofilms. Due to the complex structure and dynamic nature of biofilms, pH within biofilm can vary greatly over relatively small distances forming microgradients.

Optical methods offer the capability to determine pH values through various spatial and temporal dimensions. They also offer the ability to determine these values in a naturally-hydrated state. Two optical methods, utilising the phenomenon of fluorescence, for the rapid determination of spatial and temporal gradients of  $pH_e$  in the bulk phase of laboratory-grown dental plaque were investigated.

The first method was the use of dual-fluorophore, ratiometric, pH-sensitive nanosensors imaged through the use of CLSM. The nanosensors were produced, calibrated and applied to both planktonic and biofilm phenotypes. The nanosensors caused no determinable effect upon the viability of the bacteria tested. However, the nanosensors were deemed not suitable for such measurements due to a number of issues experienced. The nanosensors did not facilitate imaging within the biofilm, both following the addition after growth and prior to growth. This issue may be as a result of poor light penetration of the excitation laser source, poor nanosensor penetration or removal of the nanosensors during growth. Another issue that arose during the analysis of the nanosensors was as a result of photobleaching of the pH-sensitive fluorophores, but not the pH-insensitive fluorophore. This photobleaching alters the fluorescence intensity of the pH-sensitive fluorophores and, therefore, the ratio of pH-sensitive to pH-insensitive fluorophores. Due to these issues, and an inability to overcome these issues, investigation of the pH-sensitive nanosensors was ceased.

Alternative methods were investigated. The second method investigated was the use of the pH-sensitive fluorophore, SNARF<sup>®</sup>-4F 5-(and-6)-carboxylic acid and the

use of two-photon excitation fluorescence lifetime imaging microscopy. Fluorescence lifetime values were determined through the use of time-correlated single-photon counting.

Although considerable drawbacks exist in the use of currently employed methods, the determinations and visualisation of microgradients in hydrogen-ion concentration is not without difficulty. Although many of these shortcomings have been addressed, issues still arose due to interactions of the sensor and the biofilm structure and logistics, such as transport of the biofilms from growth to imaging locations. Another contemplation associated with optical imaging is the cost. One of the desired elements of a novel method to determine and visualise microgradients in pH is for it to be cost-effective. The current method of determination is comparatively cheap. Both methods investigated had sizeable expenditures, whether chemical (e.g. fluorophores) or the imaging equipment (confocal laser scanning microscope, fluorescence lifetime imaging microscopy, time-correlated single-photon counting). Moreover, the use of the equipment requires extensive and continual training. Of the two methods investigated, the use of SNARF<sup>®</sup>-4F to determine and visualise pH microgradients through the use of two-photon molecular excitation fluorescence lifetime imaging microscopy and time-correlated single-photon counting exhibited the most promise. This methodology provides extensive dynamic range, high resolution and rapid response to changes in pH. As fluorescence lifetime is an intrinsic property, variations in concentration due to the complex biofilms structure and processes are immaterial. Two-photon molecular excitation improves depth penetration allowing imaging at greater depths within the biofilm structure in comparison with single-photon molecular excitation. Also, the fluorophore, SNARF<sup>®</sup>-4F, is commercially available. The nanosensors were produced in-house and therefore are not commercially available. Furthermore, with respect to the nanosensors, extensive knowledge is required to design, produce and characterise the constructed product. With the ability to determine spatially-resolved pH coupled with the ability to visualise using a technique with excellent depth-penetration, the mapping of pH microgradients would provide greater understanding of the complex processes which occur within dental biofilms as a

result of metabolism. To this point, many of the shortcomings have been improved upon. However, the ability to determine and visualise pH microgradients in oral biofilms reflecting dental caries populations, with an appropriate level of resolution, in multiple spatial and temporal dimensions, remains elusive. Regardless, many of the properties of these two optical methods have been assessed and, although there are clearly issues, with the many benefits that each offer, and unknown properties characterised, with further research to overcome these drawbacks they may become useful. It is clear that the ability to observe the formation of pH microgradients in four dimensions is highly desirable. This capacity would be welcomed by both industry and in the clinic. The ability to assess compounds with the ability to return the resting pH in a timelier manner or retarding the pH decrease which occurs as a result of fermentation. In the clinic, a method to assess multispecies interaction with respect to pH may shine light on disparities in current knowledge. Many areas of research still exist in the field of environmental determination within dental plaque, and further extrapolated to other areas of biofilm research.

## REFERENCES

- Aamdal-Scheie, A. et al., 1996. Plaque pH and Microflora of Dental Plaque on Sound and Carious Root Surfaces. *Journal of Dental Research*, 75(11), pp.1901–1908.
- Aas, J.A. et al., 2005. Defining the Normal Bacterial Flora of the Oral Cavity. *Journal of Clinical Microbiology*, 43(11), pp.5721–5732.
- Abou Neel, E.A. et al., 2016. Demineralization-remineralization dynamics in teeth and bone. *International Journal of Nanomedicine*, 11(1), pp.4743–4763.
- Acosta, M.A. et al., 2012. Fluorescent silica particles for monitoring oxygen levels in three-dimensional heterogeneous cellular structures. *Biotechnology and bioengineering*, 109(10), pp.2663–70.
- Aguirre-Zero, O.M., Zero, D.T. & Proskin, H.M., 1993. Effect of Chewing Xylitol Chewing Gum on Salivary Flow Rate and the Acidogenic Potential of Dental Plaque. *Caries Research*, 27, pp.55–59.
- Aires, C.P. et al., 2006. Effect of sucrose concentration on dental biofilm formed in situ and on enamel demineralization. *Caries research*, 40(1), pp.28–32.
- Al-Hashimi, I.H. & Levine, M.J., 1989. Characterization of in vivo salivary-derived enamel pellicle. *Archives of oral biology*, 34(4), pp.289–295.
- Amano, A. et al., 1994. Effects of temperature stress on expression of fimbriae and superoxide dismutase by *Porphyromonas gingivalis*. *Infection and Immunity*, 62(10).
- Aylott, J.W., 2003. Optical nanosensors: An enabling technology for intracellular measurements. *The Analyst*, 128(4), pp.309–312.
- Balakrishnan, M., Simmonds, R.S. & Tagg, J.R., 2000. Dental Caries is A Preventable Infectious Disease. *Australian Dental Journal*, 45(4), pp.235–245.

- Bardow, A. et al., 2000. The buffer capacity and buffer systems of human whole saliva measured without loss of CO<sub>2</sub>. *Archives of oral biology*, 45(1), pp.1–12.
- Bardow, A. et al., 2008. The role of saliva. In O. Fejerskov & E. Kidd, eds. *Dental Caries: The Disease and its Clinical Management*. Oxford, UK: Wiley-Blackwell.
- Bates, R.G., 1973. *Determination of pH: theory and practice* 2nd ed., Wiley.
- Becker, W. et al., 2004. Fluorescence Lifetime Imaging by Time-Correlated Single-Photon Counting. *Microscopy Research and Technique*, 63(1), pp.58–66.
- De Beer, D. et al., 1994. Effects of biofilm structures on oxygen distribution and mass transport. *Biotechnology and Bioengineering*, 43(11), pp.1131–1138.
- De Beer, D. & Stoodley, P., 1995. Relation between the structure of an aerobic biofilm and transport phenomena. *Water science and technology*, 32(8), pp.11–18.
- De Beer, D., Stoodley, P. & Lewandowski, Z., 1996. Liquid flow and mass transport in heterogeneous biofilms. *Water Research*, 30(11), pp.2761–2765.
- Beighton, D., 2005. The complex oral microflora of high-risk individuals and groups and its role in the caries process. *Community dentistry and oral epidemiology*, 33(4), pp.248–55.
- Beighton, D., Smith, K. & Hayday, H., 1986. The growth of bacteria and the production of exoglycosidic enzymes in the dental plaque of macaque monkeys. *Archives of oral biology*, 31(12), pp.829–35.
- Bell, G., Emslie-Smith, D. & Patterson, C., 1980. *Textbook of Physiology*, London, UK: Churchill Livingstone Elsevier.
- Berezin, M.Y. & Achilefu, S., 2010. Fluorescence lifetime measurements and biological imaging. *Chemical reviews*, 110(5), pp.2641–84.

- Berg, J.M., Tymoczko, J.L. & Stryer, L., 2002. Primary Structure: Amino Acids Are Linked by Peptide Bonds to Form Polypeptide Chains. In J. M. Berg, J. L. Tymoczko, & L. Stryer, eds. *Biochemistry*. New York, NY, US: W H Freeman, pp. 97–103.
- Berkovitz, B.K.B., 2016. Oral Cavity. In S. Standring et al., eds. *Gray's Anatomy: The Anatomical Basis of Clinical Practice*. London, UK: Elsevier, pp. 507–533.
- Bestvater, F. et al., 2002. Two-photon fluorescence absorption and emission spectra of dyes relevant for cell imaging. *Journal of Microscopy*, 208(2), pp.108–115.
- Bhawalkar, J.D. et al., 1997. Two-Photon Photodynamic Therapy. *Journal of clinical laser medicine & surgery*, 15(5), pp.201–204.
- Born, M. & Wolf, E., 1999. Elements of the Theory of Diffraction. In M. Born & E. Wolf, eds. *Principles of Optics*. Cambridge, UK: Cambridge University Press, pp. 412–516.
- Bowden, G.H.W., 1990. Microbiology of Root Surface Caries in Humans. *Journal of dental research*, 69(5), pp.1205–1210.
- Bowen, W.H. & Birkhed, D., 1986. Dental caries: Dietary and microbiology factors. In L. Granath & W. D. McHugh, eds. *Systematized Prevention of Oral Disease; Theory and Practice*. Boca Raton: CRC Press, pp. 19–41.
- Boyar, R.M. et al., 1989. The Microflora Associated with the Development of Initial Enamel Decalcification below Orthodontic Bands in vivo in Children Living in a Fluoridated-water Area. *Journal of Dental Research*, 68(12), pp.1734–1738.
- Bradshaw, D.J. et al., 1994. Metabolic cooperation in oral microbial communities during growth on mucin. *Microbiology*, 140(12), pp.3407–3412.
- Bradshaw, D.J. et al., 1998. Role of *Fusobacterium nucleatum* and Coaggregation in Anaerobe Survival in Planktonic and Biofilm Oral Microbial Communities during Aeration. *Infection and Immunity*, 66(10), pp.4729–4732.

- Bradshaw, D.J. & Marsh, P.D., 1994. Effect of Sugar Alcohols on the Composition and Metabolism of a Mixed Culture of Oral Bacteria Grown in a Chemostat. *Caries Research*, 28, pp.251–256.
- Bradshaw, D.J., McKee, A.S. & Marsh, P.D., 1989. Effects of carbohydrate pulses and pH on population shifts within oral microbial communities in vitro. *Journal of dental research*, 68(9), pp.1298–1302.
- Brailsford, S.R. et al., 2001. The predominant aciduric microflora of root-caries lesions. *Journal of dental research*, 80(9), pp.1828–1833.
- Branda, S.S. et al., 2005. Biofilms: The matrix revisited. *Trends in Microbiology*, 13(1), pp.20–26.
- Brasselet, S. & Moerner, W., 2000. Fluorescence Behavior of Single-Molecule pH-Sensors. *Single Molecules*, 1, pp.17–23.
- Burdikova, Z. et al., 2015. Measurement of pH micro-heterogeneity in natural cheese matrices by fluorescence lifetime imaging. *Frontiers in Microbiology*, 6(March), pp.1–10.
- Busscher, H.J. & Van Der Mei, H.C., 1997. Physico-chemical interactions in initial microbial adhesion and relevance for biofilm formation. *Advances in Dental Research*, 11(1), pp.24–32.
- Capozzi, V. et al., 2012. Lactic acid bacteria producing B-group vitamins: A great potential for functional cereals products. *Applied Microbiology and Biotechnology*, 96(6), pp.1383–1394.
- Carlsson, J. et al., 1970. Early Establishment of *Streptococcus salivarius* in the Mouths of Infants. *Journal of Dental Research*, 49(2), pp.415–418.
- Casiano-Colon, A. & Marquis, R.E., 1988. Role of the arginine deiminase system in protecting oral bacteria and an enzymatic basis for acid tolerance. *Applied and Environmental Microbiology*, 54(6), pp.1318–1324.

- Caufield, P.W. et al., 2000. Natural History of *Streptococcus sanguinis* in the Oral Cavity of Infants: Evidence for a Discrete Window of Infectivity. *Infection and Immunity*, 68(7), pp.4018–4023.
- Caufield, P.W. et al., 2015. Oral Lactobacilli and Dental Caries : A Model for Niche Adaptation in Humans. *Journal of Dental Research*, (September 2015), pp.1–9.
- Cawson, R.A. & Odel, E.W., 2008. *Cawson's Essentials of Oral Pathology and Oral Medicine* 8th ed., Edinburgh: Churchill Livingstone Elsevier.
- Centonze, V.E., 2002. Introduction to multiphoton excitation imaging for the biological sciences. *Methods in cell biology*, 70, pp.129–48.
- Charlton, G., 1956. Determination of hydrogen ion concentration in the mouth—a comparison of the glass, antimony and quinhydrone micro-electrodes\*. *Australian Dental Journal*, 176, pp.174–176.
- Chauhan, V.M. et al., 2013. Mapping the Pharyngeal and Intestinal pH of *Caenorhabditis elegans* and Real-Time Luminal pH Oscillations Using Extended Dynamic Range pH-Sensitive Nanosensors. *ACS nano*, 7(6), pp.5577–5587.
- Chauhan, V.M., Burnett, G.R. & Aylott, J.W., 2011. Dual-fluorophore ratiometric pH nanosensor with tuneable pKa and extended dynamic range. *The Analyst*, 136(9), pp.1799–801.
- Chen, Y. & Periasamy, A., 2004. Characterization of two-photon excitation fluorescence lifetime imaging microscopy for protein localization. *Microscopic Research and Technique*, 63(1), pp.72–80.
- Ciardi, J.E. et al., 1977. Adsorption of *Streptococcus mutans* lipoteichoic acid to hydroxyapatite. *European journal of oral sciences*, 85(6), pp.387–391.
- Ciardi, J.E. et al., 1987. Cell-to-Cell Interaction of *Streptococcus sanguis* and *Propionibacterium acnes* on Saliva-Coated Hydroxyapatite. *Infection and Immunity*, 55(6), pp.1441–1446.

- Ciric, L. et al., 2011. In vitro assessment of shiitake mushroom (*Lentinula edodes*) extract for its antigingivitis activity. *Journal of biomedicine & biotechnology*, 2011, p.507908.
- Clark, H.A. et al., 1998. Subcellular optochemical nanobiosensors: probes encapsulated by biologically localised embedding (PEBBLEs). *Sensors and Actuators B: Chemical*, 51, pp.12–16.
- Clark, H.A., Hoyer, M., Philbert, M.A. and Kopelman, R., 1999a. Optical nanosensors for chemical analysis inside single living cells. 1. Fabrication, characterization, and methods for intracellular delivery of PEBBLE sensors. *Analytical Chemistry*, 71(21), pp.4831-4836.
- Clark, H.A., Kopelman, R., Tjalkens, R. and Philbert, M.A., 1999b. Optical nanosensors for chemical analysis inside single living cells. 2. Sensors for pH and calcium and the intracellular application of PEBBLE sensors. *Analytical Chemistry*, 71(21), pp.4837-4843.
- Clarke, J.K., 1924. On the bacterial factor in the aetiology of dental caries. *The British Journal of Experimental Pathology*, 5(3), pp.141–147.
- Coulter, W.A. & Russell, C., 1975. Continuous monitoring of pH and Eh in bacterial plaque grown on a tooth in an artificial mouth. *Applied and environmental microbiology*, 29(2), pp.141–144.
- Crusz, S.A. et al., 2012. Bursting the bubble on bacterial biofilms: a flow cell methodology. *Biofouling*, 28(8), pp.835–42.
- Cullum, B.M. & Vo-Dinh, T., 2000. The development of optical nanosensors for biological measurements. *Trends in Biotechnology*, 18, pp.822–823.
- Cunin, R. et al., 1986. Biosynthesis and metabolism of arginine in bacteria. *Microbiological reviews*, 50(3), pp.314–352.

- Curley, P.F. et al., 1992. Application of a femtosecond self-sustaining mode-locked Ti : sapphire laser to the field of laser scanning confocal microscopy. *Optical and Quantum Electronics*, 24, pp.851–859.
- Cuy, J.L. et al., 2002. Nanoindentation mapping of the mechanical properties of human molar tooth enamel. *Archives of oral biology*, 47, pp.281–291.
- Dalwai, F., 2008. *In vitro modelling of bacterial population shifts in oral biofilms*. University College London, London, UK.
- Dalwai, F., Spratt, D.A. & Pratten, J., 2006. Modeling Shifts in Microbial Populations Associated with Health or Disease. *Applied and Environmental Microbiology*, 72(5), pp.3676–3684.
- Dalwai, F., Spratt, D.A. & Pratten, J., 2007. Use of quantitative PCR and culture methods to characterize ecological flux in bacterial biofilms. *Journal of Clinical Microbiology*, 45(9), pp.3072–6.
- Dawes, C., 2004. How much saliva is enough for avoidance of xerostomia? *Caries research*, 38(3), pp.236–40.
- Dawes, C., 2003. What is the critical pH and why does a tooth dissolve in acid? *Journal of the Canadian Dental Association*, 69(11), pp.722–4.
- Dawes, C. & Macpherson, L.M.D., 1992. Effects of nine different chewing-gums and lozenges on salivary rate and pH. *Caries Research*, 26, pp.176–182.
- Dawson, R.M.C. et al., 1986. *Data for Biochemical Research* 3rd ed., Oxford, UK: Oxford Scientific Publishing.
- Deng, D.M. & ten Cate, J.M., 2004. Demineralization of dentin by *Streptococcus mutans* biofilms grown in the constant depth film fermentor. *Caries Research*, 38(1), pp.54–61.
- Denk, W., Strickler, J.H. & Webb, W.W., 1990. Two-Photon Laser Scanning Fluorescence Microscopy. *Science*, 248(4951), pp.73–76.

- Denk, W. & Svoboda, K., 1997. Photon upmanship: Why multiphoton imaging is more than a gimmick. *Neuron*, 18(3), pp.351–357.
- Desai, A.S. et al., 2013. Fluorescent nanosensors for intracellular measurements: synthesis, characterization, calibration, and measurement. *Frontiers in physiology*, 4(January), p.401.
- Dewhirst, F.E. et al., 2010. The human oral microbiome. *Journal of Bacteriology*, 192(19), pp.5002–5017.
- Diaspro, A., Chirico, G. & Collini, M., 2005. Two-photon fluorescence excitation and related techniques in biological microscopy. *Quarterly reviews of biophysics*, 38(2), pp.97–166.
- Dibdin, G.H. & Shellis, R.P., 1988. Physical and biochemical studies of *Streptococcus mutans* sediments suggest new factors linking the cariogenicity of plaque with its extracellular polysaccharide content. *Journal of dental research*, 67(6), pp.890–895.
- Donlan, R.M., 2002. Biofilms: Microbial life on surfaces. *Emerging Infectious Diseases*, 8(9), pp.881–890.
- Driessens, F.C.M., van Dijk, J.W.E. & Borggreven, J.M.P.M., 1978. Biological calcium phosphates and their role in the physiology of bone and dental tissues I. Composition and solubility of calcium phosphates. *Calcified Tissue Research*, 26(1), pp.127–137.
- Duncan, R.R., 2007. Fluorescence lifetime imaging microscopy ( FLIM ) to quantify protein-protein interactions inside cells. *Biochemical Society Transactions*, 34(5), pp.679–682.
- Eastoe, J.E., 1960. Organic Matrix of Tooth Enamel. *Nature*, pp.411–412.
- Edgar, M., Dawes, C. & O’Mullane, D., 2004. *Saliva and Oral Health* 3rd ed. M. Edgar, C. Dawes, & D. O’Mullane, eds., London, UK. British Dental Journal, pp.1-146.

- Edgar, W.M., 1992. Saliva: its secretion, composition and functions. *British Dental Journal*, 172, pp.305–312.
- Edgar, W.M. & Geddes, D.A., 1990. Chewing gum and dental health--a review. *British Dental Journal*, 168(4), pp.173–177.
- Edgar, W.M. and Higham, S.M., 1995. Role of saliva in caries models. *Advances in dental research*, 9(3), pp.235-238.
- Elias, S. & Banin, E., 2012. Multi-species biofilms: Living with friendly neighbors. *FEMS Microbiology Reviews*, 36(5), pp.990–1004.
- Ellen, R.P., Banting, D.W. & Fillery, E.D., 1985. Streptococcus mutans and Lactobacillus Detection in the Assessment of Dental Root Surface Caries Risk. *Journal of Dental Research*, 64(10), pp.1245–1249.
- Emilson, C.G. & Krasse, B., 1985. Support for and implications of the specific plaque hypothesis. *Scandinavian journal of dental research*, 93(2), pp.96–104.
- Ewers, G.J. & Greener, E.H., 1985. The electrochemical activity of the oral cavity-a new approach. *Journal of oral rehabilitation*, 12(6), pp.469–76.
- Faust, K. et al., 2012. Microbial Co-occurrence Relationships in the Human Microbiome. *PLoS Computational Biology*, 8(7), p.e1002606.
- von der Fehr, F.R. & Steinnes, E., 1966. The solubility rate of unabraded, abraded, and exposed human enamel surfaces studied by means of activation analysis. *Archives of oral biology*, 11(12), pp.1405–1418.
- Fejerskov, O., 2004. Changing paradigms in concepts on dental caries: consequences for oral health care. *Caries research*, 38(3), pp.182–91.
- Filoche, S.K. et al., 2008. Plaques from different individuals yield different microbiota responses to oral-antiseptic treatment. *FEMS immunology and medical microbiology*, 54(1), pp.27–36.

- Fisher, W.G. et al., 1997. Simultaneous Two-Photon Activation of Type-I Photodynamic Therapy Agents. *Photochemistry and photobiology*, 66(2), pp.141–55.
- Foster, J.S. & Kolenbrander, P.E., 2004. Development of a multispecies oral bacterial community in a saliva-conditioned flow cell. *Applied and environmental microbiology*, 70(7), pp.4340–8.
- French, T., So, P.T.C., Weaver Jr, D.J., Coelho-Sampaio, T., Gratton, E., Voss Jr, E.W. and Carrero, J., 1997. Two-photon fluorescence lifetime imaging microscopy of macrophage-mediated antigen processing. *Journal of microscopy*, 185(3), pp.339-353.
- Fröhlich, S., Maiwald, J.H. & Flowerdew, G., 1992. Effect of gum chewing on the pH of dental plaque. *Journal of Clinical Dentistry*, 3(3), pp.75–78.
- Gadella, T.W.J., Jovin, T.M. & Clegg, R.M., 1993. Fluorescence lifetime imaging microscopy (FLIM): Spatial resolution of microstructures on the nanosecond time scale. *Biophysical Chemistry*, 48(2), pp.221–239.
- Geddes, D.A.M., 1975. Acids produced by human dental plaque metabolism in situ. *Caries research*, 9, pp.98–109.
- Geddes, D.A.M., 1981. Studies on metabolism of dental plaque: diffusion and acid production in human dental plaque. *Frontiers of Oral Physiology*, 3, pp.78–87.
- Gerritsen, H.C. & de Grauw, K.J., 2000. Fluorescent lifetime imaging of oxygen in dental biofilm. K. Koenig, H. J. Tanke, & H. Schneckenburger, eds. *Laser Microscopy*, 4164(2000), pp.70–78.
- Gibbons, R.J. & van Houte, J., 1975. Bacterial adherence in oral microbial ecology. *Annual Reviews in Microbiology*, 29, pp.19–42.
- Gibbons, R.J., Moreno, E.C. & Etherden, I., 1983. Concentration-Dependent Multiple Binding Sites on Saliva-Treated Hydroxyapatite for *Streptococcus sanguis*. *Infection and Immunity*, 39(1), pp.280–289.

- Girkin, J.M., 2003. Optical physics enables advances in multiphoton imaging. *Journal of Physics D: Applied Physics*, 36, pp.R250–R258.
- Goldberg, M. et al., 2011. Dentin: Structure, Composition and Mineralization. *Frontiers in Bioscience: Elite Edition*, 3(1), pp.711–735.
- Göppert-Mayer, M., 1931. Über Elementarakte mit zwei Quantensprüngen. *Annalen der Physik*, 401(3), pp.273–294.
- Graber, M.L. et al., 1986. Characteristics of fluoroprobes for measuring intracellular pH. *Analytical biochemistry*, 12, pp.202–212.
- Grossman, L.I. & Brickman, B.M., 1937. Some observations of the pH of saliva. *Journal of dental research*, 16(5), pp.409–416.
- Guyton, A.C., 1991. Secretion of saliva. In *Textbook of Medical Physiology*. Philadelphia, PA: Saunders Company, pp. 711–713.
- Haffajee, A.D. et al., 1992. Subgingival temperature (III). Relation to microbial counts. *Journal of clinical periodontology*, 19(6), pp.417–422.
- Hajishengallis, G., 2014. Immunomicrobial pathogenesis of periodontitis: keystones, pathobionts, and host response. *Trends in immunology*, 35(1), pp.3–11.
- Hakonen, A. & Hulth, S., 2008. A high-precision ratiometric fluorosensor for pH: implementing time-dependent non-linear calibration protocols for drift compensation. *Analytica chimica acta*, 606(1), pp.63–71.
- Hamada, S. & Slade, H.D., 1980. Biology, immunology, and cariogenicity of *Streptococcus mutans*. *Microbiological reviews*, 44(2), pp.331–84.
- Han, J. & Burgess, K., 2010. Fluorescent indicators for intracellular pH. *Chemical reviews*, 110(5), pp.2709–28.
- Hannig, C., Hannig, M. & Attin, T., 2005. Enzymes in the acquired enamel pellicle. *European journal of oral sciences*, 113(1), pp.2–13.

- Hannig, M., 1999. Ultrastructural investigation of pellicle morphogenesis at two different intraoral sites during a 24-h period. *Clinical oral investigations*, 3(2), pp.88–95.
- Hassell, T.M., 1971. Construction of micro-antimony electrodes for use in radio telemetry of plaque pH. *Helvetica Odontologica Acta*, 15(1), pp.50–51.
- Hausler, S. & Fuqua, C., 2013. Biofilms 2012: new discoveries and significant wrinkles in a dynamic field. *Journal of bacteriology*, 195(13), pp.2947–58.
- Herp, A., Wu, A.M. & Moschera, J., 1979. Current concepts of the structure and nature of mammalian salivary mucous glycoproteins. *Molecular and Cellular Biochemistry*, 23(1), pp.27–44.
- Hidalgo, G. et al., 2009. Functional tomographic fluorescence imaging of pH microenvironments in microbial biofilms by use of silica nanoparticle sensors. *Applied and environmental microbiology*, 75(23), pp.7426–35.
- Higham, S.M., 2010. Caries Process and Prevention Strategies: The Agent.
- Higham, S.M. & Edgar, W.M., 1989a. Effects of Parafilm and cheese chewing on human dental plaque pH and metabolism. *Caries Research*, 23(1), pp.42–48.
- Higham, S.M. & Edgar, W.M., 1989b. Human dental plaque pH, and the organic acid and free amino acid profiles in plaque fluid, after sucrose rinsing. *Archives of oral biology*, 34(5), pp.329–34.
- Hille, C. et al., 2008. Time-domain fluorescence lifetime imaging for intracellular pH sensing in living tissues. *Analytical and Bioanalytical Chemistry*, 391(5), pp.1871–1879.
- van 't Hof, W. et al., 2014. Antimicrobial defense systems in saliva. A. J. M. Ligtenberg & E. C. I. Veerman, eds. *Monographs in Oral Science*, 24, pp.40–51.

- Holgerson, P. et al., 2013. Oral microbial profile discriminates breastfed from formula-fed infants. *Journal of Paediatric Gastroenterology and Nutrition*, 56(2), pp.127–136.
- Holly, F.J. & Gray, J.A., 1968. Mechanism for incipient carious lesion growth utilizing a physical model based on diffusion concepts. *Archives of Oral Biology*, 13(3), pp.319–333.
- Hooper, L. V, Littman, D.R. & MacPherson, A.J., 2012. Interactions Between the Microbiota and the Immune System. *Science*, 336, pp.1268–1273.
- Hope, C.K. et al., 2012. Reducing the variability between constant-depth film fermenter experiments when modelling oral biofilm. *Journal of applied microbiology*, 113(3), pp.601–608.
- Hope, C.K., Clements, D. & Wilson, M., 2002. Determining the spatial distribution of viable and nonviable bacteria in hydrated microcosm dental plaques by viability profiling. *Journal of applied microbiology*, 93(3), pp.448–55.
- Horiba Scientific, A., Time-resolved fluorescence lifetime measurements.
- Hornby, K. et al., 2009. Enamel benefits of a new hydroxyapatite containing fluoride toothpaste. *International dental journal*, 59(1), pp.325–331.
- Howe, P.R. & Hatch, R.E., 1917. A study of the microorganisms of dental caries. *The Journal of Medical Research*, 36(3), pp.481–492.
- Humphrey, S.P. & Williamson, R.T., 2001. A review of saliva: normal composition, flow, and function. *The Journal of prosthetic dentistry*, 85(2), pp.162–9.
- Hunter, R.C. & Beveridge, T.J., 2005. Application of a pH-sensitive fluoroprobe (C-SNARF-4) for pH microenvironment analysis in *Pseudomonas aeruginosa* biofilms. *Applied and environmental microbiology*, 71(5), pp.2501–2510.

- Hwang, J.Y. et al., 2012. Investigating photoexcitation-induced mitochondrial damage by chemotherapeutic corroles using multimode optical imaging. *Journal of biomedical optics*, 17(1), pp.0150031–01500312.
- Igarashi, K., Kamiyama, K. & Yamada, T., 1981. Measurement of pH in human dental plaque in vivo with an ion-sensitive transistor electrode. *Archives of oral biology*, 26, pp.203–207.
- Iheozor-Ejiofor, Z. et al., 2015. Water fluoridation for the prevention of dental caries ( Protocol ). *Cochrane Collaboration*, (6), pp.1–274.
- Jenkins, G.N., 1966. The refinement of foods in relation to dental caries. *Advances in Oral Biology*, 2(1), pp.67–100.
- Jenkins, S., Addy, M. & Newcombe, R., 1991. Triclosan and sodium lauryl sulphate mouthwashes: (I) Effects on salivary bacterial counts. *Journal of Clinical Periodontology*, 18, pp.140–144.
- Jenkins, S., Addy, M. & Wade, W.G., 1988. The mechanism of action of chlorhexidine: A study of plaque growth on enamel inserts in vivo. *Journal of Clinical Periodontology*, 15, pp.415–424.
- Jenkinson, H.F. & Lamont, R.J., 2005. Oral microbial communities in sickness and in health. *Trends in microbiology*, 13(12), pp.589–95.
- Jenkinson, H.F. & Lamont, R.J., 2006. Oral microbial ecology. In R. J. Lamont et al., eds. *Oral Microbiology and Immunology*. Washington DC, USA: American Society of Microbiology, pp. 89–105.
- Jenkinson, H.F. & Lamont, R.J., 1997. Streptococcal Adhesion and Colonization. *Critical Reviews in Oral Biology & Medicine*, 8(2), pp.175–200.
- Jensen, M.E., Polansky, P.J. & Schachtele, C.F., 1982. Plaque sampling and telemetry for monitoring acid production on human buccal tooth surfaces. *Archives of oral biology*, 27, pp.21–31.

- Johansson, I., 2002. Milk and dairy products: possible effects on dental health. *Food & Nutrition Research*, (12), pp.119–122.
- Johnson, I. & Spence, M.T., 2010. *The Molecular Probes Handbook - A Guide to Fluorescence Probes and Labeling Technologies* 11th Ed. I. Johnson & M. T. Z. Spence, eds., Life Technologies.
- Jones, K. & Bradshaw, S.B., 1996. Biofilm formation by the Enterobacteriaceae : A comparison between *Salmonella enteritidis*, *Escherichia coli* and a nitrogen-fixing strain of *Klebsiella pneumoniae*. *Journal of applied microbiology*, 80(4), pp.428–464.
- De Jong, M.H. & Van der Hoeven, J.S., 1987. The growth of oral bacteria on saliva. *Journal of dental research*, 66(2), pp.498–505.
- De Jong, M.H., Van der Hoeven, J.S. & Van Os, J.H., 1986. Growth of micro-organisms from supragingival dental plaque on saliva agar. *Journal of dental research*, 65(2), pp.85–88.
- Kaiser, W. & Garrett, C., 1961. Two-Photon Excitation in  $\text{CaF}_2:\text{Eu}^{2+}$ . *Physical Review Letters*, 7(6), pp.229–231.
- Kampoo, K., 2011. *Bacteriological Investigations of the Human Oral Microbiota in Health and Disease*.
- Kanapka, J.A. & Kleinberg, I., 1983. Catabolism of arginine by the mixed bacteria in human salivary sediment under conditions of low and high glucose concentration. *Archives of oral biology*, 28(11), pp.1007–1015.
- Kasha, M., 1950. Characterisation of electronic transitions in complex molecules. *Discussions of the Faraday Society*, 9, pp.14–19.
- Kashket, S., Zhang, J. & Van Houte, J., 1996. Accumulation of fermentable sugars and metabolic acids in food particles that become entrapped on the dentition. *Journal of dental research*, 75(11), pp.1885–1891.

- Kaylor, B.M., 2004. *In vivo measurement of pH in tumor and surrounding tissue using fluorescein ratio imaging.*
- Kenney, E.B. & Ash, M.M., 1969. Oxidation reduction potential of developing plaque, periodontal pockets and gingival sulci. *Journal of periodontology*, 40(11), pp.630–3.
- Kidd, E.A.M., 2011. The implications of the new paradigm of dental caries. *Journal of dentistry*, 39 Suppl 2, pp.S3-8.
- Kidd, E.A.M. & Fejerskov, O., 2004. What Constitutes Dental Caries? Histopathology of Carious Enamel and Dentin Related to the Action of Cariogenic Biofilms. *Journal of Dental Research*, 83(suppl 1), pp.C35–C38.
- Kidd, E.A.M. & Fejerskov, O., 2016. *Essentials of dental caries* 4th. E. Kidd & O. Fejerskov, eds., Oxford, UK: Oxford University Press.
- Kilian, M. et al., 2016. The oral microbiome – an update for oral healthcare professionals. *British Dental Journal*, 221(10), pp.657–666.
- Kim, S. et al., 2007. Organically modified silica nanoparticle co-encapsulating photosensitizing drug & aggregation-enhanced 2-photon absorbing fluorescent dye aggregate for TPA two-photon photodynamic therapy. *Journal of the American Chemical Society*, 129(9), pp.2669–2675.
- Kimoto, M. et al., 2006. A role of salivary carbonic anhydrase VI in dental plaque. *Archives of oral biology*, 51(2), pp.117–22.
- Kivelä, J. et al., 1999. Salivary carbonic anhydrase isoenzyme VI. *The Journal of Physiology*, 520(2), pp.315–320.
- Kleinberg, I., 2002. A Mixed-Bacteria Ecological Approach To Understanding the Role of the Oral Bacteria in Dental Caries Causation: an Alternative To Streptococcus Mutans and the Specific-Plaque Hypothesis. *Critical Reviews in Oral Biology & Medicine*, 13(2), pp.108–125.

- Kligler, I.J., 1915. A biochemical study and differentiation of oral bacteria with special reference to dental caries. *Journal of the allied dental societies*, 10, pp.141–166.
- Kolenbrander, P.E. et al., 2006. Bacterial interactions and successions during plaque development. *Periodontology 2000*, 42(5), pp.47–79.
- Kolenbrander, P.E. et al., 2002. Communication among oral bacteria. *Microbiology and Molecular Biology Reviews*, 66(3), pp.485–505.
- Kolenbrander, P.E., 2011. Multispecies communities: interspecies interactions influence growth on saliva as sole nutritional source. *International journal of oral science*, 3(2), pp.49–54.
- Kolenbrander, P.E. et al., 2010. Oral multispecies biofilm development and the key role of cell-cell distance. *Nature reviews. Microbiology*, 8(7), pp.471–80.
- Kolenbrander, P.E. & London, J., 1993. Adhere Today , Here Tomorrow : Oral Bacterial Adherence. *Journal of Bacteriology*, 175(11), pp.3247–3252.
- Kolenbrander, P.E. & London, J., 1992. Ecological Significance of Co-aggregation among Oral Bacteria. In K. C. Marshall, ed. *Advances in Microbial Ecology*. Boston, MA: Springer US, pp. 183–217.
- König, G. & Navia, M., 1995. Nutritional role of sugars. *American journal of clinical nutrition*, 62(S), pp.275–283.
- König, K., So, P.C., Mantulin, W.W., Tromberg, B.J. and Gratton, E., 1996. Two-photon excited lifetime imaging of autofluorescence in cells during UV A and NIR photostress. *Journal of microscopy*, 183(3), pp.197-204.
- Koo, H., Falsetta, M.L. & Klein, M.I., 2013. The exopolysaccharide matrix: a virulence determinant of cariogenic biofilm. *Journal of dental research*, 92(12), pp.1065–73.

- Koo Lee, Y.-E., Kopelman, R. & Smith, R., 2009. Nanoparticle PEBBLE sensors in live cells and in vivo. *Annual Review of Analytical Chemistry*, 2, pp.57–76.
- Kreth, J., Merritt, J. & Qi, F., 2009. Bacterial and Host Interactions of Oral Streptococci. *DNA and cell biology*, 28(8), pp.397–403.
- Kuramitsu, H.K. et al., 2007. Interspecies interactions within oral microbial communities. *Microbiology and molecular biology reviews: MMBR*, 71(4), pp.653–70.
- Küseler, A. et al., 1993. Accuracy and precision in vitro of Beetrode microelectrodes used for intraoral pH measurements. *Caries research*, 27(3), pp.183–190.
- Lakowicz, J.R., 2006. *Principles of fluorescence spectroscopy* 3rd Editio., Springer.
- Lamb, J.F., 1991. *Essentials of Physiology*, Oxford, UK: Blackwell Scientific Publications.
- Lamont, R.J. & Jenkinson, H.F., 2010. *Oral microbiology at a glance* 1st ed. R. J. Lamont & H. F. Jenkinson, eds., Oxford, UK: Wiley-Blackwell.
- Lamont, R.J. & Jenkinson, H.F., 2000. Subgingival colonization by Porphyromonas gingivalis. *Oral microbiology and immunology*, 15(6), pp.341–9.
- Lamster, I.B. & Ahlo, J.K., 2007. Analysis of Gingival Crevicular Fluid as Applied to the Diagnosis of Oral and Systemic Diseases. *Annals of the New York Academy of Sciences*, 1098(1), pp.216–229.
- Lappin-Scott, H.M. & Costerton, J.W., 1989. Bacterial biofilms and surface fouling. *Biofouling*, 1(4).
- Leinonen, J. et al., 1999. Salivary Carbonic Anhydrase Isoenzyme VI Is Located in the Human Enamel Pellicle. *Caries Research*, 33(3), pp.185–190.
- Lenander-Lumikari, M. & Loimaranta, V., 2000. Saliva and Dental Caries. *Advances in Dental Research*, 14(1), pp.40–47.

- Li, Y. & Burne, R.A., 2001. Regulation of the *gtfBC* and *ftf* genes of *Streptococcus mutans* in biofilms in response to pH and carbohydrate. *Microbiology (Reading, England)*, 147(Pt 10), pp.2841–8.
- Liljemark, W.F. & Gibbons, R.J., 1971. Ability of *Veillonella* and *Neisseria* Species to Attach to Oral Surfaces and Their Proportions Present Indigenously. *Infection and Immunity*, 4(3), pp.264–268.
- Lin, H.-J., Herman, P. & Lakowicz, J.R., 2003. Fluorescence lifetime-resolved pH imaging of living cells. *Cytometry. Part A : the journal of the International Society for Analytical Cytology*, 52(2), pp.77–89.
- Lin, J., 2000. Recent development and applications of optical and fiber-optic pH sensors. *Trends in Analytical Chemistry*, 19(9), pp.541–552.
- Ling, G. & Gerard, R.W., 1949. The normal membrane potential of frog sartorius fibers. *Journal of Cellular Physiology*, 34, pp.383–396.
- Lingström, P., Van Houte, J. & Kashket, S., 2015. Food starches and dental caries. *Critical Reviews in Oral Biology & Medicine*, 11(1963), pp.366–380.
- Liu, G., Tang, C.M. & Exley, R.M., 2015. Non-pathogenic *Neisseria* : members of an abundant , multi-habitat , diverse genus. *Microbiology*, 161, pp.1297–1312.
- Liu, Y.-L., Nascimento, M. & Burne, R.A., 2012. Progress toward understanding the contribution of alkali generation in dental biofilms to inhibition of dental caries. *International journal of oral science*, 4(3), pp.135–40.
- Livesey, G., 2017. Health potential of polyols as sugar replacers , with emphasis on low glycaemic properties. , (2003), pp.163–191.
- Loesche, W.J., 1976. Chemotherapy of dental plaque infections. *Oral Sciences Reviews*, 9, pp.65–107.

- Loesche, W.J., 1988. Ecology of the Oral Flora. In M. G. Newman & R. J. Nisengard, eds. *Oral Microbiology and Immunology*. Philadelphia, PA: Saunders Company, pp. 307–320.
- Loesche, W.J., 1996. Microbiology of Dental Decay and Periodontal Disease. In S. Baron, ed. *Medical Microbiology*. Galverston, TX: University of Texas.
- Loesche, W.J., 1986. Role of Streptococcus mutans in human dental decay. *Microbiological reviews*, 50(4), pp.353–80.
- Loesche, W.J. & Grossman, N.S., 2001. Periodontal Disease as a Specific, albeit Chronic, Infection: Diagnosis and Treatment. *Clinical Microbiology Reviews*, 14(4), pp.727–752.
- Van Loveren, C., 2000. Diet and dental caries: cariogenicity may depend more on oral hygiene using fluorides than on diet or type of carbohydrates. *European Journal of Paediatric Dentistry*, 1, pp.55–62.
- Van Loveren, C., 2004. Sugar Alcohols : What Is the Evidence for Caries-Preventive and Caries-Therapeutic Effects ? *Caries Research*, 38, pp.286–293.
- Lussi, A., Hellwig, E. & Klimek, J., 2012. Fluorides - mode of action and recommendations for use. *Research and Science*, 122(11), pp.1030–42.
- Mager, D.L. et al., 2003. Distribution of selected bacterial species on intraoral surfaces. *Journal of clinical periodontology*, 30(7), pp.644–54.
- Maiden, M.F.J. et al., 1998. Subgingival temperature and microbiota in initial periodontitis. *Journal of clinical periodontology*, 25(10), pp.786–793.
- Main, C. et al., 1984. Instrumentation for measurement of dental plaque thickness in situ. *Journal of Biomedical Engineering*, 6(2), pp.151–154.
- Malvern Instruments, 2000. Dynamic Light Scattering: An Introduction in 30 Minutes, pp.1–8.

- Mandel, I.D., 1987. The functions of saliva. *Journal of dental research*, 66(2S), pp.623–627.
- Manji, F. et al., 1991. A random effects model for some epidemiological features of dental caries. *Community dentistry and oral epidemiology*, 19(6), pp.324–8.
- Manning, R.H. & Edgar, W.M., 1993. pH changes in plaque after eating snacks and meals, and their modification by chewing sugared- or sugar-free gum. *British Dental Journal*, 174(7), pp.241–244.
- Marcotte, H. & Lavoie, M.C., 1998. Oral microbial ecology and the role of salivary immunoglobulin A. *Microbiology and Molecular Biology Reviews*, 62(1), pp.71–109.
- Marcotte, N. & Brouwer, A.M., 2005. Carboxy SNARF-4F as a fluorescent pH probe for ensemble and fluorescence correlation spectroscopies. *The journal of physical chemistry. B*, 109(23), pp.11819–28.
- Margolis, H.C. & Moreno, E.C., 1994. Composition and cariogenic potential of dental plaque fluid. *Critical Reviews in Oral Biology & Medicine*, 5(1), pp.1–25.
- Margolis, H.C., Duckworth, J.H. and Moreno, E.C., 1988. Composition and buffer capacity of pooled starved plaque fluid from caries-free and caries-susceptible individuals. *Journal of dental research*, 67(12), pp.1476-1482.
- Marquis, R.E., 1995. Oxygen metabolism, oxidative stress and acid-base physiology of dental plaque biofilms. *Journal of industrial microbiology*, 15(3), pp.198–207.
- Marsh, P.D., 2003. Are dental diseases examples of ecological catastrophes? *Microbiology*, 149(2), pp.279–294.
- Marsh, P.D., 1995. Dental plaque. In H. M. Lappin-Scott & J. W. Costerton, eds. *Microbial Biofilms*. Cambridge, UK: Cambridge University Press, pp. 282–300.

- Marsh, P.D., 2009. Dental plaque as a biofilm: the significance of pH in health and caries, *Compendium of continuing education in dentistry*. Jamesburg, N.J. 30(2). p. 76-87.
- Marsh, P.D., 2006. Dental plaque as a biofilm and a microbial community - implications for health and disease. *BMC oral health*, 6 Suppl 1, p.S14.
- Marsh, P.D., 2004. Dental plaque as a microbial biofilm. *Caries research*, 38(3), pp.204–11.
- Marsh, P.D., 1994. Microbial ecology of dental plaque and its significance in health and disease. *Advances in Dental Research*, 8(2), pp.263–272.
- Marsh, P.D., 2000. Role of the Oral Microflora in Health. *Microbial Ecology in Health and Disease*, 12, pp.130–137.
- Marsh, P.D. & Bowden, G.H.W., 2000. Microbial Community Interactions in Biofilms. In D. Allison et al., eds. *Symposia - Society for General Microbiology*. Cambridge: Cambridge University Press, pp. 167–198.
- Marsh, P.D. & Bradshaw, D.J., 1999. Microbial community aspects of dental plaque. In *Dental Plaque Revisited: Oral Biofilms in Health and Disease*. pp. 237–253.
- Marsh, P.D. & Bradshaw, D.J., 1997. Physiological approaches to the control of oral biofilms. *Advances in dental research*, 11(1), pp.176–186.
- Marsh, P.D. & Martin, M. V, 2009. *Oral Microbiology* 5th ed., London, UK: Churchill Livingstone Elsevier.
- Marsh, P.D., Moter, A. & Devine, D.A., 2011. Dental plaque biofilms: communities, conflict and control. *Periodontology 2000*, 55(1), pp.16–35.
- Marsh, P.D. & Nyvad, B., 2003. The oral microflora and biofilms on teeth. In O. Fejerskov & E. A. M. Kidd, eds. *Dental Caries: The Disease and its Clinical Management*. Copenhagen, DK: Blackwell Munksgaard, p. 29e48.

- Marsh, P.D. & Nyvad, B., 2009. The oral microflora and biofilms on teeth. In O. Fejerskov & E. Kidd, eds. *Dental Caries: The Disease and its Clinical Management*. New Jersey, USA: John Wiley & Sons, pp. 163–187.
- Martinez, G.M. et al., 2001. Fluorescent pH probes , Fluorescent Proteins , and Intrinsic Cellular Fluorochromes are Tools to Study Cytosolic pH (pH<sub>cyt</sub>) in Mammalian Cells . *Proceedings of SPIE*, 4259, pp.144–156.
- Masuda, M. et al., 2012. Production Potency of Folate, Vitamin B12, and Thiamine by Lactic Acid Bacteria Isolated from Japanese Pickles. *Bioscience, Biotechnology, and Biochemistry*, 76(11), pp.2061–2067.
- McClure, F.J. & McCann, H.G., 1960. Dental caries and composition of bones and teeth of white rats: Effect of dietary mineral supplements. *Archives of Oral Biology*, 2(2), pp.151–161.
- McDermid, A.S., McKee, A.S. & Marsh, P.D., 1988. Effect of environmental pH on enzyme activity and growth of *Bacteroides gingivalis* W50. *Infection and Immunity*, 56(5), pp.1096–1100.
- McHugh, W.D., 1970. *Dental Plaque: Symposium Proceedings* 1st ed., Edinburgh: Harcourt Brace/Churchill Livingstone.
- McHugh, W.D., 1999. Dental Plaque: Thirty Years On. In H. N. Newman & M. Wilson, eds. *Dental Plaque Revisited: Oral Biofilms in Health and Disease*. Cardiff: Bioline Press, pp. 1–3.
- McIntosh, J., James, W.W. & Lazarus-Barlow, P., 1922. An investigation into the aetiology of dental caries. I: The nature of the destructive agent and the production of artificial caries. *The British Journal of Experimental Pathology*, 3(3), pp.138–145.
- Meckel, A.H., 1968. The nature and importance of organic deposits on dental enamel. *Caries Research*, 2(2), pp.104–114.

- Merritt, J.H., Kadouri, D.E. & O'Toole, G.A., 2005. Growing and Analyzing Static Biofilms. *Current Protocols in Microbiology*, 1(1), Section 1B.1 pp.1-17.
- Miessler, G.L. & Tarr, D.A., 2004. Acid–Base and Donor–Acceptor Chemistry. In *Inorganic Chemistry*. New Jersey, USA: Prentice Hall, pp. 54–55.
- Mikx, F.H.M. & Van der Hoeven, J.S., 1975. Symbiosis of *Streptococcus mutans* and *Veillonella alcalescens* in mixed continuous cultures. *Archives of oral biology*, 20(7), pp.407–10.
- Milichich, G.W., 2009. Caries management in the dental practice. *Compendium of continuing education in dentistry (Jamesburg, N.J. : 1995)*, 30(2), pp.62-73.
- Miller, W.D., 1890. *The micro-organisms of the human teeth*, Philadelphia, PA: The S. S. White Dental Mfg. Co.
- Minah, G.E., Solomon, E.S. & Chu, K., 1985. The association between dietary sucrose consumption and microbial population shifts at six oral sites in man. *Archives of oral biology*, 30(5), pp.397–401.
- Moons, P., Michiels, C.W. & Aertsen, A., 2009. Bacterial interactions in biofilms. *Critical reviews in microbiology*, 35(3), pp.157–68.
- Moore, R.J. et al., 1999. Intra-oral temperature variation over 24 hours. *European journal of orthodontics*, 21(3), pp.249–61.
- Moynihan, P. & Petersen, P.E., 2007. Diet, nutrition and the prevention of dental diseases. *Public Health Nutrition*, 7(1a), pp.201–226.
- Mühlemann, H. R., & de Boever, J. (1970). Radiotelemetry of the pH of interdental areas exposed to various carbohydrates. In W. D. McHugh (Ed.), *Dental plaque* (pp. 179–186). Edinburgh: Livingstone.
- Muntz, J., 1943. Production of acids from glucose by dental plaque material. *Journal of Biological Chemistry*, 148, pp.225–236.

- Murtazina, R. et al., 2007. Tissue-specific regulation of sodium/proton exchanger isoform 3 activity in Na<sup>+</sup>/H<sup>+</sup> Exchanger Regulatory Factor 1 (NHERF1) null mice: cAMP inhibition is differentially dependent on NHERF1 and exchange protein directly activated by cAMP in ileum versus prox. *Journal of Biological Chemistry*, 282(34), pp.25141–25151.
- Nadimi, H. et al., 2011. Are sugar-free confections really beneficial for dental health ? *Nature Publishing Group*, 211(7), pp.1–5.
- Nanci, A., 2014. Dentin-Pulp Complex. In *Ten Cate's Oral Histology: Development, Structure and Function*. Elsevier Mosby, pp. 165–205.
- Nanci, A., 2014. Enamel: Development, Structure and Function. In *Ten Cate's Oral Histology: Development, Structure and Function*. Elsevier Mosby, pp. 122–164.
- Newbrun, E., 1992. Preventing dental caries: current and prospective strategies. *The Journal of the American Dental Association*, 123(5), pp.68-73.
- Nizel, A.E. & Harris, R.S., 1964. The Effects of Phosphates on Experimental Dental Caries : A Literature Review. *Journal of Dental Research*, 43(6), pp.1123–1136.
- Noomnarm, U. & Clegg, R.M., 2009. Fluorescence Lifetimes: Fundamentals and Interpretations. *Photosynthesis Research*, 101, pp.181–194.
- Nyvad, B. & Kilian, M., 1987. Microbiology of the early colonization of human enamel and root surfaces in vivo. *Scandinavian Journal of Dental Research*, 95(5), pp.369–80.
- O'Connor, N. & Silver, R.B., 2007. Ratio imaging: practical considerations for measuring intracellular Ca<sup>2+</sup> and pH in living cells. *Methods in cell biology*, 81(6), pp.415–33.
- Orland, F.J. et al., 1954b. Use of the germfree animal technic in the study of experimental dental caries. I. Basic observations on rats reared free of all microorganisms. *Journal of dental research*, 33(2), pp.147–74.

- Owen, O.W., 1949. A study of bacterial counts (lactobacilli) in saliva related to orthodontic appliances. *American Journal of Orthodontics*, 35, pp.672–678.
- Paes Leme, A.F. et al., 2008. Effects of sucrose on the extracellular matrix of plaque-like biofilm formed in vivo, studied by proteomic analysis. *Caries research*, 42(6), pp.435–43.
- Papas, A.S. et al., 1993. Caries prevalence in xerostomic individuals. *Journal of the Canadian Dental Association*, 59(2), pp.171–179.
- Park, E.J. et al., 2003. Ratiometric optical PEBBLE nanosensors for real-time magnesium ion concentrations inside viable cells. *Analytical Chemistry*, 75(15), pp.3784–3791.
- Paster, B.J. et al., 2001. Bacterial Diversity in Human Subgingival Plaque. *Journal of Bacteriology*, 183(12), pp.3770–3783.
- Paster, B.J. et al., 2006. The breadth of bacterial diversity in the human periodontal pocket and other oral sites. *Periodontology 2000*, 42, pp.80–87.
- Paster, B.J. & Dewhirst, F.E., 2009. Molecular microbial diagnosis. *Periodontology 2000*, 51, pp.38–44.
- Pawley, J.B., 2006. *Handbook of Biological Confocal Microscopy* 3rd ed. James B Pawley, ed., New York: Springer.
- Peter, M. and Ameer-Beg, S.M., 2004. Imaging molecular interactions by multiphoton FLIM. *Biology of the Cell*, 96(3), pp.231-236.
- Peters, A.C. & Wimpenny, J.W.T., 1988. A constant-depth laboratory model film fermentor. *Biotechnology and bioengineering*, 32, pp.263–270.
- Petersen, P.E., 2003. The World Oral Health Report 2003: continuous improvement of oral health in the 21st century--the approach of the WHO Global Oral Health Programme. *Community dentistry and oral epidemiology*, 31 Suppl 1, pp.3–23.

- Phillips, D. et al., 1985. Time Correlated Single-Photon Counting (TCSPC) Using Laser Excitation. *Instrumentation Science & Technology*, 14(3–4), pp.267–292.
- Pratten, J. et al., 1998. In vitro studies of the effect of antiseptic-containing mouthwashes on the formation and viability of *Streptococcus sanguis* biofilms. *J Appl Microbiol*, 84(6), pp.1149–1155.
- Pratten, J. et al., 2015. Physical disruption of oral biofilms by sodium bicarbonate: an in vitro study. *International Journal of Dental Hygiene*, (July), pp.1-6.
- Pratten, J. & Wilson, M., 1999. Antimicrobial susceptibility and composition of microcosm dental plaques supplemented with sucrose. *Antimicrobial Agents and Chemotherapy*, 43(7), pp.1595–1599.
- Pratten, J., Wilson, M. & Spratt, D.A., 2003. Characterization of in vitro oral bacterial biofilms by traditional and molecular methods. *Oral microbiology and immunology*, 18(1), pp.45–9.
- Preetha, A. & Banerjee, R., 2005. Comparison of Artificial Saliva Substitutes. *Trends in Biomaterials and Artificial Organs*, 18(2), pp.178–186.
- Preethi, B.P., Reshma, D. & Anand, P., 2010. Evaluation of flow rate, pH, buffering capacity, calcium, total proteins and total antioxidant capacity levels of saliva in caries free and caries active children: An in vivo study. *Indian Journal of Clinical Biochemistry*, 25(4), pp.425–428.
- Pucacco, L.R. et al., 1986. pH microelectrode: modified Thomas recessed-tip configuration. *Analytical biochemistry*, 153(2), pp.251–61.
- Qian, H. & Dao, M.L., 1993. Inactivation of the *Streptococcus mutans* wall-associated protein A gene (*wapA*) results in a decrease in sucrose-dependent adherence and aggregation. *Infection and Immunity*, 61(12), pp.5021–5028.
- Quivey Jr., R.G., 2006. Caries. In R. J. Lamont et al., eds. *Oral Microbiology and Immunology*. Washington DC, USA: American Society of Microbiology, pp. 233–252.

- Ramsay, G., 2014. *NHS Dental Statistics for England : 2013-14, Second Quarterly Report*,
- Raner, E. et al., 2014. pH and bacterial profile of dental plaque in children and adults of a low caries population. *Anaerobe*, 27, pp.64–70.
- Rasband, W.S., ImageJ, U. S. National Institutes of Health, Bethesda, Maryland, USA, <https://imagej.nih.gov/ij/>, 1997-2016.
- Rasmussen, T.B. & Givskov, M., 2006. Quorum-sensing inhibitors as anti-pathogenic drugs. *International Journal of Medical Microbiology*, 296(1), pp.149–156.
- Ready, D., 2002. Composition and antibiotic resistance profile of microcosm dental plaques before and after exposure to tetracycline. *Journal of Antimicrobial Chemotherapy*, 49(5), pp.769–775.
- Reema, S.D., Lahiri, P.K. & Roy, S.S., 2014. Review of casein phosphopeptides-amorphous calcium phosphate. *Chinese journal of dental research*, 17(1), pp.7–14.
- Resch-Genger, U. et al., 2008. Quantum dots versus organic dyes as fluorescent labels. *Nature methods*, 5(9), pp.763–775.
- Revsbech, N.P. & Jørgensen, B.B., 1986. Microelectrodes: their use in microbial ecology. *Adv. Microb. Ecol*, 9, pp.293–352.
- Ribeiro, C.C.C. et al., 2005. Effect of starch on the cariogenic potential of sucrose. *British Journal of Nutrition*, 94, pp.44–50.
- Ribou, A.-C., Vigo, J. & Salmon, J.-M., 2002. C-SNARF-1 as a Fluorescent Probe for pH Measurements in Living Cells: Two-Wavelength-Ratio Method versus Whole-Spectral-Resolution Method. *Journal of Chemical Education*, 79(12), p.1471.
- Richter, C. et al., 2015. Dual-fluorescence pH probe for bio-labelling. *Physical chemistry chemical physics : PCCP*, 17, pp.30590–30597.

- Roberts, A.P. & Mullany, P., 2010. Oral biofilms: a reservoir of transferable, bacterial, antimicrobial resistance. *Expert review of anti-infective therapy*, 8(12), pp.1441–50.
- Rose, M.C. & Voynow, J.A., 2006. Respiratory tract mucin genes and mucin glycoproteins in health and disease. *Physiological reviews*, 86(1), pp.245–278.
- Rudney, J.D., 1995. Does Variability in Salivary Protein Concentrations Influence Oral Microbial Ecology and Oral Health? *Critical Reviews in Oral Biology & Medicine*, 6(4), pp.343–367.
- Rugg-Gunn, A., 2013. Dental caries: strategies to control this preventable disease. *Acta medica academica*, 42(2), pp.117–30.
- Rölla, G., Robrish, S.A. & Bowen, W.H., 1977. Interaction of hydroxyapatite and protein-coated hydroxyapatite with streptococcus mutans and streptococcus sanguinis. *Acta Pathologica, Microbiologica et Immunologica Scandinavia*, 85B(5), pp.341–346.
- Santegoeds, C.M., Schramm, A. & de Beer, D., 1998. Microsensors as a tool to determine chemical microgradients and bacterial activity in wastewater biofilms and flocs. *Biodegradation*, 9(3–4), pp.159–167.
- Schachtele, C.F. et al., 1976. Bacterial interference with sucrose-dependent adhesion of oral streptococci. In *Microbial Aspect of Dental Caries*. pp. 401–412.
- Schachtele, C.F. & Jensen, M.E., 1982. Comparison of methods for monitoring changes in the pH of human dental plaque. *Journal of dental research*, 61(10), pp.1117–25.
- Schaudinn, C. et al., 2007. Bacterial Biofilms, Other Structures Seen as Mainstream Concepts. *Microbe*, 2(5), pp.231–237.

- Scheie, A.A. et al., 1992. Use of palladium touch microelectrodes under field conditions for in vivo assessment of dental plaque pH in children. *Caries research*, 26, pp.44–52.
- Schlafer, S. et al., 2011. pH landscapes in a novel five-species model of early dental biofilm. *PLoS One*, 6(9), p.e25299.
- Schlafer, S. et al., 2015. Ratiometric Imaging of Extracellular pH in Bacterial Biofilms with C-SNARF-4. *Applied and Environmental Microbiology*, 81(4), pp.1267–1273.
- Scully, C., 2013. *Oral and Maxillofacial Medicine: The Basis of Diagnosis and Treatment*, Churchill Livingstone.
- Selvig, K.A. and Selvig, S.K., 1962. Mineral content of human and seal cementum. *Journal of Dental Research*, 41(3), pp.624-632.
- Selwitz, R.H., Ismail, A.I. and Pitts, N.B., 2007. Dental caries. *The Lancet*, 369(9555), pp.51-59.
- Shi, W., Li, X. & Ma, H., 2012. A Tunable Ratiometric pH Sensor Based on Carbon Nanodots for the Quantitative Measurement of the Intracellular pH of Whole Cells. *Angewandte Chemie*, 124(26), pp.6538–6541.
- Shouji, N. et al., 2000. Anticaries Effect of a Component from Shiitake (an Edible Mushroom). *Caries Research*, 34(1), pp.94–98.
- Shu, M. et al., 2007. The relationship between dental caries status and dental plaque urease activity. *Oral microbiology and immunology*, 22(1), pp.61–6.
- Siggaard-Andersen, O., 1974. *The acid-base status of the blood* 4th ed., Baltimore, MD: Williams and Wilkins.
- Sigma-Aldrich, Sigma-Aldrich Buffer Reference Centre.
- Silver, R.B., 2003. Ratio imaging: measuring intracellular Ca<sup>++</sup> and pH in living cells. *Methods in cell biology*, 72, pp.369–87.

- Siqueira, W.L. et al., 2010. Evidence of intact histatins in the in vivo acquired enamel pellicle. *Journal of dental research*, 89(6), pp.626–30.
- Sissons, C.H., Wong, L. & Shu, M., 1998. Factors affecting the resting pH of in vitro human microcosm dental plaque and *Streptococcus mutans* biofilms. *Archives of oral biology*, 43(2), pp.93–102.
- Slomiany, B.L. et al., 1996. Salivary mucins in oral mucosal defense. *General Pharmacology*, 27(5), pp.761–771.
- So, P.T.C. et al., 2000. Two-photon excitation fluorescence microscopy. *Annual Review of Biomedical Engineering*, 2, pp.399–429.
- Socransky, S.S. & Haffajee, A.D., 1992. The bacterial etiology of destructive periodontal disease: current concepts. *Journal of periodontology*, 63(4 Suppl), pp.322–31.
- Sousa, V. et al., 2016. Microbial ecology dynamics in the progression to peri-implantitis: modelling microcosm biofilms on to titanium implant surfaces. *Clinical oral implants research*, 27(13), p.2016.
- Spence, D.E., Kean, P.N. & Sibbett, W., 1991. 60-fsec pulse generation from a self-mode-locked Ti:sapphire laser. *Optics letters*, 16(1), pp.42–44.
- Spratt, D.A. et al., 2012. Evaluation of Plant and Fungal Extracts for Their Potential Antigingivitis and Anticaries Activity. *Journal of Biomedicines and Biotechnology*, 2012, p.510198.
- Spratt, D.A. et al., 2011. Shiitake mushroom extracts disrupt *Streptococcus mutans* and *Actinomyces naeslundii* biofilms. Poster presented at: IADR General Session 2012, Iguaçú Falls, Brazil; 20–23 June, 2012.
- Spratt, D.A. & Pratten, J., 2003. Biofilms and the oral cavity. *Reviews in Environmental Science and Biotechnology*, 2, pp.109–120.

- Steinberg, D., 2015. Dental Chatter: Bacterial Cross-Talk in the Biofilm of the Oral Cavity. *Israel Journal of Chemistry*, pp.1-10.
- Stephan, R.M., 1940. Changes in hydrogen-ion concentration on tooth surfaces and in carious lesions. *Journal of the American Dental Association*, 27(5), pp.718–723.
- Stephan, R.M., 1944. Intra-oral hydrogen ion concentration associated with dental caries activity. *Journal of dental research*, 23(4), pp.257–267.
- Stephan, R.M. & Miller, B.F., 1943. A quantitative method for evaluating physical and chemical agents which modify production of acids in bacterial plaques on human teeth. *Journal of Dental Research*, 22(1), pp.63–71.
- Sternberg, C. & Tolker-Nielsen, T., 2005. Growing and Analyzing Biofilms in Flow Cells. *Current Protocols in Microbiology*, 1(B2), pp.1–15.
- Stokes, G.G., 1853. On the Change of Refrangibility of Light. *Philosophical Transactions of the Royal Society of London*, 143(January), pp.385–396.
- Stoodley, P. et al., 2002. Biofilms as complex differentiated communities. *Annual Reviews in Microbiology*, 56, pp.187–209.
- Stoodley, P. et al., 1998. Influence of hydrodynamics and nutrients on biofilm structure. *Journal of applied microbiology*, 85 Suppl 1, p.19S–28S.
- Stoodley, P., De Beer, D. & Lewandowski, Z., 1994. Liquid Flow in Biofilm Systems. *Applied and environmental microbiology*, 60(8), pp.2711–2716.
- Stoodley, P., Boyle, J.D. & Lappin-scott, H.M., 1999. Influence of flow on the structure of bacterial biofilms. In C. R. Bell, M. Brylinski, & P. Johnson-Green, eds. *Microbial Biosystems: New Frontiers*. Halifax, Canada: Atlantic Canac Society for Microbial Ecology, p. 7.

- Straub, M. and Hell, S.W., 1998. Fluorescence lifetime three-dimensional microscopy with picosecond precision using a multifocal multiphoton microscope. *Applied Physics Letters*, 73(13), pp.1769-1771.
- Stutzmann, G.E. & Parker, I., 2005. Dynamic multiphoton imaging: a live view from cells to systems. *Physiology (Bethesda, Md.)*, 20, pp.15–21.
- Sun, H. et al., 2009. Polymeric Nanosensors for Measuring the Full Dynamic pH Range of Endosomes and Lysosomes in Mammalian Cells. *Journal of Biomedical Nanotechnology*, 5(6), pp.676–682.
- Sun, H. et al., 2006. Synthesis and Characterization of Ratiometric, pH Sensing Nanoparticles with Covalently Attached Fluorescent Dyes [Supplementary information]. *Chemistry of Materials*, 18(15), pp.S1–S15.
- Sun, H., Almdal, K. & Andresen, T.L., 2011. Expanding the dynamic measurement range for polymeric nanoparticle pH sensors. *Chemical communications*, 47(18), pp.5268–70.
- Sun, Y., Day, R.N. & Periasamy, A., 2011. Investigating protein-protein interactions in living cells using fluorescence lifetime imaging microscopy. *Nature protocols*, 6(9), pp.1324–1340.
- Suntharalingam, P. & Cvitkovitch, D.G., 2005. Quorum sensing in streptococcal biofilm formation. *Trends in microbiology*, 13(1), pp.3–6.
- Svensäter, G. et al., 1997. Acid tolerance response and survival by oral bacteria. *Oral microbiology and immunology*, 12, pp.266–273.
- Sytsma, J., Vroom, J.M., De Grauw, C.J. and Gerritsen, H.C., 1998. Time-gated fluorescence lifetime imaging and microvolume spectroscopy using two-photon excitation. *Journal of Microscopy*, 191, pp.39-51.
- Szabó, I., 1974. Carbonic anhydrase activity in the saliva of children and its relation to caries activity. *Caries research*, 8(2), pp.187–191.

- Szmacinski, H. & Lakowicz, J.R., 1995. Fluorescence lifetime-based sensing and imaging. *Sensors and Actuators B: Chemical*, 29(1–3), pp.16–24.
- Szmacinski, H. & Lakowicz, J.R., 1993. Optical measurements of pH using fluorescence lifetimes and phase-modulation fluorometry. *Analytical chemistry*, 65, pp.1668–1674.
- Tadrous, P.J., 2000. Methods for imaging the structure and function of living tissues and cells: 2. Fluorescence lifetime imaging. *The Journal of pathology*, 191(3), pp.229–34.
- Takahashi, N., 2005. Microbial ecosystem in the oral cavity : Metabolic diversity in an ecological niche and its relationship with oral diseases. *International Congress Series*, 1284, pp.103–112.
- Takahashi, N. & Nyvad, B., 2008. Caries ecology revisited: microbial dynamics and the caries process. *Caries Research*, 42(6), pp.409–18.
- Takahashi, N. & Nyvad, B., 2011. The role of bacteria in the caries process: ecological perspectives. *Journal of dental research*, 90(3), pp.294–303.
- Takahashi, N. & Schachtele, C.F., 1990. Effect of pH on the growth and proteolytic activity of *Porphyromonas gingivalis* and *Bacteroides intermedius*. *Journal of dental research*, 69(6), pp.1266–1269.
- Takehita, T. et al., 2015. Dental plaque development on a hydroxyapatite disk in young adults observed using a barcoded pyrosequencing approach. *Scientific Reports*, 8136, pp.1–9.
- Telgi, R.L. et al., 2013. In vivo dental plaque pH after consumption of dairy products. *General Dentistry*, 61(3), pp.56–59.
- Tenovuo, J., 1997. Salivary parameters of relevance for assessing caries activity in individuals and populations. *Community dentistry and oral epidemiology*, 25(1), pp.82–6.

- Theilade, E., 1986. The non-specific theory in microbial etiology of inflammatory periodontal diseases. *Journal of clinical periodontology*, 13(10), pp.905–11.
- Thermo Fisher Scientific, Fluorescence SpectraViewer.  
<https://www.thermofisher.com/uk/en/home/life-science/cell-analysis/labeling-chemistry/fluorescence-spectraviewer.html>.
- Thomas, R.C., 1978. *Ion-Selective Intracellular Microelectrodes: How to Make and Use Them* 2nd ed. R. Thomas, ed., New York: Academic Press.
- Thonard, J.C., 1966. Dental caries as an infectious disease. *Journal of School Health*, 11(3), pp.152–159.
- Tinanoff, N. & Palmer, C.A., 2000. Dietary Determinants of Dental Caries and Dietary Recommendations for Preschool Children. *Journal of Public Health Dentistry*, 60(3), pp.197–206.
- Tolker-Nielsen, T. & Molin, S., 2000. Spatial Organization of Microbial Biofilm Communities. *Microbial Ecology*, 40(2), pp.75–84.
- Touger-Decker, R. & Van Loveren, C., 2003. Sugars and dental caries. *American journal of clinical nutrition*, 78(1), p.881S–892S.
- Tsien, R.Y., 1998. The green fluorescent protein. *Annual Reviews of Biochemistry*, 67(11), pp.509–44.
- VanHoudt, P., 1992. Iridium oxide pH microelectrode. *Biotechnology and Bioengineering*, 203(4), pp.601–608.
- Vratsanos, S.M., 1981. Chromatographic microanalysis of organic acids in plaque related to food cariogenicity. *Foods, nutrition and dental health*, 3, pp.89–91.
- Vratsanos, S.M. & Mandel, I.D., 1982. Comparative Plaque Acidogenesis of Caries-Resistant vs. Caries-Susceptible Adults. *Journal of Dental Research*, 61(3), pp.465–468.

- Vroom, J.M. et al., 1999. Depth penetration and detection of pH gradients in biofilms by two-photon excitation microscopy. *Applied and environmental microbiology*, 65(8), pp.3502–3511.
- Wachter, E.A. et al., 1998. Simultaneous Two-Photon Excitation Photodynamic Therapy Agents. *SPIE*, 68, pp.68–75.
- Wall, T.A. & Vujcic, M., 2015. *Research Brief: U.S. Dental Spending Continues to Be Flat*, US.
- Wang, X.-H. et al., 2014. Targetable Phosphorescent Oxygen Nanosensors for the Assessment of Tumor Mitochondrial Dysfunction By Monitoring the Respiratory Activity. *Angewandte Chemie*, 53(46), pp.12471–12475.
- Wheeler, T.T., Clark, W.B. & Birdsell, D.C., 1979. Adherence of *Actinomyces viscosus* T14V and T14AV to Hydroxyapatite Surfaces In Vitro and Human Teeth In Vivo. *Infection and Immunity*, 25(3), pp.1066–1074.
- Whelton, H., 2004. Introduction: the anatomy and physiology of salivary glands. In M. Edgar, C. Dawes, & D. O'Mullane, eds. *Saliva and Oral Health*. Lowestoft, Suffolk: British Dental Journal, pp. 1–13.
- Whitaker, J.E., Haugland, R.P. & Prendergast, F.G., 1991. Spectral and photophysical studies of benzo[c]xanthene dyes: dual emission pH sensors. *Analytical biochemistry*, 194(2), pp.330–44.
- Wiecek, J.M., 2015. *Development of an in vitro gingivitis model*.
- Wilson, M., 2005. The oral cavity and its indigenous microbiota. In M. Wilson, ed. *Microbial Inhabitants of Humans: Their Ecology and Role in Health and Disease*. Cambridge, UK: Cambridge University Press, pp. 318–372.
- Wilson, T., 1984. *Theory and Practice of Scanning Optical Microscopy* C. Sheppard, ed., Academic Press, 1984 Original from University of Minnesota.

- Wimpenny, J.W.T. & Coombs, J.P., 1983. Penetration of Oxygen into Bacterial Colonies. *Journal of General Microbiology*, 129(4), pp.1239–1242.
- Wojcicki, C.J., Harper, D.S. & Robinson, P.J., 1987. Differences in Periodontal Disease-Associated Microorganisms of Subgingival Plaque in Prepubertal, Pubertal and Postpubertal Children. *Journal of Periodontology*, 58(4), pp.219–223.
- Wolfbeis, O.S., 2004. Fiber-Optic Chemical Sensors and Biosensors. *Analytical chemistry*, 76, pp.3269–3284.
- Xiao, J. et al., 2012. The exopolysaccharide matrix modulates the interaction between 3D architecture and virulence of a mixed-species oral biofilm. *PLoS pathogens*, 8(4), p.e1002623.
- Zambon, J.J. et al., 1996. Cigarette smoking increases the risk for subgingival infection with periodontal pathogens. *Journal of periodontology*, 67(10 Suppl), pp.1050–4.
- Zaura, E. et al., 2011. The effects of fractions from shiitake mushroom on composition and cariogenicity of dental plaque microcosms in an in vitro caries model. *Journal of biomedicine & biotechnology*, 2011(1), p.135034.
- Zen, K. et al., 1992. Second messengers regulate endosomal acidification in Swiss 3T3 fibroblasts. *The Journal of cell biology*, 119(1), pp.99–110. Zero, D.T., 2004. Sugars - The arch criminal? *Caries Research*, 38(3), pp.277–285.
- Zero, D.T., van Houte, J. & Russo, J., 1986. The intra-oral effect on enamel demineralization of extracellular matrix material synthesized from sucrose by *Streptococcus mutans*. *Journal of Dental Research*, 65(6), pp.918–923.
- Zilm, P.S. & Rogers, A.H., 2007. Co-adhesion and biofilm formation by *Fusobacterium nucleatum* in response to growth pH. *Anaerobe*, 13(3–4), pp.146–52.

# **APPENDICES**

**Appendix 1. Abbreviations Used**

**Appendix 2. Glossary of Terms Used**

## **Appendix 1. Abbreviations Used**

<b>BCECF</b>	2',7'-Bis -(2-Carboxyethyl)-5-(and-6)-Carboxyfluorescein
<b>BHI</b>	Brain Heart Infusion
<b>BSA</b>	Bovine Serum Albumin
<b>CBA</b>	Columbia Blood Agar
<b>CDFF</b>	Constant Depth Film Fermenter
<b>CFU</b>	Colony Forming Units
<b>CLSM</b>	Confocal Laser Scanning Microscopy
<b>EPS</b>	Extracellular Polymeric Substance
<b>FAA</b>	Fastidious Anaerobic Agar
<b>FAM</b>	Carboxyfluorescein, (a fluorophore)
<b>FLIM</b>	Fluorescence Lifetime Imaging Microscopy
<b>FRET</b>	Förster Resonance Energy Transfer
<b>GCF</b>	Gingival Crevicular Fluid
<b>HEPA</b>	High-Efficiency Particulate Air
<b>ID</b>	Inner Diameter
<b>OD</b>	Outer Diameter
<b>OD<sub>600</sub></b>	Optical Density at 600 nm
<b>OG</b>	Oregon Green <sup>®</sup> -488, (a fluorophore)
<b>SCA IV</b>	Salivary Carbonic Anhydrase IV
<b>SNAFL</b>	Seminaphthofluorescein, (a fluorophore)
<b>SNARF</b>	Seminaphthorhodafluor, (a fluorophore)
<b>TAMRA</b>	Tetramethylrhodafluor, (a fluorophore)
<b>TCSPC</b>	Time-Correlated Single-Photon Counting

## Appendix 2. Glossary of Terms Used

- Acidogenicity:** The ability to generate acid or acidity.
- Aciduricity:** The ability to survive and grow in low pH conditions.
- Biofilm:** A consortium of microorganisms, embedded in a cell-derived, extracellular polymeric matrix attached to a surface.
- Dynamic range:** The range of pH between the minimum and maximum response of the nanosensor within the detection limit.
- Desquamation:** The shedding or sloughing of the outermost layer of epithelial cells.
- Detection limit:** The detection limit is considered to be the intersect between the linear portion of the curve and the intersect between the minimum and maximum asymptote.
- Fluorophore brightness:** Overall signal intensity, determined by the molar extinction coefficient and quantum yield.
- Microbiota:** The ecological community of commensal, symbiotic and pathogenic microorganisms found in and on all multicellular organisms.
- Molar excitation coefficient:** Also known as the molar attenuation coefficient or molar absorptivity is the intrinsic property of how strongly a chemical species attenuates (absorbs) light at a given wavelength.
- Planktonic:** A free-living organisms existing within a hydrated atmosphere.
- Quantum yield of fluorescence:** A measure of the efficiency of the fluorescence process, defined as the ratio of the number of photons emitted to the number of photons absorbed.